Biological evaluations of nanocarriers to improve the effectiveness of colorectal cancer treatment

Cabral De Sä Leitão Oliveira, A.L.

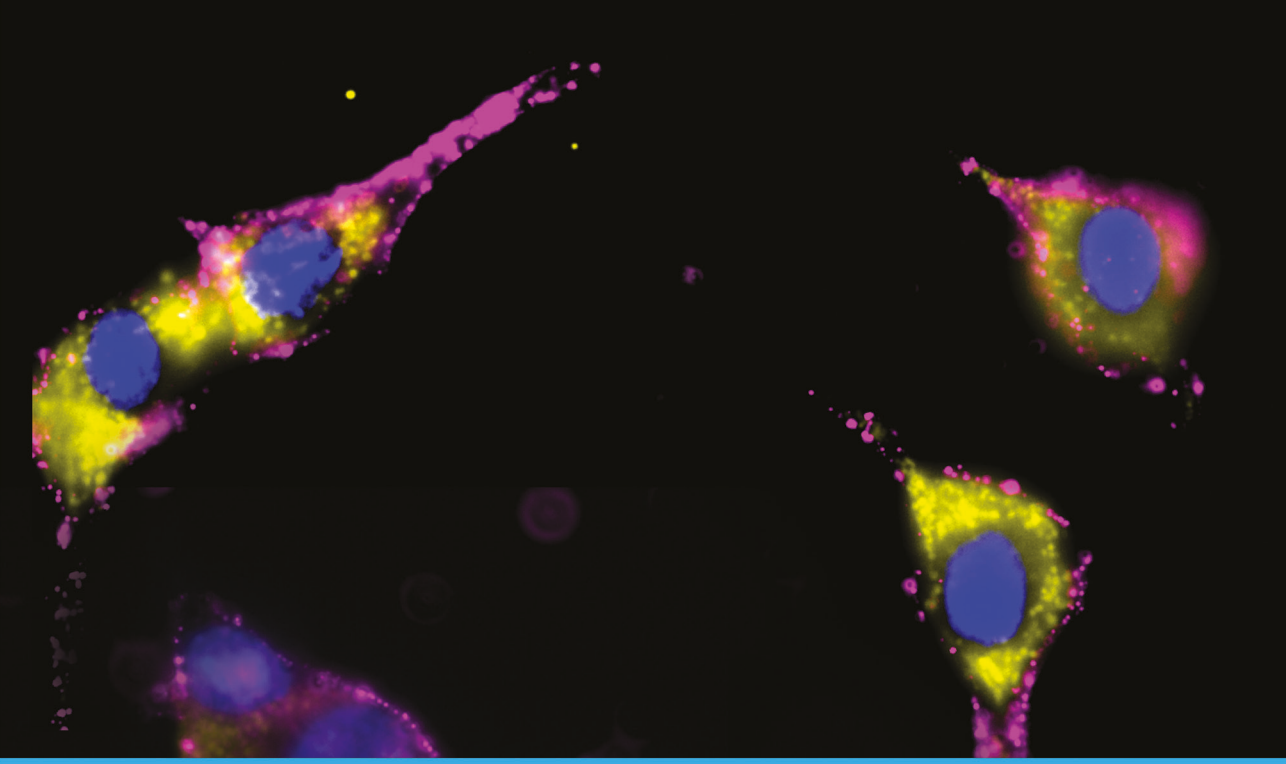

BIOLOGICAL EVALUATIONS OF NANOCARRIERS TO IMPROVE THE EFFECTIVENESS OF COLORECTAL CANCER TREATMENT

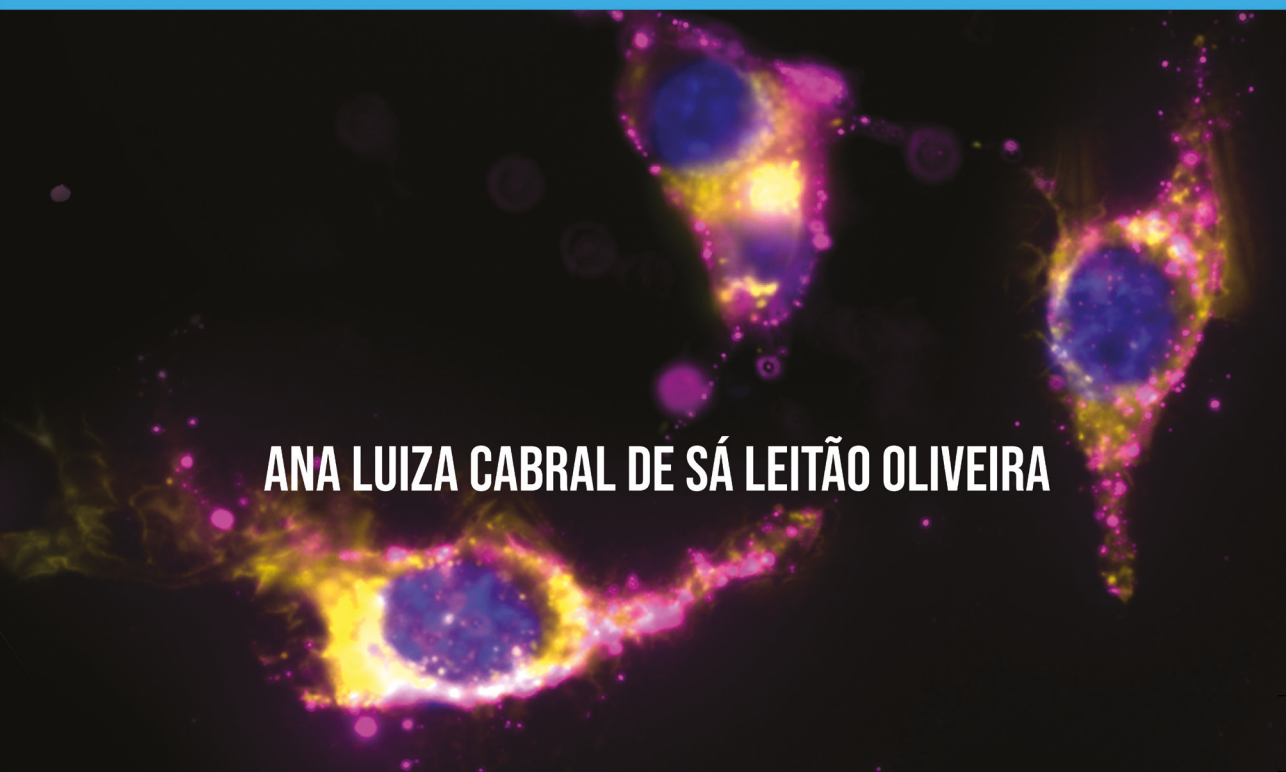

ANA LUIZA CABRAL DE SÁ LEITÃO OLIVEIRA

BIOLOGICAL EVALUATIONS OF NANOCARRIERS TO IMPROVE THE EFFECTIVENESS OF COLORECTAL CANCER TREATMENT

Ana Luiza Cabral de Sá Leitão Oliveira

Biological evaluations of nanocarriers to improve the effectiveness of colorectal cancer treatment

Proefschrift

ter verkrijging van
de graad van doctor aan de Universiteit Leiden,
op gezag van rector magnificus prof.dr.ir. H. Bijl,
volgens besluit van het college voor promoties
te verdedigen op donderdag 24 maart 2022
klokke 16.15 uur

door
Ana Luiza Cabral de Sá L. Oliveira
Geboren te Natal, Brazilië
in 1989

PROMOTOR
Prof. Dr. LF de Geus-Oei

CO-PROMOTORES
Dr. LJ Cruz Ricondo
Dr. RF de Araújo Júnior, Federal University of Rio Grande do Norte, Brazil

PROMOTIECOMMISSIE
Prof. Dr. FA Ossendorp
Dr. LH da Silva Gasparotto, Federal University of Rio Grande do Norte, Brazil.
Dr. RF de Carvalho Leitão. Federal University of Ceara, Brazil.
Prof. Dr. P Di Martino, , University of Camerino, Italy
Dr. EL Kaijzel

ISBN: 978-94-6419-452-4

LAYOUT BY: Menora Tse
PRINTED BY: Gildeprint
COVER BY: Stefano van Bovene

This thesis was financially supported by: Chipsoft B.V., Percuros B.V., Leiden University Library.

TABLE OF CONTENTS

CHAPTER I 06
Introduction

CHAPTER II 56
Cholesterol-functionalized carvedilol-loaded PLGA nanoparticles: anti-inflammatory, antioxidant, and antitumor effects

CHAPTER III 90
Effect of Oxaliplatin-Loaded Poly (d,L-Lactide-co-Glycolic Acid) (PLGA) Nanoparticles Combined with Retinoic Acid and Cholesterol on Apoptosis, Drug Resistance, and Metastasis Factors of Colorectal Cancer

CHAPTER IV 132
Maximizing the potency of oXaliplatin coated nanoparticles with folic acid for modulating tumor progression in colorectal cancer

CHAPTER V 164
Summary, General discussion and Future Perspectives

APPENDICES 184
Nederlandse samenvatting
Portuguese Summary
List of Abbreviations
List of Publications
Curriculum vitae
Ackowledgements

CHAPTER **ONE**

Ana Luiza C. de S. L. Oliveira, Timo Schomann, Lioe-Fee de Geus-Oei, Ellen Kapiteijn, Luis J. Cruz*, Raimundo F. de Araújo Júnior*.
Nanocarriers as a Tool for the Treatment of Colorectal Cancer. Pharmaceutics August 2021.
Doi: 10.3390/pharmaceutics13081321.

INTRODUCTION

Nanocarriers as a Tool for the Treatment of Colorectal Cancer

Abstract: Nanotechnology is a promising tool for the treatment of cancer. In the past decades, major steps have been made to bring nanotechnology into the clinic in the form of nanoparticle-based drug delivery systems. The great hope of drug delivery systems is to reduce the side effects of chemotherapeutics while simultaneously increasing the efficiency of the therapy. An increased treatment efficiency would greatly benefit the quality of life as well as the life expectancy of cancer patients. However, besides its many advantages, nanomedicines have to face several challenges and hurdles before they can be used for the effective treatment of tumors. Here, we give an overview of the hallmarks of cancer, especially colorectal cancer, and discuss biological barriers as well as how drug delivery systems can be utilized for the effective treatment of tumors and metastases.

Keywords: drug delivery system; nanomedicine; nanoparticles; cancer; biological barriers

1. INTRODUCTION

The development of new technologies allows the improvement of several scientific fields, such as the field of medicine, where essential discoveries have been made by applying knowledge and tools that culminate in the improvement of specialized and personalized therapy strategies [1]. The application of improved medical technologies increases the life expectancy as well as the quality of life of patients and, thereby, the standard of life of the general population. Due to technological advances, the equipment and procedures used in the clinic have become less invasive, safer, more effective and optimized. As a result, the patient's recovery time has decreased along with the risk of complications from surgery, which improves quality of life and reduces the cost of health care [2].

Nanotechnology is a consolidated ally in the search for solutions to as yet unanswered questions regarding some diseases, as well as in the improvement of existing technologies for prevention, diagnosis, control and treatment [3]. The nanomedicine area uses the properties and physical characteristics of materials, structures, devices and systems of a nanoscale size, which approaches the molecular level where changes in biological processes originate and culminate in many pathologies, such as mutated genes, protein defects and infections, among others [4].

With all the molecular knowledge available, it is possible to better understand the pathophysiology of a disease and continuously develop new tools or improve existing ones, which are applied to assist the health of patients. Such improvements are, e.g., sensors and surgical instruments that give detailed information about the location and exact size of a tumor, innovative imaging agents that are specific for a certain tissue, monitoring technologies with improved resolution and sensitivity, and mainly biomaterials with improved targeting characteristics, amongst others [5]. These medical devices are also often used in the diagnosis and treatment of disease and are associated with cell therapy to improve drug delivery, tissue engineering and tissue regeneration. Some technologies integrate multifunctional systems by combining diagnostics, targeted therapy and response tracking, which is an emerging, promising approach that is known as theranostics, a portmanteau derived from the blending of the words therapeutic (thera) and diagnostic (nostic) [6,7].

In the area of drug development, nanomedicine has a prominent role by providing potential solutions to approach challenging medical problems and needs. Nanomedicine applications can provide solutions to diagnostic problems, to therapy monitoring, as well as to the control, prevention and treatment of diseases. Within the therapeutic context, the search for a combination for better treatment efficacy is promoted through the application of innovative molecules, exploring multiple mechanisms of action and maximizing the effectiveness of known drugs, as well as their targeted, accurate and controlled delivery, in order to treat patients more effectively while reducing unwanted adverse effects [8].

2. CANCER

Cancer is a disease with genetic changes in DNA, which involves two categories of genes: oncogenes and tumor suppressor genes [9,10]. Oncogenes and tumor suppressor genes are involved in the process of carcinogenesis. Their classification is due to the type of regulation they make in the processes that lead to the promotion of the tumor: (i) if the gene promotes this process, it is called an oncogene, and (ii) if the gene prevents this process, it is called a tumor suppressor gene [11].

2.1 Characteristics of Cancer

Hanahan and Weinberg were the first to describe the specific characteristics of tumor cells in the literature [9]. Tumor cells are independent of any growth factor supply. Therefore, avoidance of growth suppressors, prevention of cell death and stimulation of angiogenesis in the environment of tumor cells are observed, and their replicative potential is maintained [9,10]. This list of characteristics was updated later with emerging characteristics (reprogramming of energy metabolism, avoidance of immune destruction) and facilitating characteristics (genomic instability, inflammation) [9,10]. These hallmarks explain the invasion/metastasis of tumors and can be used to find a new approach to diagnosis and treatment [9].

Three of these characteristics of cancer are: preventing cell death, invasion/metastasis and inflammation, which will be discussed in more detail in the next paragraphs.

2. CANCER

2.1 Characteristics of Cancer

2.1.1. Preventing Cell Death

The development of resistance to cell death, specifically to apoptosis, is one of the most important factors for the progression and survival of a cancer cell [12]. Apoptosis is a cellular suicide program that leads to the elimination of damaged or abnormal cells during development or after stress mechanisms, and this process involves a series of events that culminate in the activation of initiating caspases (caspase-2, -8, -9 or -10), and these lead to the activation of the executing caspases (caspase-3 or -7) resulting in the cleavage of specific cell substrates in the nucleus and cytoplasm that leads to cell death [12].

There are two ways of signaling cell death due to apoptosis, the extrinsic pathway (related to death receptors) and the intrinsic pathway (mitochondrial; Figure 1) [13]. The extrinsic pathway is initiated in response to the binding and activation of receptors of the tumor necrosis factor (TNF) receptor superfamily; then, there is the coupling of these by the Fas-associated death domain protein (FADD), and this subsequently leads to activation of caspase-8 and formation of a signaling complex on the plasma membrane called the death-inducing signaling complex (DISC), which in turn activates the downstream effector caspases [13]. Caspase-8 also cleaves other substrates, such as Bid, which will stimulate the release of cytochrome c and the activation of the intrinsic pathway [14].

The intrinsic pathway is initiated by the permeabilization of the mitochondrial outer membrane (MOMP—mitochondrial outer membrane permeabilization) and release of apoptogenic factors, such as cytochrome c, apoptosis-inducing factor (AIF) and second mitochondria-derived activator of caspases (SMAC), from the mitochondrial intermembrane space into the cytosol [14]. The release of cytochrome c results in the formation of apoptosomes (cytochrome c + pro-caspase-9 + APAF-1). These complexes promote the activation of caspase-9, which in turn activates effector caspases that result in the execution of apoptosis, while AIF contributes to

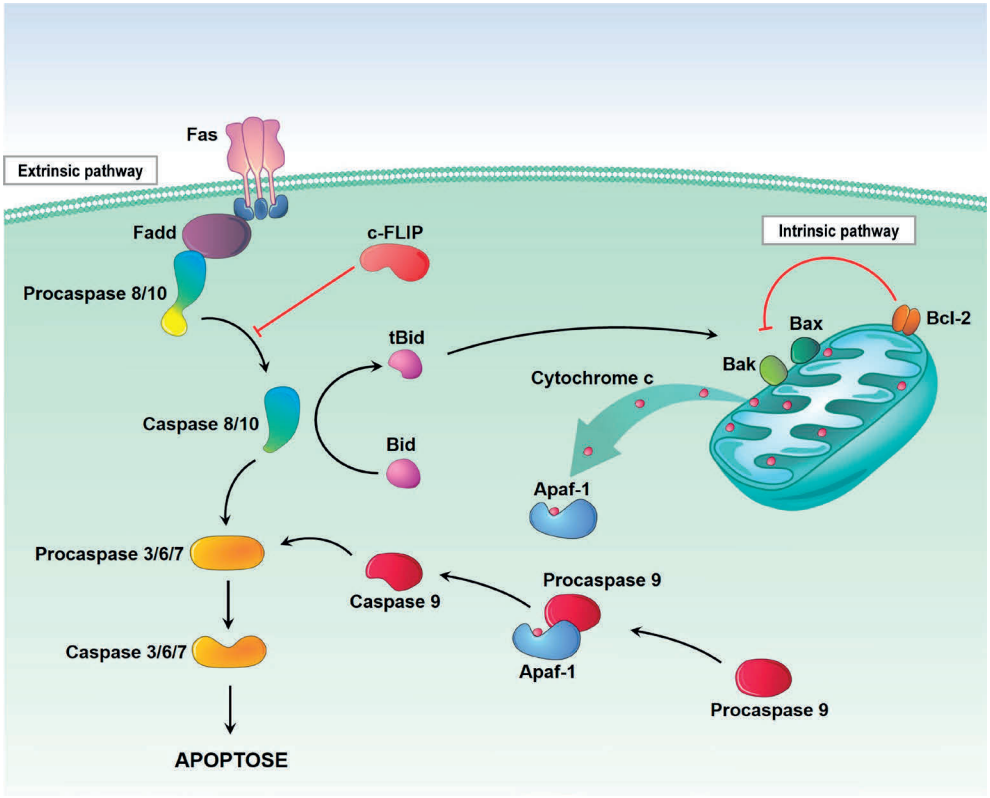

Figure 1. Pathways of apoptosis. Apoptosis can occur through two pathways: The extrinsic or the intrinsic pathway. The extrinsic pathway begins with the binding of extracellular ligands to death- promoting receptors, through the Fas-associated death domain adapter protein (FADD), then recruits procaspase-8, which in turn activates caspase-8. The intrinsic (or mitochondrial) pathway is regulated by a series of specific death-promoting molecules released from the mitochondria. Members of the pro- and antia-poptotic BCL-2 family compete on the surface of the mitochondria to control the release of cytochrome c. The released cytochrome c is associated with Apoptotic protease activating factor-1 (Apaf-1) and procaspase-9, which activate caspase-9. The two pathways share a common end point at the level of caspase-3 activation. The interaction between these pathways occurs through the Bid cleavage triggered by caspase-8. Bid's interaction with Bax or Bak in the outer mitochondrial membrane results in the release of cytochrome c. The antiapoptotic BCL-2 family can prevent such a release by direct interaction with Bax and/or Bak.

DNA fragmentation and subsequent chromosomal condensation. Next, SMAC binds to apoptosis inhibitor proteins (IAP), also promoting caspase activation [15].

The main regulators of the intrinsic pathway of apoptosis are the BCL-2 family of proteins that are classified into an antiapoptotic and proapoptotic category, which exist in a competitive flow state. The proportion in a cell can be altered due to the process of cellular stress, since, in harmful situations, BCL-2 of the proapoptotic type called pore-forming executioners are activated and trigger MOMP, which finally results in apoptosis [16].

2.1.2. Invasion/Metastasis

One of the characteristics of cancer is the ability of primary cancer cells to invade adjacent tissues and metastasize elsewhere in the body [17]. This process is complex and requires success in all its stages: from the exit of the primary tumor cells to their transition through the bloodstream, to the escape of the immune system and its stabilization and proliferation at the new location [17]. Studies that aim to understand this process in more detail can help to identify new therapeutic targets to reverse this process, which is the cause of a poor treatment prognosis and high death rates [17].

The expression of some molecules can be used as a metastasis marker. C-X-C chemokine receptor type 4 (CXCR4) is one of these markers of metastasis. Evidence shows that when its ligand, CXCL12, binds to the CXCR4 receptor, it triggers angiogenic properties [18,19]. The prognosis of cancer patients who have an overexpression of CXCR4 in cancer cells is poor, and these patients are at a high risk of recurrence [18].

The chemokine ligand 22 of the C-C motif (CCL22) is a member of the family of chemokines secreted by macrophages and tumor cells and binds to the chemokine [C-C motif] receptor 4 (CCR4) [20].

The interaction between CCL22 and the CCR4 receptor is related to cell proliferation and tumor progression. It is also responsible for attracting regulatory T cells (Treg) to tumor sites, leading to the suppression of antitumor immunity [20]. Based on this, CCL22 levels in serum can be used as a metastasis marker [20].

2.1.3. Inflammation

A wide variety of diseases, including cancer, are mediated by chronic inflammation, which contributes to the maintenance of the inflammatory tumor microenvironment (TME) and predisposes to tumorigenesis [21,22]. Chronic inflammation is characterized by sustained tissue damage and induces cell proliferation and repair. It is associated with all stages related to the formation and promotion process (increased proliferation/survival, activation of angiogenesis and metastasis) of cancer phenotypes [21,22].

Cancer-related inflammation is directly linked to genetic instability: activated leukocytes produce reactive oxygen species (ROS) and reactive nitrogen intermediates (RNI), and inflammatory cells produce cytokines and chemokines that can induce mutations and a neoplastic transformation [23]. In addition, DNA damage itself can also lead to inflammatory processes, such as the release of oncoproteins that can also activate signaling pathways related to this process, in a cycle that culminates in cancerous development [23].

Oxidative stress, a physiological state in which free radicals and ROS are present at high levels, plays an important role in the development of several diseases, including neurodegenerative, metabolic and inflammatory diseases. It has an impact on the initiation and progression of cancer and consequently on its therapy [24].

There are many biomarkers for the measurement of oxidative stress, including the production of lipid peroxidation malondialdehyde (MDA) and the antioxidant tripeptide glutathione (GSH), which can be used to identify different types of cancer. These biomarkers can verify the antioxidant status of patients and thus have great diagnostic and prognostic relevance in oncology, contributing to assessing the most appropriate treatment regime [25–27].

2. CANCER

2.2. Colorectal Cancer

Colorectal cancer (CRC) is one of the most common types of cancer: CRC takes third place in terms of incidence rate and second in terms of highest lethality rate [28]. Men are more affected by this disease than women. Risk factors that increase the prevalence of CRC include smoking, excessive alcohol intake, a sedentary lifestyle, a diet with large amounts of red and processed meat, obesity and having a family history of CRC (Figure 2) [29].

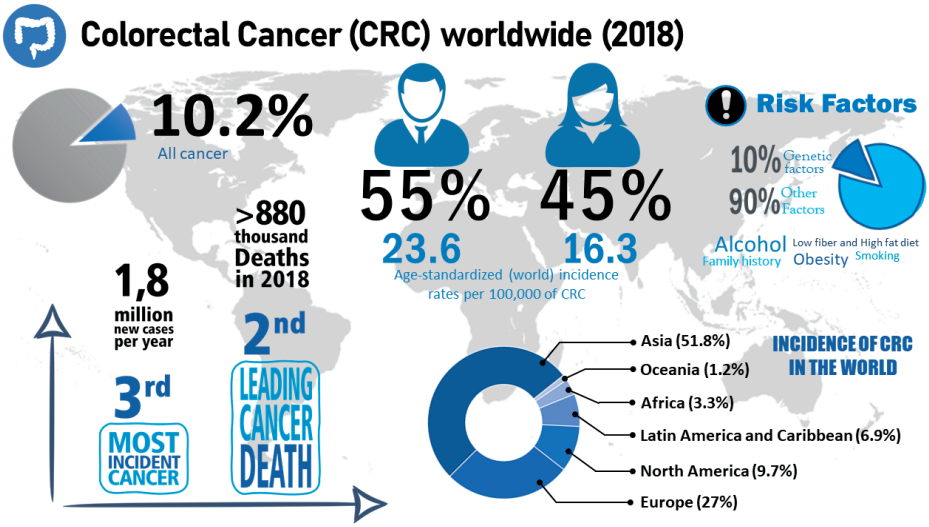

Figure 2. Characteristics of CRC. This figure presents data from CRC statistics [28], such as incidence, number of deaths and risk factors related to CRC.

CRC is a slow-developing disease, which is initiated by a single cell that has accumulated genetic and epigenetic mutations over time and, thereby, inactivated tumor suppressor genes and activated oncogenes [30,31]. The sequence of events that culminates in the appearance of the tumor is called carcinogenesis, a complex process that involves modification and mutation in genes that regulate cell growth [32]. Genome instability, named tumor initiation, is part of carcinogenesis, and it can progress to CRC in two ways. The traditional adenoma-carcinoma pathway, which takes place in 70–90% of CRCs, is initiated by a polyp that evolves to an early adenoma. On the other hand, the

serration neoplasia pathway takes place in 10–20% of CRCs and evolves from a hyperplastic polyp to a serrated polyp, ending in an adenocarcinoma [30,33].

In the colon, the epithelial renewal of the intestinal mucosa that occurs due to the loss of cells that remain on the tissue surface, and the controlled proliferation that occurs at the base of the crypt where the stem cells are located, are physiological processes. However, mutated cells can divide and reach the colonic lumen, forming discrete adenomas, which over time acquire more mutations and increase in size, developing dysplastic peculiarities that can acquire the capacity to invade other tissues. Thus, the vast majority of tumors in the colorectal region originate from precancerous polyps classified as traditional tubular adenomas, which arise when there is a dysregulation of DNA repair mechanisms, thus causing disordered cell proliferation [34–36].

The dysregulation of DNA repair mechanisms occurs due to alterations in genes that regulate cell growth. When mutated, the gene that encodes a tumor suppressor, adenomatous polyposis coli (APC), gives rise to traditional adenomas, while the oncogene BRAF, when mutated, gives rise to serrated polyps [34]. The APC mutation promotes the activation of the Wnt pathway, which leads to the chromosomal instability pathway (CIN), while BRAF mutations promote tumorigenesis through the serrated neoplasm pathway, which leads to microsatellite instability (MSI) [37]. Moreover, not all adenomas will progress to cancer, and carcinogenesis will depend on the accumulation of specific mutations. Furthermore, the time to reach the neoplastic stage will depend on the carcinogenic process and the individual's exposure to factors that influence progression, such as inflammatory processes. As an example, tumorigenesis via CIN can take 10 years or more, while tumor development via MSI can occur in a few years [38,39].

Despite having similar histopathological characteristics, different CRCs differ in clinical symptoms, response to treatment, molecular characteristics and prognosis [40]. Molecular factors have an influence on prognosis. Patients at a similar stage of the disease at the time of diagnosis may show different treatment responses and different evolutions of the disease due to heterogeneity in their molecular factors [41].

2.2.1. Treatment of Colorectal Cancer

In the past decades, chemotherapy treatment options have advanced from the use of single agents to regimens with a combined use of therapeutic agents. Additional, targeted agents that have improved treatment efficacy in metastatic disease are being used [33,42]. In addition to chemotherapeutic methods for the treatment of CRC, other therapies such as surgery, radiotherapy, targeted therapies, immunotherapy, radiofrequency ablation and palliative treatments are also available.

The choice of treatment depends on several factors, such as the location and tumor stage, which relates to tumor size, tumor growth/infiltration and the presence of locoregional and distant metastases, which are also related to the tumor microenvironment -affected genes, comorbidity and patient prognosis [43]. Thus, if CRC is diagnosed early, there is a greater chance of success in therapy, given that CRC is one of the most treatable cancers when it is discovered in the early stages [30,44].

CRC can be classified into different stages, according to the characteristics of the tumor and the involvement of the nearby lymph nodes, into the TNM classification of malignant tumors (Table 1). This classification is also used to choose the optimal treatment for the cancer patient [45].

In stage I, endoscopic examination of a pedunculated malignant polyp or surgical resection of the tumor and nearby lymph nodes is indicated. Thus, at the time of surgery, it is crucial to examine the number of lymph nodes for the correct staging of the CRC. Malignant polyps are T1 lesions where the cancerous cells have reached the muscle from the mucosa to the submucosa. They may appear benign through endoscopic analysis, but histology should be performed to check for the presence of malignant cells. After the histological analysis, it should be decided whether the endoscopic resection is sufficient or whether it is necessary to execute an

endoscopic resection of the mucosa, or other methods, such as endoscopic submucosal dissection or segmental colon resection (performed if the resection margin is less than 2 mm and there is involvement of blood vessels) [46–48].

In stage II, the surgical method is performed and the use of adjuvant chemotherapy is not indicated in most cases. According to the European Society of Medical Oncology (ESMO), the treatment using chemotherapy and adjuvants is indicated only when the following criteria are met: little tumor differentiation, vascular invasion, perineural invasion, intestinal obstruction, localized perforation and positive margins. Adjuvant chemotherapy lasts for 3–6 months on one of the following regimens shown in Table 1 [49,50]. In case of stage III, CRC treatment consists of a surgical procedure to remove the tumor, and afterwards adjuvant chemotherapy should be performed, which includes 3–6 months of FOLFOX or CAPOX. In stage IV, the CRC can be controlled by monotherapy or a combination of chemotherapy, targeted biological therapy, immunotherapy, palliative surgery, radiotherapy, and radiofrequency ablation or radio-embolization, as shown in Table 1 [51–53].

Stage of Cancer	Clinicopathological Characteristics
Stage 1	Primary tumor (T): Tis—carcinoma in situ; T1—tumor invades submucosa; T2—tumor invades muscularis propria; (N): N0—no regional lymph node metastasis; Distant metastasis (M): M0—no distant metastasis.
Stage 2	T: T3—tumor invades through muscularis propria into subserosal; T4—tumor directly invades other organs or structures, and/or perforates visceral peritoneum; N: N0—no regional lymph node metastasis; M: M0—no distant metastasis.
Stage 3	Any T; N: N1—metastasis in one to three regional lymph nodes; N2—metastasis in four or more regional lymph nodes; M: M0—no distant metastasis.
Stage 4	Any T; Any N; M: M1—distant metastasis.

Table 1. Most common treatment options based on the stage of colorectal cancer (excluding rectal cancer) using the TNM classification.

	Treatment Modalities	Chemotherapeutic Agents	Targeted Therapy (Combined with Chemo-therapy)
	Local or surgical resection of malignant polyp or surgical procedure of tumor and local lymph nodes.	Not applied	Not applied
	Surgical procedure without adjuvant chemotherapy. Adjuvant chemotherapy indicated in special cases, where high-risk characteristics are observed.	3–6 months of 5-flurouracil (FU) with leucovorin (LV), capecit-abine or combination of 5-FU with LV and oxaliplatin (FOLFOX) or capecitabine and oxaliplatin (CAPOX).	Not applied
	Surgery followed by adjuvant chemotherapy.	3–6 months of FOLFOX or CAPOX.	Not applied
	Radiotherapy, chemo-therapy, immunotherapy, targeted therapies, palliative surgery/stenting, radiofrequency ablation, radio-embolization.	FOLFOIRI, FOLFIRI (5-FU, LV and irinotecan), FOLFOX, CAPIRI (capecitabine and irinotecan), CAPOX, 5-FU with LV, irinotecan, capecitabine and trifluridine plus tipiracil (Lonsurf).	Bevaci-zumab; cetuximab/ panitu-mumab;

Oxaliplatin

Oxaliplatin (OXA) has been considered an important chemotherapeutic drug and one of the most effective for the treatment of CRC, often used in conjunction with 5-FU/leucovorin or capecitabine, called the FOLFOX or CAPOX regimen; it provides a better response rate and prolonged survival in both treatment metastases and as adjuvant therapy, being considered the gold standard for this condition [54–57]. It is believed that about 50% of patients with CRC benefit from treatment with OXA [58].

OXA is a third-generation platinum compound characterized by a diaminocyclohexane molecule. It was identified in 1976 and approved for cancer treatment only in 1996, thereby being the first platinum compound to demonstrate efficacy in the treatment of CRC [59]. OXA exerts its cytotoxic activity through direct damage to the tumor cell's DNA, through the formation of adducts, which induce the formation of DNA lesions, the interruption of DNA replication and transcription, as well as the triggering of immunological reactions that culminate in apoptosis and cell death [60,61].

As with other chemotherapeutic agents, it is known that the use of OXA is associated with certain limitations such as systemic toxicity and innate and acquired resistance, which are related to an increase in patients' morbidity and mortality [62]. This drug has a wide spectrum of adverse effects that affect the most diverse organs and can cause anemia and cytopenia; nausea, vomiting and diarrhea; mucositis and stomatitis; hearing loss; hepatic, cardiac and renal dysfunctions; neurosensory toxicity and neuropathies; as well as alopecia, anorexia and asthenia [46,47,63,64].

Resistance of tumor cells to OXA, which is one of the main reasons for treatment failure, can be caused by increased DNA repair mechanisms and increased expression of drug efflux pumps (Figure 3), as well as by genetic mutations in target pathways (such as folate, VEGF, EGF and microsatellite instability). However, these factors can

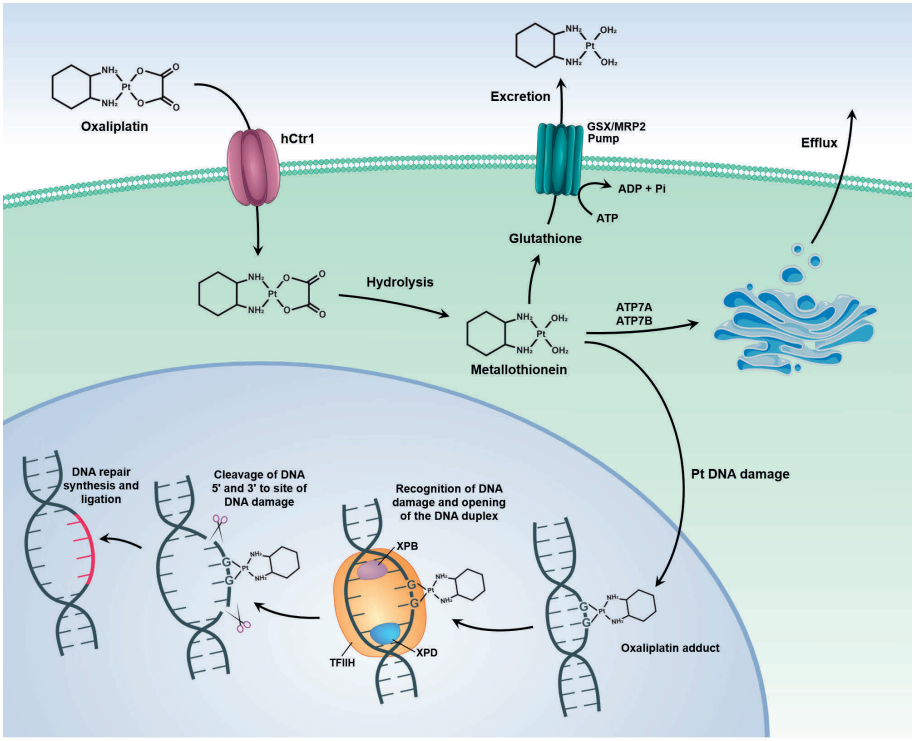

Figure 3. Tumor cell resistance mechanisms to OXA. The image shows the mechanisms of DNA repair and drug efflux.

be used as predictive markers for the response of the tumor cells to therapy [58].

Other Treatments

Radiotherapy, as well as other treatments, depends on the clinical stage of the tumor and the age of the patient. This treatment is mainly administered in patients with an advanced stage of cancer, i.e., III or IV or even nonmetastatic CRC with positive lymph nodes [48]. Several methods are used for this purpose, such as short-term radiation therapy, which has been a popular method applied in Europe for resectable rectal cancer and also in patients with locally invasive tumors [30,51].

In addition to the aforementioned treatments, palliative treatment emerges as a crucial component of standard cancer care for patients with stage IV disease, and, more recently, it has also been included in the treatment of earlier cancer stages. Palliative treatments include: combination of surgery, combined chemotherapy/targeted therapy, immunotherapy and radiotherapy regimens [52,53]. Palliative surgery is the most used for cases where patients have symptoms such as obstruction, perforation or bleeding [65]. Hence, palliative therapy for advanced CRC aims to prolong the patient's survival, providing greater quality of life and lower costs in health care [45,65].

Taken together, the choice of the approach used in the current treatments is based on the stage of evolution and progression of CRC, considering the occurrence of invasion and/or metastasis in a standardized way for all cancer patients. However, the incorporation of the use of nanoparticles (NPs) as a treatment in CRC could make the treatment more specific to the needs of each patient. The use of these NPs as a drug delivery system (DDS) may help to overcome the biological barriers that hinder conventional treatment [66,67].

3. BIOLOGICAL BARRIERS

Biological barriers are major difficulties to overcome in the use of nanosystems for the treatment of cancer patients. The unique interactions between NPs and the biological components of the body are intrinsic to each patient, making it difficult to systemically apply nanomedicine in cancer [68,69].

3.1. Reticuloendothelial System

One of the biological barriers to overcome is the mononuclear phagocyte system (MPS). This is one of the constituents of the immune system and is formed by phagocytic cells and macromolecules that can interact with NPs and trigger an immune response, which makes it difficult for nanocarriers to enter cells [70]. To escape the MPS, the physicochemical properties of the NP's surface are a key factor, which may increase their time in the blood. A good example are NPs coated with polyethylene glycol (PEG), which are able to escape the MPS, thus increasing the possibility of the drug reaching its site of action [71].

These physical and chemical properties also affect which components of the MPS will act on the NPs, as, for example, a hydrophobic surface of NPs allows them to be normally captured by the liver, spleen and later by the lungs. NPs with a hydrophilic surface have less absorption by the liver and spleen [72]. The size of the NPs is another characteristic that determines the recognition by the MPS, which has been researched. NPs bigger than 250 nm are removed by the MPS, opsonized and captured by macrophages [73]. Even if the modification of the surface reduces recognition by the MPS, complete evasion has not yet been achieved [71].

3.2. Renal System

Another difficulty when using NPs *in vivo* is the renal system, which filters the circulating blood, produces hormones and promotes homeostasis of the body [74]. When formulating NPs, the physicochemical properties must be taken into account so as not to affect the rate of renal clearance. Research has observed that a change in size, even if it is only by 2 nm (from 6 to 8 nm), can affect kidney clearance, because the smaller the size, the higher the clearance rate [71,75].

However, changing the size of NPs to prevent or decelerate renal clearance can affect the performance of NPs. One way to solve this problem would be the formulation of biodegradable nanosystems, which could be eliminated more easily by the kidneys. However, they can alter the delivery of the drug by altering the surface load [71,76]. Thus, before formulating the DDS, one must choose which are the main benefits that are necessary for their objective [71,76].

3.3. Blood-Brain Barrier

The blood-brain barrier (BBB) is a structure that protects the brain. As a consequence, blood vessels of the BBB only allow specific molecules to pass through, to allow nutrition of the central nervous system and to prevent the entry of harmful agents [77]. Normal BBB is formed by brain capillary endothelial cells and is organized as a barrier that surrounds brain capillaries. It has specific transporters that deliver essential biomolecules to the brain, while larger molecules cross the barrier through receptor-mediated transcytosis [77].

On the other hand, the BBB can be an obstacle for the systemic treatment of diseases, such as cancer, in the central nervous system. During progression, brain tumors alter the BBB, which then becomes the blood-tumor barrier (BTB), being quite heterogeneous and consisting of capillaries with the following characteristics: (i) continuous and without perforations (such as the vasculature of a healthy brain), (ii) continuous and having perforations (changes permeability) and (iii) noncontinuous (with interendothelial gaps). Even though it is more permeable to smaller and larger molecules, the BTB still possesses BBB characteristics, making it one of the biggest obstacles in the treatment of brain tumors and metastases [78,79].

Brain tumors or brain metastasis have high rates of tumor recurrence, even after initial surgical interventions and pharmacological treatments, since the delivery of pharmaceutical active agents to invasive cells behind the BBB is a challenge. To increase BBB permeability in cancer patients, current treatments consist of direct, intraventricular or intracerebral injections, infusion and even implantation. However, these therapies are toxic, can cause infections and can improperly release medications, which can lead to the accumulation of the drug in the ventricles, subarachnoid space, cerebrospinal fluid or blood [80,81].

NPs seem to be a good method to overcome the BBB, since the functionalization of their surface and their size can be changed [80]. Gold NPs (AuNPs) have been investigated for their advantages, such as stability, ability to interact with light, synthesis of different sizes, and functionalization with peptides, proteins and other biomolecules. Additionally, they can be visualized easily with computed tomography (CT), a noninvasive procedure for patients [82].

3.4. Pathophysiological Barriers in Cancer

Finally, pathophysiological barriers are another challenge for nanoformulations. The enhanced permeability and retention (ERP) effect, attributed to the deficiency of lymphatic vessels in the tumor, causes the intratumoral accumulation of NPs [76,83]. The tumor-associated

angiogenesis process leads to the formation of irregular vessels, with more gaps, promoting an increase in factors such as nitric oxide, VEGF, tumor necrosis factor (TNF) and bradykinin, making it difficult for NPs to enter and act. The proliferation of tumor cells leads to stress in the TME, causing compression of the vessels, making it difficult for NPs to penetrate the tumor tissue [76,84].

In addition to the physicochemical properties of NPs, already mentioned characteristics of the TME, such as the ERP effect and the pressure of tumor cells, are the factors that influence the entry of NPs into the tumor. Furthermore, the location of the tumor, the type of cancer, the stage of cancer and other factors intrinsic to each patient affect the penetration of NPs [85]. Therefore, measures must be taken to facilitate the penetration of NPs into tumors, such as previous treatments to reduce the pressure of the TME, as well as the inhibition of signaling by VEGF and TGFβ, thus minimizing the stress of the TME and increasing entry of the NPs into the tumor [76].

4. NANOPARTICLES AS DRUG DELIVERY SYSTEMS

Among nanomedicine projects, studies on NPs that are used for the purpose of drug delivery are one of the most widespread. NPs are complex molecules, composed of superficial layers, which can be functionalized with a variety of elements (such as ions and surfactants), cores (different chemical materials) and nuclei (central portion) [86]. Several methods can be used for their synthesis, which can be classified into either the destructive approaches starting from a larger molecule, called “top-down”, or the constructive ones, called “bottom-up”. They can also be characterized with different morphological, structural and optical techniques in order to thus obtain control of their reactivity, resistance and other properties [86].

The formulation of NPs, which can be used as DDSs, occurs through the association of active drugs with colloidal nanostructures of a size smaller than a micrometer and a large surface area in relation to their volume. The type of material used for these nanostructures can include organic (such as polymers, dendrimers, solid lipids, micelles and liposomes), inorganic (such as silica, gold, quantum dots, carbon NPs and nanotubes) and hybrid nanocarriers, which combine the advantages of both materials (Figure 4) [87].

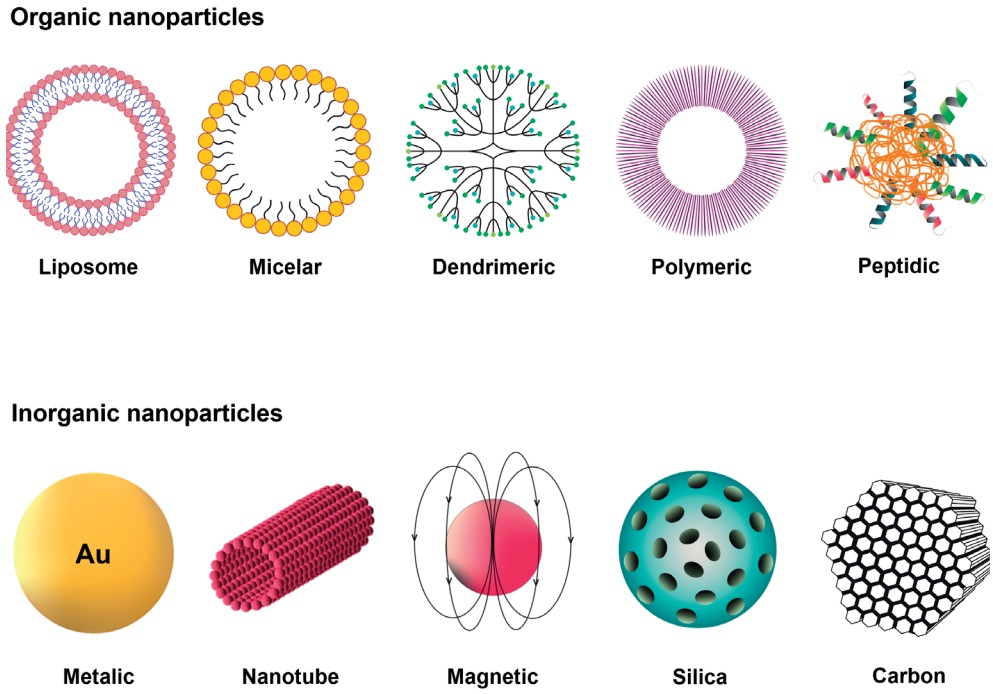

Figure 4. Different representations of the two large groups of NPs. These NPs are commonly used for biomedical applications and offer a significant potential as DDSs for cancer. They are divided into organic or inorganic, depending on the kind of material used for their composition.

Polymer-lipid hybrid NPs (PLHNPs) are an example of hybrid nanocarriers for cancer therapy; this nanosystem has a polymeric core where the drug is encapsulated, surrounded by a lipid layer. The combination of polymeric NPs and liposomes increases the biodistribution of the system, in addition to overcoming the limitations that each system would have alone [88–90]. Another example of a hybrid nanocarrier is mesoporous silica NPs (MSNs) covalently bonded with poly (oligo(ethylene glycol) monomethyl ether methacrylate) (POEGMA) and targeting peptide (RDG) to perform system stabilization and deliver the drug 5-fluorouracil (5-FU) in a targeted and effective manner. This hybrid nanocarrier has a better efficacy against CRC than the free drug, thus showing the importance of hybrid nanosystems and how they can be efficient in cancer therapy [91].

Among the organic NPs are the micelles, which are spherical macromolecules formed by a hydrophilic outer layer and a hydrophobic interior in an aqueous solution [92]. This type of nanocarrier is thermodynamically

stable as well as considered nontoxic and safe due to its composition of biocompatible material, being able to transport hydrophobic drugs, *in vivo*, inside or on the surface through a covalent connection with the carrier [92]. Its small diameter allows for the gradual administration of drugs and prevents their recognition by the immune system and their filtration by the spleen epithelial cells. In addition, the micelles can be modified in order to alter their functionalization, thus promoting the delivery of the drug and prolonging the therapeutic effect of the drug [92]. As an example of micellar nanoparticles, researchers recently formulated micellar NPs targeting small-sized trastuzumab by removing a surfactant that produced concentrated phthalocyanines with strong near-infrared absorption. In combating tumor lymph node metastases in CRC *in vitro* and *in vivo*, targeted micellar phthalocyanine (T-MP) showed promising results [93].

Liposomes are spherical lipid vesicles composed of a lipid outer layer and an aqueous interior, with variable sizes ranging from nm to μm [94,95]. They are biocompatible and stable colloidal macromolecules. Their structure, being very specific, allows for the fusion of membranes with the target cell. Liposomes can encapsulate hydrophobic drugs, promoting solubilization in water and prolonging the release of drugs that have a short half-life, which is of great importance for cancer therapy and other diseases [94,96]. Moreover, the functionalization of liposomes is advantageous: PEGylated liposomes have a longer half-life in the circulation, and various other ligands (such as proteins, carbohydrates and peptides) can also be used on the surface of the liposome in order to reach the tumor site [97]. A recent study formulated and characterized liposomes containing irinotecan (IRI) to treat CRC; this research achieved a reduction in prostaglandins in colonic tissue in addition to a reduction in tumors in mice, demonstrating promising results with these vesicles [98].

In addition to the abovementioned systems, the most-used system for delivering and targeting anticancer drugs are polymeric NPs. They are solid colloidal systems formed by the polymerization of monomers or polymers that surround the drug [99]. Their structure can vary in size and molecular weight depending on the method of preparation. This variation in structure can produce nanocapsules, where the drug is confined in an aqueous cavity and is surrounded by a single polymeric membrane or nanospheres, in which the drug is dispersed within the particles [100]. The

formulation of nanocapsules and nanospheres is complex. Nevertheless, these NPs have many advantages: they are biocompatible, stable, have a nontoxic nature and large-scale production is feasible [101].

Inorganic NPs are also widely studied as agents in antitumor therapy. Among them are AuNPs that have versatile physical and chemical properties, such as surface plasmon resonance (SPR), a large surface-to-volume ratio, fluorescence quenching and the ability to form stable chemical bonds with groups containing sulfur and nitrogen [102]. AuNPs are effective for medical imaging purposes and medication administration, due to their shape and diameter (1 to 150 nm) [103]. This nanosystem contains a large surface area that can be adjusted for drug loading, conjugation or binding of genetic material, thus enabling drug solubility, stability and more useful pharmacokinetic parameters [103,104]. Studies have shown that AuNPs reduce the population of tumor-associated fibroblasts and type I collagen production in CRC. In addition, AuNPs decrease vascular endothelial growth factor (VEGF) signals via the Akt signaling pathway, thereby reducing the pressure applied by the tumor and increasing vascular permeability (reviewed in [92]). A disadvantage of using these NPs must be noted: the possible toxicity, since recent research has shown that smaller AuNPs can accumulate in organs, such as the brain, kidney, liver, spleen and lung, and can be internalized by cells, promoting more cellular toxicity [105,106]. AuNP systems containing cetuximab (cetuximab-AuNPs) have shown promising results in *in vitro* studies against CRC. Cetuximab is a monoclonal antibody against the epidermal growth factor receptor (EGFR), and it has been widely investigated since EGFR is overexpressed in CRC and plays important roles in tumor survival. Thus, when blocked, EGFR would reduce damage caused by tumor cells. Results showed the cytotoxicity of cetuximab-AuNPs to cancer cells, with NPs mainly possessing a size of 60 nm. It was also possible to analyze the change in the expression of biomarkers on the surface of the cancer cell, where, after treatment with cetuximab-AuNPs, there was a greater expression of epithelial cell markers: epithelial cell adhesion molecule (EpCAM), melanoma cell adhesion molecule (MCAM) and human epidermal growth factor receptor-3 [107].

Silica NPs are studied for targeting drugs to tumors, as they are more advantageous than other inorganic NPs due to their ability to release drugs and their biodegradability [97]. Within the category of silica NPs, there are mesoporous silica NPs (MSNs) that are attractive due to their physicochemical properties: adjustment of the particle size (about 10 nm), adjustment of the pore size between 2 to 50 nm (according to the shape and size of the drug) and greater surface area linked to low cytotoxicity [97]. In addition, MSNs have a rich surface of silanol groups, which can be changed with molecules and functional groups such as polymers, metals, metal oxides and targeting binders, among others, for the final function of MSNs [97]. Anti-miR-155-loaded MSNs modified with polymerized dopamine (PDA) and AS1411 aptamer (MSNs-anti-miR-155@PDA-Apt) were used in a study to assess their therapeutic potential against CRC. miR-155 is expressed at high levels in the CRC TME, so the researchers studied miR-155 and its correlation with NF-kB. The results showed that there was a correlation between NF-kB and miR-155, and that NP MSNs-anti-miR-155@PDA-Apt were promising for the treatment of CRC [108]. The physicochemical properties of the material can also be adjusted by modifying its compositions, dimensions, shapes and surfaces, thereby creating more effective, biodegradable, biocompatible, targeted and responsive products [109]. Currently, a considerable number of potential drugs and those that are already in use would benefit from improvements in their pharmacokinetics and biopharmaceutical properties [110]. The NPs can carry drugs by various methods, such as encapsulation and surface fixation. They efficiently penetrate through barriers, such as cell membranes, and deliver the drug to the target site [111].

The use of DDSs is a strategy that has been developed and widely investigated to improve the transport of drugs to the site of action in target cells or tissues. More specifically, it is defined by the enhancement of bioavailability through nanoengineering, which improves the pharmacological and therapeutic properties of the DDSs [112]. DDSs have also become relevant with regard to the: (i) solubility of hydrophobic drugs; (ii) reduction of systemic toxicity, enzymatic degradation and side effects; (iii) creation of absorption and targeting mechanisms; (iv) increased specificity and efficiency; (v) continued release to maintain the therapeutic dose; and (vi) structure of various special applications such as ocular, neurological and anticancer therapy [113,114].

4. NANOPARTICLES AS DRUG DELIVERY SYSTEMS

Some characteristics are desirable for the design of biological NPs, such as: (i) chemical compatibility with physiological solutions; (ii) ease in designing and modifying; (iii) natural composition of material; and (iv) biocompatible, biodegradable and noncytotoxic nature [115]. When used as a strategy to fight cancer, the NPs used as DDS have an additional feature, besides advancing the bioavailability and solubility of drugs. Tumor cell-specific binding systems can be added to the surface of NPs, which protects healthy tissues, resulting in decreased cytotoxicity [67,116].

4.1. Poly-Lactic-Co-Glycolic Acid

The effectiveness of NPs, organic ones in particular (liposomes, micelles, polymers, dendrimers), is remarkable due to the biocompatibility and biodegradation of these systems [117]. Thus, polymers stand out in the delivery of drugs due to their formulation, stability, longer half-life and nontoxic nature [117]. Polymeric NPs consist of nanospheres or nanocapsules, and the preparation methods of such nanosystems vary depending on the drug to be encapsulated and the route of administration. However, there are two general methods of preparing polymeric NPs: the “top-down” and the “bottom-up” methods, and both methods used generate products that are obtained with aqueous colloidal suspensions. The steps of the technique that are used in the “top-down” method include: emulsion evaporation, emulsion diffusion, coacervation and nanoprecipitation. The “bottom-up” method steps include: emulsion polymerization, interfacial polymerization, interfacial polycondensation and molecular inclusion. Thus, both use organic solvents to dissolve the polymer. Therefore, the solvent must be removed in subsequent reactions to avoid compound toxicity [118,119].

Polymers are classified by their form of extraction, which can be natural or synthetic. Among the natural ones, the most studied are: chitosan, alginate, dextran, and polymers such as pullulan and hyaluronic acid (HA). Among the synthetic polymers, polylactic acid (PLA), poly-ε-caprolactone (PCL), PEG and poly-lactic-co-glycolic acid (PLGA) are the most frequently studied [120].

PLGA, also known as “smart polymer”, is a biodegradable synthetic

polymer that started to be used in the early 1970s in the composition of absorbable filaments of surgical articles [121]. Its application has been extended in the last decades, becoming one of the most successful DDSs due to its remarkable properties: its biocompatibility, sustained release, nontoxicity, nonimmunogenicity, easy adaptation of the polymer to various types of drugs and hydrolysis result in endogenous and easily metabolized compounds [122–124].

Regarding its physicochemical properties, PLGA is a linear aliphatic copolymer made of lactic acid and glycolic acid monomers in different proportions. PLGA is quite adaptable and can be processed in completely amorphous or highly crystalline forms, in almost any shape and size, being able to encapsulate the most diverse molecules (both hydrophobic and hydrophilic) [125,126]. In addition, PLGA is soluble in a wide range of common solvents, including chlorinated solvents, tetrahydrofuran and ethyl acetate [127]. All these and other characteristics can still be modulated by structural changes, which makes PLGA suitable for various biomedical devices and which promotes improvements in drug stability, degradation, release and targeting [125].

In the clinic, PLGA NPs have already been used as DDSs in various pathological conditions, such as different types of tumors [128–132], bone metastasis [133], tuberculosis [134], leishmaniasis [135,136], fungal infections [137], bacterial infections [138,139], atherosclerosis [140], inflammation [141,142], cystic fibrosis [143] and glaucoma [144]. An example of PLGA NPs investigated as therapy for CRC are the PLGA nanoparticles encapsulated in **α**-mangostine (Mang-NPs). These nanoparticles have demonstrated the ability to inhibit the viability of CRC cells, epithelial-mesenchymal transition, formation of colonies and to induce apoptosis. Mang-NPs were also able to inhibit the signaling of the Notch pathway by reducing the expression of Notch receptors (Notch1 and Notch2). Thus, polymer-based Mang-NP nanoparticles are potential therapeutic targets, demonstrating the potential of polymers in CRC therapy [145].

4.2. Properties of Nanocarriers

When formulating NPs, some characteristics need to be ideal in order to use them as a DDS, such as size, shape, solubility, surface charge and

targeting capacities. These characteristics must be controlled during the formulation process of the NPs and can be measured at the end [67].

4.2.1. Physicochemical Properties

With regard to size, two factors must be taken into account and balanced: (i) internalization by cells and (ii) clearance from the system of the organism *in vivo* [67]. The smaller the NPs, the greater the levels of cellular internalization. However, NPs smaller than 10 nm will be more easily eliminated by renal clearance. In addition, larger NPs (>200 nm) are eliminated from the bloodstream more quickly, by the complement system, and will accumulate in the liver and spleen [146].

In addition to the size, the shape of the NPs affects the surface-area-to-volume ratio, which changes the NPs' pharmacokinetic properties, cell internalization and toxicity. Thereby, the shape influences the effectiveness of the DDS [147,148]. The shape of NPs is crucial to determine the drug's destination *in vivo*, as the shape influences the permanence in the bloodstream, the uptake of the NPs by macrophages and the biodistribution [149]. Currently, most of the nanocarriers studied are spherical, but nonspherical nanocarriers are promising because they are hydrodynamic, spending more time circulating. The shape of the NPs interferes with biodistribution: aspheric nanocarriers accumulate less in the liver than spherical ones [149,150].

Another important feature is the surface chemistry, which determines the surface charge, hydrophobia and ligands, among others. This parameter plays a fundamental role in the interaction of the nanocarrier system with the biological microenvironment, as it influences colloidal behavior, interactions with plasma proteins and transmembrane permeability, thus being able to change the direction of the nanocarriers *in vivo* [151].

In the case of nanocarriers in cancer therapy, the surface charge is important. Cells in the human body have a predominantly negative charge on their surface (−40 to −80 mV). However, the surface of tumor cells is even more negatively charged, since the cell membrane contains more negative phospholipids, such as chorionic gonadotropin, anionic RNA residues and sialic acid. In contrast, the surfaces of normal cells in the human body have higher amounts of phospholipids with a neutral charge [152]. Nanosystems with high positive charges are nonspecific and can interact with the surface of blood vessels, being internalized by cells and eliminated from the blood circulation. Therefore, the surface charge must be analyzed in order not to interact with other cellular components in the circulation and thus be able to reach the TME [153,154].

Another important characteristic of NPs is their stability in solution, which is reflected by the absolute value of the zeta potential. Zeta potential values between 0 mV and ± 5 mV are not ideal, as they indicate the high instability of the NPs and consequently a rapid aggregation, whereas values greater than ± 30 mV are desirable and indicate the stability of the colloidal system [155]. Such a desirable zeta potential, which will ensure the stability of the system, can be acquired by modifying the surface of the particle through the addition of a coating. Various coatings can be used for this purpose, such as acrylate, bovine serum albumin (BSA), citrate, N-acetyl cysteine, polyacrylic acid (PAA), PEG and polyvinyl pyrrolidone (PVP) [155].

4.2.2. Solubility, Degradation and Clearance

The ability to solubilize a drug is one of the many advantages of nanomedicine. Many drugs used to treat cancer are insoluble in water and require the administration of aggressive solvents. As an example, the use of paclitaxel requires polyethoxylated castor oil, and, to avoid side effects of the solvent, corticosteroids and antihistamines are administered to patients [156,157]. Importantly, due to its benefits, Abraxane®, the albumin- based NP containing paclitaxel, has been approved by the FDA as a therapy against various types of cancer. It causes less neutropenia and has a lower risk of hypersensitivity reactions [158,159].

To be successful, NPs must also be formulated with the ability to escape from phagocytic cells and endolysosomes in order to reach the cytosol of tumor cells. In this way, different nanocarriers have been created to reach the site of action [160]. A good example is the coating of NPs with polymers containing amine groups (such as PLGA); these polymers are able to evade endosomes due to the "proton-sponge effect" [160]. Nanosystems that use the "proton-sponge effect" contain cations on their surface, which sequester protons through the proton pump, thereby increasing the amount of water molecules within the endosomes, leading to the swelling and subsequent rupture of the endosomal vesicle [160].

In addition to escaping degradation, nanocarriers must be formulated in order to avoid rapid clearance in the bloodstream. The main system that carries out the elimination of nanosystems is the MPS, also known as the reticuloendothelial system (RES), which is composed of the liver (Kupffer cells), spleen and bone marrow. This system retains and eliminates NPs [161].

Nanosystems without surface changes are quickly recognized by macrophages of the MPS. One way to avoid this phenomenon is to add nonionic polymers or surfactants to the surface of the system, which allows a longer circulation of NPs [162,163]. PEG is a polymer that has exceptional physical properties, such as water solubility, total biodegradability and a high degree of conformational entropy, being ideal on the surface of NPs to improve stability and prolong the circulation of the nanocarrier [162,164]. Thereby, PEG increases the systemic circulation time of the NPs [165].

4.2.3. Targeting

Nanomedicine has allowed an improvement in traditional therapies, which would normally be swiftly cleared from and are widely distributed throughout the body [166]. The use of targets, specific for tumor cells, through their addition on the surface of NPs, allows

the drug to be delivered to a specific tissue [167]. This targeted DDS increases the efficiency of the drug by accumulating in the target tissue and decreases the drug's side effects elsewhere in the body [166]. For the targeting of drugs, there are two basic strategies: passive or active targeting. Passive targeting is based on the physical and chemical properties of the NPs and their retention at the disease site, using blood irrigation and vessel permeability. Active targeting, on the other hand, depends on an interaction between a ligand on the surface of the NPs and exclusive receptors on the target cells, providing a better performance by increasing the uptake of the NPs and thereby the effectiveness of the drug [168]. There are several types of moieties, ranging from small organic compounds, such as trisodium citrate, to large polymers, such as polyethylene glycols. In addition, functional biomolecules, such as proteins, hyaluronic acid, folic acid (FA), carbohydrates/polysaccharides, lipids, antibodies and oligonucleotides, can be applied as targets (Figure 5) [169,170].

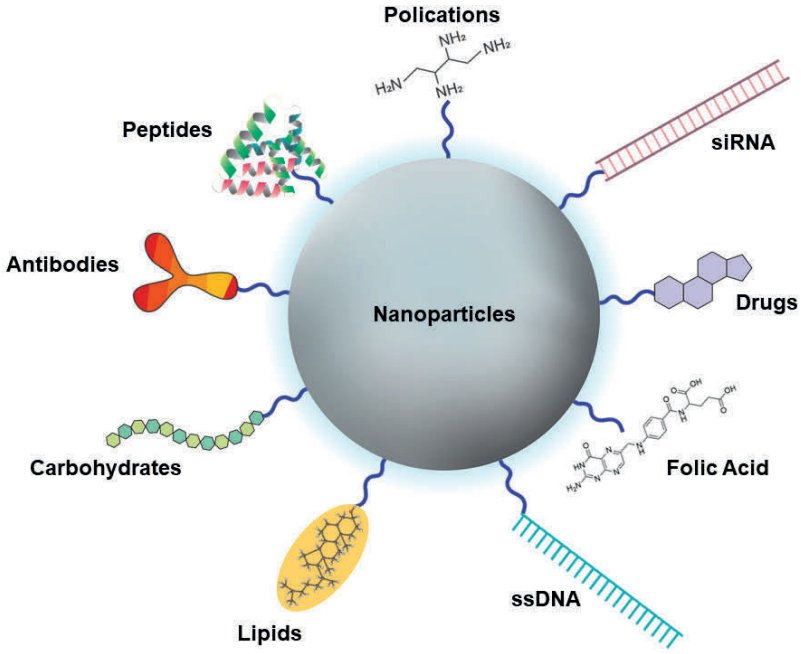

Figure 5. Delivery strategies for the active targeting of NPs. Graphical representation of surface modified NPs with targeting molecules (antibodies, peptides, lipids and carbohydrates) for the delivery of cancer drugs.

The use of antibodies on the surface of NPs to target tumor cells is a promising strategy for their specific high-affinity binding to target cells. An example is the use of cetuximab or matuzumab on the surface of liposomes for drug delivery in CRC [171]. This antibody binds to the EGFR, which is overexpressed in several types of cancer such as colorectal carcinoma. The antibody promotes the inhibition of EGFR signaling, thereby reducing a factor that is responsible for tumor development and progression [172,173].

Carbohydrates, such as galactose, are a category that is widely used to target NPs. This molecule binds to the asialoglycoprotein (ASGP) receptor, found in abundance in liver tumor cells [174]. Research carried out shows that the galactose-lithocholic acid-PEG-lacto-bionic acid nanosystem that carries doxorubicin (DOX) increases the internalization of NPs by human liver cancer cells (SK-HEP-1), promoting the death of tumor cells and reducing tumor growth when compared to untargeted NPs [175].

Another molecule that has been widely studied for its characteristics in directing the delivery of NPs is HA, a natural polysaccharide present in the human body which constitutes the extracellular matrix and is biodegradable, chemically modifiable and hydrophilic drawing attention in the field of nanomedicine [176,177]. In addition, its CD44 receptor is overexpressed on the surface of the tumor cells of many types of cancer, and its interaction with the ligand is related to tumor progression, infiltration and metastasis [178]. Thus, formulations of NPs containing HA have been of major interest for cancer therapy. As an example, micelles formulated with HA-PLGA containing DOX demonstrated an increased uptake and greater cytotoxicity for human colon cancer cells when compared to a system without HA [179].

One of the most used biomolecules as a target in NPs is cholesterol (CHOL), an indispensable structural component of cell membranes. CHOL has attracted attention in recent years for providing structural

and functional improvements in DDSs with regard to their size, drug load, encapsulation efficiency, hydrophobicity, biocompatibility and biodegradability [180].

It is also important to highlight the role of CHOL in tumor cells, since tumor cells require more nutrients due to their high rate of proliferation [181]. Consequently, more CHOL is needed for the formation of new cell membranes and to maintain tumor progression. Therefore, conjugation with CHOL selectively targets the NPs for tumor cells and allows for an increased drug concentration with a desired therapeutic effect inside the cell [181]. This active targeting will facilitate the capture of NPs in cancer cells via endocytosis [182]. Since tumor cells, compared to normal cells, require higher amounts of CHOL due to their high metabolism, this will increase the internalization of CHOL and, consequently, the internalization of the NPs as well as the drug they carry [181,182].

An alternative to improve targeting and to reduce side effects are FA ligands, which recently gained popularity. FA is known for its high affinity to folate receptors, which are often overexpressed in tumor cells, thereby promoting the selective uptake of NPs. In addition, FA is an important vitamin for DNA biosynthesis and is widely consumed by proliferating cells [183,184]. Folate receptors are overexpressed in, for example, colorectal, lung, breast, ovarian and endometrium cancers [183]. The properties of FA, such as stability, nonimmunogenicity, simple conjugation chemistry and rapid internalization, are advantageous over other ligands. In addition, this vitamin improves cytotoxic and apoptotic activity. Therefore, FA has the potential to be used in many types of cancer treatments [185–187].

4.3. Application of Nanoparticles As Drug Delivery Systems for Cancer Treatment

Current cancer treatment approaches face challenges regarding disease control and patient survival, which result from a failure to control metastasis, promotion of systemic toxicity, adverse effects and drug resistance, and subsequent death [188–190]. The characteristics of the tumor, such as the fact that the molecular environment of

solid tumors is unstable due to the accumulation of several genetic mutations over successive cell cycles, also contribute to treatment failure [191]. The genetic variability of the tumor depends on the tumor type, the tumor growth site, the intrinsic characteristics of each patient and the occurrence of metastases, among others [192,193]. Due to this variability, the success rate related to the treatment of solid-tumor cancers is still minimal. Therapeutic failures of medications are often connected to difficulties regarding an efficient direction to the tumor sites, i.e., targeting, and their ability to penetrate physical barriers. The immunosuppressive TME is also a barrier to the chemical recognition of drug molecules and promotes genetic changes in cancer cells, leading to drug tolerance [194,195].

Characteristics that are intrinsic to solid tumors make it difficult to achieve therapeutic efficacy. These characteristics are: the histo-pathological structure, the insufficiency of specific antigens and an immunosuppressive microenvironment. The stroma of solid tumors develops a physical barrier that inhibits and regulates the movement of fluids, gases and cells, and which is also able to limit the influx of drug molecules [196]. The tumor stroma, in addition to acting as a structural support for the development of the tumor, also contributes to new genetic and molecular changes [196]. Moreover, the tumor's immuno-suppressive microenvironment is a barrier to the action of chemother-apeutics, promoting genetic changes in cancer cells that lead to drug tolerance [197]. These factors make it difficult for the drugs to penetrate the tumor mass, thereby promoting a delay in the patient's clinical responses and even disease progression [198].

In order to improve antitumor therapy, several studies based on targeted or personalized therapies and even immunotherapy trials are being developed [195]. These studies resulted in the identification of molecules expressed by tumor cells as well as released growth factors, proteins, chemokines and cytokines that were associated with tumors, in order to develop individualized treatment [195,199,200].

Targeted or personalized therapy can be achieved through the use of DDSs when chemotherapy is incorporated into NPs and specific targeting molecules are added to the surface. As a consequence, the targeting of the therapeutic compound to the specific tumor site can promote therapeutic efficacy and reduce adverse effects. Adverse effects would be caused by chemotherapy alone, due to a lack of specificity and selectivity for the tumor sites during systemic administration [199,200]. In addition, DDSs have a longer circulation time due to their favorable pharmacokinetics, which delay elimination and/or excretion. Prolonged circulation results from the nanometric size of the DDSs as well as their composition containing tumor site-specific targeting moieties [201,202].

The TME strongly promotes angiogenesis, which leads to leaky spacings in the endothelial vessels and, consequently, a high vascular permeability. The space between tumor vascular cells depends on the type of tumor, ranging from 100 nm to 800 nm, which allows molecules within this size range to reach the tumor tissue [160]. In tumor blood vessels, there is also a significant absence of pericyte cells, which are important for the stabilization and support of blood vessels as well as smooth muscle cell layers. These structural changes cause a high vascular pressure, with a larger influx of molecules [160]. In addition, these factors, which are associated with the reduction of lymphatic drainage in tumors, ensure that the nanometric agents preferentially reach the tumor site and, due to their size, accumulate in this tissue [203–205]. This process is known as the EPR effect. Therefore, the size of the DDSs, their prolonged circulation and the characteristics of the tumor vessels allow for the majority of the nanometric agents to accumulate in the tumor tissue and release their therapeutic content in a target-specific manner, thereby avoiding side effects [206].

The search for better treatments has led to NPs being used as DDSs and diagnostic tools as well as for the molecular imaging of gene delivery approaches [207]. Several formulations have already been approved for use in the clinic by the US Food and Drug Administration (FDA) or the European Medicines Agency (EMA). Once approved, NPs have proven their safety and efficacy in humans and, if commercialized, are likely to meet standards of good manufacturing practice [207]. The first approved formulation was Doxil®, a liposome used to deliver

DOX, and the most recently approved NP is Apealea®, a micelle system used to deliver Paclitaxel (PTX) [207]. For Doxil®, these approvals by the FDA and EMA took place in 1995 and 1996, respectively, and Apealea® was approved by the EMA in 2018 [158,207]. Approvals were granted for several types of systems, such as liposomes, polymeric micelles, albumin or inorganic NPs [207]. The design characteristics of these already approved nanomedicines are similar, such as the inclusion of PEGylated or non-PEGylated structures, encapsulating a single drug [207].

Some of these formulations are already available for use in the clinic, while others are in Phase II/III clinical trials; most of these are used for intravenous administration, but some have been developed for intratumoral administration [207]. Among these, several nanomedicines are being tested in solid cancers and CRC. A cyclodextrin-based NP-camptothecin conjugate is currently in clinical trials for the treatment of CRC. This conjugate NP will be used for theranostics via intravenous administration but has not yet been clinically approved [207].
Taken together, nanosystems need to meet several of the above-mentioned properties at the same time to be suitable as efficient DDSs.

5. CONCLUSIONS

Novel theranostic tools provided by cutting-edge nanotechnology could be helpful in overcoming the challenge faced in the treatment of patients with cancer. This review presents an overview of state-of-the-art nanomedicine-based cancer therapies, with special attention paid to CRC. This review does not only explore alternatives for the treatment of tumors by means of NPs but also highlights several strategies to hurdle these biological barriers which prevent effective treatment.

The biological barriers discussed in this review include the reticuloendothelial system, the renal system, the blood-brain barrier and several other pathophysiological barriers in cancer. Once these barriers are overcome, nanoformulations benefit from the ERP effect of the TME, which results in

intratumoral accumulation and treatment.

Nevertheless, factors such as the location of the tumor, tumor characteristics and the TME are different for each patient and affect the penetration of the DDS. Therefore, future nanotechnologies for drug delivery need to be tailored to tumor biology, which will significantly increase the efficacy of the treatment and, at the same time, reduce the side effects of anticancer drugs that arise from systemic administration. Therefore, the application of novel nanotechnologies increases the quality of life of patients and their life expectancy in general.

REFERENCES

1. Fornaguera, C.; García-Celma, M.J. Personalized Nanomedicine: A Revolution at the Nanoscale. J. Pers. Med. 2017, 7, 12. [CrossRef] [PubMed]
2. Pautler, M.; Brenner, S. Nanomedicine: Promises and challenges for the future of public health. Int. J. Nanomed. 2010, 5, 803–809. [CrossRef]
3. Ventola, C.L. The nanomedicine revolution: Part 1: Emerging concepts. Pharm. Ther. 2012, 37, 512–525.
4. Kim, B.Y.S.; Rutka, J.T.; Chan, W.C.W. Nanomedicine. N. Engl. J. Med. 2010, 363, 2434–2443. [CrossRef] [PubMed]
5. Duncan, R.; Gaspar, R. Nanomedicine(s) under the Microscope. Mol. Pharm. 2011, 8, 2101–2141. [CrossRef]
6. Sharma, R.; Mody, N.; Agrawal, U.; Vyas, S.P. Theranostic Nanomedicine; A Next Generation Platform for Cancer Diagnosis and Therapy. Mini Rev. Med. Chem. 2017, 17, 1746–1757. [CrossRef]
7. Siddhardha, B.; Parasuraman, P. Chapter 3-Theranostics application of nanomedicine in cancer detection and treatment. In Nanomaterials for Drug Delivery and Therapy; Grumezescu, A.M., Ed.; William Andrew Publishing: Norwich, NY, USA, 2019; pp. 59–89.
8. Soares, S.; Sousa, J.; Pais, A.; Vitorino, C. Nanomedicine: Principles, Properties, and Regulatory Issues. Front. Chem. 2018,6, 360. [CrossRef]
9. Hanahan, D.; Weinberg, R.A. The Hallmarks of Cancer. Cell 2000, 100, 57–70. [CrossRef]
10. Nenclares, P.; Harrington, K.J. The biology of cancer. Medicine 2020, 48, 67–72. [CrossRef]
11. Bashyam, M.D.; Animireddy, S.; Bala, P.; Naz, A.; George, S.A. The Yin and Yang of cancer genes. Gene 2019, 704, 121–133. [CrossRef]
12. Fernald, K.; Kurokawa, M. Evading apoptosis in cancer. Trends Cell Biol. 2013, 23, 620–633. [CrossRef]
13. Fulda, S. Evasion of apoptosis as a cellular stress response in cancer. Int. J. Cell Biol. 2010, 2010, 370835. [CrossRef]
14. Bai, L.; Wang, S. Targeting Apoptosis Pathways for New Cancer Therapeutics. Annu. Rev. Med. 2014, 65, 139–155. [CrossRef]
15. Bratton, S.B.; Salvesen, G.S. Regulation of the Apaf-1-caspase-9 apoptosome. J. Cell Sci. 2010, 123, 3209–3214. [CrossRef]
16. Warren, C.F.A.; Wong-Brown, M.W.; Bowden, N.A. BCL-2 family isoforms in apoptosis and cancer. Cell Death Dis. 2019,10, 177. [CrossRef]
17. Fares, J.; Fares, M.Y.; Khachfe, H.H.; Salhab, H.A.; Fares, Y. Molecular principles of metastasis: A hallmark of cancer revisited.Signal Transduct. Target. Ther. 2020, 5, 28. [CrossRef] [PubMed]
18. Silinsky, J.; Grimes, C.; Driscoll, T.; Green, H.; Cordova, J.; Davis, N.K.; Li, L.; Margolin, D.A. CD 133+ and CXCR4+ colon cancer cells as a marker for lymph node metastasis. J. Surg. Res. 2013, 185, 113–118. [CrossRef] [PubMed]
19. Xu, C.; Zheng, L.; Li, D.; Chen, G.; Gu, J.; Chen, J.; Yao, Q. CXCR4 overexpression is correlated with poor prognosis in colorectal cancer. Life Sci. 2018, 208, 333–340. [CrossRef] [PubMed]
20. Wei, Y.; Wang, T.; Song, H.; Tian, L.; Lyu, G.; Zhao, L.; Xue, Y. C-C motif chemokine 22 ligand (CCL22) concentrations in sera of gastric cancer patients are related to peritoneal metastasis and predict recurrence within one year after radical gastrectomy.J. Surg. Res. 2017, 211, 266–278. [CrossRef] [PubMed]
21. Figueiredo, C.R.L.V. The unusual paradox of cancer-associated inflammation: An update. J. Bras. Patol. Med. Lab. 2019, 55, 321–332. [CrossRef]

22. Singh, N.; Baby, D.; Rajguru, J.P.; Patil, P.B.; Thakkannavar, S.S.; Pujari, V.B. Inflammation and cancer. Ann. Afr. Med. 2019, 18, 121–126. [CrossRef]
23. Korniluk, A.; Koper, O.; Kemona, H.; Dymicka-Piekarska, V. From inflammation to cancer. Ir. J. Med. Sci. 2017, 186, 57–62. [CrossRef] [PubMed]
24. Saha, S.K.; Lee, S.B.; Won, J.; Choi, H.Y.; Kim, K.; Yang, G.-M.; Dayem, A.A.; Cho, S.-G. Correlation between Oxidative Stress, Nutrition, and Cancer Initiation. Int. J. Mol. Sci. 2017, 18, 1544. [CrossRef] [PubMed]
25. Didžiapetriene˙, J.; Kazbariene˙, B.; Tikuišis, R.; Dulskas, A.; Dabkevic˘iene˙, D.; Lukosevic˘iene˙, V.; Kontrimavic˘iu¯te˙, E.; Sužiede˙lis, K.; Ostapenko, V. Oxidant/Antioxidant Status of Breast Cancer Patients in Pre- and Post-Operative Periods. Medicina 2020, 56, 70. [CrossRef]
26. Zalewska-Ziob, M.; Adamek, B.; Kasperczyk, J.; Romuk, E.; Hudziec, E.; Chwalin´ska, E.; Dobija-Kubica, K.; Rogozin´ski, P.; Brulin´ski, K. Activity of Antioxidant Enzymes in the Tumor and Adjacent Noncancerous Tissues of Non-Small-Cell Lung Cancer. Oxidative Med. Cell. Longev. 2019, 2019, 2901840. [CrossRef] [PubMed]
27. Oh, B.; Figtree, G.; Costa, D.; Eade, T.; Hruby, G.; Lim, S.; Elfiky, A.; Martine, N.; Rosenthal, D.; Clarke, S.; et al. Oxidative stress in prostate cancer patients: A systematic review of case control studies. Prostate Int. 2016, 4, 71–87. [CrossRef] [PubMed]
28. Bray, F.; Ferlay, J.; Soerjomataram, I.; Siegel, R.L.; Torre, L.A.; Jemal, A. Global cancer statistics 2018: GLOBOCAN estimates of incidence and mortality worldwide for 36 cancers in 185 countries. CA A Cancer J. Clin. 2018, 68, 394–424. [CrossRef] [PubMed]
29. Brenner, H.; Chen, C. The colorectal cancer epidemic: Challenges and opportunities for primary, secondary and tertiary prevention. Br. J. Cancer 2018, 119, 785–792. [CrossRef]
30. Dekker, E.; Tanis, P.J.; Vleugels, J.L.A.; Kasi, P.M.; Wallace, M.B. Colorectal cancer. Lancet 2019, 394, 1467–1480. [CrossRef]
31. Mahasneh, A.; Al-Shaheri, F.; Jamal, E. Molecular biomarkers for an early diagnosis, effective treatment and prognosis of colorectal cancer: Current updates. Exp. Mol. Pathol. 2017, 102, 475–483. [CrossRef]
32. Klaunig, J.E. Chapter 8-Carcinogenesis. In An Introduction to Interdisciplinary Toxicology; Pope, C.N., Liu, J., Eds.; Academic Press: Cambridge, MA, USA, 2020; pp. 97–110.
33. Kuipers, E.J.; Grady, W.M.; Lieberman, D.; Seufferlein, T.; Sung, J.J.; Boelens, P.G.; van de Velde, C.J.H.; Watanabe, T. Colorectal cancer. Nat. Rev. Dis. Primers 2015, 1, 15065. [CrossRef] [PubMed]
34. Nguyen, L.H.; Goel, A.; Chung, D.C. Pathways of Colorectal Carcinogenesis. Gastroenter ology 2020, 158, 291–302.[CrossRef] [PubMed]
35. Mizutani, S.; Yamada, T.; Yachida, S. Significance of the gut microbiome in multistep colorectal carcinogenesis. Cancer Sci. 2020,111, 766–773. [CrossRef]
36. Loke, Y.L.; Chew, M.T.; Ngeow, Y.F.; Lim, W.W.D.; Peh, S.C. Colon Carcinogenesis: The Interplay between Diet and Gut Microbiota.Front. Cell Infect. Microbiol. 2020, 10, 603086. [CrossRef]
37. Cheng, X.; Xu, X.; Chen, D.; Zhao, F.; Wang, W. Therapeutic potential of targeting the Wnt/β-catenin signaling pathway in colorectal cancer. Biomed. Pharmacother. 2019, 110, 473–481. [CrossRef] [PubMed]
38. Abu-Ghazaleh, N.; Chua, W.J.; Gopalan, V. Intestinal microbiota and its association with colon cancer and red/processed meat consumption. J. Gastroenterol. Hepatol. 2021, 36, 75–88. [CrossRef] [PubMed]
39. Harada, S.; Morlote, D. Molecular Pathology of Colorectal Cancer. Adv. Anat. Pathol. 2020, 27, 20–26. [CrossRef]

40. Rodriguez-Salas, N.; Dominguez, G.; Barderas, R.; Mendiola, M.; García-Albéniz, X.; Maurel, J.; Batlle, J.F. Clinical relevance of colorectal cancer molecular subtypes. Crit. Rev. Oncol. Hematol. 2017, 109, 9–19. [CrossRef]
41. Nguyen, H.T.; Duong, H.Q. The molecular characteristics of colorectal cancer: Implications for diagnosis and therapy (Review).Oncol. Lett. 2018, 16, 9–18. [CrossRef]
42. Stintzing, S. Management of colorectal cancer. F1000Prime Rep. 2014, 6, 108. [CrossRef]
43. Marley, A.R.; Nan, H. Epidemiology of colorectal cancer. Int. J. Mol. Epidemiol. Genet. 2016, 7, 105–114.
44. Mauri, G.; Sartore-Bianchi, A.; Russo, A.-G.; Marsoni, S.; Bardelli, A.; Siena, S. Early-onset colorectal cancer in young individuals. Mol. Oncol. 2019, 13, 109–131. [CrossRef]
45. Ahmed, M. Colon Cancer: A Clinician's Perspective in 2019. Gastroenterol. Res. 2020, 13, 1–10. [CrossRef]
46. Grigorian, A.; O'Brien, C.B. Hepatotoxicity Secondary to Chemotherapy. J. Clin. Transl. Hepatol. 2014, 2, 95–102. [CrossRef] [PubMed]
47. Oun, R.; Moussa, Y.E.; Wheate, N.J. The side effects of platinum-based chemotherapy drugs: A review for chemists. Dalton Trans.2018, 47, 6645–6653. [CrossRef] [PubMed]
48. National Guideline Alliance part of the Royal College of Obstetricians and Gynaecologists. Preop erative Radiotherapy and Chemoradiotherapy for Rectal Cancer: Colorectal Cancer (Update): Evidence Review C2; National Institute for Health and Care Excellence (UK) Copyright © NICE 2020: London, UK, 2020.
49. Petrelli, F.; Rulli, E.; Labianca, R.; Lonardi, S.; Rosati, G.; Dotti, K.; Ronzoni, M.; Pella, N.; Pusceddu, V.; Banzi, M.; et al. Overall survival with 3 or 6 months of adjuvant chemotherapy in Italian TOSCA phase 3 randomised trial. Ann. Oncol. Off. J. Eur. Soc. Med. Oncol. 2021, 32, 66–76. [CrossRef] [PubMed]
50. André, T.; Meyerhardt, J.; Iveson, T.; Sobrero, A.; Yoshino, T.; Souglakos, I.; Grothey, A.; Niedzwiecki, D.; Saunders, M.; Labianca,R.; et al. Effect of duration of adjuvant chemotherapy for patients with stage III colon cancer (IDEA collaboration): Final results from a prospective, pooled analysis of six randomised, phase 3 trials. Lancet Oncol. 2020, 21, 1620–1629. [CrossRef]
51. Myint, A.S.; Gérard, J.P. Role of radiotherapy in the treatment of rectal cancer in older patients. Eur. J. Surg. Oncol. J. Eur. Soc. Surg. Oncol. Br. Assoc. Surg. Oncol. 2020, 46, 349–357. [CrossRef]
52. Röhrl, K.; Guren, M.G.; Småstuen, M.C.; Rustøen, T. Symptoms during chemotherapy in colorectal cancer patients. Supportive Care Cancer Off. J. Multinatl. Assoc. Supportive Care Cancer 2019, 27, 3007–3017. [CrossRef]
53. Odgaard, M.; Lohse, N.; Petersen, A.J.; Bæksgaard, L. Oncological treatment and outcome of colorectal cancer in Greenland. Int. J. Circumpolar Health 2018, 77, 1546069. [CrossRef]
54. Gustavsson, B.; Carlsson, G.; Machover, D.; Petrelli, N.; Roth, A.; Schmoll, H.J.; Tveit, K.M.; Gibson, F. A review of the evolution of systemic chemotherapy in the management of colorectal cancer. Clin. Colorectal Cancer 2015, 14, 1–10. [CrossRef]
55. André, T.; Boni, C.; Mounedji-Boudiaf, L.; Navarro, M.; Tabernero, J.; Hickish, T.; Topham, C.; Zaninelli, M.; Clingan, P.; Bridgewater, J.; et al. Oxaliplatin, Fluorouracil, and Leucovorin as Adjuvant Treatment for Colon Cancer. N. Engl. J. Med. 2004, 350, 2343–2351. [CrossRef] [PubMed]
56. Comella, P.; Casaretti, R.; Sandomenico, C.; Avallone, A.; Franco, L. Role of oxaliplatin in the treatment of colorectal cancer.Clin. Risk Manag. 2009, 5, 229–238. [CrossRef] [PubMed]
57. Pectasides, D.; Karavasilis, V.; Papaxoinis, G.; Gourgioti, G.; Makatsoris, T.; Raptou, G.; Vrettou, E.; Sgouros, J.; Samantas, E.; Basdanis, G.; et al. Randomized phase III clinical trial comparing the combination of capecitabine and oxaliplatin (CAPOX) with the combination of 5-fluorouracil,

leucovorin and oxaliplatin (modified FOLFOX6) as adjuvant therapy in patients with operated high-risk stage II or stage III colorectal cancer. BMC Cancer 2015, 15, 384. [CrossRef]
58. Bahrami, A.; Amerizadeh, F.; Hassanian, S.M.; ShahidSales, S.; Khazaei, M.; Maftouh, M.; Ghayour-Mobarhan, M.; Ferns, G.A.; Avan, A. Genetic variants as potential predictive biomarkers in advanced colorectal cancer patients treated with oxaliplatin-based chemotherapy. J. Cell. Physiol. 2018, 233, 2193–2201. [CrossRef]
59. Ashrafizadeh, M.; Zarrabi, A.; Hushmandi, K.; Hashemi, F.; Hashemi, F.; Samarghandian, S.; Najafi, M. MicroRNAs in cancer therapy: Their involvement in oxaliplatin sensitivity/resistance of cancer cells with a focus on colorectal cancer. Life Sci. 2020, 256, 117973. [CrossRef] [PubMed]
60. Alcindor, T.; Beauger, N. Oxaliplatin: A review in the era of molecularly targeted therapy. Curr. Oncol. 2011, 18, 18–25.[CrossRef] [PubMed]
61. Seetharam, R.; Sood, A.; Goel, S. Oxaliplatin: Pre-clinical perspectives on the mechanisms of action, response and resistance.Ecancermedicalscience 2009, 3, 153. [CrossRef]
62. Braun, M.S.; Seymour, M.T. Balancing the efficacy and toxicity of chemotherapy in colorectal cancer. Ther. Adv. Med. Oncol. 2011,3, 43–52. [CrossRef]
63. Gaurav, S.; Durgadas, A.; Rajshree, K.; Ravindra, K.R. Oxaliplatin for Colorectal Cancer Therapy: A Review. Clin. Cancer Drugs2018, 5, 13–27. [CrossRef]
64. Weickhardt, A.; Wells, K.; Messersmith, W. Oxaliplatin-induced neuropathy in colorectal cancer. J. Oncol. 2011, 2011, 201593. [CrossRef] [PubMed]
65. Osagiede, O.; Spaulding, A.C.; Frank, R.D.; Merchea, A.; Uitti, R.; Ailawadhi, S.; Kelley, S.; Coliba seanu, D. Predictors of palliative treatment in stage IV colorectal cancer. Am. J. Surg. 2019, 218, 514–520. [CrossRef] [PubMed]
66. Blanco, E.; Shen, H.; Ferrari, M. Principles of nanoparticle design for overcoming biological barriers to drug delivery.Nat. Biotechnol. 2015, 33, 941–951. [CrossRef] [PubMed]
67. Pavitra, E.; Dariya, B.; Srivani, G.; Kang, S.M.; Alam, A.; Sudhir, P.R.; Kamal, M.A.; Raju, G.S.R.; Han, Y.K.; Lakkakula, B.; et al. Engineered nanoparticles for imaging and drug delivery in colorectal cancer. Semin. Cancer Biol. 2019. [CrossRef] [PubMed]
68. Toy, R.; Peiris, P.M.; Ghaghada, K.B.; Karathanasis, E. Shaping cancer nanomedicine: The effect of particle shape on the *in vivo* journey of nanoparticles. Nanomedicine 2014, 9, 121–134. [CrossRef]
69. Kim, S.M.; Faix, P.H.; Schnitzer, J.E. Overcoming key biological barriers to cancer drug delivery and efficacy. J. Control. Release Off.J. Control. Release Soc. 2017, 267, 15–30. [CrossRef]
70. Tang, Y.; Wang, X.; Li, J.; Nie, Y.; Liao, G.; Yu, Y.; Li, C. Overcoming the Reticuloendothelial System Barrier to Drug Delivery with a "Don't-Eat-Us" Strategy. ACS Nano 2019, 13, 13015–13026. [CrossRef]
71. Lungu, I.I.; Grumezescu, A.M.; Volceanov, A.; Andronescu, E. Nanobiomaterials Used in Cancer Therapy: An Up-To-Date Overview. Molecules 2019, 24, 3547. [CrossRef]
72. Nie, S. Understanding and overcoming major barriers in cancer nanomedicine. Nanomedicine 2010, 5, 523–528. [CrossRef]
73. Roh, Y.G.; Shin, S.W.; Kim, S.Y.; Kim, S.; Lim, Y.T.; Oh, B.K.; Um, S.H. Protein Nanoparticle Fabrication for Optimized Reticuloendothelial System Evasion and Tumor Accumulation. Langmuir ACS J. Surf. Colloids 2019, 35, 3992–3998. [CrossRef]
74. Tecklenborg, J.; Clayton, D.; Siebert, S.; Coley, S.M. The role of the immune system in kidney disease. Clin. Exp. Immunol. 2018,192, 142–150. [CrossRef]
75. Yu, M.; Zheng, J. Clearance Pathways and Tumor Targeting of Imaging Nanoparticles. ACS Nano 2015, 9, 6655–6674. [CrossRef]
76. von Roemeling, C.; Jiang, W.; Chan, C.K.; Weissman, I.L.; Kim, B.Y.S. Breaking Down the Barriers to Precision Cancer Nanomedicine. Trends Biotechnol. 2017, 35, 159–171. [CrossRef] [PubMed]

77. Liebner, S.; Dijkhuizen, R.M.; Reiss, Y.; Plate, K.H.; Agalliu, D.; Constantin, G. Functional morphology of the blood-brain barrier in health and disease. Acta Neuropathol. 2018, 135, 311–336. [CrossRef]
78. Wang, D.; Wang, C.; Wang, L.; Chen, Y. A comprehensive review in improving delivery of small-molecule chemotherapeutic agents overcoming the blood-brain/brain tumor barriers for glioblastoma treatment. Drug Deliv. 2019, 26, 551–565. [CrossRef]
79. Arvanitis, C.D.; Ferraro, G.B.; Jain, R.K. The blood-brain barrier and blood-tumour barrier in brain tumours and metastases.Nat. Rev. Cancer 2020, 20, 26–41. [CrossRef]
80. Alphandéry, E. Nano-Therapies for Glioblastoma Treatment. Cancers 2020, 12, 242. [CrossRef]
81. Tang, W.; Fan, W.; Lau, J.; Deng, L.; Shen, Z.; Chen, X. Emerging blood-brain-barrier-crossing nanotechnology for brain cancer theranostics. Chem. Soc. Rev. 2019, 48, 2967–3014. [CrossRef]
82. Wong, K.H.; Riaz, M.K.; Xie, Y.; Zhang, X.; Liu, Q.; Chen, H.; Bian, Z.; Chen, X.; Lu, A.; Yang, Z. Review of Current Strategies for Delivering Alzheimer's Disease Drugs across the Blood-Brain Barrier. Int. J. Mol. Sci. 2019, 20, 381. [CrossRef] [PubMed]
83. Kalyane, D.; Raval, N.; Maheshwari, R.; Tambe, V.; Kalia, K.; Tekade, R.K. Employment of enhanced permeability and retention effect (EPR): Nanoparticle-based precision tools for targeting of therapeutic and diagnostic agent in cancer. Mater. Sci. Eng. C Mater Biol. Appl. 2019, 98, 1252–1276. [CrossRef] [PubMed]
84. Dhaliwal, A.; Zheng, G. Improving accessibility of EPR-insensitive tumor phenotypes using EPR-adaptive strategies: Designing a new perspective in nanomedicine delivery. Theranostics 2019, 9, 8091–8108. [CrossRef]
85. Golombek, S.K.; May, J.-N.; Theek, B.; Appold, L.; Drude, N.; Kiessling, F.; Lammers, T. Tumor targeting via EPR: Strategies to enhance patient responses. Adv. Drug Deliv. Rev. 2018, 130, 17–38. [CrossRef]
86. Khan, I.; Saeed, K.; Khan, I. Nanoparticles: Properties, applications and toxicities. Arab. J. Chem. 2019, 12, 908–931. [CrossRef]
87. Lombardo, D.; Kiselev, M.A.; Caccamo, M.T. Smart Nanoparticles for Drug Delivery Application: Development of Versatile Nanocarrier Platforms in Biotechnology and Nanomedicine. J. Nanomater. 2019, 2019, 3702518. [CrossRef]
88. Mohanty, A.; Uthaman, S.; Park, I.-K. Utilization of Polymer-Lipid Hybrid Nanoparticles for Targeted Anti-Cancer Therapy.Molecules 2020, 25, 4377. [CrossRef] [PubMed]
89. Rizwanullah, M.; Alam, M.; Harshita; Mir, S.R.; Rizvi, M.M.A.; Amin, S. Polymer-Lipid Hybrid Nanoparticles: A Next-Generation Nanocarrier for Targeted Treatment of Solid Tumors. Curr. Pharm. Des. 2020, 26, 1206–1215. [CrossRef]
90. Ghorbanizamani, F.; Moulahoum, H.; Zihnioglu, F.; Timur, S. Nanohybrid carriers: The yin-yang equilibrium between natural and synthetic in biomedicine. Biomater. Sci. 2020, 8, 3237–3247. [CrossRef]
91. Pan, G.; Jia, T.T.; Huang, Q.X.; Qiu, Y.Y.; Xu, J.; Yin, P.H.; Liu, T. Mesoporous silica nanoparticles (MSNs)-based organic/inorganic hybrid nanocarriers loading 5-Fluorouracil for the treatment of colon cancer with improved anticancer efficacy. Colloids Surf. B Biointerfaces 2017, 159, 375–385. [CrossRef] [PubMed]
92. Ghorbani, F.; Kokhaei, P.; Ghorbani, M.; Eslami, M. Application of different nanoparticles in the diagnosis of colorectal cancer.Gene Rep. 2020, 21, 100896. [CrossRef]
93. Feng, H.-Y.; Yuan, Y.; Zhang, Y.; Liu, H.-J.; Dong, X.; Yang, S.-C.; Liu, X.-L.; Lai, X.; Zhu, M.-H.; Wang, J.; et al. Targeted Micellar Phthalocyanine for Lymph Node Metastasis Homing and Photothermal Therapy in an Orthotopic Colorectal Tumor Model. Nanomicro Lett. 2021, 13, 145. [CrossRef] [PubMed]

94. Chaturvedi, V.K.; Singh, A.; Singh, V.K.; Singh, M.P. Cancer Nanotechnology: A New Revolution for Cancer Diagnosis and Therapy. Curr. Drug Metab. 2019, 20, 416–429. [CrossRef] [PubMed]
95. Trucillo, P.; Campardelli, R.; Reverchon, E. Liposomes: From Bangham to Supercritical Fluids. Processes 2020, 8, 22. [CrossRef]
96. Gurunathan, S.; Kang, M.-H.; Qasim, M.; Kim, J.-H. Nanoparticle-Mediated Combination Therapy: Two-in-One Approach for Cancer. Int. J. Mol. Sci. 2018, 19, 3264. [CrossRef] [PubMed]
97. Montané, X.; Bajek, A.; Roszkowski, K.; Montornés, J.M.; Giamberini, M.; Roszkowski, S.; Kowalczyk, O.; Garcia-Valls, R.; Tylkowski, B. Encapsulation for Cancer Therapy. Molecules 2020, 25, 1605. [CrossRef]
98. Huang, J.R.; Lee, M.H.; Li, W.S.; Wu, H.C. Liposomal Irinotecan for Treatment of Colorectal Cancer in a Preclinical Model. Cancers2019, 11, 281. [CrossRef]
99. Awasthi, R.; Roseblade, A.; Hansbro, P.M.; Rathbone, M.J.; Dua, K.; Bebawy, M. Nanoparticles in Cancer Treatment: Opportunities and Obstacles. Curr. Drug Targets 2018, 19, 1696–1709. [CrossRef]
100. Pandey, P.; Dureja, H. Recent Patents on Polymeric Nanoparticles for Cancer Therapy. Recent Pat. Nanotechnol. 2018, 12,155–169. [CrossRef]
101. Aghebati-Maleki, A.; Dolati, S.; Ahmadi, M.; Baghbanzhadeh, A.; Asadi, M.; Fotouhi, A.; Yousefi, M.; Aghebati-Maleki, L. Nanoparticles and cancer therapy: Perspectives for application of nanopar ticles in the treatment of cancers. J. Cell. Physiol. 2020, 235, 1962–1972. [CrossRef]
102. Bai, X.; Wang, Y.; Song, Z.; Feng, Y.; Chen, Y.; Zhang, D.; Feng, L. The Basic Properties of Gold Nanoparticles and their Applications in Tumor Diagnosis and Treatment. Int. J. Mol. Sci. 2020, 21, 2480. [CrossRef] [PubMed]
103. Sztandera, K.; Gorzkiewicz, M.; Klajnert-Maculewicz, B. Gold Nanoparticles in Cancer Treatment. Mol. Pharm. 2019, 16,1–23. [CrossRef]
104. Núñez, C.; Estévez, S.V.; Del Pilar Chantada, M. Inorganic nanoparticles in diagnosis and treatment of breast cancer. J. Biol. Inorg. Chem. JBIC A Publ. Soc. Biol. Inorg. Chem. 2018, 23, 331–345. [CrossRef] [PubMed]
105. Peng, J.; Liang, X. Progress in research on gold nanoparticles in cancer management. Medicine 2019, 98, e15311. [CrossRef]
106. Lasagna-Reeves, C.; Gonzalez-Romero, D.; Barria, M.A.; Olmedo, I.; Clos, A.; Sadagopa Ramanujam, V.M.; Urayama, A.; Vergara, L.; Kogan, M.J.; Soto, C. Bioaccumulation and toxicity of gold nanoparticles after repeated administration in mice. Biochem. Biophys. Res. Commun. 2010, 393, 649–655. [CrossRef]
107. El Hallal, R.; Lyu, N.; Wang, Y. Effect of Cetuximab-Conjugated Gold Nanoparticles on the Cytotoxicity and Phenotypic Evolution of Colorectal Cancer Cells. Molecules 2021, 26, 567. [CrossRef] [PubMed]
108. Li, Y.; Duo, Y.; Bi, J.; Zeng, X.; Mei, L.; Bao, S.; He, L.; Shan, A.; Zhang, Y.; Yu, X. Targeted delivery of anti-miR-155 by functionalized mesoporous silica nanoparticles for colorectal cancer therapy. Int. J. Nanomed. 2018, 13, 1241–1256. [CrossRef] [PubMed]
109. Zhang, Y.; Chan, H.F.; Leong, K.W. Advanced materials and processing for drug delivery: The past and the future. Adv. Drug Deliv. Rev. 2013, 65, 104–120. [CrossRef] [PubMed]
110. Parveen, S.; Misra, R.; Sahoo, S.K. Nanoparticles: A boon to drug delivery, therapeutics, diagnostics and imaging.Nanomed. Nanotechnol. Biol. Med. 2012, 8, 147–166. [CrossRef] [PubMed]
111. Werengowska-Ciec´wierz, K.; Wis´niewski, M.; Terzyk, A.P.; Furmaniak, S. The Chemistry of Bioconjugation in Nanoparticles-Based Drug Delivery System. Adv. Condens. Matter Phys. 2015, 2015, 198175. [CrossRef]

112. Kumar, A.; Mansour, H.M.; Friedman, A.J.; Blough, E. Nanomedicine in Drug Delivery. 2013.
113. Mirza, A.Z.; Siddiqui, F.A. Nanomedicine and drug delivery: A mini review. Int. Nano Lett. 2014, 4, 94. [CrossRef]
114. Somwanshi, S.; Dola, R.; Siddheshwa, S.; Mereka, A.; Godg, R.; Patta, S. Nanomedicine drug delivery system. J. Asian J. Biomed. Pharm. Sci 2013, 3, 9–15.
115. Korrapati, P.S.; Karthikeyan, K.; Satish, A.; Krishnaswamy, V.R.; Venugopal, J.R.; Ramakrishna, S. Recent advancements in nanotechnological strategies in selection, design and delivery of biomolecules for skin regeneration. Mater. Sci. Eng. C 2016, 67, 747–765. [CrossRef]
116. Chandran, S.P.; Natarajan, S.B.; Chandraseharan, S.; Mohd Shahimi, M.S.B. Nano drug delivery strategy of 5-fluorouracil for the treatment of colorectal cancer. J. Cancer Res. Pract. 2017, 4, 45–48. [CrossRef]
117. Indoria, S.; Singh, V.; Hsieh, M.F. Recent advances in theranostic polymeric nanoparticles for cancer treatment: A review.Int. J. Pharm. 2020, 582, 119314. [CrossRef] [PubMed]
118. Zielin´ska, A.; Carreiró, F.; Oliveira, A.M.; Neves, A.; Pires, B.; Venkatesh, D.N.; Durazzo, A.; Lucarini, M.; Eder, P.; Silva, A.M.; et al. Polymeric Nanoparticles: Production, Characterization, Toxicology and Ecotoxicology. Molecules 2020, 25, 3731. [CrossRef]
119. Krishnaswamy, K.; Orsat, V. Chapter 2—Sustainable Delivery Systems Through Green Nanotech nology. In Nano- and Microscale Drug Delivery Systems; Grumezescu, A.M., Ed.; Elsevier: Amsterdam, The Netherlands, 2017; pp. 17–32.
120. Taghipour-Sabzevar, V.; Sharifi, T.; Moghaddam, M.M. Polymeric nanoparticles as carrier for targeted and controlled delivery of anticancer agents. Delivery 2019, 10, 527–550. [CrossRef]
121. Kapoor, D.N.; Bhatia, A.; Kaur, R.; Sharma, R.; Kaur, G.; Dhawan, S. PLGA: A unique polymer for drug delivery. Ther. Deliv. 2015, 6, 41–58. [CrossRef]
122. Danhier, F.; Ansorena, E.; Silva, J.M.; Coco, R.; Le Breton, A.; Préat, V. PLGA-based nanoparticles: An overview of biomedical applications. J. Control. Release 2012, 161, 505–522. [CrossRef] [PubMed]
123. Naves, L.; Dhand, C.; Almeida, L.; Rajamani, L.; Ramakrishna, S.; Soares, G. Poly(lactic-co-glycolic) acid drug delivery systems through transdermal pathway: An overview. Prog. Biomater. 2017, 6, 1–11. [CrossRef] [PubMed]
124. Qi, F.; Wu, J.; Li, H.; Ma, G. Recent research and development of PLGA/PLA microspheres/ nanoparticles: A review in scientific and industrial aspects. Front. Chem. Sci. Eng. 2019, 13, 14–27. [CrossRef]
125. Makadia, H.K.; Siegel, S.J. Poly Lactic-co-Glycolic Acid (PLGA) as Biodegradable Controlled Drug Delivery Carrier. Polymers 2011, 3, 1377–1397. [CrossRef] [PubMed]
126. Sun, X.; Xu, C.; Wu, G.; Ye, Q.; Wang, C. Poly(Lactic-co-Glycolic Acid): Applications and Future Prospects for Periodontal Tissue Regeneration. Polymers 2017, 9, 189. [CrossRef] [PubMed]
127. Mir, M.; Ahmed, N.; Rehman, A.U. Recent applications of PLGA based nanostructures in drug delivery. Colloids Surf. B Biointerfaces 2017, 159, 217–231. [CrossRef] [PubMed]
128. Babu, A.; Amreddy, N.; Muralidharan, R.; Pathuri, G.; Gali, H.; Chen, A.; Zhao, Y.D.; Munshi, A.; Ramesh, R. Chemodrug delivery using integrin-targeted PLGA-Chitosan nanoparticle for lung cancer therapy. Sci. Rep. 2017, 7, 14674. [CrossRef]
129. Cole, A.J.; David, A.E.; Wang, J.; Galbán, C.J.; Yang, V.C. Magnetic brain tumor targeting and biodistribution of long-circulating PEG-modified, cross-linked starch-coated iron oxide nanoparticles. Biomaterials 2011, 32, 6291–6301. [CrossRef]
130. Dhas, N.L.; Ige, P.P.; Kudarha, R.R. Design, optimization and *in-vitro* study of folic acid conju gated-chitosan functionalized PLGA nanoparticle for delivery of bicalutamide in prostate cancer. Powder Technol. 2015, 283, 234–245. [CrossRef]

131. Venugopal, V.; Krishnan, S.; Palanimuthu, V.R.; Sankarankutty, S.; Kalaimani, J.K.; Karupiah, S.; Kit, N.S.; Hock, T.T. Anti-EGFR anchored paclitaxel loaded PLGA nanoparticles for the treatment of triple negative breast cancer. *In-vitro* and *in-vivo* anticancer activities. PLoS ONE 2018, 13, e0206109. [CrossRef]
132. Pandey, P.; Rahman, M.; Bhatt, P.C.; Beg, S.; Paul, B.; Hafeez, A.; Al-Abbasi, F.A.; Nadeem, M.S.; Baothman, O.; Anwar, F.; et al. Implication of nano-antioxidant therapy for treatment of hepatocellular carcinoma using PLGA nanoparticles of rutin. Nanomed. Nanotechnol. Biol. Med. 2018, 13, 849–870. [CrossRef]
133. Ramanlal Chaudhari, K.; Kumar, A.; Megraj Khandelwal, V.K.; Ukawala, M.; Manjappa, A.S.; Mishra, A.K.; Monkkonen, J.; Ramachandra Murthy, R.S. Bone metastasis targeting: A novel approach to reach bone using Zoledronate anchored PLGA nanoparticle as carrier system loaded with Docetaxel. J. Control. Release Off. J. Control. Release Soc. 2012, 158, 470–478. [CrossRef] [PubMed]
134. Kumar, G.; Sharma, S.; Shafiq, N.; Khuller, G.K.; Malhotra, S. Optimization, i*n vitro–in vivo* evalu ation, and short-term tolerability of novel levofloxacin-loaded PLGA nanoparticle formulation. J. Pharm. Sci. 2012, 101, 2165–2176. [CrossRef] [PubMed]
135. Van de Ven, H.; Vermeersch, M.; Matheeussen, A.; Vandervoort, J.; Weyenberg, W.; Apers, S.; Cos, P.; Maes, L.; Ludwig, A. PLGA nanoparticles loaded with the antileishmanial saponin β-aescin: Factor influence study and *in vitro* efficacy evaluation. Int. J. Pharm. 2011, 420, 122–132. [CrossRef] [PubMed]
136. Singh, P.K.; Jaiswal, A.K.; Pawar, V.K.; Raval, K.; Kumar, A.; Bora, H.K.; Dube, A.; Chourasia, M.K. Fabrication of 3-O-sn- Phosphatidyl-L-serine Anchored PLGA Nanoparticle Bearing Ampho tericin B for Macrophage Targeting. Pharm. Res. 2018, 35, 60. [CrossRef] [PubMed]
137. Arasoglu, T.; Mansuroglu, B.; Derman, S.; Gumus, B.; Kocyigit, B.; Acar, T.; Kocacaliskan, I. Enhancement of Antifungal Activity of Juglone (5-Hydroxy-1,4-naphthoquinone) Using a Poly(d,l-lactic-co-glycolic acid) (PLGA) Nanoparticle System. J. Agric. Food Chem. 2016, 64, 7087–7094. [CrossRef] [PubMed]
138. Gomes, C.; Moreira, R.G.; Castell-Perez, E. Poly (DL-lactide-co-glycolide) (PLGA) nanoparticles with entrapped transcinnamaldehyde and eugenol for antimicrobial delivery applications. J. Food Sci. 2011, 76, N16-24. [CrossRef] [PubMed]
139. Hill, M.; Cunningham, R.N.; Hathout, R.M.; Johnston, C.; Hardy, J.G.; Migaud, M.E. Formulation of Antimicrobial Tobramycin Loaded PLGA Nanoparticles via Complexation with AOT. J. Funct. Biomater. 2019, 10, 26. [CrossRef]
140. Sanchez-Gaytan, B.L.; Fay, F.; Lobatto, M.E.; Tang, J.; Ouimet, M.; Kim, Y.; van der Staay, S.E.M.; van Rijs, S.M.; Priem, B.; Zhang, L.; et al. HDL-Mimetic PLGA Nanoparticle To Target Atheroscle rosis Plaque Macrophages. Bioconjugate Chem. 2015, 26, 443–451. [CrossRef] [PubMed]
141. Khanal, S.; Adhikari, U.; Rijal, N.P.; Bhattarai, S.R.; Sankar, J.; Bhattarai, N. pH-Responsive PLGA Nanoparticle for Controlled Payload Delivery of Diclofenac Sodium. J. Funct. Biomater. 2016, 7, 21. [CrossRef]
142. Pereira, A.; Brito, G.A.C.; Lima, M.L.S.; Silva Júnior, A.A.D.; Silva, E.D.S.; de Rezende, A.A.; Bortolin, R.H.; Galvan, M.; Pirih, F.Q.; Araújo Júnior, R.F.; et al. Metformin Hydrochloride-Loaded PLGA Nanoparticle in Periodontal Disease Experimental Model Using Diabetic Rats. Int. J. Mol. Sci. 2018, 19, 488. [CrossRef]
143. Vij, N.; Min, T.; Marasigan, R.; Belcher, C.N.; Mazur, S.; Ding, H.; Yong, K.T.; Roy, I. Development of PEGylated PLGA nanoparticle for controlled and sustained drug delivery in cystic fibrosis. J. Nanobiotechnol. 2010, 8, 22. [CrossRef]

144. Yang, H.; Tyagi, P.; Kadam, R.S.; Holden, C.A.; Kompella, U.B. Hybrid Dendrimer Hydrogel/PLGA Nanoparticle Platform Sustains Drug Delivery for One Week and Antiglaucoma Effects for Four Days Following One-Time Topical Administration. ACS Nano 2012, 6, 7595–7606. [CrossRef]
145. Chandra Boinpelly, V.; Verma, R.K.; Srivastav, S.; Srivastava, R.K.; Shankar, S. β-Mangostin-encap sulated PLGA nanoparticles inhibit colorectal cancer growth by inhibiting Notch pathway. J. Cell. Mol. Med. 2020, 24, 11343–11354. [CrossRef] [PubMed]
146. Hoshyar, N.; Gray, S.; Han, H.; Bao, G. The effect of nanoparticle size on *in vivo* pharmacokinetics and cellular interaction. Nanomedicine 2016, 11, 673–692. [CrossRef]
147. Caldorera-Moore, M.; Guimard, N.; Shi, L.; Roy, K. Designer nanoparticles: Incorporating size, shape and triggered release into nanoscale drug carriers. Expert Opin. Drug Deliv. 2010, 7, 479–495. [CrossRef] [PubMed]
148. Venkataraman, S.; Hedrick, J.L.; Ong, Z.Y.; Yang, C.; Ee, P.L.R.; Hammond, P.T.; Yang, Y.Y. The effects of polymeric nanostructure shape on drug delivery. Adv. Drug Deliv. Rev. 2011, 63, 1228–1246. [CrossRef] [PubMed]
149. Zhao, Z.; Ukidve, A.; Krishnan, V.; Mitragotri, S. Effect of physicochemical and surface properties on *in vivo* fate of drug nanocarriers. Adv. Drug Deliv. Rev. 2019, 143, 3–21. [CrossRef]
150. Ernsting, M.J.; Murakami, M.; Roy, A.; Li, S.D. Factors controlling the pharmacokinetics, biodistri bution and intratumoral penetration of nanoparticles. J. Control. Release Off. J. Control. Release Soc. 2013, 172, 782–794. [CrossRef]
151. Chakraborty, S.; Dhakshinamurthy, G.S.; Misra, S.K. Tailoring of physicochemical properties of nanocarriers for effective anti-cancer applications. J. Biomed. Mater. Res. Part A 2017, 105, 2906–2928. [CrossRef] [PubMed]
152. Saadat, M.; Zahednezhad, F.; Zakeri-Milani, P.; Reza Heidari, H.; Shahbazi-Mojarrad, J.; Valizadeh, H. Drug Targeting Strategies Based on Charge Dependent Uptake of Nanoparticles into Cancer Cells. J. Pharm. Pharm. Sci. A Publ. Can. Soc. Pharm. Sci. Soc. Can. Des Sci. Pharm. 2019, 22, 191–220. [CrossRef] [PubMed]
153. Chen, X.; Liu, L.; Jiang, C. Charge-reversal nanoparticles: Novel targeted drug delivery carriers. Acta Pharm. Sin. B 2016, 6,261–267. [CrossRef]
154. Zhang, M.; Chen, X.; Li, C.; Shen, X. Charge-reversal nanocarriers: An emerging paradigm for smart cancer nanomedicine.J. Control. Release Off. J. Control. Release Soc. 2020, 319, 46–62. [CrossRef]
155. Abbas, Q.; Yousaf, B.; Amina; Ali, M.U.; Munir, M.A.M.; El-Naggar, A.; Rinklebe, J.; Naushad, M. Transformation pathways and fate of engineered nanoparticles (ENPs) in distinct interactive environmental compartments: A review. Environ. Int. 2020, 138, 105646. [CrossRef]
156. Kundranda, M.N.; Niu, J. Albumin-bound paclitaxel in solid tumors: Clinical development and future directions. Drug Des. Dev.2015, 9, 3767–3777. [CrossRef]
157. Caraglia, M.; Marra, M.; Misso, G.; Lamberti, M.; Salzano, G.; De Rosa, G.; Abbruzzese, A. Tumour-specific uptake of anti-cancer drugs: The future is here. Curr. Drug Metab. 2012, 13, 4–21. [CrossRef]
158. Wolfram, J.; Ferrari, M. Clinical cancer nanomedicine. Nano Today 2019, 25, 85–98. [CrossRef] [PubMed]
159. Guo, S.; Vieweger, M.; Zhang, K.; Yin, H.; Wang, H.; Li, X.; Li, S.; Hu, S.; Sparreboom, A.; Evers, B.M.; et al. Ultra-thermostable RNA nanoparticles for solubilizing and high-yield loading of paclitaxel for breast cancer therapy. Nat. Commun. 2020, 11, 972. [CrossRef]
160. Sun, T.; Zhang, Y.S.; Pang, B.; Hyun, D.C.; Yang, M.; Xia, Y. Engineered nanoparticles for drug delivery in cancer therapy.Angew. Chem. 2014, 53, 12320–12364. [CrossRef] [PubMed]

161. Wei, Y.; Quan, L.; Zhou, C.; Zhan, Q. Factors relating to the biodistribution & clearance of nanoparticles & their effects on *in vivo* application. Nanomed. Nanotechnol. Biol. Med. 2018, 13, 1495–1512. [CrossRef]
162. Nogueira, E.; Gomes, A.C.; Preto, A.; Cavaco-Paulo, A. Folate-targeted nanoparticles for rheumatoid arthritis therapy.Nanomed. Nanotechnol. Biol. Med. 2016, 12, 1113–1126. [CrossRef]
163. Gorbet, M.J.; Ranjan, A. Cancer immunotherapy with immunoadjuvants, nanoparticles, and checkpoint inhibitors: Recent progress and challenges in treatment and tracking response to immunotherapy. Pharmacol. Ther. 2020, 207, 107456. [CrossRef]
164. Dadwal, A.; Baldi, A.; Kumar Narang, R. Nanoparticles as carriers for drug delivery in cancer. Artif. Cells Nanomed. Biotechnol.2018, 46, 295–305. [CrossRef]
165. Soe, Z.C.; Poudel, B.K.; Nguyen, H.T.; Thapa, R.K.; Ou, W.; Gautam, M.; Poudel, K.; Jin, S.G.; Jeong, J.-H.; Ku, S.K.; et al. Folate-targeted nanostructured chitosan/chondroitin sulfate complex carriers for enhanced delivery of bortezomib to colorectal cancer cells. Asian J. Pharm. Sci. 2019, 14, 40–51. [CrossRef]
166. Jahan, S.T.; Sadat, S.M.A.; Walliser, M.; Haddadi, A. Targeted Therapeutic Nanoparticles: An Immense Promise to Fight against Cancer. J. Drug Deliv. 2017, 2017, 9090325. [CrossRef] [PubMed]
167. Ahmad, A.; Khan, F.; Mishra, R.K.; Khan, R. Precision Cancer Nanotherapy: Evolving Role of Multifunctional Nanoparticles for Cancer Active Targeting. J. Med. Chem. 2019, 62, 10475–10496. [CrossRef]
168. Yoo, J.; Park, C.; Yi, G.; Lee, D.; Koo, H. Active Targeting Strategies Using Biological Ligands for Nanoparticle Drug Delivery Systems. Cancers 2019, 11, 640. [CrossRef]
169. Heuer-Jungemann, A.; Feliu, N.; Bakaimi, I.; Hamaly, M.; Alkilany, A.; Chakraborty, I.; Masood, A.; Casula, M.F.; Kostopoulou, A.; Oh, E.; et al. The Role of Ligands in the Chemical Synthesis and Applications of Inorganic Nanoparticles. Chem. Rev. 2019, 119, 4819–4880. [CrossRef]
170. Muhamad, N.; Plengsuriyakarn, T.; Na-bangchang, K. Application of active targeting nanoparticle delivery system for chemotherapeutic drugs and traditional/herbal medicines in cancer therapy: A systematic review. Int. J. Nanomed. 2018, 13, 3921–3935. [CrossRef]
171. Akbarzadeh Khiavi, M.; Safary, A.; Barar, J.; Ajoolabady, A.; Somi, M.H.; Omidi, Y. Multifunctional nanomedicines for targeting epidermal growth factor receptor in colorectal cancer. Cell. Mol. Life Sci. 2020, 77, 997–1019. [CrossRef]
172. Eloy, J.O.; Petrilli, R.; Trevizan, L.N.F.; Chorilli, M. Immunoliposomes: A review on functionalization strategies and targets for drug delivery. Colloids Surf. B Biointerfaces 2017, 159, 454–467. [CrossRef]
173. Moradpour, Z.; Barghi, L. Novel Approaches for Efficient Delivery of Tyrosine Kinase Inhibitors. Journal of pharmacy & pharmaceutical sciences: A publication of the Canadian Society for Pharmaceutical Sciences, Societe canadienne des sciences pharmaceutiques. J. Pharm. Pharm. Sci. 2019, 22, 37–48. [CrossRef]
174. Li, Y.L.; Zhu, X.M.; Liang, H.; Orvig, C.; Chen, Z.F. Recent Advances in Asialoglycoprotein Receptor and Glycyrrhetinic Acid Receptor-Mediated and/or pH Responsive Hepatocellular Carcino ma-Targeted Drug Delivery. Curr. Med. Chem. 2020. [CrossRef]
175. Xia, Y.; Zhong, J.; Zhao, M.; Tang, Y.; Han, N.; Hua, L.; Xu, T.; Wang, C.; Zhu, B. Galactose-modified selenium nanoparticles for targeted delivery of doxorubicin to hepatocellular carcinoma. Drug Deliv. 2019, 26, 1–11. [CrossRef]
176. Li, M.; Sun, J.; Zhang, W.; Zhao, Y.; Zhang, S.; Zhang, S. Drug delivery systems based on CD44-tar geted glycosaminoglycans for cancer therapy. Carbohydr. Polym. 2021, 251, 117103. [CrossRef]

177. Kim, K.; Choi, H.; Choi, E.S.; Park, M.-H.; Ryu, J.-H. Hyaluronic Acid-Coated Nanomedicine for Targeted Cancer Therapy.Pharmaceutics 2019, 11, 301. [CrossRef] [PubMed]
178. Sakurai, Y.; Harashima, H. Hyaluronan-modified nanoparticles for tumor-targeting. Expert Opin. Drug Deliv. 2019, 16, 915–936. [CrossRef] [PubMed]
179. Lee, S.Y.; Kang, M.S.; Jeong, W.Y.; Han, D.-W.; Kim, K.S. Hyaluronic Acid-Based Theranostic Nanomedicines for Targeted Cancer Therapy. Cancers 2020, 12, 940. [CrossRef] [PubMed]
180. Kumari, P.; Muddineti, O.S.; Rompicharla, S.V.K.; Ghanta, P.; BBN, A.K.; Ghosh, B.; Biswas, S. Cholesterol-conjugated poly(D, L-lactide)-based micelles as a nanocarrier system for effective delivery of curcumin in cancer therapy. Drug Deliv. 2017, 24, 209–223. [CrossRef] [PubMed]
181. Varan, G.; Öncül, S.; Ercan, A.; Benito, J.M.; Ortiz Mellet, C.; Bilensoy, E. Cholesterol-Targeted Anticancer and Apoptotic Effects of Anionic and Polycationic Amphiphilic Cyclodextrin Nanoparticles. J. Pharm. Sci. 2016, 105, 3172–3182. [CrossRef] [PubMed]
182. Lee, J.-J.; Lee, S.Y.; Park, J.-H.; Kim, D.-D.; Cho, H.-J. Cholesterol-modified poly(lactide-co-glycolide) nanoparticles for tumor- targeted drug delivery. Int. J. Pharm. 2016, 509, 483–491. [CrossRef]
183. Low, P.S.; Kularatne, S.A. Folate-targeted therapeutic and imaging agents for cancer. Curr. Opin. Chem. Biol. 2009, 13,256–262. [CrossRef]
184. Souho, T.; Lamboni, L.; Xiao, L.; Yang, G. Cancer hallmarks and malignancy features: Gateway for improved targeted drug delivery. Biotechnol. Adv. 2018, 36, 1928–1945. [CrossRef] [PubMed]
185. Samadian, H.; Hosseini-Nami, S.; Kamrava, S.K.; Ghaznavi, H.; Shakeri-Zadeh, A. Folate-conjugated gold nanoparticle as a new nanoplatform for targeted cancer therapy. J. Cancer Res. Clin. Oncol. 2016, 142, 2217–2229. [CrossRef]
186. Fernández, M.; Javaid, F.; Chudasama, V. Advances in targeting the folate receptor in the treatment/imaging of cancers. Chem. Sci.2018, 9, 790–810. [CrossRef]
187. Yang, B.; Ni, X.; Chen, L.; Zhang, H.; Ren, P.; Feng, Y.; Chen, Y.; Fu, S.; Wu, J. Honokiol-loaded polymeric nanoparticles: An active targeting drug delivery system for the treatment of nasopharyngeal carcinoma. Drug Deliv. 2017, 24, 660–669. [CrossRef] [PubMed]
188. Le Tourneau, C.; Delord, J.P.; Gonçalves, A.; Gavoille, C.; Dubot, C.; Isambert, N.; Campone, M.; Trédan, O.; Massiani, M.A.; Mauborgne, C.; et al. Molecularly targeted therapy based on tumour molecular profiling versus conventional therapy for advanced cancer (SHIVA): A multicentre, open-label, proof-of-concept, randomised, controlled phase 2 trial. Lancet Oncol. 2015, 16, 1324–1334. [CrossRef]
189. Amiri-Kordestani, L.; Basseville, A.; Kurdziel, K.; Fojo, A.T.; Bates, S.E. Targeting MDR in breast and lung cancer: Discriminating its potential importance from the failure of drug resistance reversal studies. Drug Resist. Update 2012, 15, 50–61. [CrossRef] [PubMed]
190. Rodgers, G.M., 3rd; Becker, P.S.; Blinder, M.; Cella, D.; Chanan-Khan, A.; Cleeland, C.; Coccia, P.F.; Djulbegovic, B.; Gilreath, J.A.; Kraut, E.H.; et al. Cancer- and chemotherapy-induced anemia. J. Natl. Compr. Cancer Netw. JNCCN 2012, 10, 628–653. [CrossRef]
191. Takeshima, H.; Ushijima, T. Accumulation of genetic and epigenetic alterations in normal cells and cancer risk. NPJ Precis. Oncol.2019, 3, 7. [CrossRef]
192. Mroz, E.A.; Rocco, J.W. The challenges of tumor genetic diversity. Cancer 2017, 123, 917–927. [CrossRef]
193. Tiong, K.-L.; Yeang, C.-H. Explaining cancer type specific mutations with transcriptomic and epigenomic features in normal tissues. Sci. Rep. 2018, 8, 11456. [CrossRef]
194. Wagner, J.; Wickman, E.; DeRenzo, C.; Gottschalk, S. CAR T Cell Therapy for Solid Tumors: Bright Future or Dark Reality?Mol. Ther. 2020, 28, 2320–2339. [CrossRef]

195. Maeda, H.; Khatami, M. Analyses of repeated failures in cancer therapy for solid tumors: Poor tumor-selective drug delivery, low therapeutic efficacy and unsustainable costs. Clin. Transl. Med. 2018, 7, 11. [CrossRef]
196. Werb, Z.; Lu, P. The Role of Stroma in Tumor Development. Cancer J. 2015, 21, 250–253. [CrossRef]
197. Zhang, H.; Ye, Z.-L.; Yuan, Z.-G.; Luo, Z.-Q.; Jin, H.-J.; Qian, Q.-J. New Strategies for the Treatment of Solid Tumors with CAR-T Cells. Int. J. Biol. Sci. 2016, 12, 718–729. [CrossRef] [PubMed]
198. Cruz, E.; Kayser, V. Monoclonal antibody therapy of solid tumors: Clinical limitations and novel strategies to enhance treatment efficacy. Biol. Targets Ther. 2019, 13, 33–51. [CrossRef]
199. Wei, Q.Y.; Xu, Y.M.; Lau, A.T.Y. Recent Progress of Nanocarrier-Based Therapy for Solid Malig nancies. Cancers 2020, 12, 2783.[CrossRef] [PubMed]
200. Nurgali, K.; Jagoe, R.T.; Abalo, R. Editorial: Adverse Effects of Cancer Chemotherapy: Anything New to Improve Tolerance and Reduce Sequelae? Front. Pharm. 2018, 9, 245. [CrossRef] [PubMed]
201. Zhang, S.-q.; Fu, Q.; Zhang, Y.-j.; Pan, J.-x.; Zhang, L.; Zhang, Z.-r.; Liu, Z.-m. Surface loading of nanoparticles on engineered or natural erythrocytes for prolonged circulation time: Strategies and applications. Acta Pharmacol. Sin. 2021. [CrossRef]
202. Zhong, L.; Xu, L.; Liu, Y.; Li, Q.; Zhao, D.; Li, Z.; Zhang, H.; Zhang, H.; Kan, Q.; Wang, Y.; et al. Trans formative hyaluronic acid-based active targeting supramolecular nanoplatform improves long circulation and enhances cellular uptake in cancer therapy. Acta Pharm. Sin. B 2019, 9, 397–409. [CrossRef]
203. McDonald, D.M.; Choyke, P.L. Imaging of angiogenesis: From microscope to clinic. Nat. Med. 2003, 9, 713–725. [CrossRef]
204. Kang, H.; Rho, S.; Stiles, W.R.; Hu, S.; Baek, Y.; Hwang, D.W.; Kashiwagi, S.; Kim, M.S.; Choi, H.S. Size-Dependent EPR Effect of Polymeric Nanoparticles on Tumor Targeting. Adv. Healthc. Mater. 2020, 9, 1901223. [CrossRef]
205. Maeda, H. Tumor-selective delivery of macromolecular drugs via the EPR effect: Background and future prospects. Bioconjug Chem.2010, 21, 797–802. [CrossRef]
206. Kobayashi, H.; Watanabe, R.; Choyke, P.L. Improving conventional enhanced permeability and retention (EPR) effects; what is the appropriate target? Theranostics 2013, 4, 81–89. [CrossRef] [PubMed]
207. Norouzi, M.; Amerian, M.; Amerian, M.; Atyabi, F. Clinical applications of nanomedicine in cancer therapy. Drug Discov. Today2020, 25, 107–125. [CrossRef] [PubMed]
208. Anselmo, A.C.; Mitragotri, S. Nanoparticles in the clinic. 2016, 1, 10–29, doi:https://doi.org/10.1002/btm2.10003.

CHAPTER **TWO**

Ana Luiza C. de S. L. Oliveira, Alaine M. dos Santos-Silva, Arnóbio A. da Silva-Júnior, Vinícius B. Garcia, Aurigena A. de Araújo, Lioe-Fee de Geus-Oei, Alan B. Chan, Luis J. Cruz and Raimundo F. de Araújo Júnior.

Cholesterol-functionalized carvedilol-loaded PLGA nanoparticles: anti-inflammatory, antioxidant, and antitumor effects. Journal of Nanoparticle Research. May 2020.

Doi: 10.1007/s11051-020-04832-8

CHOLESTEROL -FUNCTIONALIZED CARVEDILOL-LOADED PLGA NANOPARTICLES: ANTI-INFLAMMATORY, ANTIOXIDANT, AND ANTITUMOR EFFECTS

Abstract: The inflammation has been identified as factor of tumor progression, which has increased the interest and use of molecules with anti-inflammatory and antioxidant activities in the cancer treatment. In this study, the antioxidant, anti-inflammatory, and antitumor potentials of carvedilol was explored in a different approach. The cholesterol (CHO) was investigated as facilitated agent in the action of carvedilol-loaded nanoparticles. Different formulations exhibited spherical and stable nanoparticle with mean diameter size < 250 nm. The cholesterol changed the copolymer-drug interactions and the encapsulation efficiency. The *in vitro* cancer study was performed using murine colorectal cancer cell line (CT-26) to observe the cell viability and apoptosis on MTS assay and flow cytometry, respectively. The experiments have demonstrated that cholesterol improved the performance of drug-loaded nanoparticles, which was much better than free drug. The *in vivo* inflammation peritonitis model revealed that carvedilol-loaded nanoparticles increased the level of glutathione and leukocyte migration mainly when the funcionalized drug-loaded nanoparticles were tested, in a lower dose than the free drug. As hypothesized, the experimental data suggest that cholesterol-functionalized carvedilol-loaded PLGA nanoparticles can be a novel and promising approach in the inflammation-induced cancer therapy since showed anti-inflammatory, antioxidant, and antitumor effects.

Keywords: Cancer; Inflammation; Oxidative stress; Colloidal nanocarriers; Functionalized nanoparticles; Drug delivery systems.

INTRODUCTION

Inflammation and cancer are two interrelated pathological processes, it is well known that inflammation plays a role in tumor progression and that anti-inflammatory therapy can be an ally in the treatment of tumor development (Coussens and Werb 2002; Ghuman et al. 2017). Colorectal cancer (CRC) is an example of cancer whose risk factor is inflammatory bowel disease, which participates in the process of tumor progression (West et al. 2015). The inflammation-mediated CRC tumorigenesis mechanism is correlated to an action of pro-inflammatory cytokines and reactive oxygen species, activating transcription factors, such as NF-kB and STAT3, involved in tumor proliferation pathways and apoptosis inhibition (Elinav et al. 2013; Ghuman et al. 2017; Taniguchi and Karin 2018). The development of new anticancer approach that can take cancer cells to apoptosis, without the harmful side effects caused by conventional cancer therapies, is one of exciting chal lenges of modern medicine. Even though carvedilol (CVDL) is classified as a non-selective beta-adrenergic receptor blocker (β1, β2), which has been used for treating hypertension, angina pectoris, small myocardial infarction, tachyarrhythmia, and congestive heart failure (Balaha et al. 2016), studies have shown that it has also antioxidant, anti-inflammatory, pro-apoptotic, antifibrotic, antiproliferative, and anticancer properties (Araújo Júnior et al. 2016; Areti et al. 2017; De Araujo et al. 2018; Félix et al. 2017; Yao et al. 2016).

As one alternative to the smart use of drug efficiency, nanoparticles can be used as drug delivery systems (DDSs) enable to increase the solubility of hydrophobic drugs, the distribution of higher drug concentrations to target areas due to an Enhanced Permeation and Retention (EPR) effect and provides the sustained and controlled release of encapsulated drugs. This can lead to lower doses of drugs, thus reducing side effects (Goyal et al. 2016; Lee et al. 2015). Different types of nanoparticles (NPs) can be formulated such as liposomes, dendrimers, carbon nanotubes, inorganic, and NPs based on proteins and polymers, each with their own properties. Poly (D, L-lactide-co-glycolide) (PLGA) is a type of polymer approved by the European Medicines Agency (EMA) and Food and Drug Administration (FDA), applied in the development of DDSs (Masloub et al. 2016; Ramezanpour et al. 2016). In this way, nanoparticles can be used for targeted site-specific de livery, which facilitates their internalization into cancer cells and for co-delivering multiple factors to the same cell/tissue

site (Bahrami et al. 2017; Kapadia et al. 2015; Milling et al. 2017). Several targeting ligands are used for drug delivery such as antibodies, peptides, folate, glycoproteins, and cholesterol (CHOL) (Bahrami et al. 2017; Varan et al. 2016). Cholesterol is an important structural component in cells which is involved in many biological processes such as endocytosis of materials and proliferation of cancer and metastasis. Cancer cells have rapid metabolism, requiring more nutrients. Therefore, CHOL is required for synthesizing new membranes (Lee et al. 2016; Varan et al. 2016). In this context, the large number of reports on PLGA NPs used as drug delivery systems for cancer treatment highlights the potential of PLGA NPs as carriers of cancer therapy drugs.

Therefore, the aim of the present study was to verify the *in vitro* and *in vivo* performance of carvedilol-loaded polymeric nanoparticles and the effects of mod ifying particle surfaces induced by CHOL to improve cell uptake of carvedilol as a chemotherapy agent. The interactions among the involved compounds and physicochemical properties of distinct formulations were carefully monitored using an analytical approach. Enhancing the biological efficacy in the inflammatory process and against tumor cells by carvedilol-loaded polymeric induced by CHOL is an interesting and relevant achievement which is not yet reported in literature.

EXPERIMENTAL SECTION

Reagents

For formulation of the nanoparticles, the following compounds were used: copolymer PLGA (poly (lactic-coglycolic acid) (Sigma-Aldrich, Saint Louis, MO, EUA), CVDL (Espaço Pharma®, RN, Brazil), CHOL (92.5%, Vetec®, Sigma-Aldrich, Saint Louis, MO, USA), and poly vinyl alcohol (PVA) with viscosimetric molecular mass of 4.7 × 104 g/mol Vetec (São Paulo, Brazil). The organic solvents: acetone (ACE) and dichloromethane (DCM) (were purchased from Labsynth® (São Paulo, Brazil). Dimethyl sulfoxide (DMSO) was purchased from Sigma-Aldrich (CA, USA). For *in vitro* assays, the following reagents were used: CellTiter 96 AQueous One Solution (MTS) solution (Promega Corporation, Madison, WI), DAPI (Life Technologies, the Netherlands), and Annexin V-FITC (BD Pharmingen, CA, USA). Purified water (1.3 µS) was obtained from reverse osmosis purification equipment model OS50 LX (Gehaka, SP, Brazil). All other chemicals and reagents were

of analytical grade.

Preparation and Characterization of Nanoparticles

Nanoparticles were prepared by the emulsification- solvent evaporation method (Pooja et al. 2016; Zhu et al. 2012), following a previously standardized nanoparticulate system (dos Santos-Silva et al. 2017). First, the organic phase (OP) (6 mL) containing the PLGA was injected into the aqueous phase (AP) (14 mL containing the solution of PVA surfactant in water) under magnetic stirring at 720 rpm at 25 °C. The AP was previously filtered using 0.45-µm membranes. Emulsification was followed in Ultra-turrax equipment (IKA Labortechnik, Germany) at 25 °C for 18 min and evaporation of the solvent occurred under magnetic stirring at 720 rpm overnight. Samples were placed in hermetically sealed glass flasks and stored at 5 °C in a freezer.

Preparation of Surface-Modified Nanoparticles

Surface-modified and CHOL NPs were prepared as in the “Preparation and characterization of nanoparticles” section. The CHOL was inserted in a ratio of 1:10 relative to the CVDL in the polymeric OP following the same evaluation procedure in which nanoparticles were not functionalized. Preparation of drug-loaded nanoparticles

The PLGA 1.0% w/v solution in the OP composed by DCM:ACE at 25:75 v/v was injected in the aqueous solution of PVA 0.5% w/v, using a burette in a flow of 1.0 mL/min under magnetic stirring at 720 rpm. Emulsification followed a stirring speed of 20,000 rpm for 18 min (dos Santos-Silva et al. 2017). Different concentrations of drug were dissolved with the polymer in the organic solvent to supply drug/copolymer ratios of 1:2.5, 1:5, 1:10, and 1:20 relative to the PLGA.

Particle Size and Zeta Potential Measurements

Mean particle size and polydispersity index (PdI) were assessed by using the dynamic light scattered (DLS) by the particle size analyzer (Zetasizer Nano ZS, Malvern instruments, Malvern, UK) at 659-nm wavelength,

temperature of 25 ± 2 °C, and an angle of 173° to the incident beam. Zeta potential measurements were performed in the same equipment using Zeta Potential Analyzer software by electrophoretic mobility. The measurements average of ten determinations for each sample diluted at 1:100 (v/v) with purified water were carried out in triplicate and data expressed as mean ± standard deviation (SD).

Atomic Force Microscopy

The topographic image and the surface of the particles in atomic resolution of drug-free and CVDL-loaded nanoparticles were observed by using atomic force microscopy (AFM) images. The dispersions were freshly diluted in a ratio of 1:25 (v/v) using purified water and placed on a glass coverslips, dried under a desiccator for 24 h, and then analyzed in an AFM SPM-9700 Shimadzu microscope (Tokyo, Japan) at room temperature with a non-contact cantilever and 1-Hz scanning (Dos Santos-Silva et al. 2019).

Physicochemical Stability

The drug-free nanoparticles and CVDL-loaded nanoparticles were hermetically stored for 7 weeks in closed flasks at 5 °C. The samples were collected at intervals of 7 days and had their size and zeta potential evaluates. The measurements were performed using the parameters described in the “Particle size and zeta potential measurements” section. Attenuated total reflectance Fourier transform infrared spectroscopy. The drug-copolymer interactions in the nanoparticles without carvedilol (NP), carvedilol-loaded (NP CVDL), and carvedilol-loaded functionalized with cholesterol (NP CVDL CHOL) were assessed by attenuated total reflectance Fourier transform infrared spectroscopy (ATR-FTIR). The colloidal dispersion of nanoparticles was concentrated using the vacuum concentrator (Labconco Centrivap) for 7–8 h. The spectra were recorded with a resolution of 4 cm−1 between 4000 and 500 cm−1 at 20 scans, for pure compounds (PLGA, CVDL, CHOL), and polymeric nanoparticles in a SHIMADZU IR Prestige 21 FTIR-ATR spectrophotometer (Tokyo, Japan).

Drug Loading Efficiency

The samples were centrifuged for during 60 min at 4 °C (Eppendorf® Microcentrifuge 5404R) at 16.0 ×g using the ultra-centrifugal filter

(Sartorius®, Vivaspin 2, Ultra-15 MWCO 10 kDa). The drug in the supernatant was analyzed at 241 nm, which was the maximum absorption wavelength for the CVDL using the previously validated UV-Vis spectrophotometry. All analyses were performed in triplicate, and the data expressed as mean ± standard deviation (SD). The encapsulation efficiency (EE%) was calculated using Eq. (1), as described by Dos Santos Silva (dos Santos Silva et al. 2019)

.

$$EE\ (\%) = (\text{total drug} - \text{drug in the supernatant}) / = \text{total drug} \times 100$$

In Vitro Drug Release Performance

In vitro drug release analyzed was made using static Franz vertical diffusion cells (Crown Scientific, Sommerville, USA) thermostatted at 37 ± 0.5 °C. First, 3.0 mL of distinct nanoparticles (NP CVDL, NP CVDL CHOL) and CVDL solution were applied and hermetically sealed in the donor compartment and separated from the receptor compartment by a synthetic cellulose acetate 0.45-µm filter, previously hydrated for 24 h in phosphate buffer solution (PBS). The receptor compartment was filled with 11.0 mL of PBS adjusted for pH 7.4, which remained under magnetic stirring at 360 rpm during the entire experiment. Aliquots of 1.0 mL were withdrawals at seven specific intervals (30 to 600 min) and analyzed by previously validated UV spectrophotometry at 241 nm. The same volume of freshly buffered solution replaced the medium to maintain the sink conditions (Ng et al. 2010). The release data were then analyzed using linear regression according to mathematical models to determine the release mechanism of carvedilol from its NPs. The correlation coefficient [R] was determined in each case, and the orders of release were accordingly determined.

In Vitro Anti-CRC Studies

Cell line and cultivation

The murine CRC cell line CT-26 (CT-26.WT, ATCC® CRL-2638™; ATCC, Manassas, VA, USA) was cultivated in Dulbecco's Modified Eagle Medium (DMEM) (Thermo Fisher Scientific, MA, USA) supplemented

with 10% (v/v) fetal bovine serum (FBS) and 1% antibiotics (penicillin/ streptomycin) in 37 °C incubator with atmosphere of 5% CO2 and was passaged twice a week by removing the adherent cells with trypsin/ EDTA in buffered saline.

Cell viability assay (MTS)

MTS assay for the PLGA nanoparticles conjugated with CVDL was determined based on the reduction of the MTS tetrazolium compound to formazan product by living cells in culture. CT-26 cell lines were plated in 96-well plates with a density of 3 × 103 cells/well. Applications of free CVDL and drug-loaded nanoparticles at concentrations of 0.3 µg/mL, 0.78 µg/mL, 1.56 µg/ mL, 3.12 µg/mL, and 6.2 µg/mL were then performed after 24 h under culture conditions (De Araujo et al. 2018). MTS solution was added to medium without cells as a blank control. Treatments were evaluated at 24 h and 48 h by the addition of 20 µL/ well of MTS solution after replacing the treatment medium with a new one. After incubation for 2 h, the fluorescence was measured using a microplate reader (VersaMax Molecular Devices, Sunnyvale, CA) with absorbance being measured at 490 nm. All data points represent triplicates for each treatment.

Evaluation of *in vitro* cell death

The effect of free CVDL and nanoconjugates on CT-26 cells was determined by double-labeled flow cytometry with Annexin V-FITC and DAPI, which enables identifying apoptotic and necrotic cells through loss of membrane integrity. Cell lines were arranged in 24-well plates with a density of 1 × 104 cells/well, at a total volume of 500 µL. After 24 h of incubation under culture conditions, the cells were treated with the samples at doses of 0.3 µg/mL, 0.78 µg/mL, and 1.56 µg/ mL at 24 h and 48 h. The cells were obtained after each period by collecting the supernatant from the wells, washing with PBS, trypsinization, and centrifugation at 3200 rpm at 4 °C for 5 min. Finally, they were labeled with Annexin V-FITC and DAPI, and analyzed with BD LSR-II (BD Biosciences, CA, USA) and FlowJo soft ware version 7.6.5 (Tree Star Inc., CA, USA).

In vivo Inflammation and Oxidative Stress Studies

Animal preparation

Female Swiss mice at 9 weeks old (40 ± 2.0 g) were obtained from the UFRN Vivarium Center of Biosciences. Animals were maintained under standard 12-h light/dark cycle, 22 ± 0.1 °C, and 50–55% humidity with ad libitum access for food and water. The mice were subjected to 12-h fasting prior to the experiments. Euthanasia was performed with a subcutaneous administration of 90 mg/kg sodium thiopental (0.5%, Tiopentax, Cristália, São Paulo, Brazil). This study was carried out in strict accordance with the recommendations in the Guide for the Care and Use of Laboratory Animals of the National Institutes of Health. The protocol was approved by the Committee on the Ethics of Animal Experiments of the UFRN (CEUA, Permit Number: 001/2015).

The carrageenan-induced peritonitis model

Mice were randomly distributed into twelve groups (n = 5/group). The mice were orally pre-treated with a vehicle (0.9% saline solution)/carrageenan group, drug-free nanoparticle (NP) (1 mL of a 1 mg/mL preparation), free CVDL (3 mg/kg and 0.3 mg/kg), NP CVDL (0.3 mg/kg, 0.1 mg/kg and 0.05 mg/kg), NP CVDL CHOL (0.3 mg/kg, 0.1 mg/kg, and 0.05 mg/kg), or Diclofenac (10 mg/kg) in order to evaluate the effect of PLGA, the association of PLGA with CVDL or CVDL and CHOL combined on leukocyte recruitment into the peritoneal cavity. After 30 min, 0.25 mL of a 1% carrageenan solution (Sigma-Aldrich, São Paulo, Brazil) was intraperitoneally (i.p.) injected. The sham group received a vehicle (1 mL water/10 g) and a 0.9% sterile saline solution intraperitoneal injection (0.1 mL/10 g) (Ribeiro et al. 1991). Then, the mice were euthanized 4 h later with an overdose of 90 mg/kg sodium thiopental. Three milliliters of saline solution was then injected into each abdominal cavity and peritoneal fluid was collected and diluted (1:20) in Turk's solution. A total leukocyte count was performed for each sample with a Neubauer counting chamber.

The samples were stored at − 80 °C for subsequent analyses of malondialdehyde (MDA) and total glutathione (GSH) levels.

Glutathione levels

GSH levels assessment was performed according to the method described by Anderson (Anderson 1985). Briefly, 100 µL of each inflammatory lavage was diluted in a 5% trichloroacetic acid (TCA)/ distilled water solution and centrifuged at 10,000 rpm for 15 min at 4 °C. Each standard dilution (20 µL), TCA solution (20 µL, Vetec, São Paulo, Brazil) for the blank, and each sample supernatant (20 µL) were added to 96-well plates in duplicate. In addition, 15 µL PBS-EDTA, 20 µL dithiobisnitrobenzoic acid (DTNB) solution, and 140 µL NADPH were added to each well. After an incubation step at 30 °C for 5 min, 15 µL of an enzyme solution and GSH reductase (Sigma-Aldrich, São Paulo, Brazil) were added to each well. Absorbance values at 412 nm were recorded by spectrocopical UV/VIS analysis (Biotek, São Paulo, Brazil) for 3 min. Total GSH content was calculated based on interpolations from a standard curve that was generated with purified glutathione (γ-L-Glutamyl-L-cysteinyl-glycine, GSH, Sig- ma-Aldrich, São Paulo, Brazil, G4251). The results of this assay are expressed in nanomoles per microliter of sample.

Malonyldialdehyde assay

Malonyldialdehyde (MDA) is a product of lipid peroxidation.
To quantify the increase in free radicals in liver sample, MDA content was measured via the assay described by Esterbauer and Cheeseman (Esterbauer and Cheeseman 1990). First, each sample (50 µl) was diluted in Tris HCl buffer (250 µL, 20 mM) (Trizma hydrochloride, Sigma Aldrich, São Paulo, Brazil) in distilled water (20 mM, pH 7.4). Peritoneal fluid samples were homogenized and centrifuged (10.000 rpm for 10 min at 4 °C), then 750 µL of 10.3 mM 1-methyl-2-phenylindole and 225 µL HCl (37%) were added to each sample. Samples were incubated in a water bath for 40 min at 45 °C, and centrifuged at 10.000 rpm for 5 min at 4 °C. Absorbance values at 586 nm were recorded with a spectroscopic UV/VIS analysis (Biotek, São Paulo, Brazil) and the results were interpolated from a standard

curve that was established with 1,1,3,3- tetraethoxypropane. The results from this assay are expressed as nanomoles per microliter of sample.

Statistical analysis

All analyses of nanoparticles were performed in triplicate and data expressed as mean ± standard deviation (SD). The significant differences between the groups were calculated using the analysis of variance (ANOVA) and the Bonferroni's test as indicated, in which $p < 0.05$ was considered statistically significant.

RESULTS

Preparation and characterization of nanoparticles

Figure 1a shows the results of the nanoparticles prepared for emulsification-solvent evaporation method, using a concentration of PLGA 1.0% and PVA 0.5%, with solvent ratio DCM: ACE 25:75 (v/v). Nanoparticles were prepared as CVDL-free nanoparticles (NP) and nanoparticles in different CVDL: copolymer ratios (NP CVDL 1:10, NP CVDL 1:5, and NP CVDL 1:2.5) (Fig. 1a). The nanoparticles showed the formation of the smallest particles (209.1 ± 2.03 nm at 373.4 ± 19.3 nm, desirable values of zeta potential (− 2.0 ± 4.2 mV at − 5.7 ± 1.3 mV) and polydispersity index (0.137 ± 0.01 at 0.248 ± 0.07). The highest drug loading efficiency (95.06 ± 0.4%) was observed for the nanoparticle containing CVDL:PLGA weight-ratio of 1:10, which corresponds to a final drug concentration in the nanoparticle of 1 mg/mL. CHOL was inserted as functionalizing substance in this best drug:polymer ratio. The results obtained are shown in Table 1. A slight increase in particle size was observed when NP CVDL (227.3 ± 9.07 nm) and NP CVDL CHOL were compared (234.7 ± 18.7 nm), and a consequent decrease in encapsulation efficiency (95.06 ± 0.4 at 37.45 ± 1.8)

Nanoparticles	Diameter (nm) ± SD	PDI (nm) ± SD	ZP (mV) ± SD	EE% ± SD
NP	209.1 ± 2.03	0.137 ± 0.01	-1.03 ± 0.2	-
NP CVDL	227.3 ± 9.07	0.223 ± 0.03	-2.04 ± 0.2	95.06 ± 0.4
NP CVDL CHOL	234.7 |± 18.7	0.081 ± 0.01	2.08 ± 0.1	37.45 ± 1.8

Table 1. Results of diameter, polydispersity index, zeta potential and encapsulation efficiency in the analysis of the chosen nanoparticles.

Notes: PDI (Polydispersity Index), nm (Nanometer), Standard Deviation (SD), Millivolt (mV).

RESULTS

Preparation and characterization of nanoparticles

The AFM images (Fig. 1) assessed topography aspects such as the shape and the surface of particles. The 2D images were obtained for the nanoparticles without drug (Fig. 1(B1)), the nanoparticle with drug in the proportion of 1:10 (Fig. 1(B2)), and the nanoparticle with drug and CHOL were observed in 2D and 3D images, respectively (Fig. 1(B3, B4)). Both drug-free, drug-containing nanoparticles and drug-containing functionalized nanoparticles showed slightly spherical shapes with smooth and uniform surfaces.

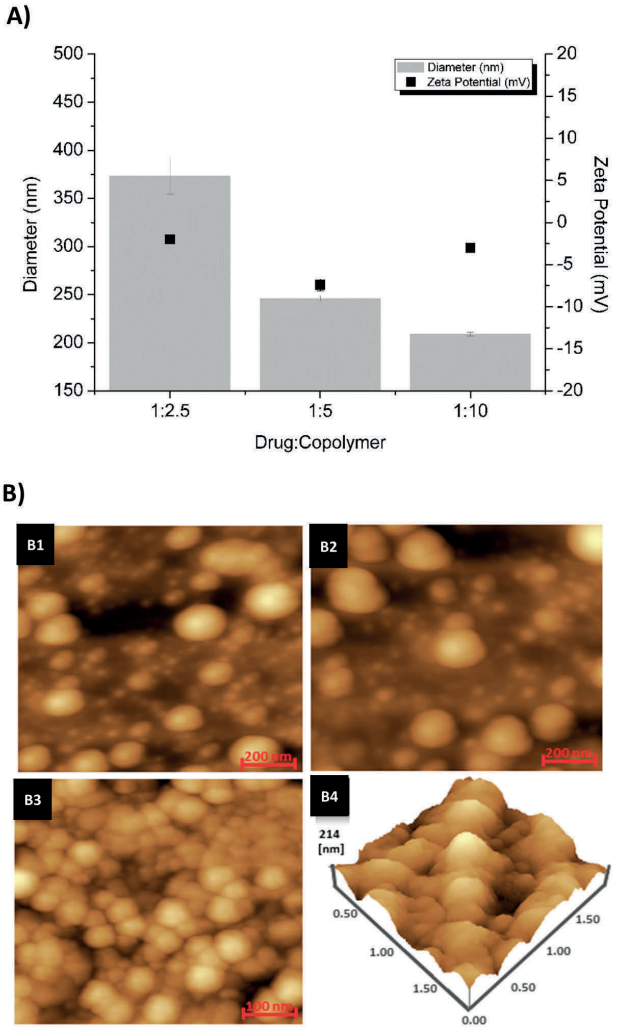

Figure 1. Mean diameter and zeta potential as a function of concentration of the drug: PLGA copolymer. b AFM images of (B1) NP, (B2) NP CVDL, and (B3, B4) NP CHOL in 2D and 3D respectively.

Fig. 2: a ATR-FTIR spectra for pure compounds (CVDL, PLGA, and CHOL) and nanoparticles (NP, NP CVDL, and NP CHOL). b Experimental *in vitro* release profile from CVDL solution and nanoparticles CVDL content (NP CDVL and NP CHOL). c Physicochemical stability is expressed in mean diameter and zeta potential as a function of storage time for the drug-free nanoparticles (NP) and drug-loaded nanoparticles (NP CVDL and NP CHOL). Note: The data are expressed as mean ± standard deviation (SD) (n = 3)

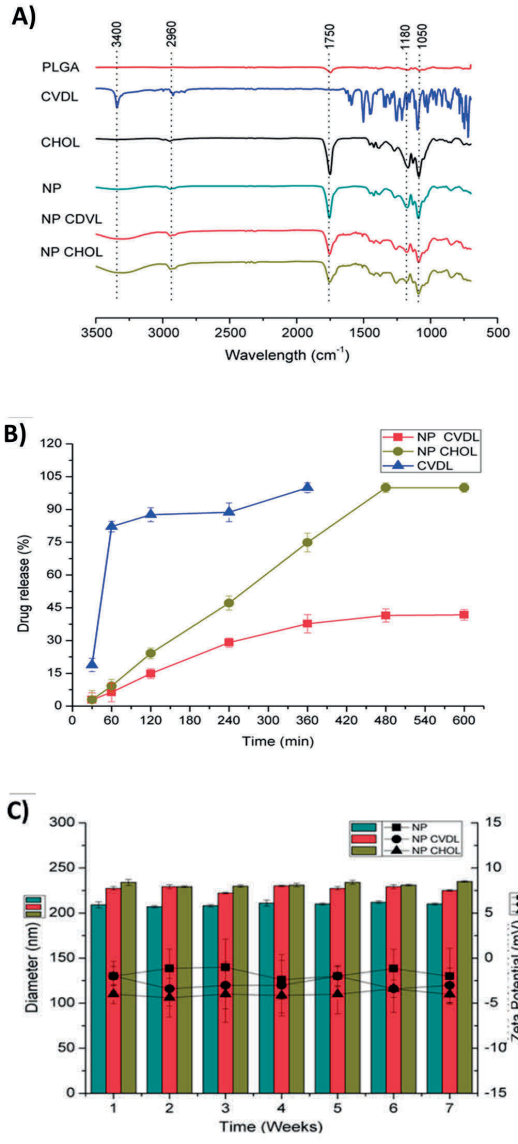

Figure 2 a shows the comparisons of the ATR-FTIR spectrum bands for the pure compounds (CVDL, PLGA, and CHOL), for the drug-free nanoparticle (NP), for the nanoparticle with the drug (NP CVDL), and for the functionalized nanoparticle with the drug (NP CVDL CHOL). The result was presented mainly comparing the bands of the nanoparticle with drug with the bands of the pure compounds, still highlighting the behavior of the functionalized nanoparticles. Carvedilol showed N–H peak of aromatic amines at 3400 cm−1 and weak peak of angular deformation N–H bonds at 1.580 cm−1 used to characterize secondary amines of the drug structure. It is possible to observe peaks of aliphatic C–H between 2960 and 2850 cm−1, while bands of C=C vibrations of aromatic nuclei are observed between 1600 and 1450 cm−1. The isolated PLGA showed characteristic absorption peaks with significant N–C stretch peaks close to 1300 cm−1 and C=O monomeric peaks of the carboxylic acid at about 1750 cm−1. The CHOL spectrum alone shows a broad band

RESULTS
Preparation and characterization of nanoparticles

between 3250 and 3500 cm−1 due to the elongation vibration of the O–H bond. The NP, NP CVDL, and NP CVDL CHOL specters were also compared (Fig.2a). In the spectrum of NPs, the peaks in the region of 1750 cm−1, 1180 cm−1, and 1050 cm−1 stand out, respectively, corresponding to monomeric peaks of the C=O, aliphatic peaks of the C–N and C–O peaks present in the aromatic group.

Figure 2 b shows the release profile of CVDL and distinct formulations of the CVDL-loaded polymeric nanoparticles. The successful drug efficiency in the PLGA nanoparticles, previously demonstrated, assured the desired slow release rate for all formulations (Danhier et al. 2012; Hans and Lowman 2002; Lee et al. 2016). We further subjected the data to four different diffusion kinetic linear models, which include the first-order model, the Bhaskar model, the modified Freundlich model, and parabolic model [Araújo et al.]. The calculated parameters are shown in Table 2. In these equations, Mt/M∞, t, and k correspond to the fractional drug release, release time and release rate constant, respectively. The a is a constant whose chemical significance is not clearly resolved. The Bhaskar model showed the best correlation (R = 0.96 ± 0.02 to 0.97 ± 0.02) for all

Formu-lations	Kinetic Match			
a (R ± DS)	First order	Bhaskar	Freundlich	Parabolic Diffusion
NP CVDL	0.0059 h^{-1} (0.91 ± 0.02)	0.52 $h^{0.65}$ (0.97 ± 0.02)	42.16 h (0.92 ± 0.03)	1.26 $h^{-0.5}$ (0.59 ± 0.03)
NP CVDL CHOL	0.0059 h^{-1} (0.90 ± 0.03)	0.52 $h^{0.65}$ (0.96 ± 0.02)	50.43 h (0.93 ± 0.03)	0.30 $h^{-0.5}$ (0.47 ± 0.03)

Table 2. Fitting parameters of different kinetic models applied for the *in vitro* CVDL release from PLGA nanoparticles.

formulations.

The physicochemical stability test was performed to monitor the time-dependent changes in the NP, NP CVDL, and NP CVDL CHOL. The analysis intervals were 7 days (for 7 weeks). The performed tests were of particle size, polydispersity index, and zeta potential, as shown in Fig. 2c. Analyses from the first to the seventh week particle size for NP values ranged from ~ 209 to 213 nm, and the PDI values ranged from ~ 0.130 to 0.165 nm. The particle size for NP CVDL ranged from ~ 227 to 233 nm and the PDI values ranged from ~ 0.223 to 0.229 nm. The particle size for NP CVDL CHOL ranged from ~ 234 to 239 nm and the PDI values ranged from ~ 0.081 to 0.109 nm. The zeta potential for all formulations ranged from ~ − 2 to − 4 mV.

In vitro anti-CRC studies

The results obtained with MTS assay showed that after the time points treatment with free CVDL, NP, NP CVDL, and NP CVDL CHOL, the proliferation of the CRC cell line CT-26 was compared with the negative control. The NP treatment did not alter the cell line viability after 24 h and 48 h (Fig. 3a, b).

After 24 h of treatment, CVDL (3.12 μg/mL and 6.25 μg/mL) decreased the proliferation rate of CT-26, $p < 0.01$ and $p < 0.05$, respectively. NP CVDL CHOL also showed the same result in a lower dose (0.78 μg/ mL, $p < 0.01$) (Fig. 3a). There was a decrease in the CT- 26 cell viability when NP CVDL was used in 0.35 μg/ mL ($p < 0.05$), 1.56 μg/mL, ($p < 0.0001$), 3.12 μg/mL ($p < 0.0001$), and 6.25 μg/mL ($p < 0.0001$) doses for 48 h. Free CVDL and NP CVDL CHOL presented similar activity after 48 h by reducing the proliferation of the tumor line with the same statistical value ($p < 0.0001$) at 0.78 μg/mL, 1.56 μg/mL, 3.12 μg/mL, and 6.25 μg/mL concentrations (Fig. 3b).

According to the flow cytometry, Fig. 2 shows the percentage of cell death of the treatments with free CVDL, NP CVDL, and NP CVDL CHOL (0.35 μg/ mL, 0.78 μg/mL, 1.56 μg/mL) for 24-h or 48-h treatment when compared with the negative control. The percentage is the sum of Annexin V-FITC-positive/ DAPI-negative and Annexin V-FITC-positive/DAPI- positive cells. Dot plots of flow cytometry for 24 (A) hours and 48 h (B) are shown in supplementary material.

RESULTS
In vitro anti-CRC studies

All the samples presented antitumor activity in both time points. After 24 h, the treatment at 0.35 μg/mL concentration increased the total death with CVDL ($p < 0.001$), NP CVDL ($p < 0.0001$), and NP CVDL CHOL ($p < 0.0001$). The NP CVDL also increased the total death at 0.78 μg/mL, $p < 0.05$ (Fig. 3c). When treatment time was increased to 48 h, the quantity of death also increased, in which CVDL 0.78 μg/mL induced cell death ($p < 0.0001$), as well as NP CDVL and NP CVDL CHOL for the three doses used ($p < 0.0001$) (Fig. 3d).

When free CVDL with NP CVDL and NP CVDL CHOL at the same concentration is compared, it is observed that there is a difference between antitumor activity of the nanoconjugates and the free CVDL. An increase in this activity for the three evaluated concentrations was observed at 48 h (Fig. 3e). The p values for this comparison are as follows: (i) for 0.35 μg/mL, CVDL vs NP CVDL ($p < 0.0001$) and CVDL vs NP CVDL CHOL ($p < 0.0001$); (ii) for 0.78 μg/mL, CVDL vs NP CVDL ($p < 0.0001$) and CVDL vs NP CVDL CHOL ($p < 0.0001$); and (iii) for 1.56 μg/mL, CVDL vs NP CVDL ($p < 0.01$) and CVDL vs NP CVDL CHOL ($p < 0.0001$) (Fig. 3e).

Fig. 3: Antitumor activity of nanoparticles in CT-26 cells. a, b Mean cell viability of CT-26 cells treated with CVDL, NP, NP CVDL, and NP CVDL CHOL for 24 h (a) and 48 h (b). The concentrations used were as follows: 0.35 μg/mL, 0.78 μg/mL, 1.56 μg/mL, 3.12 μg/mL, and 6.2 μg/mL. All treatment groups were compared with the negative control group (****$p < 0.0001$, **$p < 0.01$, *$p < 0.05$). c, d The mean cell death statistic of the treatments of free CVDL, NP CVDL, and NP CVDL CHOL at CT-26 cells at 24 h (c) and 48 h (d) when compared with the negative control (*$p < 0.05$, ***$p < 0.001$, and ****$p < 0.0001$). Negative control and 25% DMSO were used. The concentrations of CVDL, NP CVDL, and NP CVDL CHOL used were as follows: 0.35 μg/mL, 0.78 μg/mL, and 1.56 μg/mL. e Comparison between CVDL, NP CVDL, and NP CVDL CHOL at the concentrations 0.35 μg/mL, 0.78 μg/mL, and 1.56 μg/mL. The duration of treatment of CT-26 cells was 48 h (**$p < 0.01$ and ****$p < 0.0001$)

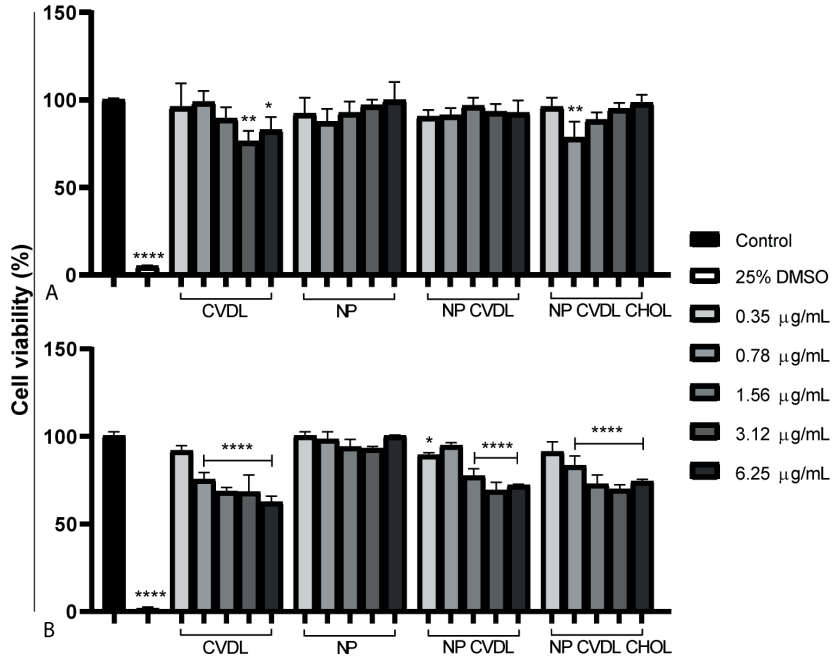
Cell viability (%)
150
100
50
0
A
B
****
**
*
CVDL
NP
NP CVDL
NP CVDL CHOL
Control
25% DMSO
0.35 μg/mL
0.78 μg/mL
1.56 μg/mL
3.12 μg/mL
6.25 μg/mL

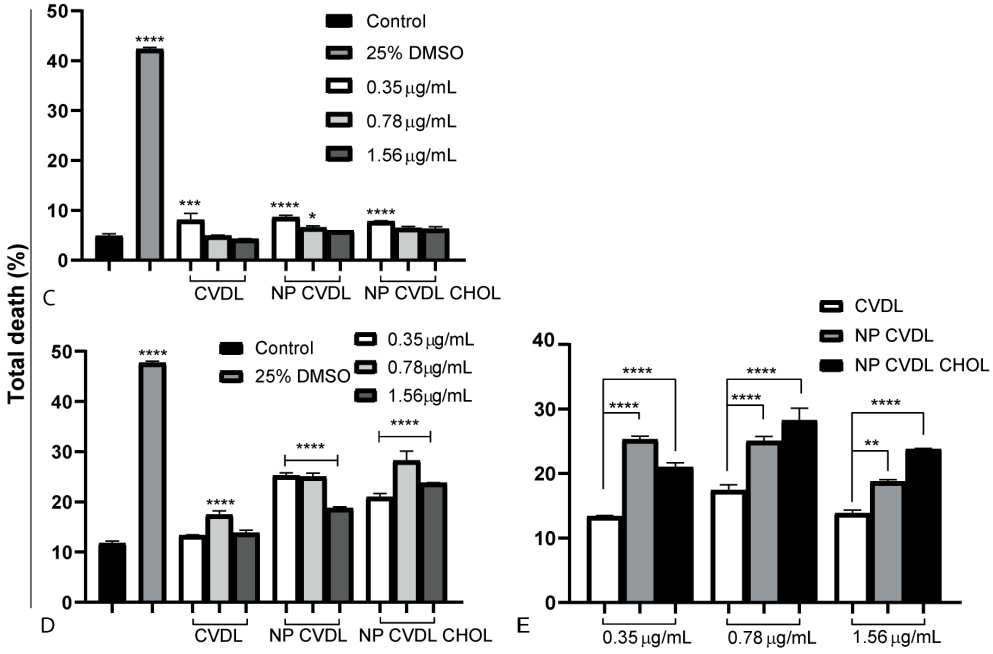
Total death (%)
50
40
30
20
10
0
C
D
E
Control
25% DMSO
0.35 μg/mL
0.78 μg/mL
1.56 μg/mL
***
****
*
CVDL
NP CVDL
NP CVDL CHOL

RESULTS

In vivo inflammation and oxidative stress studies

Global leukocyte counting was used in this study to evaluate the leukocyte migration to the injury sites. As shown in Fig. 4a, every tested treatment proved to be efficient in reducing the inflammation in comparison with the positive control group ($p < 0.0001$). No significant difference was observed when the NP groups were compared with the gold standard treatment group (diclofenac) and CVDL 3 mg/kg ($p > 0.05$). There was no difference among the NP group and the NP CVDL and NP CVDL CHOL combination groups in this parameter.

GSH levels (Fig. 4b) were higher in all the treated groups than in the positive control group ($p < 0.0001$), proving that PLGA is involved in antioxidant processes. Interestingly, NP lead to higher GSH levels than the NP CVDL ($p < 0.0001$), but the addition of CHOL seems to boost the antioxidant effects of NP, since no difference was observed between NP group and the NP CVDL CHO (0.05 mg/kg) group ($p > 0.05$), whereas the levels were higher in the NP CVDL CHOL (0.1 mg/kg) and NP CVDL CHOL (0.3 mg/kg) ($p < 0.0001$).

MDA is a secondary product of lipid peroxidation caused by oxidative stress. If there is an inflammatory process in course, MDA levels are expected to be increased, whereas GSH should remain low or decreased (Falcao et al. 2018). All tested treatments in this study were able to prevent oxidative stress and therefore MDA levels were kept low compared with the positive control (Fig. 4c) ($p < 0.0001$).

DISCUSSION

The nanoparticles obtained by the emulsification-solvent evaporation method showed the formation of small particles and desirable zeta potential values. Similar particle size results as in the paper about carvedilol- loaded solid lipid nanoparticles for intranasal drug delivery had already been obtained in later works, where a concentration of 0.5–2.5% surfactant obtained a particle size in the range 174.35 nm ± 1.34 to 492.40 nm ± 8.20 (Qi et al. 2013). The best results were obtained with

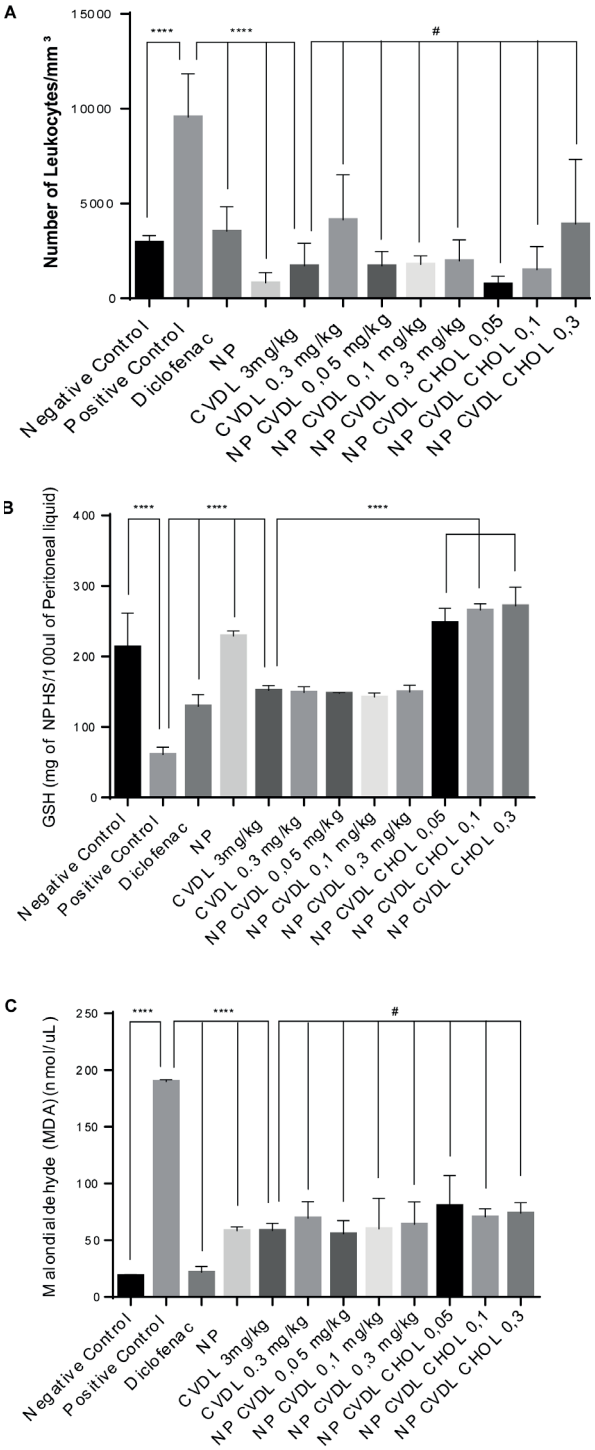

Fig. 4: a Number of leukocytes, b glutathione levels, and c malondialdehyde. ANOVA followed by Bonferroni's multiple comparisons test. ****$p < 0.0001$, #$p > 0.05$

particles smaller than 300 nm and are ideal because they are smaller and have better adsorption (Aboud et al. 2016). The zeta potential reflects the surface charge of the particles, and the use of PLGA as the main polymer dispersed in the organic phase gave us a negative zeta potential in all results as expected (Table 1). This can be explained by considering the anionic nature of the polymer (Némethová et al. 2017). The choice of three ratios of drug:copolymer is justified because factors such as the nature and concentration of the polymer in the organic phase, the polarities of the solvents, the nature and ratio of the internal/external phases, and the nature and concentration of the surfactants are essential. Therefore, it was necessary to choose which of the nanoparticles among the various ratios have the best results among such factors (Baena-Aristizábal et al. 2016). The highest drug loading efficiency was observed in the formulation containing CVDL:PLGA in the weight ratio of 1:10. Other papers dealing with carvedilol nanoparticles have shown incorporation efficiency of up to 97%, being slightly higher than ours. However, the drug amount used was greater than 1 mg/mL (Luxenhofer 2015). Thus, we had higher incorporation efficiency for the drug quantity. The drug proportion plays a critical role in determining drug loading, particle size, and particle size distribution, as well as the physical stability of the resulting products (El-Say et al. 2018). In this same reasoning, CHOL was incorporated as a functionalizing substance to increase the targeting for cancer cells, where there was a slight increase in particle size and a consequent decrease in encapsulation efficiency. Variations in particle size are indicative that there was an interaction between the copolymer and the drug. In addition, smaller particle size is also indicative of a larger surface area which directly reflects the encapsulation efficiency (de Oliveira et al. 2013).

The AFM images assed topography aspects such as the shape and the surface of particles. Comparisons of the images of CVDL-free nanoparticles with CVDL- loaded nanoparticles and drug-loaded functionalized nanoparticles confirmed that the drug loading did not affect the formation of sub 250-nm spherical nanoparticles, corroborating the particle size measurements performed by DLS. The analysis of the AFM tip over the surface of nanoparticles records the topography, elucidating the shape and giving information about the size and surface of particles after to desiccants the samples. The more spherical and uniform the particle

size, the better the release kinetics of the drug (Bazylińska et al. 2014; Doquet and Barkia 2016; M. Hoo et al. 2008).

By analyzing the infrared spectra of the nanoparticles, it is possible to observe slight shortening of peaks while adding drug and CHOL, as in the regions of 1750 cm−1, 1180 cm−1, and 1050 cm−1 which respectively corresponded to monomeric peaks of the C=O, derivative of PLGA. Peaks of the C–N aliphatic and C–O peaks were present in the aromatic group. These changes in the spectrum are indicative of the incorporation of CVDL as well as of CHOL to the nanoparticles.

The Bhaskar model explains that the drug release rate in the particles may be limited (1-MT/M ∞) Kb = t0.65 + b). This fact suggests that the drug release was controlled by diffusion dependent on the drug loading ratio from spherical particles (Gocalinska et al. 2015). This result also corroborates AFM data (Neupane et al. 2014). However, it is possible to observe that the systems show a controlled release for at least 600 min (although with a low percentage of release), differently from the drug that released 100% in the first minutes. Similar results were found in a work on CVDL-loaded solid lipid nanoparticles to improve the oral bioavailability, in which a maximal release of 25% of CVDL from the nanoparticles was found (Venishetty et al. 2012). Thus, our work brings even more favorable release results. In addition, the previous work does not address what kind of kinetic model causes release, which makes a difference. This capacity of nanoparticulate systems to maintain the entrapped drug into polymeric matrix in the release medium potentially improve the biological activity. This fact avoids the CVDL release before the nanoparticles arrive to the target cells, mainly considering the internalization of nanoparticles by endocytosis phenomena (Cheng et al. 2014; Lin et al. 2010; Son and Kim 2010).

Good results were obtained within the analysis in the stability study of the nanoparticles containing CVDL:PLGA at the 1:10 ratio and the nanoparticle without the drug (Fig. 2c). There were no significant variations between particle size and zeta potential values over the 7 weeks, as the zeta potential values remained positive without large variations and the particle size remained below 250 nm. Previous studies with nanoparticles generally do not report the physical stability of proposed formulations or just consider small intervals of hours or days. These results show that there

were no instability phenomena such as creaming, flocculation, sedimentation, phase separation, or coalescence (Binder et al. 2014; Grouchko et al. 2014).

The MTS viability assay is based on the ability of viable cells to transform a tetrazolium salt into a soluble formazan product through their mitochondrial activity (Malich et al. 1997). In this work, the antiproliferative activity of the samples after 24 h of incubation showed that the free CVDL (3.12 µg/mL and 6.25 µg/mL) and NP CVDL CHOL (0.78 µg/mL) were able to decrease the proliferation of tumor cells when compared with the control. Increasing the incubation time of the treatment (48 h) also increased the amount of non-viable cells.

All compounds induced cell death by flow cytometry at both treatment times, although the amount of total cell death was more significant after 48 h. This result confirms the data observed in the MTS, corroborating that the release of the drug by the nanoparticles occurs later (Liu et al. 2015). Low-dose CVDL (0.35 µg/mL) does not induce cell death when compared with control at 48 h, whereas NP CVDL and NP CVDL CHOL induce cell death; this outcome is an important finding which can prevent side effects in future use as an antitumor agent. It may be possible to use less amount of CVDL when encapsulated in nanoparticles and thus reduce likely side effects when higher doses of the drug are used (Waghela et al. 2015). There is a difference between the amount of cell death when comparing the free CVDL and the nanoparticle systems at the same concentration (Fig. 3e). This result demonstrates the increased efficiency of the antitumor activity of CVDL when present in a functionalized system (Wang et al. 2018). NP CVDL CHOL showed greater efficiency in inducing cell death than NP CVDL at doses 0.78 µg/mL and 1.56 µg/mL at 48 h, and this data corroborates other works which showed the promising cholesterol-targeting characteristic (Kong et al. 2019; Lee et al. 2016; Li et al. 2018; Mazumdar et al. 2018).

Many studies have proven that PLGA is an efficient delivery system of different active components, mainly if functionalized with cholesterol (Lee et al. 2016; Mazumdar et al. 2018). In this study, the treatment with NP CVDL CHOL (0.05 mg/kg and 0.1 mg/kg) is more efficient in decreasing

leukocyte migration as well as increasing the GSH levels at all tested doses (0.05 mg/kg, 0.1, and 0.3 mg/kg) than free CVDL and NP CVDL. As shown in Fig. 4, NP CVDL or NP CVDL CHOL (0.05 mg/kg) show similar activity regarding leukocyte levels, MDA and GSH when these data are compared with free CVDL at a concentration of 3 mg/kg. Thus, using functionalized nanoparticles with CHOL decreased the amount of CVDL without compromising its anti-inflammatory and antioxidant effects. These results suggest that PLGA nanoparticles functionalized with cholesterol can enhance the cellular uptake of pharmacological compounds, preventing lipid peroxidation and leukocyte migration in inflammatory processes (Alqahtani et al. 2015; Astete et al. 2011; Nallamuthu et al. 2013; Pereira et al. 2018).

CONCLUSION

In this study, we successfully developed carvedilol-loaded polymeric nanoparticles and improved cell uptake of carvedilol as chemotherapy agent. Nanoparticles have shown suitable structure features as small and stable particles able to induce both the high encapsulation efficiency and the slow drug release profile for CVDL. The data presented indicates that the NP CVDL CHOL can be used as a drug carrier with promising antitumor, antioxidant, and anti-inflammatory activity.

APPENDIX TO CHAPTER 2

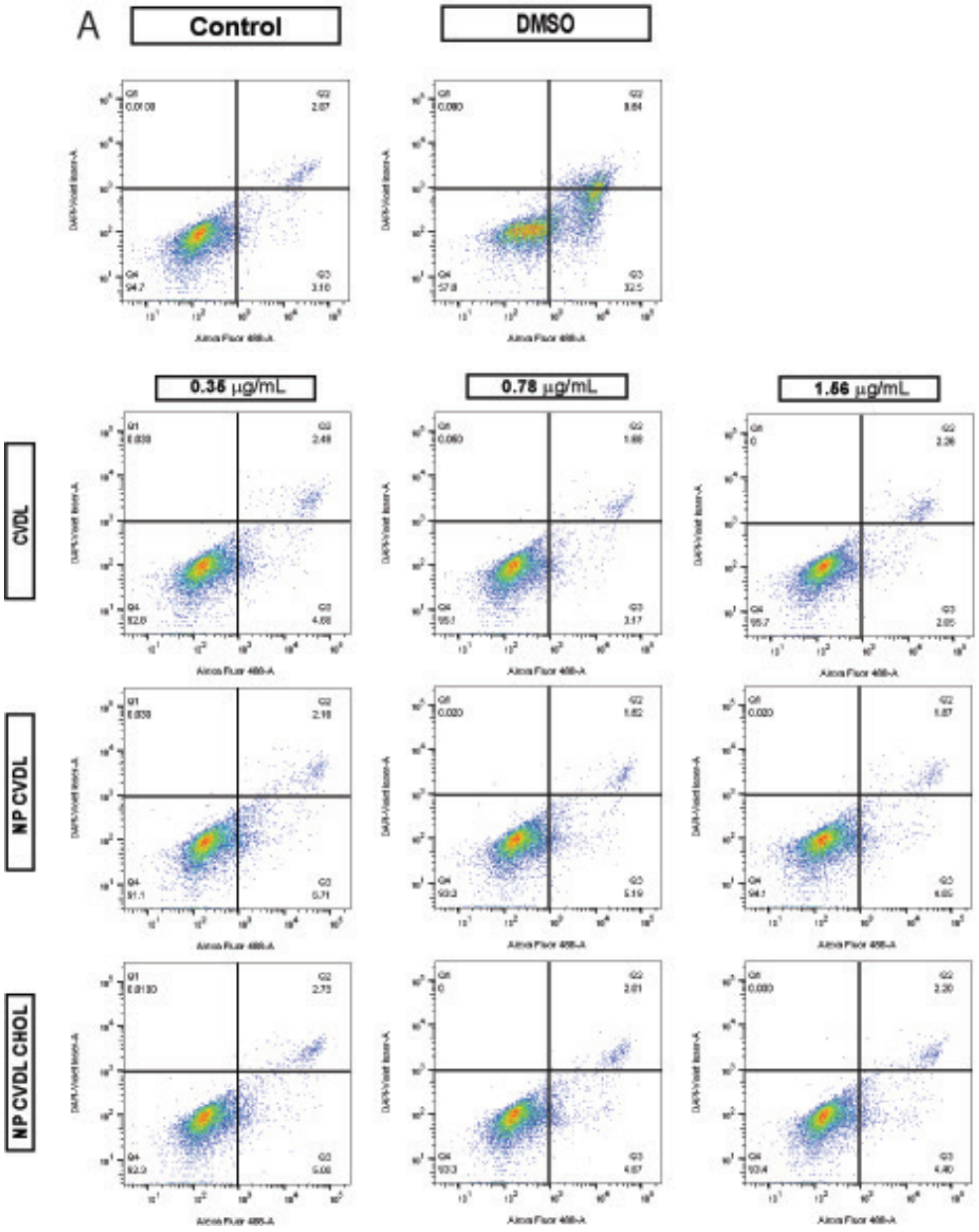

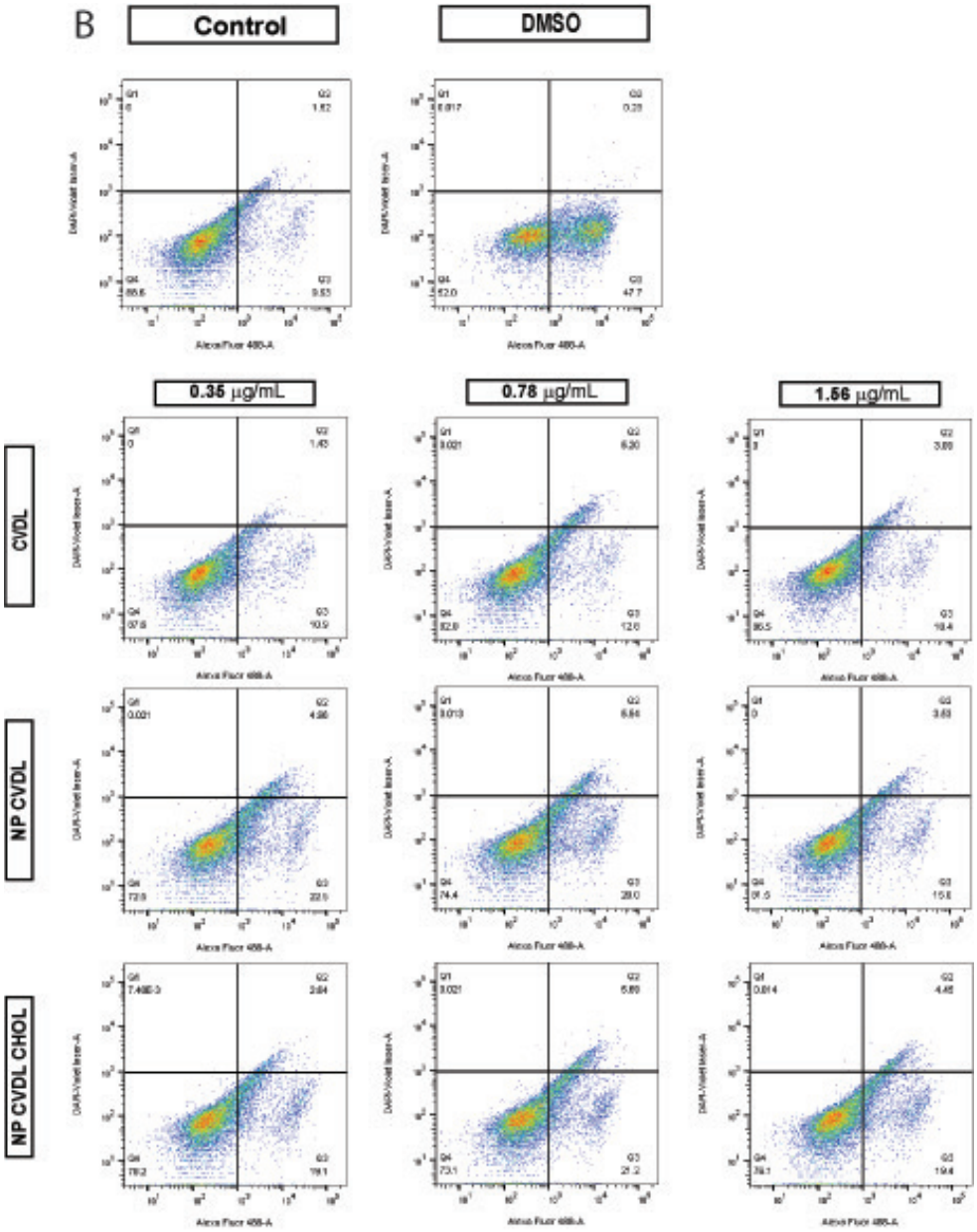
B
Control
DMSO
0.35 µg/mL
0.78 µg/mL
1.56 µg/mL
CVDL
NP CVDL
NP CVDL CHOL

REFERENCES

1. Aboud HM, El Komy MH, Ali AA, El Menshawe SF, Abd Elbary A (2016) Development, optimi zation, and evaluation of carvedilol-loaded solid lipid nanoparticles for intranasal drug delivery AAPS. Pharm Sci Tech 17:1353–1365. https://doi. org/10.1208/s12249-015-0440-8.
2. Alqahtani S et al (2015) Cellular uptake, antioxidant and antiproliferative activity of entrapped α-tocopherol and γ- tocotrienol in poly (lactic-co-glycolic) acid (PLGA) and chitosan covered PLGA nanoparticles (PLGA-Chi). J Colloid Interface Sci 445:243–251. https://doi.org/10.1016/j. jcis.2014.12.083.
3. Anderson ME (1985) Determination of glutathione and glutathione disulfide in biological samples. Methods Enzymol 113: 548–555.
4. Araújo Júnior RF, Garcia VB, RFdC L, GAdC B, EdC M, PMM G, de Araújo AA (2016) Carvedilol improves inflammatory response, oxidative stress and fibrosis in the alcohol-induced liver injury in rats by regulating Kuppfer cells and hepatic stellate cells. PLoS One 11:e0148868. https://doi. org/10.1371/journal.pone.0148868.
5. Areti A, Komirishetty P, Kumar A (2017) Carvedilol prevents functional deficits in peripheral nerve mitochondria of rats with oxaliplatin-evoked painful peripheral neuropathy. Toxicol Appl Pharmacol 322:97–103. https://doi. org/10.1016/j.taap.2017.03.009.
6. Astete CE, Dolliver D, Whaley M, Khachatryan L, Sabliov CM (2011) Antioxidant poly(lactic-co-gly colic) acid nanoparticles made with alpha-tocopherol-ascorbic acid surfactant. ACS Nano 5:9313–9325. https://doi.org/10.1021/nn102845t.
7. Baena-Aristizábal CM, Fessi H, Elaissari A, Mora-Huertas CE (2016) Biodegradable microparticles preparation by double emulsification—solvent extraction method: a systematic study. Colloids Surf A Physicochem Eng Asp 492:213– 229. https://doi.org/10.1016/j.colsurfa.2015.11.067.
8. Bahrami B, Hojjat-Farsangi M, Mohammadi H, Anvari E, Ghalamfarsa G, Yousefi M, Jadidi-Ni aragh F (2017) Nanoparticles and targeted drug delivery in cancer therapy. Immunol Lett 190:64–83. https://doi.org/10.1016/j. imlet.2017.07.015.
9. Balaha M, Kandeel S, Barakat W (2016) Carvedilol suppresses circulatin g a nd hepati c IL-6 responsible for hepatocarcinogenesis of chronically damaged liver in rats. Toxicol Appl Pharmacol 311. https://doi.org/10.1016/j. taap.2016.10.012.
10. Bazylińska U, Lewińska A, Lamch Ł, Wilk KA (2014) Polymeric nanocapsules and nanospheres for encapsulation and long sustained release of hydrophobic cyanine-type photosensitizer. Colloids Surf A Physicochem Eng Asp 442:42–49. https://doi.org/10.1016/j.colsurfa.2013.02.023.
11. Binder K, Virnau P, Statt A (2014) Perspective: the Asakura Oosawa model: a colloid prototype for bulk and interfacial phase behavior. J Chem Phys 141:140901. https://doi. org/10.1063/1.4896943.
12. Cheng Y, Morshed R, Auffinger B, Tobias AL, Lesniak MS (2014) Multifunctional nanoparticles for brain tumor diagnosis and therapy Adv Drug Deliv Rev 0:42–57 doi:https://doi. org/10.1016/j. addr.2013.09.006, 66.
13. Choi DG, Venkatesan J, Shim MS (2019) Selective anticancer therapy using pro-oxidant drug-loaded chitosan-fucoidan nanoparticles. Int J Mol Sci 20:20. https://doi.org/10.3390/ ijms20133220
14. Coussens LM, Werb Z (2002) Inflammation and cancer. Nature 420:860–867. https://doi. org/10.1038/nature01322
15. Danhier F, Ansorena E, Silva JM, Coco R, Le Breton A, Preat V (2012) PLGA-based nanopar ticles: an overview of biomedi- cal applications. J Control Release 161:505–522. https://doi. org/10.1016/j.jconrel.2012.01.043

16. De Araujo RF Jr et al (2018) Apoptosis in human liver carcinoma caused by gold nanoparticles in combination with carvedilol is mediated via modulation of MAPK/Akt/mTOR pathway and EGFR/FAAD proteins. Int J Oncol 52:189–200. https://doi.org/10.3892/ijo.2017.4179
17. de Oliveira AM, Jäger E, Jäger A, Stepánek P, Giacomelli FC (2013) Physicochemical aspects behind the size of biodegradable polymeric nanoparticles: a step forward. Colloids Surf A Physicochem Eng Asp 436:1092–1102. https://doi. org/10.1016/j.colsurfa.2013.08.056
18. Doquet V, Barkia B (2016) Combined AFM, SEM and crystal plasticity analysis of grain boundary sliding in titanium at room temperature. Mech Mater:103–127. https://doi. org/10.1016/j. mechmat.2016.09.001
19. dos Santos Silva AM et al (2019) Hydrophilic and hydrophobic polymeric benznidazole-loaded nanoparticles: physicochemical properties and *in vitro* antitumor efficacy. Journal of Drug Delivery Science and Technology 51:700–707. https://doi.org/10.1016/j.jddst.2019.04.005
20. dos Santos-Silva AM, de Caland LB, de ALC SLO, de Araújo- Júnior RF, Fernandes-Pedrosa MF, Cornélio AM, da Silva- Júnior AA (2017) Designing structural features of novel benznida zole-loaded cationic nanoparticles for inducing slow drug release and improvement of biological efficacy. Mater Sci Eng C 78:978–987. https://doi.org/10.1016/j. msec.2017.04.053
21. Dos Santos-Silva AM et al (2019) Self-assembled benznidazole- loaded cationic nanoparticles containing cholesterol/sialic acid: physicochemical properties, *in vitro* drug release and *in vitro* anticancer efficacy. Int J Mol Sci 20. https://doi. org/10.3390/ijms20092350
22. El-Hammadi MM, Delgado ÁV, Melguizo C, Prados JC, Arias JL (2017) Folic acid-decorated and PEGylated PLGA nanoparticles for improving the antitumour activity of 5-fluorouracil. Int J Pharm 516:61–70. https://doi.org/10.1016/j. ijpharm.2016.11.012
23. Elinav E, Nowarski R, Thaiss CA, Hu B, Jin C, Flavell RA (2013) Inflammation-induced cancer: crosstalk between tumours, immune cells and microorganisms. Nat Rev Cancer 13: 759–771. https://doi.org/10.1038/nrc3611
24. El-Say K, Hosny KM, Alkhalidi H (2018) Quality by design approach to screen the formulation and process variables influencing the characteristics of carvedilol solid lipid nanoparticles. J Drug Deliv Sci Technol:45–168. https://doi. org/10.1016/j.jddst.2018.03.010
25. Esterbauer H, Cheeseman KH (1990) Determination of aldehydic lipid peroxidation products: malonaldehyde and 4- hydroxynonenal. Methods Enzymol 186:407–421
26. Falcao TR et al (2018) Crude extract and fractions from Eugenia uniflora Linn leaves showed anti-inflammatory, antioxidant, and antibacterial activities. BMC Complement Altern Med 18:84. https://doi.org/10.1186/s12906-018-2144-6
27. Félix L et al (2017) Carvedilol exacerbate gentamicin-induced kidney mitochondrial alterations in adult rat. Exp Toxicol Pathol 69:83–92. https://doi.org/10.1016/j.etp.2016.11.006
28. Ghuman S et al (2017) Serum inflammatory markers and colorectal cancer risk and survival. Br J Cancer 116:1358–1365. https://doi.org/10.1038/bjc.2017.96
29. Gocalinska A, Manganaro M, Dimastrodonato V, Pelucchi E (2015) Evaluation of defect density by top-view large scale AFM on metamorphic structures grown by MOVPEvol 349. doi:https://doi. org/10.1016/j.apsusc.2015.05.070
30. Goyal R, Macri LK, Kaplan HM, Kohn J (2016) Nanoparticles and nanofibers for topical drug delivery. J Control Release 240:77–92. https://doi.org/10.1016/j.jconrel.2015.10.049
31. Grouchko M, Roitman P, Zhu X, Popov I, Kamyshny A, Su H, Magdassi S (2014) Merging of metal nanoparticles driven by selective wettability of silver nanostructures. Nat Commun 5: 2994. https://doi.org/10.1038/ncomms3994

32. Hans ML, Lowman A (2002) Biodegradable nanoparticles for drug delivery and targeting. Curr Opinion Solid State Mater Sci 6:319. https://doi.org/10.1016/S1359-0286(02)00117-1
33. Hoo CM, Starostin N, West P, Mecartney M (2008) A comparison of atomic force microscopy (AFM) and dynamic light scattering (DLS) methods to characterize nanoparticle size distribution. J Nanopart Res 10. https://doi.org/10.1007/s11051- 008-9435-7
34. Kapadia CH, Perry JL, Tian S, Luft JC, DeSimone JM (2015) Nanoparticulate immunotherapy for cancer. J Control Release 219:167– 180. https://doi.org/10.1016/j. jconrel.2015.09.062
35. Kong ZL, Kuo HP, Johnson A, Wu LC, Chang KLB (2019) Curcumin-loaded mesoporous silica nanoparticles markedly enhanced cytotoxicity in hepatocellular carcinoma cells. Int J Mol Sci:20. https://doi.org/10.3390/ijms20122918
36. Lee BK, Yun YH, Park K (2015) Smart nanoparticles for drug delivery: boundaries and opportu nities. Chem Eng Sci 125: 158–164. https://doi.org/10.1016/j.ces.2014.06.042
37. Lee J-J, Lee SY, Park J-H, Kim D-D, Cho H-J (2016) Cholesterol- modified poly(lactide-co-gly colide) nanoparticles for tumor- targeted drug delivery. Int J Pharm 509:483–491. https://doi.org/10.1016/j.ijpharm.2016.06.008
38. Li H, Tong Y, Bai L, Ye L, Zhong L, Duan X, Zhu Y (2018) Lactoferrin functionalized PEG-PLGA nanoparticles of shikonin for brain targeting therapy of glioma. Int J Biol Macromol 107:204–211. https://doi.org/10.1016/j. ijbiomac.2017.08.155
39. Lin J, Zhang H, Chen Z, Zheng Y (2010) Penetration of lipid membranes by gold nanoparticles: insights into cellular up- take, cytotoxicity, and their relationship. ACS Nano 4:5421– 5429. https://doi.org/10.1021/nn1010792
40. Liu P et al (2015) Development of alendronate-conjugated poly (lactic-co-glycolic acid)-dextran nanoparticles for active targeting of cisplatin in osteosarcoma. Sci Rep 5:17387– 17387. https://doi.org/10.1038/srep17387
41. *In vitro* cytotoxicity of 20 chemicals using human cell lines. Toxicology 124:179–192. https://doi.org/10.1016/S0300- 483X(97)00151-0
42. Masloub SM, Elmalahy MH, Sabry D, Mohamed WS, Ahmed SH (2016) Comparative evaluation of PLGA nanoparticle delivery system for 5-fluorouracil and curcumin on squamous cell carcinoma. Arch Oral Biol 64:1–10. https://doi.org/10.1016/j.archoralbio.2015.12.003
43. Mazumdar S, Italiya KS, Sharma S, Chitkara D, Mittal A (2018) Effective cellular internalization, cell cycle arrest and improved pharmacokinetics of tamoxifen by cholesterol based lipopolymeric nanoparticles. Int J Pharm 543:96–106. https://doi.org/10.1016/j.ijpharm.2018.03.022
44. Milling L, Zhang Y, Irvine DJ (2017) Delivering safer immunotherapies for cancer. Adv Drug Deliv Rev 114:79–101. https://doi.org/10.1016/j.addr.2017.05.011
45. Nallamuthu I, Parthasarathi A, Khanum F (2013) Thymoquinone- loaded PLGA nanoparticles: antioxidant and anti-microbial properties vol 2. doi:https://doi.org/10.3329/icpj.v2 i12.17017
46. Némethová V et al (2017) Intracellular uptake of magnetite nanoparticles: a focus on physi co-chemical characterization and interpretation of *in vitro* data. Mater Sci Eng C 70:161–168. https://doi.org/10.1016/j.msec.2016.08.064
47. Neupane YR, Srivastava M, Ahmad N, Kumar N, Bhatnagar A, Kohli K (2014) Lipid based nanocarrier system for the potential oral delivery of decitabine: formulation design, character ization, ex vivo, and *in vivo* assessment. Int J Pharm 477:601–612. https://doi.org/10.1016/j.ijpharm.2014.11.001
48. Ng SF, Rouse JJ, Sanderson FD, Meidan V, Eccleston GM (2010) Validation of a static Franz diffusion cell system for *in vitro* permeation studies. AAPS PharmSciTech 11:1432–1441. https://doi.org/10.1208/s12249-010-9522-9

49. Pereira MC et al (2018) Effect of nanoencapsulation using PLGA on antioxidant and antimi crobial activities of guabiroba fruit phenolic extract. Food Chem 240:396–404. https://doi.org/10.1016/j.foodchem.2017.07.144
50. Pooja D, Tunki L, Kulhari H, Reddy BB, Sistla R (2016) Optimization of solid lipid nanoparticles prepared by a single emulsification-solvent evaporation method. Data Brief 6:15– 19. https://doi.org/10.1016/j.dib.2015.11.038
51. Qi F, Zhang X, Li S (2013) A novel method to get methotrexatum/ layered double hydroxides intercalation compounds and their release properties. J Phys Chem Solids 74:1101–1108. https://doi.org/10.1016/j.jpcs.2013.03.005
52. Ramalho MJ, Sevin E, Gosselet F, Lima J, Coelho MAN, Loureiro JA, Pereira MC (2018) Recep tor-mediated PLGA nanoparticles for glioblastoma multiforme treatment. Int J Pharm 545: 84–92. https://doi.org/10.1016/j.ijpharm.2018.04.062
53. Ramezanpour M, Leung SSW, Delgado-Magnero KH, Bashe BYM, Thewalt J, Tieleman DP (2016) Computational and experimental approaches for investigating nanoparticle-
54. Luxenhofer R (2015) Polymers and nanomedicine: considerations on variability and repro ducibility when combining complex systems. Nanomedicine (Lond) 10:3109–3119. https://doi.org/10.2217/nnm.15.139
55. Malich G, Markovic B, Winder C (1997) The sensitivity and specificity of the MTS tetrazolium assay for detecting the *in vitro* cytotoxicity of 20 chemicals using human cell lines. Toxicology 124:179–192. https://doi.org/10.1016/S0300- 483X(97)00151-0
56. Masloub SM, Elmalahy MH, Sabry D, Mohamed WS, Ahmed SH (2016) Comparative evaluation of PLGA nanoparticle delivery system for 5-fluorouracil and curcumin on squamous cell carcinoma. Arch Oral Biol 64:1–10. https://doi.org/10.1016
57. /j.archoralbio.2015.12.003
58. Mazumdar S, Italiya KS, Sharma S, Chitkara D, Mittal A (2018) Effective cellular internalization, cell cycle arrest and improved pharmacokinetics of tamoxifen by cholesterol based lipopolymeric nanoparticles. Int J Pharm 543:96–106. https://doi.org/10.1016/j.ijpharm.2018.03.022
59. Milling L, Zhang Y, Irvine DJ (2017) Delivering safer immunotherapies for cancer. Adv Drug Deliv Rev 114:79–101. https://doi.org/10.1016/j.addr.2017.05.011
60. Nallamuthu I, Parthasarathi A, Khanum F (2013) Thymoquinone- loaded PLGA nanoparticles: antioxidant and anti-microbial properties vol 2. doi:https://doi.org/10.3329/icpj.v2 i12.17017
61. Némethová V et al (2017) Intracellular uptake of magnetite nanoparticles: a focus on physi co-chemical characterization and interpretation of *in vitro* data. Mater Sci Eng C 70:161–168. https://doi.org/10.1016/j.msec.2016.08.064
62. Neupane YR, Srivastava M, Ahmad N, Kumar N, Bhatnagar A, Kohli K (2014) Lipid based nanocarrier system for the potential oral delivery of decitabine: formulation design, character ization, ex vivo, and *in vivo* assessment. Int J Pharm 477:601–612. https://doi.org/10.1016/j.ijpharm.2014.11.001
63. Ng SF, Rouse JJ, Sanderson FD, Meidan V, Eccleston GM (2010) Validation of a static Franz diffusion cell system for *in vitro* permeation studies. AAPS PharmSciTech 11:1432–1441. https://doi.org/10.1208/s12249-010-9522-9
64. Pereira MC et al (2018) Effect of nanoencapsulation using PLGA on antioxidant and antimi crobial activities of guabiroba fruit phenolic extract. Food Chem 240:396–404. https://doi.org/10.1016/j.foodchem.2017.07.144
65. Pooja D, Tunki L, Kulhari H, Reddy BB, Sistla R (2016) Optimization of solid lipid nanoparticles prepared by a single emulsification-solvent evaporation method. Data Brief 6:15– 19. https://doi.org/10.1016/j.dib.2015.11.038

66. Qi F, Zhang X, Li S (2013) A novel method to get methotrexatum/ layered double hydroxides intercalation compounds and their release properties. J Phys Chem Solids 74:1101–1108. https://doi.org/10.1016/j.jpcs.2013.03.005
67. Ramalho MJ, Sevin E, Gosselet F, Lima J, Coelho MAN, Loureiro JA, Pereira MC (2018) Recep tor-mediated PLGA nanoparticles for glioblastoma multiforme treatment. Int J Pharm 545: 84–92. https://doi.org/10.1016/j.ijpharm.2018.04.062
68. Ramezanpour M, Leung SSW, Delgado-Magnero KH, Bashe BYM, Thewalt J, Tieleman DP (2016) Computational and experimental approaches for investigating nanoparticle-based drug delivery systems. Biochim Biophys Acta Biomembr 1858:1688–1709. https://doi.org/10.1016/j.bbamem.2016.02.028
69. Ribeiro RA, Flores CA, Cunha FQ, Ferreira SH (1991) IL-8 causes *in vivo* neutrophil migration by a cell-dependent mechanism. Immunology 73:472–477
70. Son S, Kim WJ (2010) Biodegradable nanoparticles modified by branched polyethylenimine for plasmid DNA delivery. Biomaterials 31:133–143. https://doi.org/10.1016/j. biomaterials.2009.09.024
71. Taniguchi K, Karin M (2018) NF-kappaB, inflammation, immunity and cancer: coming of age. Nat Rev Immunol 18:309– 324. https://doi.org/10.1038/nri.2017.142
72. Varan G, Öncül S, Ercan A, Benito JM, Ortiz Mellet C, Bilensoy E (2016) Cholesterol-targeted anticancer and apoptotic effects of anionic and polycationic amphiphilic cyclodextrin nano particles. J Pharm Sci 105:3172–3182. https://doi. org/10.1016/j.xphs.2016.06.021
73. Venishetty VK, Chede R, Komuravelli R, Adepu L, Sistla R, Diwan PV (2012) Design and evalu ation of polymer coated carvedilol loaded solid lipid nanoparticles to improve the oral bioavail ability: a novel strategy to avoid intraduodenal administration. Colloids Surf B: Biointerfaces 95:1–9. https://doi.org/10.1016/j.colsurfb.2012.01.001
74. Waghela BN, Sharma A, Dhumale S, Pandey SM, Pathak C (2015) Curcumin conjugated with PLGA potentiates sustainability, anti-proliferative activity and apoptosis in human colon carcinoma cells. PLoS One 10:e0117526–e0117526. https://doi.org/10.1371/journal.pone.0117526
75. Wang W, Chen T, Xu H, Ren B, Cheng X, Qi R, Liu H, Wang Y, Yan L, Chen S, Yang Q, Chen C (2018) Curcumin-loaded solid lipid nanoparticles enhanced anticancer efficiency in breast cancer. Molecules:23. https://doi.org/10.3390 /molecules23071578
76. West NR, McCuaig S, Franchini F, Powrie F (2015) Emerging cytokine networks in colorectal cancer. Nat Rev Immunol 15: 615–629. https://doi.org/10.1038/nri3896
77. Yao K, Zhang WW, Yao L, Yang S, Nie W, Huang F (2016) Carvedilol promotes mitochondrial biogenesis by regulating the PGC-1/TFAM pathway in human umbilical vein endothelial cells (HUVECs). Biochem Biophys Res Commun 470:961–966. https://doi.org/10.1016/j.bbrc.2016.01.089
78. Zhu M, Shi J, He Q, Zhang L, Chen F, Chen Y (2012) An emulsification-solvent evaporation route to mesoporous bioactive glass microspheres for bisphosphonate drug delivery. J Mater Sci 47:2256. https://doi.org/10.1007/s10853-011- 6037-z.

CHAPTER **THREE**

Ana Luiza C. de S. L. Oliveira, Raimundo Fernandes de Araújo Júnior*, Thaís Gomes de Carvalho, Alan B. Chan, Timo Schomann, Filippo Tamburini, Lioe-Fee de Geus-Oei and Luis J. Cruz*.

Effect of Oxaliplatin-Loaded Poly (d,L-Lactide-co-Glycolic Acid) (PLGA) Nanoparticles Combined with Retinoic Acid and Cholesterol on Apoptosis, Drug Resistance, and Metastasis Factors of Colorectal Cancer. Pharmaceutics.. Feb 2020. Doi: 10.3390/pharmaceutics12020193.

EFFECT OF OXALIPLATIN -LOADED POLY PLGA NANOPARTICLES COMBINED WITH RETINOIC ACID AND CHOLESTEROL ON APOPTOSIS, DRUG RESISTENCE, AND METASTASIS FACTORS OF COLORECTAL CANCER

Abstract: Apoptosis signaling pathways, drug resistance, and metastasis are important targets to develop new cancer treatments. We developed cholesterol-coated Poly(d,l-Lactide-co-Glycolic Acid) (PLGA) nanoparticles for effective encapsulation and delivery of retinoic acid and oxaliplatin to analyze their antitumor activity in colorectal cancer. The cell viability and proliferation of tumoral cells lines (CT-26 and SW-480) decreased when compared to control *in vitro* after treatment with the nanoparticles. In addition, apoptosis of CT-26 cells increased. Importantly, cytoprotection of nontumor cells was detected. Expression of pro-apoptotic proteins was upregulated, while anti-apoptotic proteins were downregulated either *in vitro* or *in vivo*. In addition, drug resistance and metastasis factors were downregulated *in vivo*. Human colorectal tumors that highly expressed BCL-2 and Ki-67 had a greater tendency towards death within 60 months. Our results show that loading oxaliplatin combined with retinoic acid and cholesterol in a nanoparticle formulation enables determination of optimal antitumor activity and subsequent treatment efficacy.

Keywords: PLGA nanoparticles; oxaliplatin; colorectal cancer; drug resistance; apoptosis

INTRODUCTION

Colorectal cancer (CRC) is the third most commonly occurring malignancy around the world with significant morbidity and mortality rates. Every year, 1.2 million people are diagnosed with CRC [1–4]. Evasion of apoptosis is one of the hallmarks of cancer, in general, and correlated to drug resistance and metastatic spread, which urges the development of new drugs [5–7]. Apoptosis occurs through the extrinsic pathway or intrinsic pathway. Both pathways converge at the activation of caspase-3, which then induces other caspases downstream of caspase-3 and eventually leads to apoptosis of the cancer cells [6,8].

Oxaliplatin (OXA) is used to treat CRC, in combination with other drugs. OXA binds to nucleophilic molecules and forms adducts that inhibit gene transcription [9,10]. Unfortunately, tumor resistance to OXA treatment is not uncommon and can occur via a mutation in the intrinsic apoptosis pathway, which results in metastatic spread [7,11]. In addition, toxic effects are also observed. Neurotoxicity through reversible sensory neuropathy or chronic cumulative neuropathy is frequently observed [12].

To overcome these limitations of OXA, a drug delivery system (DDS) that can increase efficacy and reduce adverse effects by increasing the circulation time and bioavailability of the drug can be used [13]. This would result in a high resistance to clearance and increased concentration of the drug in the target tissues, thus, requiring lower doses of drugs [14]. One of the most widely used DDSs is the biodegradable and biocompatible copolymer poly (d,l-lactic-co-glycolic acid) (PLGA) due to its metabolite monomers: Lactic acid and glycolic acid. This polymer is approved by the Food and Drug Administration (FDA) and the European Medicine Agency (EMA) in several clinically applied DDS [15]. Nanoparticles (NPs) are a form of DDS. The commonly utilized techniques for the preparation of NPs are the nanoprecipitation technique [16], the emulsification solvent extraction/evaporation method [17,18], the emulsification solvent diffusion [19,20], and the double emulsion solvent evaporation [21]. The choice of a particular method of encapsulation is mainly determined by the solubility and molecular stability of the drug. In this study, we prepared NPs made from PLGA using the emulsification solvent extraction/evaporation method.

Cholesterol (CHO) is involved in the endocytosis of materials as well as cancer proliferation and metastasis. Different types of cells have different

amounts of cholesterol in their membranes. This difference becomes clearer when comparing healthy cells with cancer cells. Cancer cells have a high proliferation rate. Thus, the membranes of these cells are synthesized rapidly, which requires more nutrients and leads to higher CHO content of the membrane [22,23].

Retinoic acid (RA) binds to the heterodimers of the retinoic acid receptor (RARs) and the retinoid X receptor (RXRs) present in the nuclear membrane of cancer cells, which leads to growth inhibition, differentiation, or apoptosis in these cells. Studies have shown that, when used in combination with chemotherapeutic agents such as OXA, those characteristics of RA lead to increased cytotoxicity and decreased side effects via synergistic action of therapeutic agents [24–26].

In this study, PLGA, OXA, CHO, and RA were combined to formulate distinct NPs for the delivery of drugs to targeted cells. It is expected that CHO-coated PLGA NPs have an enhanced tumor-targetability when compared to exclusive PLGA NPs. Therefore, the aim of the present work was to evaluate the biological efficacy of OXA against CRC cells when co-encapsulated with RA in CHO-coated PLGA NPs.

2. MATERIALS AND METHODS

2.1. Preparation of PLGA Nanoparticles

The PLGA NPs were synthesized using a solvent extraction/evaporation method [27,28]. We hypothesized the emulsification solvent extraction/evaporation technique could result in better encapsulation yield of hydrophilic (OXA) and hydrophobic (RA) molecules simultaneously. Briefly, 100 mg of PLGA (Corbion, Amsterdam, The Netherlands) were dissolved in 3 mL of dichloromethane (DCM). Depending on the PLGA NPs, the following substances were added: 20 mg of OXA (European Pharmacopoeia Reference Standards), 0.5 mg of IR-780 iodide (Sigma-Aldrich, St. Louis, MO, USA), and/or 20 mg of RA (Sigma-Aldrich, St. Louis, MO, USA). The solution containing the NPs constituents was added dropwise to 25 mL of aqueous 2.5% (w/v) polyvinyl alcohol (PVA) and emulsified using a sonicator (250 watt, Sonifier 250; Branson, Danbury, CT, USA). PVA acted as a surfactant molecule, which stabilized the emulsion nanoparticles, avoided aggregation, and prevented them

from coalescing with each other. In addition, PVA acted as an effective stabilization and the PVA surfactant molecules allowed us to achieve small particle size and narrow size distribution. A very low concentrations of PVA remained on the surface of nanoparticles [29]. The solution was transferred to a new vial that contained an air-dried solution of 20 mg CHO (Avati Polar Lipids, Alabaster, AL, USA), dissolved in 0.4 mL of chloroform, and homogenized by sonication. After evaporating the solvent, the NPs were collected by centrifugation and lyophilized for 3 days. The concentration of each encapsulated constituent was determined by reverse phase high-performance liquid chromatography (RP-HPLC), as described elsewhere [30,31].

2.2. Physicochemical Properties of PLGA NPs

PLGA NPs were characterized by average size, polydispersity index, and surface charge (zeta-potential) by dynamic light scattering. PLGA NP samples were measured for size using a Zetasizer (Nano ZS, Malvern Ltd., Worcestershire, UK), and were analyzed for surface charge by laser Doppler electrophoresis on the same device.

2.3. Atomic Force Microscope (AFM)

The shape and surface of PLGA NPs were visualized by AFM. The nanoparticle dispersion was deposited and left to dry overnight on the mica for analysis using a JPK NanoWizard® 3 NanoOptics AFM System (JPK BioAFM Business, Berlin, Germany) with intermittent contact mode cantilevers (70 kHz). Raw data (height (measured) trace) obtained from the microscope were processed with JPKSPM Data Processing software using the plane flattening algorithm.

2.4. Viability Assay

An initial screening was performed by adding free OXA (5 µg/mL, 10 µg/mL, 25 µg/mL, 50 µg/mL, 100 µg/mL, and 200 µg/mL) to the CT-26 plated in a 96-well plate. Then a second assay was performed using free OXA as well as all PLGA NPs formulation systems (Table 1) at

concentrations of 5 µg/mL, 10 µg/mL, and 25 µg/mL. Culture medium without drug (negative) and 25% DMSO (positive) were used as controls. After incubation for 24, 48, or 72 h, 20 µL/well of MTS [3-(4,5-dimethylthiazol-2-yl)- 5-(3-carboxymethoxyphenyl)-2-(4-sulfophenyl)-2H-tetrazolium, inner salt] (Promega Corporation, Madison, WI, USA) solution was added and incubated for 3 h. Absorbance was measured at 490nm.

Samples	Loading oxaliplatin efficiency (µg/mg NPs)	Loading retinoic efficiency (µg/mg NPs)	Size ± S.D. (nm)	PDI (Polydispersity Index)	Zeta potential ± S.D. (mV)
NPs 1 (OXA, RA)-CHO	44	40	801.7 ±165.4	0.598	-21.4 ±8.4
NPs 2 (OXA)-CHO	48	--	678.3 ±118.5	0.694	-25.8 ±15.9
NPs 3 (RA)-CHO	--	46	539.8 ±87.6	0.438	-28.5 ±16.1
NPs 4 (empty)-CHO	--	--	443.1 ±27.1	0.253	-23.6 ±9.13
NPs 5 (empty)	--	--	496.7 ±35.35	0.255	-28.8 ±8.6
NPs 6 (OXA)	55	--	391.5 ±60.53	0.182	-29.6 ±9.9
NPs 7 (OXA, RA)	46	44	505.6 ±64.30	0.199	-27.6 ±42.1

Table 1: Physicochemical properties of Poly(D,L-Lactide-co-Glycolic Acid) (PLGA) nanoparticles (NPs). Determination of retinoic acid (RA) and oxaliplatin (OXA) content, size distribution, and zeta-potential of PLGA NPs. Particles were characterized by Dynamic Light Scattering (DLS) and zeta-potential measurements. Particle size data represent the mean value ± standard deviation (SD) of dynamic light scattering data. Zeta-potential data represent the mean value ± SD of 10 readings. OXA and RA contents of PLGA NPs were determined by particle digestion and measured by reversed-phase high-performance liquid chromatography (RP-HPLC) analysis.

For SW-480 cells, Hoechst labelling and flow cytometric analysis were performed. The cells were cultured in a 96-well plate for 24 h. Next, free OXA (5 µg/mL, 25 µg/mL, 50 µg/mL), NPs 1, and NPs 2 (5 µg/mL, 25 µg/mL, 50 µg/mL) were added and incubated for 24 and 48 h. Afterwards, the cells were labelled with Hoechst, measured with a flow cytometer BD LSR II (BD Biosciences, San Jose, CA, USA) and analyzed with FlowJo (version 10.1, BD Life Sciences, Franklin Lakes, NJ, USA).

2.5. Detection of Cell Death and Proliferation by Flow Cytometry

CT-26 was arranged in 24-well plates and treated with free OXA and PLGA NPs (NPs 1, NPs 2, NPs 6, and NPs 7, 5 µg/mL and 25 µg/mL) for 24 and 48 h. For 3T3 cells, the same experimental design was performed during the 48 h of treatment. At each time point, the cells were labeled with Annexin V- fluorescein isothiocyanate (FITC) (BD Biosciences, San Jose, CA, USA) and 4,6-diamidino-2-phenylindole (DAPI) (Thermo Fisher Scientific, Cambridge, MA, USA), and analyzed with a flow cytometry.

For proliferation analyses, CT-26 and SW-480 cells were seeded in 12-well plates. The following day, the cells were treated with 25 µg/mL of free OXA and 5 µg/mL of PLGA NPs (NPs 1 and NPs 2) for 48 h. After treatment, the cells were incubated with the allophycocyanin (APC)-conjugated anti-mouse Ki-67 (1:100) (Thermo Fisher Scientific, Cambridge, MA, USA). The analyses were performed as described above.

2.6. Immunofluorescence, FADD, BCL-2, and Caspase-3 Activity

CT-26 cells and SW-480 cells were treated with OXA (5 µg/mL and 25 µg/mL) and PLGA NPs (NPs 1 and NPs 2, both 5 µg/mL) for 24 and 48 h. At each time point, CT-26 cells were incubated with the primary antibodies (Abcam, Burlingame, CA, USA), fas-associated protein with death domain (FADD) (ab24533), BCL-2 (ab32124), and caspase-3 (ab13847), and SW-480 cells were incubated with caspase-3 (ab13847). The primary antibody was detected with goat anti-rabbit Alexa Fluor 555 secondary antibody (ab150078; Abcam) and DAPI was used for

nuclear staining. Specimens were examined with a Leica DM5500 B fluorescence microscope, equipped with a Leica DFC365 FX digital camera. Digital images were acquired and stored using Leica Application Suite X (LAS X) software.

2.7. Internalization of PLGA NPs by Cells and Visualization by Fluorescence Imaging

CT-26 cells were seeded on 12-mm coverslips placed at the bottom of a 12-well plate. After 24 h of incubation, NPs 1 and NPs 2 (5 µg/mL) were added. After 4 h and 24 h of incubation with NPs, the cells were stained with a membrane stain and the nuclei were counterstained with DAPI. For the visualization, a Leica DM5500 B fluorescence microscope was used as described above.

2.8. CRC Xenograft Models and Treatment Regimens

For xenographic tumor induction, a suspension of CT-26 cells (5×106) was subcutaneously injected into the right flank of male Balb/c mice. The protocol was approved by the Committee on the Ethics of Animal Experiments of the UFRN (Universidade Federal do Rio Grande do Norte) (CEUA, permit number: 170.020/2019).

Once the tumor volume reached 3–4 mm [32], the animals were categorized into four groups (N = 8, each group) and treated intratumorally three times in 15 days with: (1) Control (CTRL) = 5 mg/kg saline solution, (2) OXA = 5 mg/kg, (3) NPs 1 = 5 mg/kg, and (4) NPs 2 = 5 mg/kg. Then, the tumor size was monitored every two days for 21 days or until the tumor reached a volume of 2000 mm3 [33,34]. Their size was calculated with the following equation [35]:

$$\text{Volume} = (\text{length} \times \text{width}^2 \times 0.523))$$

Animals were euthanized with (80 mg/kg, i.p.) 2% thiopental (Cristália, São Paulo, Brazil) on day 21. Subcutaneous tumor masses were harvested and immediately frozen at −80 ◦C for qPCR analysis. Other tumors fragments were immersed in 10% paraformaldehyde for histopathological analysis.

2.9. Immunohistochemical Staining of FADD, APAF-1, and BCL-2

From tumors of each treatment group, 4-µm-thin tissue sections were cut using a microtome and transferred to gelatin-coated slides [36]. Tissue sections were incubated with primary antibodies anti-FADD (ab24533), anti-apoptotic protease activating factor 1 (APAF-1) (ab2001), and BCL-2 (ab32124; Abcam, Burlingame, CA, USA) at 4 ◦C overnight. Slices were washed with phosphate-buffered saline (PBS) and incubated with a streptavidin/Haptoglobin Related Protein (HRP)-conjugated secondary antibody (Biocare Medical, Concord, CA, USA). Immunoreactivity to the various proteins was visualized with a colorimetric-based detection kit following the protocol provided by the manufacturer (TrekAvidin-HRP Label + Kit from Biocare Medical, Pacheco, USA). Light microscopy (Nikon Eclipse 2000 equipped with Nikon DS-Fi2; Nikon Corporation, Tokyo, Japan) with a high-power objective (40×) was used to acquire digital images. The intensity of cell immunostaining was scored as follows: 1 = absence of positive cells, 2 = small number of positive cells or isolated cells, 3 = moderate number of positive cells, and 4 = large number of positive cells. Labelling intensity was evaluated by two previously trained examiners in a double-blind fashion.

2.10. Analysis of mRNA Expression

Total RNA was extracted from fragments of tumor tissue with a trizol reagent (Invitrogen Co., Carlsbad, CA, USA) and the SV Total RNA Isolation System (Promega, Madison, WI, USA). Real-time quantitative PCR analyses of β-actin, FADD, APAF-1, multidrug resistance protein 1 (MDR1), survivin, C-X-C chemokine receptor type 4 (CXCR4), and monocyte-derived chemokine (CCL22) mRNAs were performed with SYBR Green Mix in the Applied Biosystems1 7500 FAST system (Applied Biosystems, Foster City, CA, USA), according to a standard protocol with the primers listed in Table 2.

The standard PCR conditions were as follow: 50 ◦C for 2 min and 95 ◦C for 10 min, followed by 40 30-s cycles at 94 ◦C, a variable annealing primer temperature for 30 s, and 72 ◦C for 1 min. Mean threshold cycle

mRNA	Oligonucleotides Primers		Temper-ature
β-actina	5' AAC TTT GGC ATCGTG GAA GG 3'	5'GTGGATGCAGGGAT-GATGTTC 3'	60°C
FAAD	5' AGAAGAAGAACG-CCTCGGTG 3'	5' GCTCACAGATTCCTG-GGCTT 3'	56.5°C
APAF-1	5'TTCCAGTGGCAAGGA-CACAG 3'	5` CCACTCTCCACAGG-GACAAC 3'	56..8°C
MDR1	5' TCAGCAACAG-CAGTCTGGAG 3'	5' ACTATGAGCACAC-CAGCACC 3'	55.2°C
Survivin	5'AGAACAAAATTG-CAAAGGAGACA 3'	5'GGCATGTCACTCAG-GTCCAA 3'	55.2°C
CXCR4	5'ACCTCGGT-GTCCTCTTGCTGTCCA3'	5'GCTTGACGTTG-GCTCTGGCGATGT`3	56.5°C
CCL22	5'GAGACAACAGTGGTC-CCAGG 3'	5` CTGGCACTGT-CAATCCCTGT 3'	56..8°C

Table 2: Primer sequences used for PCR.

(Ct) values were used to calculate the relative expression levels of the target genes for the experimental groups, relative to those in the negative control group; expression data were normalized relative to the housekeeping gene β-actin using the 2−ΔΔCt formula.

2.11. Primary CRC Tissue Microarray

Biopsies were obtained from 180 patients undergoing surgical resection of CRC at the Cancer Referral Center of Natal, Brazil. Additional clinical information has been previously described together with the method to generate the tissue microarray (TMA) blocks [37]. This research was approved by the institutional committee (No. 030/0030/2006, 20th July, 2006).

For immunohistochemistry (IHC), anti-BCL-2, anti-caspase-8, and anti-Ki-67 antibody were used (Abcam, Burlingame, CA, USA) at a dilution of 1:1500. The number of positive cells within each TMA core was counted under a light microscope with a high-power magnification (40×).

2. MATERIALS AND METHODS

2.11. Primary CRC Tissue Microarray

BCL-2, caspase-8, and Ki-67 expression in the tumor tissue and surrounding stromal tissue was independently assessed by two researchers, who were blinded to the clinical data. Disease staging was performed according to the modified Dukes' criteria classification [37].

2.12. Statistical Analysis

All *in vitro* experiments or *in vivo* were performed in triplicate and a one-way ANOVA was used, followed by Bonferroni's post hoc test for parametric data and Kruskal–Wallis test followed by a Dunn's multiple comparison test. A p-value of <0.05 was considered to be statistically significant ($p < 0.05$, $p < 0.01$, $p < 0.001$, and $p < 0.0001$). Statistical significance was measured using parametric testing of the TMA samples, assuming equal variance, with a standard t-test for two paired samples used to assess the difference between test and control samples, unless stated otherwise. The probability of survival over time compared to positivity of immunohistochemical labeling for Ki-67, caspase-8, and BCL-2 was estimated using Kaplan–Meier product limit survival curves with a log-rank (Mantel–Cox) comparison test.

3. RESULTS

3.1. Preparation and Physicochemical Properties of PLGA NPs

We loaded NPs with OXA and then studied their therapeutic potential (Table 1). Besides the empty NPs (control), each batch was a combination of the following compounds: OXA, RA, and CHO. CHO improved and facilitated the uptake of the PLGA NPs into cancer cells. First, the PLGA NPs were characterized to ascertain their size and surface charge (Table 1). The average size ranged from 400 nm to 800 nm in diameter. The average zeta potential ranged between −21.4 mV and −29.6 mV. Figure 1 shows two representative examples of AFM analysis of PLGA NPs, which revealed that all PLGA NPs were spherical in shape with a uniform size distribution.

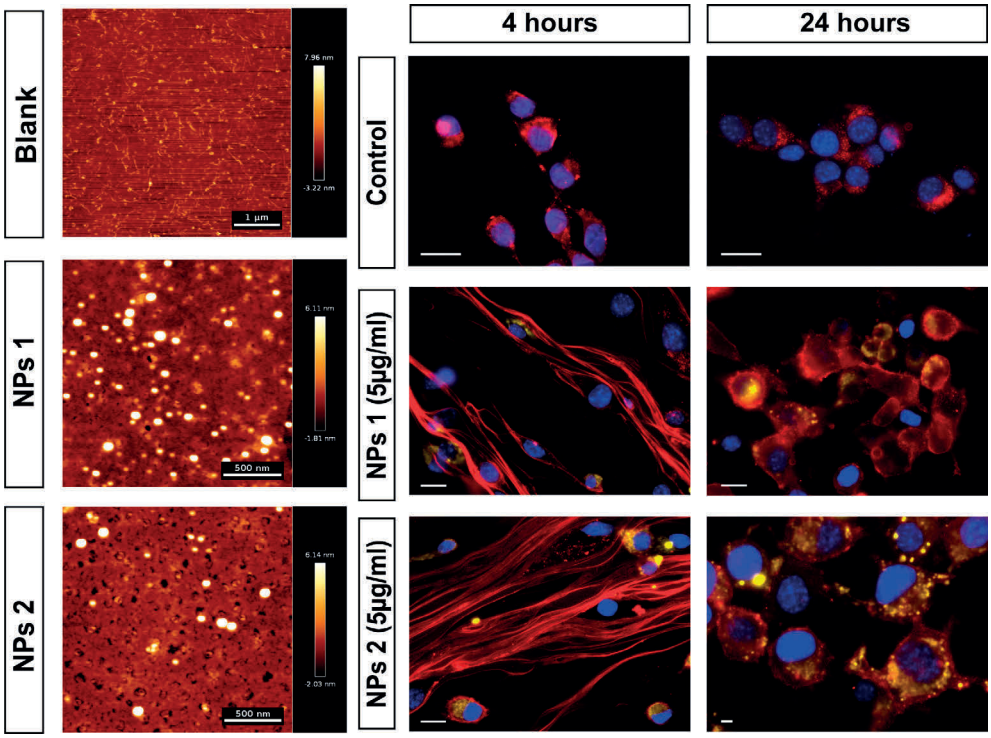

Figure 1. Representative AFM images of blank glass, NPs 1 and NPs 2 in alternating contact (AC) mode in air (scale bar = 500 µm) are showed in the left column of the panel. Fluorescence images in the right columns of the panel show the internalization of NPs by CT-26 cells. The nanoparticles (yellow) were detected in all treated groups and time points. Scale bar: 20 µm.

3.2. Viability Assay

After incubation with the samples for 24 and 48 h, the viability of CT-26 was assessed by MTS assay in a concentration-dependent manner (Figure 2A,B). To assess the possible improvement of drug efficacy, two cell viability tests were performed: (1) With free OXA and (2) with CHO-coated PLGA NPs containing OXA and/or RA. The range of 5 µg/mL to 200 µg/mL of OXA highly reduced cell viability after 24 and 48 h (Figure S1). However, concentrations of 5, 10, and 25 µg/mL of this chemotherapeutic agent were closest to the half maximal inhibitory concentration (IC50). Therefore, these concentrations were used in a second step.

NPs 1, NPs 2, NPs 6, and NPs 7 reduced cell viability comparable to free OXA. Cell proliferation reduced in a dose-dependent manner, thereby, confirming the efficacy and successful uptake of our nanoparticulate systems (Figure 2A,B). The others system, i.e., NPs 3, NPs 4, and NPs 8, did not demonstrate satisfactory cytotoxicity for CT-26 cells because they did not have OXA in their composition. The formulation of NPs 5 (empty control) did not show cytotoxicity, confirming that PLGA is biocompatible and did not influence the results (Figure 2A,B).

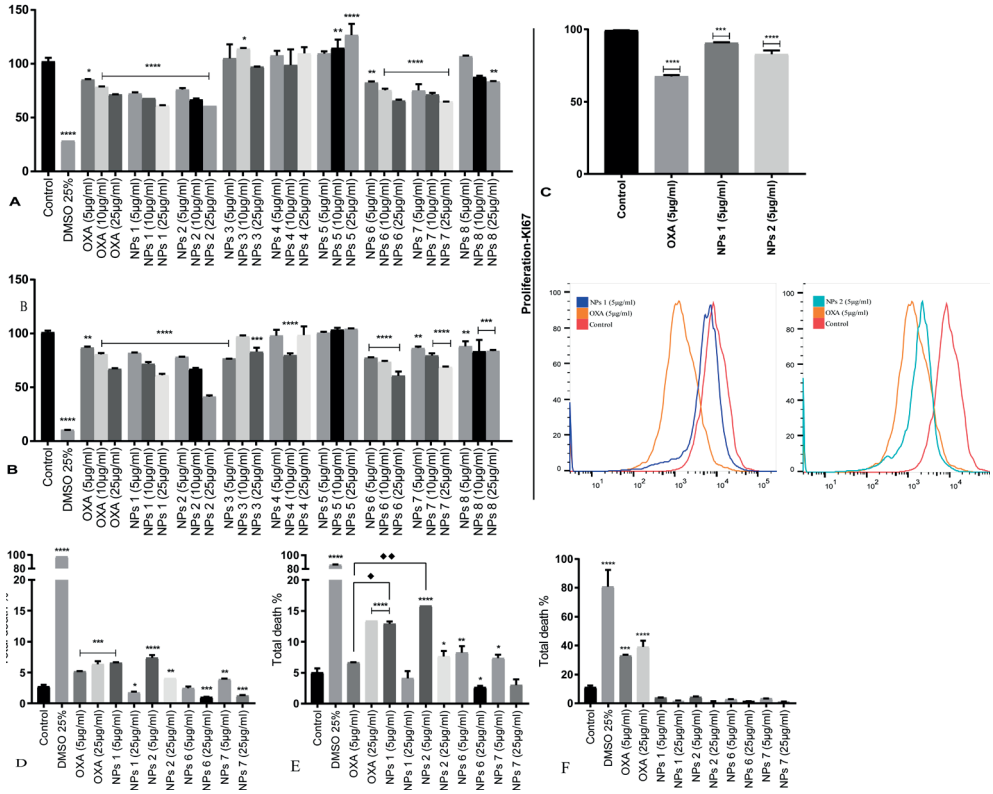

Figure 2. Cell viability (A,B), proliferation (C), total death for CT-26 for 24 h (D), total death for CT-26 for 48 h (E) and total death for 3T3 cells for 48 h (F). Mean cell proliferation of CT-26 cells treated with OXA and PLGA NPs for 24 h (A) and 48 h (B). Ki-67 immunostaining of CT-26 cells treated with OXA (5 µg/mL), NPs 1 (5 µg/mL), and NPs 2 (5 µg/mL) and compared to negative control for 48 h (C). The statistic of the treatments for the total death when compared to the negative control is displayed (* $p < 0.05$, ** $p < 0.01$, *** $p < 0.001$, and **** $p < 0.0001$). Comparison between OXA (5 µg/mL) and NPs 1 (5 µg/mL, ◆) as well as between OXA (5 µg/mL) and NPs 2 (5 µg/mL, ◆◆).

3. RESULTS

3.2. Viability Assay

To evaluate the effect of free OXA, NPs 1, and NPs 2 on the viability of the human CRC cell line SW-480, cells were treated with doses of 5, 25, and 50 µg/mL for 24 and 48 h. The results showed that free OXA as well as the NPs induced cell death, as determined by Hoechst labelling and flow cytometric analysis (Figure 3A,B). Thus, in conclusion, free OXA as well as NPs 1 and NPs 2 (5 µg/mL and 25 µg/mL) showed cytotoxicity in CT-26 and SW-480 cells after 24 and 48 h of incubation.

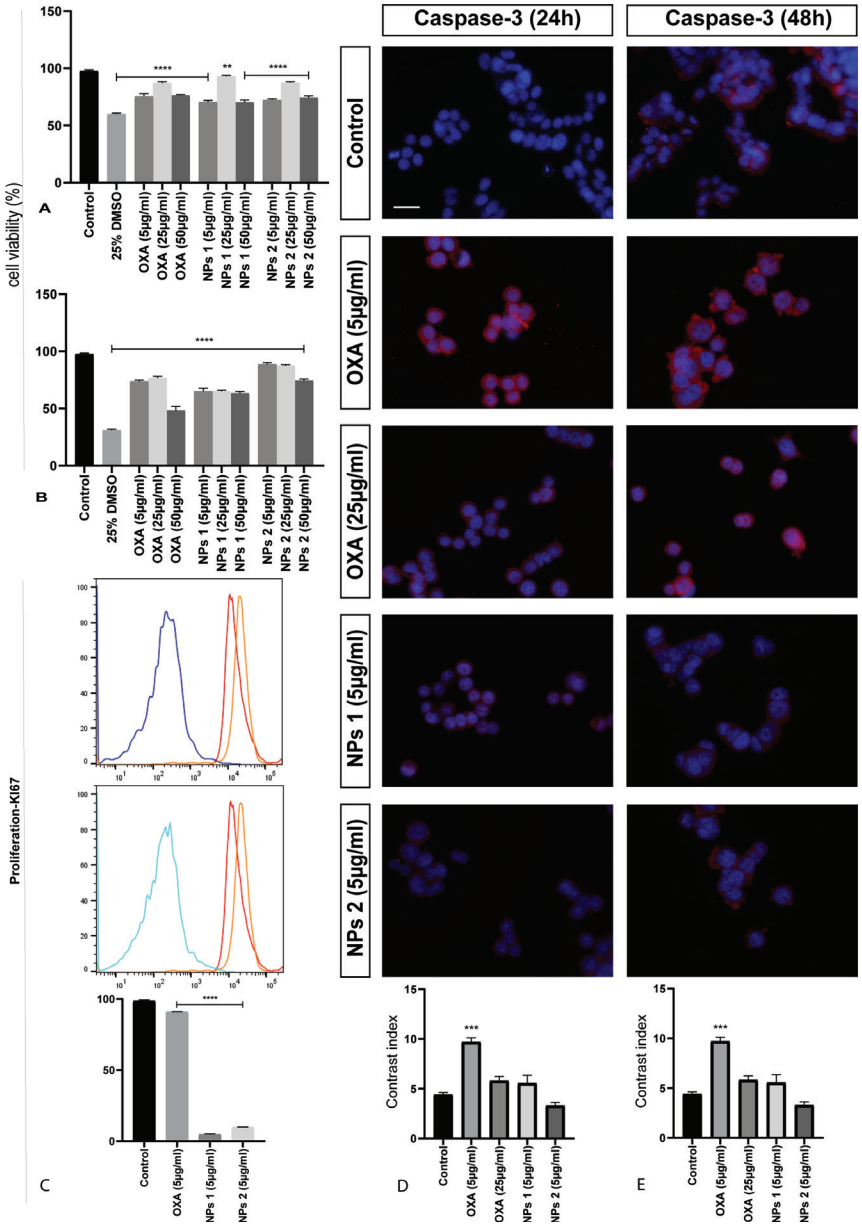

Figure 3. Cell viability, proliferation, and detection of caspase-3 of SW-480 cells. Mean cell proliferation of SW-480 cells treated with OXA and PLGA NPs for 24 h (A) and 48 h (B). All treatment groups were compared to the negative control group (**** $p < 0.0001$ and ** $p < 0.01$). Ki-67 immunostaining of SW-480 cells treated with OXA, NPs 1, and NPs 2, and compared to negative control for 48 h (C). All treatments were statistically significant (**** $p < 0.0001$). Representative photomicrographs of caspase-3 in SW-480 cells stained with 4,6-diamidino-2-phenylindole (DAPI) (blue) and anti-caspase-3 antibody (red). Contrast index for caspase-3 after 24 h (D) and 48 h (E) (*** $p < 0.001$). Scale bar: 50 µm.

3.3. Detection of Apoptosis and Proliferation by Flow Cytometry

The dot plots generated by flow cytometric analysis show counts of cells with initial apoptosis (Annexin V-FITC-positive/DAPI-negative) in the lower right quadrant, while the upper right quadrant represents late apoptosis (Annexin V-FITC-positive/DAPI-positive) (Figures S2–S4). The total apoptosis was calculated with the sum of early (Q3) and late (Q2) apoptotic cells.

In CT-26 cells, the antitumor activity of OXA (5 μg/mL and 25 μg/mL) induced apoptosis after 24 h ($p < 0.001$, Figure 2D). However, after 48 h, only a concentration of 25 μg/mL OXA showed significant activity ($p < 0.0001$, Figure 2E). Similarly, NPs 1 (5 μg/mL, $p < 0.001$), NPs 2 (5 μg/mL and 25 μg/mL, $p < 0.0001$ and $p < 0.01$, respectively), and NPs 7 (5 μg/mL, $p < 0.01$) induced apoptosis after 24 h (Figure 2D). However, unlike free OXA, NPs 1 (5 μg/mL, $p < 0.0001$), NPs 2 (5 μg/mL and 25 μg/mL, $p < 0.0001$ and $p < 0.05$, respectively), NPs 6 (5 μg/mL, $p < 0.01$), and NPs 7 (5 μg/mL, $p < 0.05$) induced apoptosis after 48 h (Figure 2E). When compared to free OXA at the same concentration, NPs 1 (5 μg/mL, $p < 0.0001$) and NPs 2 (5 μg/mL, $p < 0.0001$) showed statistically significant antitumor activity after 48 h (Figure 2E). Importantly, our NPs did not induce apoptosis in nontumor 3T3 cells at any dose (Figure 2F). However, nontumor cells showed a significant death rate when exposed to free OXA (5 μg/mL and 25 μg/mL, $p < 0.001$ and $p < 0.0001$, respectively) after 48 h (Figure 2F).

A Ki-67 immunostaining was performed on CT-26 cells to evaluate the cell growth fraction after treatment with free OXA (5 μg/mL), NPs 1 (5 μg/mL), and NPs 2 (5 μg/mL), which was expressed in the G1, S, and G2/M cell cycle phases and was absent in resting (G0) cells. CT-26 cells treated with NPs 1 and NPs 2 showed a higher Ki-67 expression ($p < 0.001$ and $p < 0.0001$, respectively) than free OXA when compared to the negative control ($p < 0.0001$, Figure 2C). However, SW-480 cells treated with NPs 1 and NPs 2 exhibited a lower Ki-67 expression than free OXA when compared to the negative control ($p < 0.0001$, Figure 3C).

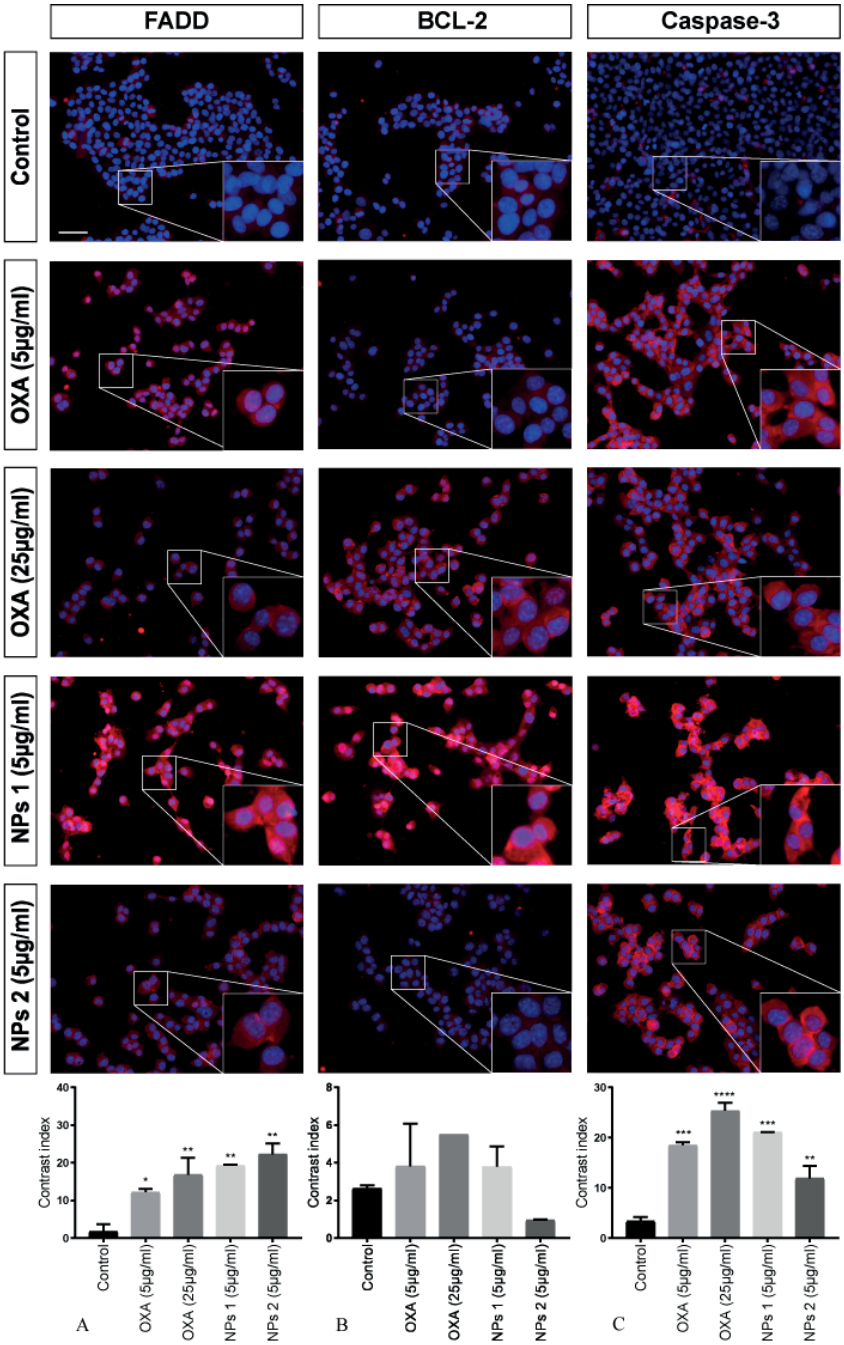

Figure 4. Detection of fas-associated protein with death domain (FADD), BCL-2, and caspase-3 after 24 h of treatment. CT-26 cells stained with DAPI (blue), anti-FADD, anti-BCL-2, and anti-caspase-3 antibodies (red). Contrast index for FADD, * $p < 0.05$, ** $p < 0.01$ (A); BCL-2, $p > 0.05$ (B); and caspase-3, ** $p < 0.01$, *** $p < 0.001$, **** $p < 0.0001$ (C). Scale bar: 50 µm.

3.4. Immunofluorescence of FADD, BCL-2, and Caspase-3

To investigate the activated apoptosis pathway in CT-26 cells treated with free OXA and NPs 1 and NPs 2, three different proteins were investigated by means of immunofluorescence microscopy.

After treating with OXA (5 µg/mL and 25 µg/mL), NPs 1 (5 µg/mL), and NPs 2 (5 µg/mL), antibody staining (FADD and caspase-3) was statistically significant when compared to the control for all samples after 24 h. However, BCL-2 staining did not show significant results ($p > 0.05$, Figure 4). For FADD, it was $p < 0.05$, $p < 0.01$, $p < 0.01$, and $p < 0.01$, respectively, and for caspase-3 it was $p < 0.001$, $p < 0.0001$, $p < 0.001$, and $p < 0.01$, respectively.

Our analysis showed significant FADD staining for NPs 1 (5 µg/mL, $p < 0.05$) and NPs 2 (5 µg/mL, $p < 0.05$) only 48 h after treatment. However, a decrease in BCL-2 immunoreactivity for all treatments ($p < 0.001$, $p < 0.01$, $p < 0.01$, $p < 0.001$) was observed. When compared to the control, caspase-3 staining of CT-26 treated with OXA, NPs 1, and NPs 2 was significant ($p < 0.01$ for all treatments, Figure 5).

When caspase-3 staining was evaluated in SW-480 cells, a higher expression of caspase-3 was perceived in cells treated with OXA (5 µg/mL, $p < 0.01$) when compared to control cells after 24 and 48 h (Figure 3D,E). However, OXA (25 µg/mL), NPs 1 (5 µg/mL), and NPs 2 (5 µg/mL) did not show significant caspase-3 expression when compared to the control.

3.5. Internalization of NPs by CT-26 Cells

Internalization of NPs 1 and NPs 2 by CT-26 cells was studied using fluorescence microscopy (Figure 1). After 4 h and 24 h of incubation, the cell membranes were stained to visualize internalization of NPs 1 and NPs 2 by cells. NPs 1 and NPs 2 showed accumulation within the cells at both time points.

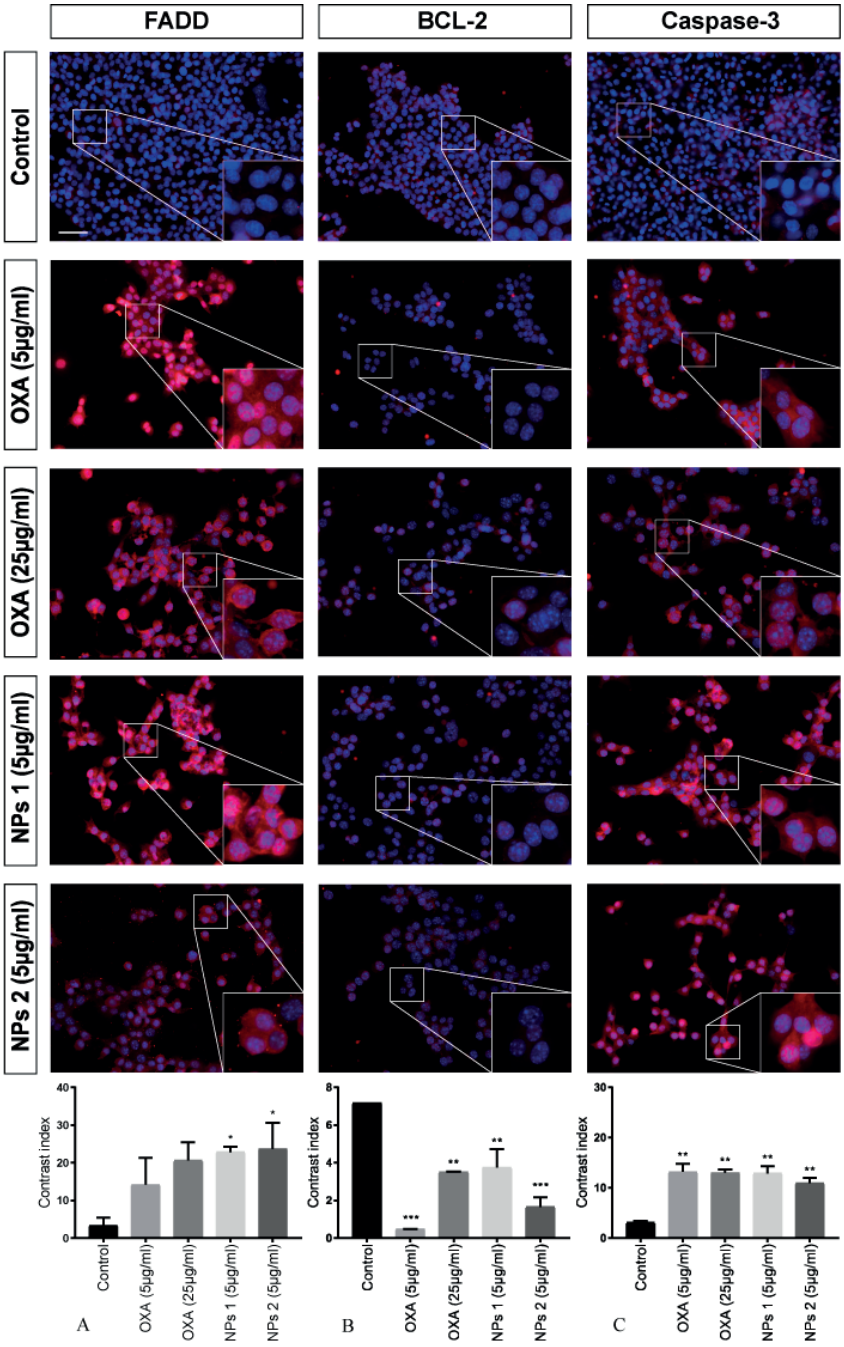

Figure 5. Detection of FADD, BCL-2, and caspase-3 after 48 h of treatment. CT-26 cells stained with DAPI (blue), anti-FADD, anti-BCL-2, and anti-caspase-3 antibodies (red). Contrast index for FADD, * $p < 0.05$ (A); BCL-2, ** $p < 0.01$, *** $p < 0.001$ (B); and caspase-3, ** $p < 0.01$ (C). Scale bar: 50 µm.v

3.6. *In Vivo* Study

To confirm whether NPs 1 and NPs 2 were more efficient DDSs to downregulate apoptosis pathways, drug resistance, and metastasis factors *in vivo* when compared to free OXA, the expression of FADD, APAF-1, BCL-2, caspase-3, MDR1, survivin, CXCR4, and CCL22 was observed in tumors of Balb/c mice using qPCR and/or immunohistochemistry. As shown in Figure 6, tumor growth and volume decreased in groups treated with free OXA, NPs 1, and NPs 2 (5 mg/kg, $p < 0.0001$). After 15 days of treatment with free OXA (5 mg/kg), NPs 1 (5 mg/kg), and NPs 2 (5 mg/kg), immunohistochemical analyses revealed an increased expression of FADD (Figure 7A,B, $p < 0.0001$) and caspase-3 (Figure 7A,D, $p < 0.0001$), and a decreased expression of BCL-2 (Figures 7A and 8C, $p < 0.0001$ for NPs 1 and $p < 0.001$ for OXA and NPs 2) in tumors of Balb/c mice when compared to the control group. A comparison between the different treatment groups showed a higher expression of FADD and caspase-3 in tumors of groups treated with NPs 1 (Figures 7B and 8D) than in groups treated with free OXA and NPs 2. On the other hand, BCL-2 had a lower expression in groups treated with NPs 1 (Figure 7C) than in the other two groups. Indeed, genes of FADD and APAF-1 were evaluated in tumors by means of RT-PCR after 15 days of treatment. From the gene expression analysis, it was observed that the increase of FADD was statistically significant in groups treated with free OXA (5 mg/kg) and NPs 1 (5 mg/kg) when compared with the control (Figure 7E, $p < 0.05$ and $p < 0.001$, respectively). The increase of APAF-1 was statistically significant in groups treated with NPs 1 (5 mg/kg) and NPs 2 (5 mg/kg) when compared to the control (Figure 7E, $p < 0.001$ and $p < 0.05$, respectively). When the gene expression of FADD and APAF-1 is compared between the treatment groups, it is apparent that their expression was higher after treatment with NPs 1 than after treatment with either free OXA or NPs 2 (Figure 7E).

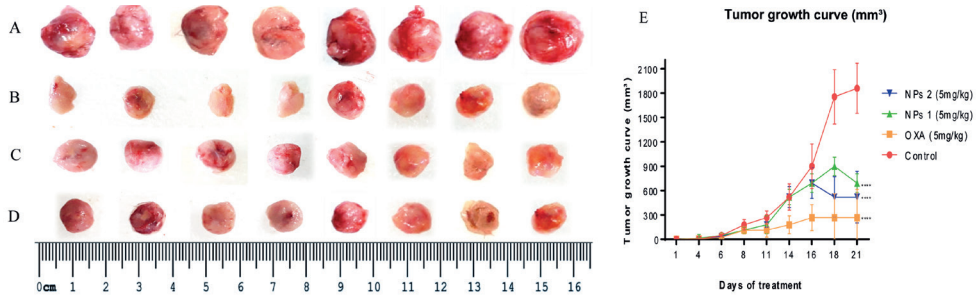

Figure 6. Morphology of all the tumors collected from (A) control, (B) OXA (5 mg/kg), (C) NPs 1 (5 mg/kg), and (D) NPs 2 (5 mg/kg) mice. Tumor growth curve of the Balb/c xenografts with different treatments (E). All treatment groups were compared to the negative control group (**** $p < 0.0001$).

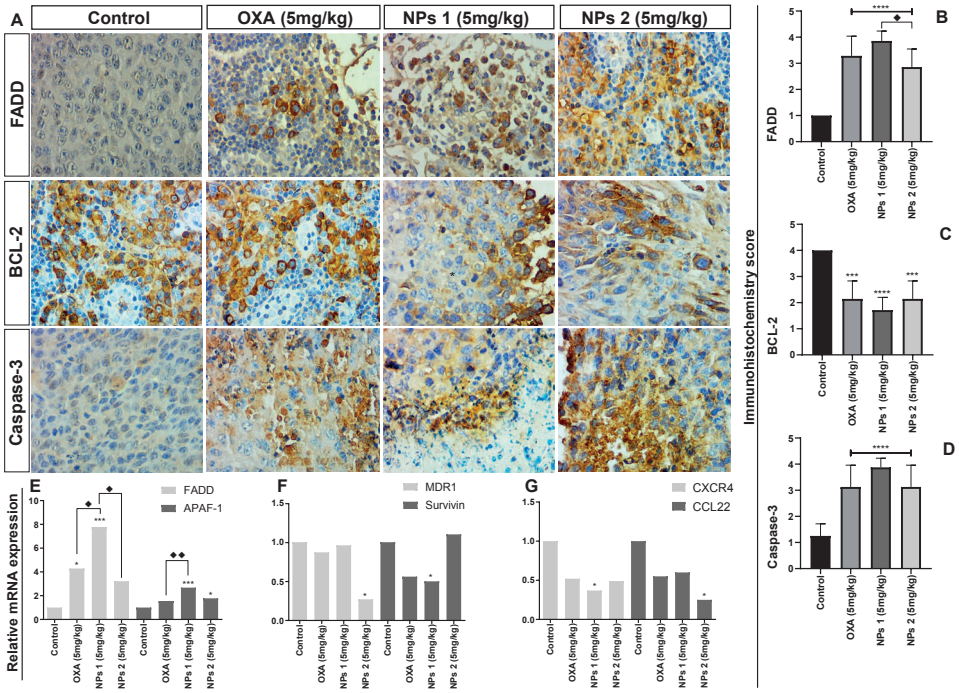

Figure 7. Analysis of apoptosis, drug resistance, and metastasis factors. Representative photomicrographs of immunohistochemistry of tumor fragments of mice receiving different treatments (A). Immunohistochemistry score by anti-FADD (B), anti-BCL-2 (C), anti-caspase-3 (D), relative messenger ribonucleic acids (mRNA) expression by RT-PCR for FADD and apoptotic protease activating factor 1 (APAF -1) (E), multidrug resistance protein 1 (MDR1) and survivin (F), and C-X-C chemokine receptor type 4 (CXCR4), and monocyte-derived chemokine (CCL22) (G). All treatment groups were compared to the negative control group (**** $p < 0.0001$). Comparison between OXA (5 mg/kg) and NPs 1 (5 mg/kg, ◆ $p < 0.05$) as well as between OXA (5 mg/kg) and NPs 2 (5 mg/kg, ◆◆ $p < 0.01$) was also performed ($p < 0.0001$ for both). Magnification: 40×.

3. RESULTS

3.6. *In Vivo* Study

The gene expression analysis of drug resistance and metastasis factors was also evaluated by RT-PCR. Based on Figure 7F, the expression of MDR1 and survivin genes, which are involved in drug resistance, was reduced after treatment with NPs. The MDR1 gene expression decreased after treatment with NPs 2 (5 mg/kg, $p < 0.05$), while the survivin gene expression decreased after treatment with NPs 1 (5mg/kg, $p < 0.05$). As metastasis is one of the biggest concerns of cancer management strategies, we investigated two genes from chemokines related to metastasis by means of RT-PCR. When compared to the control group, NPs 1 was able to reduce CXCR4 gene expression while NPs 2 decreased the CCL22 gene expression (Figure 7G, both $p < 0.05$).

3.7. Expression of Anti-Apoptosis and Pro-Apoptosis Proteins in Primary Colorectal Tumors

Apoptosis is associated with several other processes of tumor progression, like drug resistance, cell proliferation, and metastasis. Here, we evaluated if the expression of BCL-2, caspase-8, and Ki-67 would be associated with poor prognosis in tumors with low (1/2) and high (3/4) modified Dukes' classification of the patients in primary CRC. High expression of BCL-2 was an indication of recurrence of the CRC ($p = 0.0001$, Figure 8). In addition, patients who showed high expression of caspase-8 indicated a greater tendency towards death within 60 months of follow-up, although our data were not statically significant ($p = 0.10$, Figure 8). Furthermore, high expression of BCL-2 and caspase-8 was associated with more aggressive tumors, as represented by lymph node involvement ($p = 0.0002$ for both), modified Dukes' criteria grade ($p = 0.0001$ and $p = 0.07$, respectively), and proliferation by Ki-67 ($p = 0.04$ and $p = 0.0001$, respectively, Table 3). These results show that the synthesis of new drug systems to specifically target apoptosis, especially in human primary tumor of aggressive cancers, is necessary as part of a novel cancer management strategy.

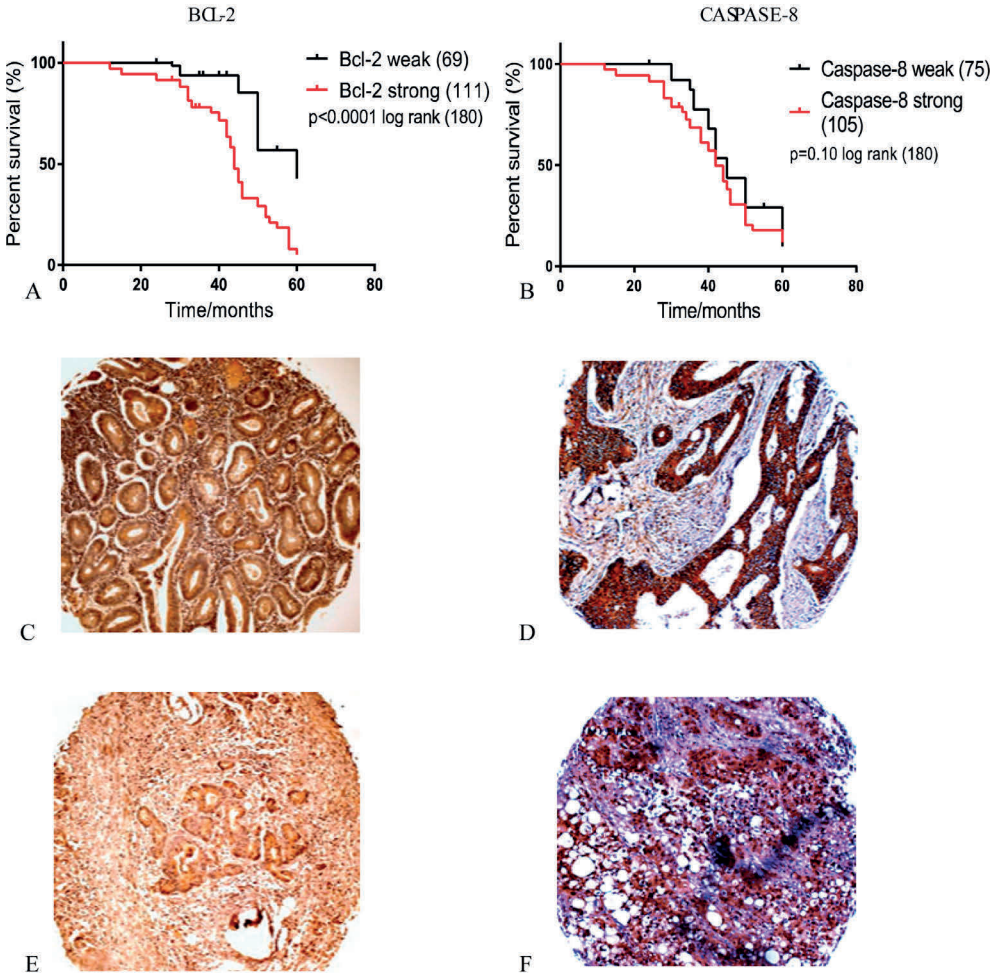

Figure 8. Expression of BCL-2 and caspase-8 in primary colorectal tumors. (A) Kaplan–Meier survival curve estimated by BCL-2 staining in colorectal cancer (CRC) tumors (log-rank × 2 = 30.75, p < 0.0001), (B) Kaplan–Meier survival estimated by caspase-8 staining in CRC tumors (log-rank × 2 = 2.61, p = 0.10). Immunohistochemical staining for BCL-2 and caspase-8 in colorectal carcinoma. Colorectal adenocarcinoma with a high modified Dukes' classification ("3" and "4") showing: (C) Strong cytoplasmic staining of BCL-2, and (E) weak BCL-2 cytoplasmic staining. Strong cytoplasmic staining of caspase-8 (D), and (F) weak caspase-8. Magnification: 40×.

	Caspase-8 (n=180)		
	Weak	Strong	p Value
Number of patients	75 (41.6%)	105 (58.3%)	-
Lymph node status			
Negative	15(20%)	03(2.86%)	0.0002[1]
Positive	60(80%)	102(97.14%)	
Modified Dukes´ Criteria Grade			
Low (I and II)	25(33.3%)	07 (6.67%)	0.0001[1]
High (III and IV)	50(66.7%)	98 (93.33%)	
KI67			
< 10 %	02 (2.7%)	02 (1.9%)	0.04[2]
11-25%	18 (24%)	11 (10.48%)	
>25%	55(73.3%)	92 (87.62%)	

Table 3 . Expression of BCL-2 and caspase-8 in primary colorectal tumors. (A) Kaplan–Meier survival curve estimated by BCL-2 staining in colorectal cancer (CRC) tumors (log-rank × 2 = 30.75, p < 0.0001), (B) Kaplan–Meier survival estimated by caspase-8 staining in CRC tumors (log-rank × 2 = 2.61, p = 0.10). Immunohistochemical staining for BCL-2 and caspase-8 in colorectal carcinoma. Colorectal adenocarcinoma with a high modified Dukes' classification ("3" and "4") showing: (C) Strong cytoplasmic staining of BCL-2, and (E) weak BCL-2 cytoplasmic staining. Strong cytoplasmic staining of caspase-8 (D), and (F) weak caspase-8. Magnification: 40×.

4. DISCUSSION

Evasion of apoptosis is one of the major causes of tumor progression. In this study, we identified increased expression of BCL-2 and caspase-8 in human CRC. In addition, we demonstrated that increased expression of BCL-2 and caspase-8 is associated with proliferation (Ki-67), a high invasion grade, and a positive lymph node status. This suggests a growth advantage of tumor cells with high expression of caspase-8 in the pathogenesis of CRC, which is consistent with previous studies [38–41]. However, previous studies showed that inactivating mutations of the caspase-8 genes are rare in human colorectal carcinomas [42]. There is growing evidence that caspase-8 does not just act as an inducer of apoptosis, but

	Bcl-2 (n=180)		
	Weak	Strong	p Value
	69 (38.33%)	111 (41.67%)	-
	39(56.52%)	23(20.72%)	0.0002[1]
	30(43.48%)	88(79.28%)	
	41(59.42%)	35(31.53%)	0.07[1]
	28(40.58%)	76(68.47%)	
	09(13.05%)	24(21.62%)	0.0001[2]
	11(15.94%)	52(46.85%)	
	49(71,01%)	35(31.53%)	

also in metastasis [43]. Induction of cell death is one of the challenges for the development of new drugs, especially in aggressive tumors with a high level of mortality.

Based on evidences that tumor progression is associated with failing cell control mechanisms, we designed OXA-loaded PLGA NPs combined with RA and CHO to assess the improvement of the antitumor activity of OXA. Firstly, we evaluated the cytotoxicity of OXA-containing NPs in CT-26 cells. The data showed that OXA-containing NPs 1, NPs 2, NPs 6, and NPs 7 possess a cytotoxic activity (after 24 and 48 h), which was similar to the free drug. However, NPs 1 and NPs 2 exhibited a higher cytotoxic activity than others NPs after 48 h. According to these results, we decided to assess the cytotoxicity of NPs 1 and NPs 2 in SW-480 cells. Both NPs showed to have cytotoxic activity in this cell line. These results revealed that RA and CHO helped OXA to inhibit the cell viability in CT-26 as well as SW-480 cells, probably by increasing the availability or potentializing the cytotoxic effects of OXA inside of cells [23,44,45].

4. DISCUSSION

OXA is a third-generation platinum drug, which inhibits DNA replication [46]. However, the obtained efficacy is suboptimal due to the aggressive side effects OXA and drug resistance of cancer cells [46–48]. The pro-apoptotic activities of NPs and OXA were analyzed by flow cytometry for both CT-26 and nontumor cells. NPs 1, NPs 2, NPs 6, and NPs 7 had pro-apoptotic activity at a concentration of 5 µg/mL in the tumor cell line at 24 and 48 h. However, NPs 1 and NPs 2 exhibited a higher pro-apoptotic activity than higher concentrations of free OXA. Interestingly, they also reduced the total apoptosis in the nontumor cell line. Previous studies reported that NPs-encapsulated chemotherapeutic agents induce apoptosis in several tumor cell lines without interfering with nontumor cell lines [49,50]. This result indicates that it is possible to use lower concentrations of OXA when it is encapsulated in a nanoparticulate DDS. In addition, it is possible to combine OXA with CHO and RA. Due to their high proliferation rate, tumor cells require higher amounts of CHO than nontumor cells. Thus, coating with CHO facilitates the internalization of NPs and, thereby, increases the delivery of OXA into tumor cells. This improves the efficiency of the system and decreases the adverse effects that are related to the cumulative impact of OXA on patients [12,23,51]. Our study contributed to this knowledge and, in addition, we did not observe significant cell death in nontumor cells. This indicates that these nanoparticulate DDSs (NPs 1 and NPs 2) can have a protective effect on nontumor cells, while selectively targeting tumor cells.

High uptake of NPs by tumor cells and effective intracellular drug release are necessary to achieve an enhanced therapeutic effect in clinic trials. The uptake of NPs 1 and NPs 2 by CT-26 cells was investigated after 4 h and 24 h, which revealed that our NPs were mainly located in the cytoplasm close to the nucleus. It is worth mentioning that the CHO-coated NPs combined with RA (NPs 1 and NPs 2) showed rapid uptake and improved therapeutic efficacy through induction of apoptosis in CRC cells [23,52]. Therefore, our results indicate the importance of CHO for the increased capture and internalization of DDS in the treatment of CRC [23,53].

The pro-apoptotic activity of free OXA (5 µg/mL and 25 µg/mL), NPs 1 (5 µg/mL), and NPs 2 (5 µg/mL) in CT-26 cells was confirmed by immunoreactivity of caspase-3, FADD, and BCL-2, which are involved in the extrinsic

and intrinsic apoptosis pathway. The extrinsic pathway was activated by all compounds within 24 h, but only NPs 1 and NPs 2 induced a positive immunoreactivity to FADD after 48 h. These results show that our OXA-containing nanoparticulated DDS exhibits a prolonged activity as compared to the free drug, which suggests an increased bioavailability inside the cancer cells [45,51,52]. Since immunoreactivity for BCL-2 was observed only after 48 h, our data suggests that the NPs act primarily by activating the extrinsic pathway. Previous studies give evidence for a strong correlation between intrinsic apoptosis and cell proliferation in tumor progression [44,54]. The expression of Ki-67 is strongly associated with (tumor) cell proliferation and growth, and is widely used in routine pathological investigations as a proliferation marker [55]. Owing to high cell proliferation, frequently associated with the Ki-67 protein labeling index, Ki-67 may be a promising factor for targeted molecular therapies [55]. In this study, NPs 1 (5 µg/mL) and NPs 2 (5 µg/mL) strongly decreased the expression of Ki-67 in SW-480 cells but not in CT-26 cells. Interestingly, this result corroborates findings in the literature by describing the anti-apoptotic protein BCL-2 as an inhibitor of p53, a pro-apoptotic and suppressor protein [56]. Since mutated p53 can also induce a G2/M cell cycle and stimulate Ki-67, our NPs 1 and NPs 2 were able to induce extrinsic apoptosis, which has an independent path of BCL-2 and p53 and showed that the BCL-2-p53-Ki-67 path is common in aggressive tumors [57]. In our study, we found that NPs 1 and NPs 2 induced apoptosis via the extrinsic path and blocked the proliferation of cancer cells, thereby, suggesting that the NPs act on different signaling pathways.

With the aim to observe the efficiency of NPs in an animal model, we inoculated CT-26 cells subcutaneously in the flank of Balb/c mice and, when the tumors reached 4 mm, the mice were treated with free OXA, NPs 1, and NPs 2 (all 5 mg/kg), respectively, 3 times over a period of 2 weeks. Based on the expression of FADD, BCL-2, and caspase-3, our *in vivo* results suggested that NPs 1 induced apoptosis more than NPs 2, especially through the extrinsic pathway, corroborating with our *in vitro* results. One of the advantages of RA combined with OXA and CHO, is that CHO increases internalization of nanoparticles as described above and, therefore, increased amounts of RA can act directly on the regulation of apoptotic pathway proteins and at the tumor microenvironment as demonstrated by Watabe et al. [53].

4. DISCUSSION

High levels of CXCR4, a receptor correlated with tumor malignancy, and CCL22, a member of the chemokine family, are related to migration, invasion, and metastasis in various tumors, leading to a poor prognosis and malignant progression [58–61]. Our results show that NPs 1 and NPs 2 decrease CXCR4 and CCL22 expression in the primary microenvironment, which indicates that our nanoparticulated DDSs act as important modulators of metastatic sites. Drug resistance to OXA is a problem, which reduces its effectiveness and increases the chances of metastasis, thereby, limiting tumor treatment with this drug. In this study, when analyzing primary tumors treated with free OXA as well as NPs 1 and NPs 2, we observed downregulation of multidrug resistance (MDR), such as, MDR1 expression by NPs 2 and survivin by NPs 1. This proves that encapsulation of drugs decreases drug resistance since NPs were taken up by endocytosis by passing drug efflux pumps which are altered in tumor cells [62,63]. Drug efflux pumps expressed on human cancer cells majorly contribute to MDR, especially those related to P-gp also known as multidrug resistance protein 1 (MDR1) and surviving [64]. These results suggest that CHO functionalized PLGA nanoparticles loaded with anti-cancer drug OXA and chemosensitizer RA enhanced therapeutic potential by modulating MDR of tumor cells through RA and enhanced the anticancer activity of DDSs. Dual drug loaded nanoparticles revealed better therapeutic efficacy with enhanced expression or downregulation of pro-apoptotic/anti-apoptotic proteins and downregulation of metastastic factors, such as CXCR4 and CCL22.

An upregulation of apoptosis in the microenvironment of human primary tumors is the key point to reduce proliferation and metastasis and, consequently, improve the survival of patients. Here, we designed a system of OXA-loaded NPs combined with RA and CHO to study their efficiency in inducing apoptosis and regulating proliferation, drug resistance, and metastatic factors. Taken together, the data presented in this study indicated that nanoparticulate DDSs (NPs 1 and NPs 2) possess antitumor activity in CRC cells *in vitro* and *in vivo*, which is preferentially mediated by the extrinsic apoptosis pathway. *In vivo* results also suggest that NPs 1 and NPs 2 downregulate resistance to OXA and metastasis factors. Cytoprotective activity based on the non-induction of cell death in nontumor cells is combined with the antitumor activity and modulation of the tumoral

microenvironment, indicating that these systems are safe candidates for drug delivery that can be used for the treatment of cancer with decreased adverse effects.

APPENDIX TO CHAPTER 3

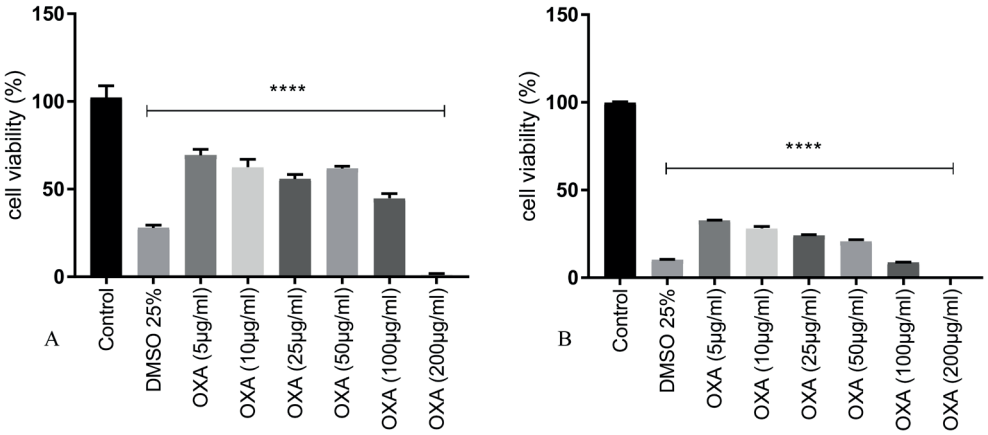

Figure S1. Mean cell proliferation of CT-26 cells treated with OXA for 24 h. (A) and 48 (B) hours. The concentrations used were: 5 µg/mL, 10 µg/mL, 25 µg/mL, 50 µg/mL, 100 µg/mL, and 200 µg/mL. All treatment groups were compared to the negative control group (**** $p < 0.0001$).

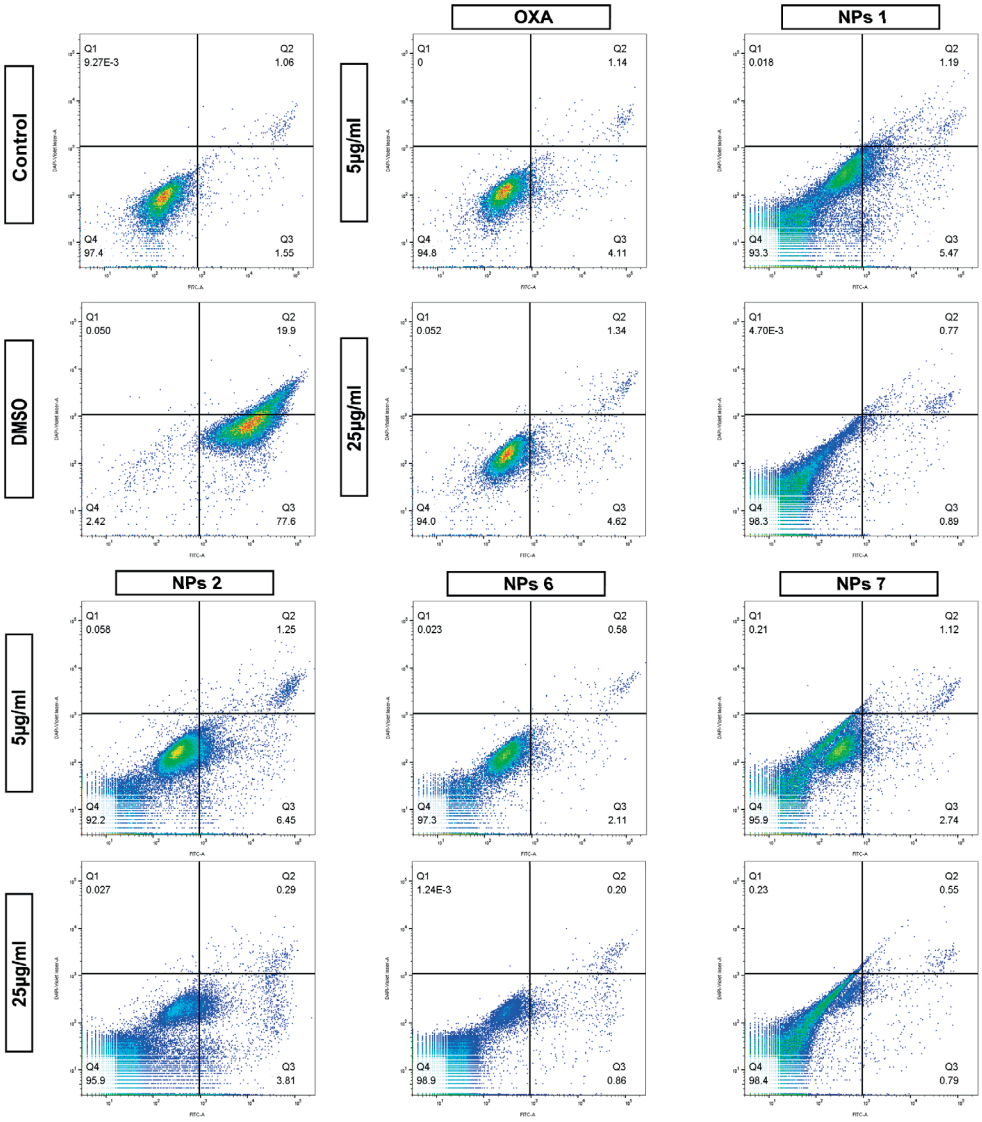

Figure S2. Flow cytometry to determine apoptosis. Dot plots of flow cytometry with the effect of different doses of OXA, DMSO, and NPs on early and late apoptotic CT-26 cells after 24 h. are displayed.

APPENDIX TO CHAPTER 3

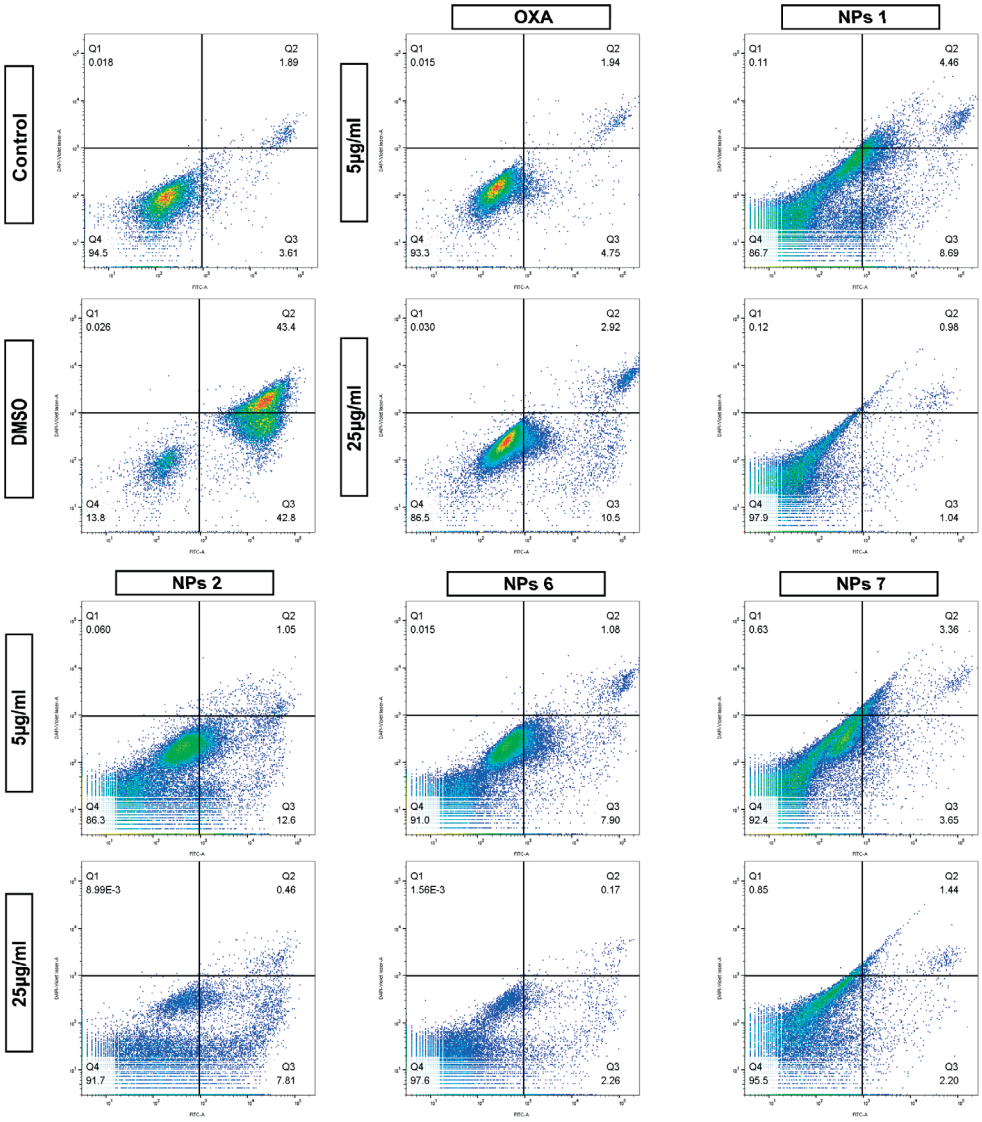

Figure S3. Flow cytometry to determine apoptosis. Dot plots of flow cytometry with the effect of different doses of OXA, DMSO, and NPs on early and late apoptotic CT-26 cells at 48 h. are displayed.

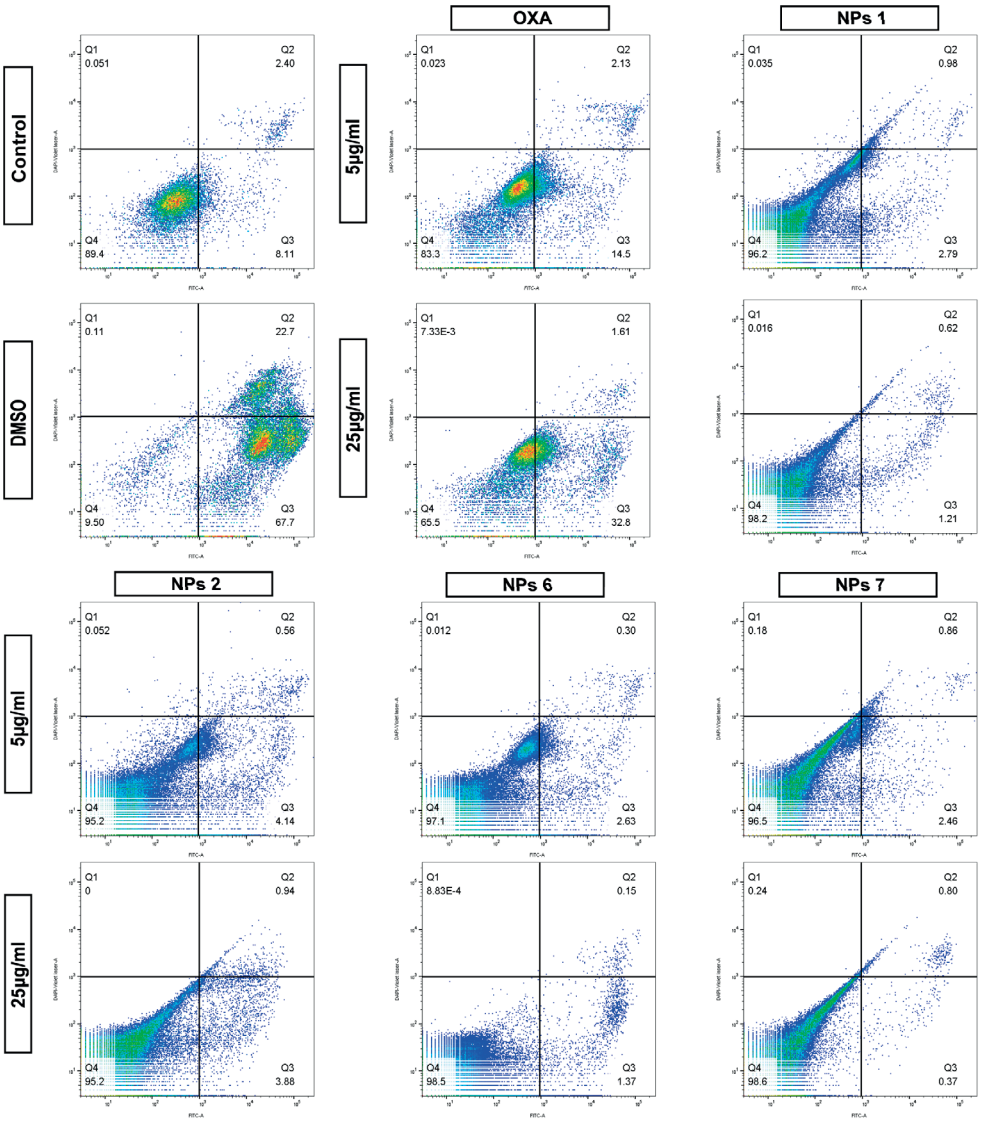

Figure S4. Flow cytometry to determine apoptosis. Dot plots of flow cytometry with the effect of different doses of oxaliplatin, DMSO, and NPs, on early and late apoptosis in 3T3 cells at 48 h. are displayed.

REFERENCES

1. Kacan, T.; Nayir, E.; Altun, A.; Kilickap, S.; Babacan, N.A.; Ataseven, H.; Kaya, T. Antitumor activity of sorafenib on colorectal cancer. J. Oncol. Sci. 2016, 2, 53–57. [CrossRef]
2. Wang, X.; Song, Z.-J.; He, X.; Zhang, R.-Q.; Zhang, C.-F.; Li, F.; Wang, C.-Z.; Yuan, C.-S. Antitumor and immunomodulatory activity of genkwanin on colorectal cancer in the APCMin/+ mice. Int. Immunopharmacol. 2015, 29, 701–707. [CrossRef] [PubMed]
3. Zhang, F.; Lu, Y.-X.; Chen, Q.; Zou, H.-M.; Zhang, J.-M.; Hu, Y.-H.; Li, X.-M.; Zhang, W.-J.; Zhang, W.; Lin, C.; et al. Identification of NCK1 as a novel downstream effector of STAT3 in colorectal cancer metastasis and angiogenesis. Cell. Signal. 2017, 36, 67–78. [CrossRef] [PubMed]
4. Ferlay, J.; Soerjomataram, I.; Dikshit, R.; Eser, S.; Mathers, C.; Rebelo, M.; Parkin, D.M.; Forman, D.; Bray, F. Cancer incidence and mortality worldwide: Sources, methods and major patterns in GLOBOCAN 2012. Int. J. Cancer 2015, 136, E359–E386. [CrossRef] [PubMed]
5. Krakstad, C.; Chekenya, M. Survival signalling and apoptosis resistance in glioblastomas: Opportunities for targeted therapeutics. Mol. Cancer 2010, 9, 135. [CrossRef]
6. Ahmed, F.F.; Abd El-Hafeez, A.A.; Abbas, S.H.; Abdelhamid, D.; Abdel-Aziz, M. New 1,2,4-triazole-Chalcone hybrids induce Caspase-3 dependent apoptosis in A549 human lung adenocarcinoma cells. Eur. J. Med. Chem. 2018, 151, 705–722. [CrossRef]
7. Hu, T.; Li, Z.; Gao, C.-Y.; Cho, C.H. Mechanisms of drug resistance in colon cancer and its thera peutic strategies. World J. Gastroenterol. 2016, 22, 6876–6889. [CrossRef]
8. Asweto, C.O.; Wu, J.; Alzain, M.A.; Hu, H.; Andrea, S.; Feng, L.; Yang, X.; Duan, J.; Sun, Z. Cellular pathways involved in silica nanoparticles induced apoptosis: A systematic review of *in vitro* studies. Environ. Toxicol. Pharmacol. 2017, 56, 191–197. [CrossRef]
9. Zhang, H.; Song, H.; Yuan, R.; Zhang, X.; Yu, H.; Zhao, Y.; Jiang, T. Polyene phosphatidylcholine overcomes oxaliplatin resistance in human gastric cancer BGC823 cells. Biochem. Biophys. Res. Commun. 2018, 497, 108–114. [CrossRef]
10. Zhang, P.; Chen, Z.; Ning, K.; Jin, J.; Han, X. Inhibition of B7-H3 reverses oxaliplatin resistance in human colorectal cancer cells. Biochem. Biophys. Res. Commun. 2017, 490, 1132–1138. [CrossRef]
11. Indran, I.R.; Tufo, G.; Pervaiz, S.; Brenner, C. Recent advances in apoptosis, mitochondria and drug resistance in cancer cells. Biochim. Biophys. Acta 2011, 1807, 735–745. [CrossRef] [PubMed]
12. Hong, Z.-P.; Wang, L.-G.; Wang, H.-J.; Ye, W.-F.; Wang, X.-Z. Wogonin exacerbates the cytotoxic effect of oxaliplatin by inducing nitrosative stress and autophagy in human gastric cancer cells. Phytomedicine 2018, 39, 168–175. [CrossRef] [PubMed]
13. Kumar, B.; Jajodia, K.; Kumar, P.; Gautam, H. Recent advances in nanoparticle-mediated drug delivery. J. Drug Deliv. Sci. Technol. 2017, 41, 260–268. [CrossRef]
14. Zang, X.; Zhao, X.; Hu, H.; Qiao, M.; Deng, Y.; Chen, D. Nanoparticles for tumor immunotherapy. Eur. J. Pharm. Biopharm. 2017, 115, 243–256. [CrossRef] [PubMed]
15. Masloub, S.M.; Elmalahy, M.H.; Sabry, D.; Mohamed, W.; Hassan, S. Comparative evaluation of PLGA nanoparticle delivery System for 5-fluorouracil and curcumin on squamous cell carcinoma. Arch. Oral Biol. 2016, 64, 1–10. [CrossRef] PubMed]
16. Benita, S. Microencapsulation: Methods and Industrial Applications, 2nd ed.; CRC Press: Boca Raton, FL, USA, 2005.
17. Yang, Y.-Y.; Chung, T.-S.; Ping Ng, N. Morphology, drug distribution, and *in vitro* release profiles of biodegradable polymeric microspheres containing protein fabricated by double-emulsion solvent extraction/evaporation method. Biomaterials 2001, 22, 231–241. [CrossRef]
18. Jelvehgari, M.; Montazam, S.H. Comparison of microencapsulation by emulsion-solvent

extraction/ evaporation technique using derivatives cellulose and acrylate-methacrylate copolymer as carriers. Jundishapur J. Nat. Pharm. Prod. 2012, 7, 144–152.
19. Imbrogno, A.; Piacentini, E.; Drioli, E.; Giorno, L. Preparation of uniform poly-caprolactone Microparticles by membrane emulsification/solvent diffusion process. J. Membr. Sci. 2014, 467, 262–268. [CrossRef]
20. Imbrogno, A.; Dragosavac, M.M.; Piacentini, E.; Vladisavljevic´, G.T.; Holdich, R.G.; Giorno, L. Polycaprolactone multicore-matrix particle for the simultaneous encapsulation of hydrophilic and hydrophobic compounds produced by membrane emulsification and solvent diffusion processes. Colloids Surf. B Biointerfaces 2015, 135, 116–125. [CrossRef]
21. Iqbal, M.; Zafar, N.; Fessi, H.; Elaissari, A. Double emulsion solvent evaporation techniques used for drug encapsulation. Int. J. Pharm. 2015, 496, 173–190. [CrossRef]
22. Varan, G.; Öncül, S.; Ercan, A.; Benito, J.M.; Ortiz Mellet, C.; Bilensoy, E. Cholesterol-Targeted Anticancer and Apoptotic Effects of Anionic and Polycationic Amphiphilic Cyclodextrin Nanoparticles. J. Pharm. Sci. 2016, 105, 3172–3182. [CrossRef] [PubMed]
23. Lee, J.-J.; Lee, S.Y.; Park, J.-H.; Kim, D.-D.; Cho, H.-J. Cholesterol-modified poly(lactide-co-glycolide) nanoparticles for tumor-targeted drug delivery. Int. J. Pharm. 2016, 509, 483–491. [CrossRef] [PubMed]
24. Akanda, M.H.; Rai, R.; Slipper, I.J.; Chowdhry, B.Z.; Lamprou, D.; Getti, G.; Douroumis, D. Delivery of retinoic acid to LNCap human prostate cancer cells using solid lipid nanoparticles. Int. J. Pharm. 2015, 493, 161–171. [CrossRef] [PubMed]
25. Nagar, P.; Goyal, P.; Gupta, A.; Sharma, A.K.; Kumar, P. Synthesis, characterization and evaluation of retinoic acid-polyethylene glycol nanoassembly as efficient drug delivery system. Nano Struct. Nano Objects 2018, 14, 110–117. [CrossRef]
26. Chen, M.-C.; Hsu, S.-L.; Lin, H.; Yang, T.-Y. Retinoic acid and cancer treatment. BioMedicine 2014, 4, 22. [CrossRef]
27. Cruz, L.J.; Tacken, P.J.; Rueda, F.; Domingo, J.C.; Albericio, F.; Figdor, C.G. Chapter eight—Targeting Nanoparticles to Dendritic Cells for Immunotherapy. In Methods in Enzymology; Düzgünes¸, N., Ed.; Academic Press: Cambridge, MA, USA, 2012; Volume 509, pp. 143–163.
28. Cruz, L.J.; Tacken, P.J.; Eich, C.; Rueda, F.; Torensma, R.; Figdor, C.G. Controlled release of antigen and Toll-like receptor ligands from PLGA nanoparticles enhances immunogenicity. Nanomed icine 2017, 12, 491–510. [CrossRef]
29. Urbaniak, T.; Musiał, W. Influence of Solvent Evaporation Technique Parameters on Diameter of Submicron Lamivudine-Poly-β-Caprolactone Conjugate Particles. Nanomaterials 2019, 9, 1240. [CrossRef]
30. Tel, J.; Lambeck, A.J.A.; Cruz, L.J.; Tacken, P.J.; de Vries, I.J.M.; Figdor, C.G. Human Plasmacytoid Dendritic Cells Phagocytose, Process, and Present Exogenous Particulate Antigen. J. Immunol. 2010, 184, 4276–4283. [CrossRef]
31. Cruz, L.J.; Tacken, P.J.; Fokkink, R.; Joosten, B.; Stuart, M.C.; Albericio, F.; Torensma, R.; Figdor, C.G. Targeted PLGA nano- but not microparticles specifically deliver antigen to human dendritic cells via DC-SIGN *in vitro*. J. Control. Release 2010, 144, 118–126. [CrossRef]
32. Zhang, W.; Wang, F.; Hu, X.; Liang, J.; Liu, B.; Guan, Q.; Liu, S. Inhibition of colorectal cancer liver metastasis in BALB/c mice following intratumoral injection of oncolytic herpes simplex virus type 2 for the induction of specific antitumor immunity. Oncol. Lett. 2019, 17, 815–822. [CrossRef]
33. Liu, L.; Mayes, P.A.; Eastman, S.; Shi, H.; Yadavilli, S.; Zhang, T.; Yang, J.; Seestaller-Wehr, L.; Zhang, S.-Y.; Hopson, C.; et al. The BRAF and MEK Inhibitors Dabrafenib and Trametinib: Effects on Immune Function and in Combination with Immunomodulatory Antibodies Targeting PD-1, PD-L1, and CTLA-4. Clin. Cancer Res. 2015, 21, 1639. [CrossRef] [PubMed]

34. Liu, Y.; Zhang, N.; Cao, Q.; Cui, X.; Zhou, Q.; Yang, C. The effects of propofol on the growth behavior of hepatoma xenografts in Balb/c mice. Biomed. Pharmacother. 2017, 90, 47–52. [CrossRef]
35. Liu, H.; Xu, H.W.; Zhang, Y.Z.; Huang, Y.; Han, G.Q.; Liang, T.J.; Wei, L.L.; Qin, C.Y.; Qin, C.K. Ursode oxycholic acid induces apoptosis in hepatocellular carcinoma xenografts in mice. World J. Gastroenterol. 2015, 21, 10367–10374. [CrossRef] [PubMed]
36. de Carvalho, T.G.; Garcia, V.B.; de Araújo, A.A.; da Silva Gasparotto, L.H.; Silva, H.; Guerra, G.C.B.; de Castro Miguel, E.; de Carvalho Leitão, R.F.; da Silva Costa, D.V.; Cruz, L.J.; et al. Spherical neutral gold nanoparticles improve anti-inflammatory response, oxidative stress and fibrosis in alcohol-methamphetamine-induced liver injury in rats. Int. J. Pharm. 2018, 548, 1–14. [CrossRef] [PubMed]
37. Araújo Jr, R.F.; Lira, G.A.; Vilaça, J.A.; Guedes, H.G.; Leitão, M.C.A.; Lucena, H.F.; Ramos, C.C.O. Prognostic and diagnostic implications of MMP-2, MMP-9, and VEGF-β expressions in colorectal cancer. Pathol. Res. Pract. 2015, 211, 71–77. [CrossRef] [PubMed]
38. Um, H.-D. Bcl-2 family proteins as regulators of cancer cell invasion and metastasis: A review focusing on mitochondrial respiration and reactive oxygen species. Oncotarget 2016, 7, 5193–5203. [CrossRef] [PubMed]
39. Xu, B.; Zhou, Z.G.; Li, Y.; Wang, L.; Yang, L.; Zhou, B.; Liu, H.Y.; Song, J.M.; Zeng, Y.J.; Wang, R.; et al. Clinicopathological Significance of Caspase-8 and Caspase-10 Expression in Rectal Cancer. Oncology 2008, 74, 229–236. [CrossRef] [PubMed]
40. Heijink, D.M.; Kleibeuker, J.H.; Jalving, M.; Boersma-van Ekb, W.; Koornstra, J.J.; Wesseling, J.; de Jong, S. Independent Induction of Caspase-8 and cFLIP Expression during Colorectal Carcinogenesis in Sporadic and HNPCC Adenomas and Carcinomas. Anal. Cell. Pathol. 2007, 29, 409–419. [CrossRef]
41. Sträter, J.; Herter, I.; Merkel, G.; Hinz, U.; Weitz, J.; Möller, P. Expression and prognostic significance of APAF-1, caspase-8 and caspase-9 in stage II/III colon carcinoma: Caspase-8 and caspase-9 is associated with poor prognosis. Int. J. Cancer 2010, 127, 873–880. [CrossRef]
42. Kim, H.S.; Lee, J.W.; Soung, Y.H.; Park, W.S.; Kim, S.Y.; Lee, J.H.; Park, J.Y.; Cho, Y.G.; Kim, C.J.; Jeong, S.W.; et al. Inactivating mutations of caspase-8 gene in colorectal carcinomas. Gastroenterology 2003, 125, 708–715. [CrossRef]
43. Graf, R.P.; Keller, N.; Barbero, S.; Stupack, D. Caspase-8 as a Regulator of Tumor Cell Motility. Curr. Mol. Med. 2014, 14, 246–254. [CrossRef] [PubMed]
44. Abbaszadeh-Goudarzi, K.; Shokri, F.; Hosseini, M.; Jadidi-Niaragh, F.; Ghalamfarsa, G.; Saboor-Yaraghi, A. Synergistic induction of apoptosis in B-cell chronic lymphocytic leukemia cells after treatment with all-Trans retinoic acid in combination with interleukin-21 and rituximab. J. Cancer Res. Ther. 2016, 12, 1278. [CrossRef] [PubMed]
45. Sutar, Y.B.; Telvekar, V.N. Chitosan based copolymer-drug conjugate and its protein targeted polyelectrolyte complex nanoparticles to enhance the efficiency and specificity of low potency anticancer agent. Mater. Sci. Eng. C 2018, 92, 393–406. [CrossRef] [PubMed]
46. Tummala, S.; Kumar, M.N.; Pindiprolu, S.K. Improved anti-tumor activity of oxaliplatin by encapsulating in anti-DR5 targeted gold nanoparticles. Drug Delivr. 2016, 23, 3505–3519. [CrossRef]
47. Alian, O.M.; Azmi, A.S.; Mohammad, R.M. Network insights on oxaliplatin anti-cancer mecha nisms. Clin. Transl. Med. 2012, 1, 26. [CrossRef]
48. Zori Comba, A.; Blajman, C.; Richardet, E.; Bella, S.; Vilanova, M.; Cóppola, F.; Van Kooten, M.; Rodger, J.; Giglio, R.; Balbiani, L.; et al. A randomised phase II study of oxaliplatin alone versus oxaliplatin combined with 5-fluorouracil and folinic acid (Mayo Clinic regimen) in previously untreated metastatic colorectal cancer patients. Eur. J. Cancer 2001, 37, 1006–1013. [CrossRef]

49. Prado Almeida, E.D.; Vieira Dipieri, L.; Rosseti, F.C.; Maldonado Marchetti, J.; Lopes Badra Bentley, M.V.; de Souza Nunes, R.; Sarmento, V.H.V.; Giroldo Valério, M.E.; Rodrigues, J.J.; Martins Montalvão, M.; et al. Skin permeation, biocompatibility and antitumor effect of chloroaluminum phthalocyanine associated to oleic acid in lipid nanoparticles. Photodiagnosis Photodyn. Ther. 2018, 24, 262–273. [CrossRef]
50. Kumar, S.; Sangwan, P.; Lather, V.; Pandita, D. Biocompatible PLGA-oil hybrid nanoparticles for high loading and controlled delivery of resveratrol. J. Drug Deliv. Sci. Technol. 2015, 30, 54–62. [CrossRef]
51. Rompicharla, S.V.K.; Bhatt, H.; Shah, A.; Komanduri, N.; Vijayasarathy, D.; Ghosh, B.; Biswas, S. Formulation optimization, characterization, and evaluation of *in vitro* cytotoxic potential of curcumin loaded solid lipid nanoparticles for improved anticancer activity. Chem. Phys. Lipids 2017, 208, 10–18. [CrossRef]
52. Lee, C.S.; Kim, H.; Yu, J.; Yu, S.H.; Ban, S.; Oh, S.; Jeong, D.; Im, J.; Baek, M.J.; Kim, T.H. Doxorubi cin-loaded oligonucleotide conjugated gold nanoparticles: A promising *in vivo* drug delivery system for colorectal cancer therapy. Eur. J. Med. Chem. 2017, 142, 416–423. [CrossRef]
53. Watabe, H.; Soma, Y.; Ito, M.; Kawa, Y.; Mizoguchi, M. All-trans Retinoic Acid Induces Differenti ation and Apoptosis of Murine Melanocyte Precursors with Induction of the Microphthalmia-As sociated Transcription Factor. J. Investig. Dermatol. 2002, 118, 35–42. [CrossRef] [PubMed]
54. C Tsamandas, A.; Kardamakis, D.; Tsiamalos, P.; Liava, A.; Tzelepi, V.; Vassiliou, V.; Petsas, T.; Vagenas, K.; Zolota, V.; Scopa, C. The Potential Role of Bcl-2 Expression, Apoptosis and Cell Proliferation (Ki-67 Expression) in Cases of Gastric Carcinoma and Correlation with Classic Prognostic Factors and Patient Outcome. Anticancer Res. 2009, 29, 703–709. [PubMed]
55. Li, L.T.; Jiang, G.; Chen, Q.; Zheng, J.N. Ki67 is a promising molecular target in the diagnosis of cancer (review). Mol. Med. Rep. 2015, 11, 1566–1572. [CrossRef] [PubMed]
56. Lowe*, M.H.a.S. The p53–Bcl-2 connection.Cell Death and Differentiation. Cell Death Differ. 2006, 13. [CrossRef]
57. Toussaint, O.; Royer, V.; Salmon, M.; Remacle, J. Stress-induced premature senescence and tissue ageing. Biochem. Pharmacol. 2002, 64, 1007–1009. [CrossRef]
58. Vedagiri, H.; Helga Jenifer, M.; Sneha Mirulalini, G. Integrative analysis of CXCR4/CXCL12 axis gene expression alterations in breast cancer and its prognostic relevance. Gene Rep. 2018, 11, 6–11. [CrossRef]
59. Pollino, S.; Palmerini, E.; Dozza, B.; Bientinesi, E.; Piccinni-Leopardi, M.; Lucarelli, E.; Righi, A.; Benassi, M.S.; Pazzaglia, L. CXCR4 in human osteosarcoma malignant progression. The response of osteosarcoma cell lines to the fully human CXCR4 antibody MDX1338. J. Bone Oncol. 2019, 17, 100239. [CrossRef]
60. Mandal, P.K.; Biswas, S.; Mandal, G.; Purohit, S.; Gupta, A.; Majumdar, A.; Roy Chowdhury, S.; Bhattacharyya, A. CCL2 conditionally determines CCL22-dependent Th2-accumulation during TGF-β-induced breast cancer progression. Immunobiology 2018, 223, 151–161. [CrossRef]
61. Wei, Y.; Wang, T.; Song, H.; Tian, L.; Lyu, G.; Zhao, L.; Xue, Y. C-C motif chemokine 22 ligand (CCL22) concentrations in sera of gastric cancer patients are related to peritoneal metastasis and predict recurrence within one year after radical gastrectomy. J. Surg. Res. 2017, 211, 266–278. [CrossRef]
62. Yan, X.; Li, P.; Zhan, Y.; Qi, M.; Liu, J.; An, Z.; Yang, W.; Xiao, H.; Wu, H.; Qi, Y.; et al. Dihydroartemisinin suppresses STAT3 signaling and Mcl-1 and Survivin expression to potentiate ABT-263-induced apoptosis in Non-small Cell Lung Cancer cells harboring EGFR or RAS mutation. Biochem. Pharmacol. 2018, 150. [CrossRef]

63. Lv, T.; Li, Z.; Xu, L.; Zhang, Y.; Chen, H.; Gao, Y. Chloroquine in combination with aptamer modified nanocomplexes for tumor vessel normalization and efficient erlotinib/Survivin-shRNA co-de livery to overcome drug resistance in EGFR-mutated NSCLC. Acta Biomater. 2018, 76. [CrossRef]
64. Kapse-Mistry, S.; Govender, T.; Srivastava, R.; Yergeri, M. Nanodrug delivery in reversing multidrug resistance in cancer cells. Front. Pharmacol. 2014, 5. [CrossRef]

CHAPTER **FOUR**

Ana Luiza C. de S. L. Oliveira, Luana Zerillo, Luis J. Cruz*, Timo Schomann, Alan B. Chan, Thaís Gomes de Carvalho, Shirley Vitória de P. Souza, Aurigena A. Araújo, Lioe-Fee de Geus-Oei, Raimundo F. de Araújo Júnior*.

Maximizing the potency of oxaliplatin coated nanoparticles with folic acid for modulating tumor progression in colorectal cancer. Materials Science and Engineering: C. January 2021. DOI: 10.1016/j.msec.2020.111678.

MAXIMIZING THE POTENCY OF OXALIPLATIN COATED NANOPARTICLES WITH FOLIC ACID FOR MODULATING TUMOR PROGRESSION IN COLORECTAL CANCER

Abstract: One of the challenges of nanotechnology is to improve the efficacy of treatments for diseases, in order to reduce morbidity and mortality rates. Following this line of study, we made a nanoparticle formulation with a small size, uniform surfaces, and a satisfactory encapsulation coefficient as a target for colorectal cancer cells. The results of binding and uptake prove that using the target system with folic acid works: Using this system, cytotoxicity and cell death are increased when compared to using free oxaliplatin. The data show that the system maximized the efficiency of oxaliplatin in modulating tumor progression, increasing apoptosis and decreasing resistance to the drug. Thus, for the first time, our findings suggest that PLGA-PEG-FA increases the antitumor effectiveness of oxaliplatin by functioning as a facilitator of drug delivery in colorectal cancer.

Keywords: Drug delivery system, Oxaliplatin, Folic acid, Apoptosis, Drug resistance.

INTRODUCTION

Nowadays, cancer is one of the leading reasons for death worldwide. The number of incidence and mortality has increased in the last decades, and it is expected that the number will continue to grow [1,2]. Colorectal cancer (CRC), considered rare in the past, is now becoming more frequent and new therapeutical approaches are emerging to fight CRC, such as the use of nanomedicine to improve established therapies [3–5].

Tumor mass develops as a result of a sequence of malignant events, and some characteristics of the tumor cells are common to all types of tumor cells. One of them is the ability to prevent apoptosis [6,7]. Apoptosis is a biological process that occurs through the extrinsic and intrinsic pathways, converging on a common path that will end with cell death. The activation of these pathways helps to stop the progression of tumors [8,9].

Oxaliplatin (OXA) is a chemotherapeutic agent, a third-generation platinum, that has been used in the treatment of CRC in therapeutic regimes [4,10,11]. This drug acts mainly against tumor cells by binding to DNA. Subsequently, OXA forms adducts in GC-rich areas in the DNA, activating the DNA replication and transcription processes [12,13]. Mechanisms of resistance to OXA are reported as one of the major causes of failure in the treatment of CRC, due to the accumulation of enzymes and detoxification transporters (leading to increased detoxification), resulting in decreased intracellular amount of drugs and accumulation of repair enzymes by excision of nucleotides [11,12,14].

Drug delivery systems (DDSs) may be used to overcome the limitations of OXA treatment. This can be realized by adjusting the dose of the chemotherapeutic agent, increasing the internalization of the drug in the cells and enhancing bioavailability, which will lead to increased drug efficiency, and a decrease in adverse effects and drug resistance [15–17]. Currently, poly (D,L-lactide-co-glycolic acid) (PLGA) is widely used as a DDS due to its biocompatibility and biodegradability characteristics [18,19]. PLGA polymer nanoparticles can be designed with surface modifications; an example is the addition of hydrophilic and polymeric polyethylene glycol (PEG), which prevents interactions with macrophages or phagocytes, guaranteeing the delivery and distribution of drugs in the tumor environment [18–21].

These nanoparticles can have their surfaces modified with the addition of targeting molecules, which increases the selectivity, applicability and effectiveness of DDS [22]. An example for a nanoparticle targeting is folic acid (FA), that interacts with the folate receptor, which is overexpressed in a wide range of human cancers, but is very low in healthy tissues [21,23]. Targeted PLGA nanoparticles have been used in the development of a DDS for the treatment of cancer; they improve the antitumor activity of drugs by inducing apoptosis, reducing side effects, suppressing metastasis, and decreasing resistance to drugs [4,5].

Based on the above, the aim of this study is to formulate a novel modified FA-PLGA nanoparticles loaded with OXA to enhance the effect of this drug against colorectal cancer. Our nanoparticle system can target CRC cells and amplify the anti-tumor activity of OXA. In this study, for the first time we combined PLGA, FA, and OXA, we designed, characterized, and evaluated anti-tumor activity in murine colon carcinoma cells of the modified FA-PLGA nanoparticles loaded with OXA.

2. MATERIALS AND METHODS

2.1. Reagents

PLGA (PURASORB® PDLG 5002A 50:50, inherent viscosity 0.20 dL/g, MW =17,000) was obtained from Carbion PURAC (Amsterdam, the Netherlands); polyvinyl alcohol (PVA) (87–89% hydrolyzed, typical MW 13.000-23.000), N-(3-dimethylaminopropyl)-N'-ethylcarbodiimide hydrochloride (EDC, ≥98.0%), N-hydroxysuccinimide (NHS, 98%), methylene chloride, dimethylformamide (99.8%), chloroform (99%), and triethylamine (TEA, 99.5%) were purchased from Sigma- Aldrich (Steinheim, Germany). PEG with diamine group (NH2-PEG- NH2, MW 3143) was obtained from Iris Biotech (Biotech GmbH, Marktredwitz, Germany). The solvent used to prepare the nanoparticles, and dichloromethane (DCM, 99.8%) were purchased from Sigma- Aldrich (Darmstadt, Germany). The NPs were all loaded with NIR dye (IR-780 Iodide) purchased from Sigma-Aldrich (Zwijndrecht, the Netherlands) and OXA (Sigma-Aldrich, Darmstadt, Germany). The target FA was obtained from Sigma-Aldrich (Steinheim, Germany). The *in vitro* studies were performed using Dulbecco's modified Eagle's medium (DMEM) (Gibco Laboratories, Grand Island, USA), Fetal Bovine Serum (FBS)

(Bodinco BV, Alkmaar, the Netherlands), trypsin/EDTA (Gibco Technologies, Grand Island, NY, USA), CellTiter 96 AQueous One Solution (MTS) solution (Promega Corporation, Madison, WI, USA), 4,6- diamidino-2-phenylindole (DAPI) (Thermo Fisher Scientific, Cambridge, MA, USA), DiD cell-labeling solution (Thermo Fisher Scientific, Cambridge, MA, USA), V-FITC (BD Pharmigen, CA, USA), To-pro 3 iodide (642/661) (Invitrogen, Eugene, USA) and Tween-20 (Promega, Madison, WI, USA). All primary and the secondary antibodies were purchased from Abcam, Burlingame, CA, USA. The *in vivo* studies were performed using streptavidin/Haptoglobin Related Protein (HRP)-conjugated secondary antibody (Biocare Medical, Concord, CA, USA), colorimetric-based detection kit (TrekAvidin-HRP Label Kit from Biocare Medical, Pacheco, USA), trizol reagent (Invitrogen Co., Carlsbad, CA, USA), SV Total RNA Isolation System (Promega, Madison, WI, USA) and SYBR Green MiX in the Applied Biosystems1 7500 FAST system (Applied Biosystems, Foster City, CA, USA).

2.2. Synthesis of polymers as well as preparation and characterization of nanoparticles

The polymers PLGA-PEG and PLGA-PEG-FA were synthesized in 4 different steps (Fig. 1A) using the single-emulsion solvent evaporation method [24], and were characterized by H-NMR (Proton nuclear magnetic resonance). For the nanoparticles loaded with near infrared 780 dye (NIR) and co-loaded with OXA, a double-emulsion solvent evaporation method of water-oil-water (W/O/W) was used [25].

An optical measure was performed to test the amount of FA conjugated with PLGA-PEG as follows: a solution of PLGA-PEG-FA was measured with Amersham Biosciences Ultrospec 2100 pro, UV/Vis Spectrophotometer and Absorbance was read at 350 nm [26,27].

In order to determine the encapsulation efficiency [28] and the loading content of the NIR dye and OXA, a solution of nanoparticles was measured for the NIR dye content using an Odyssey Infrared Imager 9120 (LI-COR) scanner at 800 nm. The concentration of OXA was determined by reversed-phase high-performance liquid chromatography

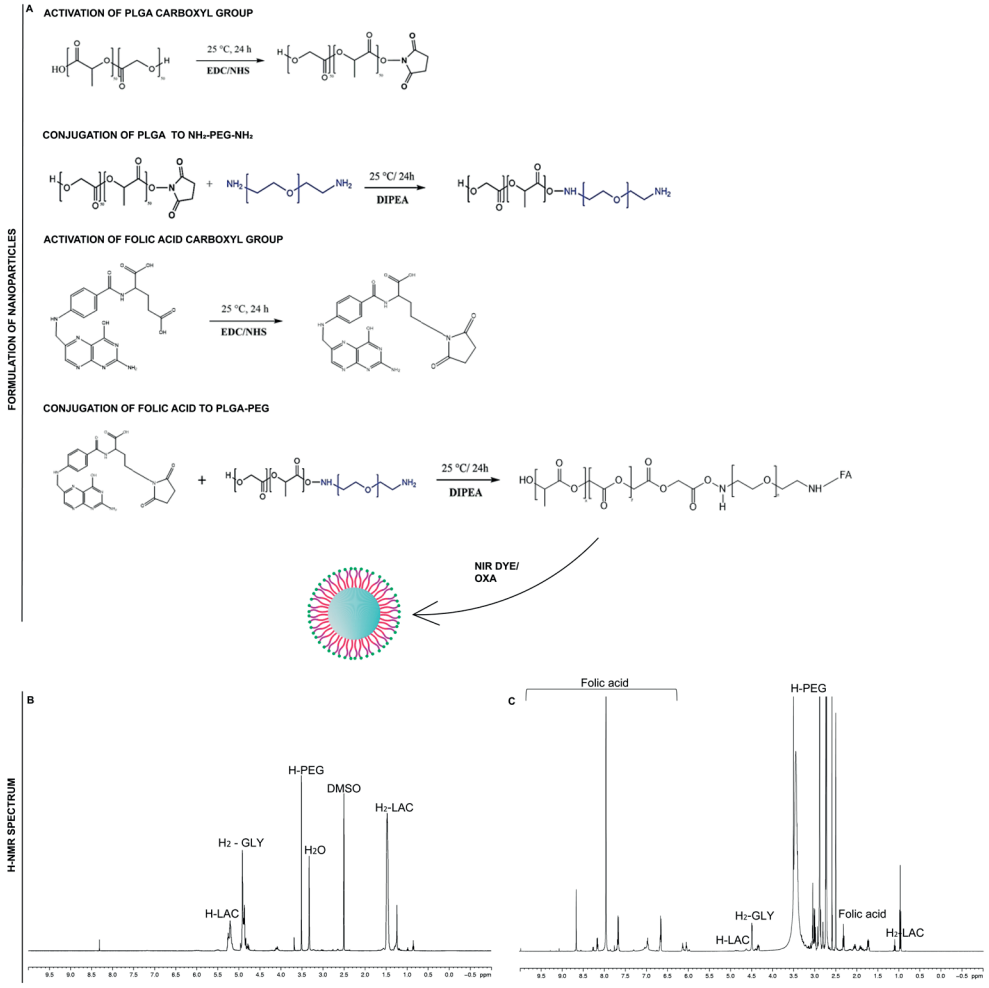

Figure 1. Formulation and characterization of nanoparticles. (A) Schematic illustration of formulation of PLGA-PEG-FA co-polymer and nanoparticles. H-NMR spectrum: (B) PLGA-PEG and (C) PLGA-PEG-FA co-polymers.

(RP-HPLC).

2.3. Morphology and physicochemical properties of nanoparticles

To visualize and characterize the structure of the nanoparticles, transmission electron microscopy (TEM) was used. A droplet of 3 µL of the nanoparticle solution was imaged in a Tecnai 12 Biotwin transmission electron microscope (FEI, the Netherlands), equipped with a LaB6

filament operated at 120 kV. The average size of the nanoparticles and their polydispersity index (PDI) were determined by dispersing the nanoparticles in MilliQ water using Dynamic Light Scattering (DLS). The stability of the nanoparticles was determined by measurement of their zeta potential (Zetasizer Nano S90, Malvern Instruments, Worcestershire, UK). The zeta potential analysis of the nanoparticles was performed by DLS.

2.4. Drug release studies

The *in vitro* drug release of OXA from PLGA nanoparticles was evaluated in phosphate-buffered saline (PBS) with pH 7.4 as release medium. Briefly, 1 mg of the freeze-dried nanoparticles [PLGA-PEG OXA and PLGA-PEG (OXA)-FA] were resuspended in PBS (1 mg/mL), triplicate for each formulation, and incubated at 37 ◦C under continuous shaking (300 rpm). At predetermined time points the nanoparticles were separated by centrifugation (12.000 rpm for 20 min), 150 µL aliquots were sampled and 150 µL of fresh and warm PBS added to release medium. The aliquots were maintained at 20 ◦C and, at the end of experiment, the concentration of OXA in the supernatant was measured spectrophotometrically at **λ** = 240 nm (Ultrospec 2100 pro).

2.5. Binding assay and uptake assay

Murine colorectal carcinoma (CT-26) cells were seeded in a black-walled 96-well cell culture microplate and incubated with PLGA-PEG and PLGA-PEG-FA at 10 µg/mL for 0, 1, 2, 8, or 24 h. For the binding assay, the plate was maintained at 4 ◦C, while the plate was maintained at 37 ◦C for the uptake assay. After the different time points, nuclei of the cells were stained with To-pro 3 iodide dye, which is detectable at 700 nm. The plate was imaged with an Odyssey Infrared Imager 9120 (LICOR) scanner using 700 nm and 800 nm channels to visualize the cell nuclei

and NIR-loaded nanoparticles, respectively.

2.6. Internalization of nanoparticles by cells and fluorescence imaging

The CT-26 cells were plated and treated with PLGA-PEG and PLGA-PEG-FA at 10 µg/mL. After 4, 8, 24, and 48 h, the cells were stained with DiD and DAPI. For the visualization of nanoparticles (yellow), cell membrane (pink), and nucleus (blue), a Leica DM5500 B fluorescence microscope equipped with a Leica DFC365 FX digital camera (Leica) was used. Digital images were acquired, analyzed, and stored using Leica Application Suite X (LAS X) software.

2.7. Viability test

The cells were cultured and free OXA, PLGA-PEG, PLGA-PEG (OXA) and PLGA-PEG-FA (OXA) at concentrations of 1 µg/mL, 5 µg/mL, 10 µg/ mL, 20 µg/mL, and 50 µg/mL, respectively, were added; positive (25% DMSO) and negative controls were included. After 24, 48 or 72 h of treatment, MTS [3-(4,5-dimethylthiazol-2-yl)-5-(3-carboxymethoxyphenyl)-2-(4-sulfophenyl)-2H-tetrazolium, innersalt] solution was added to the wells and incubated for 3 h. Absorbance was measured at 490 nm using Molecular Devices VERSAmax Tunable Microplate Reader.

2.8. Detection of cell death by flow cytometry and immunofluorescence

CT-26 cells were plated and treated with free OXA and PLGA nanoconjugates [PLGA-PEG (OXA) and PLGA-PEG-FA (OXA)] at 10 µg/mL and 20 µg/mL for 24 and 48 h. After each period, the cells intended for flow cytometric analysis were labelled with Annexin V-FITC and DAPI, sorted with a BD FACS Canto II (BD Biosciences, CA, USA), and analyzed with FlowJo software, version 10.1 (Tree Star Inc., CA, USA). For immunofluorescence, the cells were incubated with the primary antibodies, anti-FAS-associated protein with death domain (FADD) rabbit (2.5:100), anti-apoptotic protease activating factor 1 (APAF-1) rabbit (1:100), and anti-caspase-3 rabbit (1:200), in blocking solution at 4 ◦C overnight. The primary antibody was detected with Alexa Fluor 555 anti-rabbit secondary antibody diluted at 1:300 in blocking buffer. DAPI (1:1000)

in phosphate-buffered saline was used for nuclear staining. Samples were examined with a Leica DM5500 B fluorescence microscope, as mentioned above.

2.9. CRC xenograft *in vivo* models and treatment regimens

For the animal model, the CT-26 cells (5 106) was subcutaneously injected into the right flank of male Balb/c mice. When the tumor volume achieved 3-4 mm [29], the animals were organized into four groups with five animals each, and were treated intratumorally three times in 15 days with injection dose of 5 mg/Kg. The groups for this experiment were, (1) Saline 5 mg/Kg saline solution, (2) OXA 5 mg/Kg, (3) PLGA-PEG (OXA) 5 mg/Kg and (4) PLGA-PEG-FA (OXA) 5 mg/Kg = The tumor size was measured every two days during 21 days or until the tumor reached a volume of 2000 mm3 [30,31]. For calculate their volume, was used the equation below [32]:

$$\text{Volume} = (\text{length} \times \text{width}^2 \times 0.523).$$

In the end of the experiment the animals were euthanized (80 mg/Kg, i.p.) 2% thiopental (Crista´lia, Sa˜o Paulo, Brazil) and the subcutaneous tumor was removed and collected, half of the tumor was immediately stored at 80 ◦C for qPCR analysis and the other part were placed in 10% paraformaldehyde for histopathological analysis. Therefore, the protocol was accepted by the Committee on the Ethics of Animal Experiments of the UFRN (Universidade Federal do Rio Grande do Norte) (CEUA, permit number: 222.011/2020).

2.10. Immunohistochemical staining of caspase-3 and survivin

The tumors of each group were cut using a microtome. Tissue sections were stored with primary antibodies anti-caspase-3 (CUSABIO CSB-PA 140280) and anti-survivin (NOVUS NB 500-201SS) at 4 ◦C overnight. Then, the fragments were washed with phosphate-buffered saline and incubated with a streptavidin/haptoglobin-related protein (HRP)-conjugated secondary antibody.

The proteins showed immunoreactivity with the use of colorimetric-based detection kit following the protocol provided by the manufacturer. To obtain digital images, a high-power objective (40) light microscopy (Nikon Eclipse 2000 equipped with Nikon DS-Fi2; Nikon Corporation, Tokyo, Japan) was used. For analysis the intensity of cell immunostaining, two trained examiners in a double-blind evaluated the labelling intensity. The immunoreactivity was analyzed based on the scores with minor modifications [33] for which the and the percentage (P) of tumor cells with characteristic staining (from an undetectable level or 0%, for homogeneous staining or 100%) and estimate of the intensity (I) of staining (1, weak staining; 2, moderate staining; and 3, strong staining). The result of the scores is obtained by multiplying the value of the percentage of cells marked by the intensity of the mark.

2.11. Analysis of mRNA expression

The RNA extraction from tumor tissue was realized using a trizol reagent and SV Total RNA Isolation System. For real-time quantitative polymerase chain reaction (PCR) analyses, a SYBR Green MiX was used in the β-actin, FADD, APAF-1, multidrug resistance protein 1 (MDR1), survivin, C-X-C chemokine receptor type 4 (CXCR4), and monocyte-derived chemokine (CCL22) messenger ribonucleic acids (mRNAs). The primers are listed in Table S1.

The standard PCR conditions were followed [4]. Mean threshold cycle (Ct) values were used to calculate the relative expression levels of the target genes for the experimental groups, relative to those in the negative control group; expression data were normalized relative to the housekeeping gene β-actin using the 2—ΔΔCt formula.

2.12. Statistical analysis

All *in vitro* experiments were performed in triplicate. The significant

differences between the groups were calculated using the analysis of variance (ANOVA) and the Bonferroni's test, as indicated. A p-value of <0.05 was considered to be statistically significant ($p < 0.05$, $p < 0.01$, $p < 0.001$, and $p < 0.0001$).

3. RESULTS

3.1. Synthesis and characterizations of nanoparticles

The success of PLGA-PEG and PLGA-PEG-FA polymers was confirmed by H-NMR analysis. It was possible to identify the PLGA groups [-CH2- and — CH3 peaks of poly(D,L-lactide), d = 5.2–5.3 and 1.5 ppm; CH2- peak of poly (glycolide), d 4.8–4.9 ppm], the PEG group (d= 3.6 ppm), and the characteristic peaks of the folic acid (d= 4.5, 6.6, 7.6, and 8.6 ppm) (Fig. 1B and C).

The average size, the zeta potential and the percentage encapsulation efficiency of the nanoparticles are displayed in Table 1, and the DLS curves at Supplementary materials (Fig. 1S). All nanoparticles were negatively charged as determined by measurement of their zeta potential. In average, 64.68% percent of FA was conjugated to PEG-PLGA as well as 64.06% conjugated to PLGA-PEG-FA (OXA). The percentage of encapsulation efficiency of OXA for PLGA-PEG NPs was 55% and for PLGA-PEG-FA nanoparticles it was 50% (Table 1).

The morphology of the nanoparticles was visualized by TEM microscopy and revealed that all generated nanoparticles were spherical, with a smooth surface and uniform sizes (Fig. 2A–D).

NPs	Size ± SD (nm)	PDI	Zeta potential ± SD (mV)	% FA bound to PLGA -PEG	EE% NIR	EE% OXA
PLGA-PEG	197.3 ± 0.52	0.01	-20.1 ± 5.09	--	39.03	--
PLGA-PEG (OXA)	198.5 ± 0.67	0.04	-20.8 ± 4.07	--	37.14	55
PLGA-PEG -FA	180.8 ± 1.35	0.04	-24.5 ± 5.07	64.68	26.05	--
PLGA-PEG -FA (OXA)	201.3 ± 1.78	0.06	-23.6 ± 9.51	64.06	24.09	50

Table 1. Diameter, polydispersity index, zeta potential, percentage of FA bound to PLGA- PEG as well as encapsulation efficiency (EE%) of NIR dye and OXA in the analysis of the chosen nanoparticles.

Notes. PDI (Polydispersity Index), nm (Nanometer), Standard Deviation (SD), Millivolt (mV).encapsulation efficiency (EE%) of NIR dye and OXA in the analysis of the chosen nanoparticles.

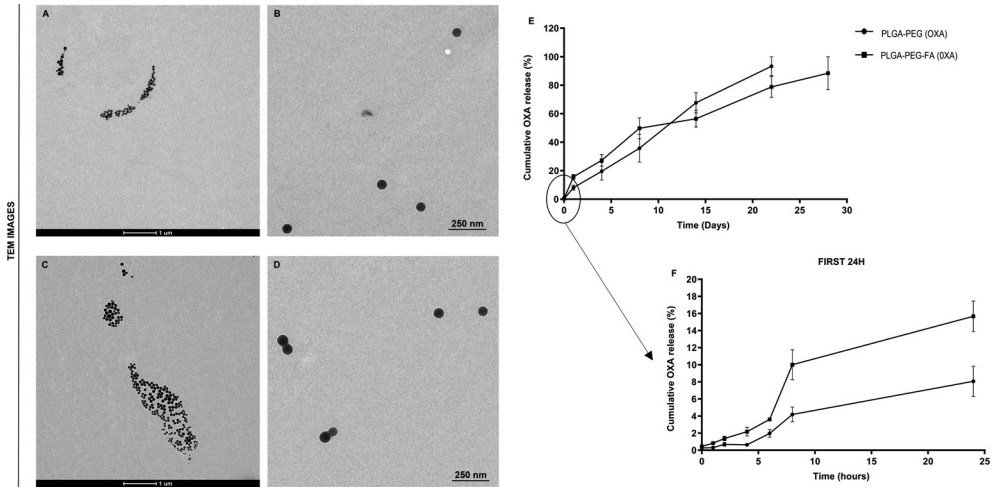

Figure 2 Morphology images, and Drug release studies of nanoparticles. Morphology images of nanoparticles obtained by TEM: (A, B) PLGA-PEG (OXA) and (C, D) PLGA-PEG-FA (OXA). The graphs show the percentage of cumulative release of OXA in PBS, when the drug is encapsulated in two systems, PLGA-PEG and PLGA-PEG- FA. (E) Cumulative release throughout the experiment. (F) Cumulative release in the first 24 h of the experiment.

3.2. Drug release studies

The PLGA-PEG system demonstrating through the results obtained slow, gradual and progressive release. The release study of OXA from PLGA-PEG (OXA) and PLGA-PEG-FA (OXA) in PBS initially showed different patterns with about 16% of OXA released within the first 24 h for PLGA-PEG-FA (0XA) and 7% of OXA for the PLGA-PEG (OXA) (Fig. 2F). However, after 8 days, PLGA-PEG-FA (OXA) started released slowly then PLGA-PEG (OXA). The OXA release for was 100% around 23 days, while until the end of the experiment (28 days), the PLGA-PEG-FA (OXA) did not release all amount of OXA (Fig. 2E).

3.3. Binding and uptake assay

In Fig. 3, the nanoparticle with the target FA (PLGA-PEG-FA) showed higher binding and uptake than the nanoparticle without the target FA (PLGA-PEG). For binding assay there is no statistical difference between the nanoparticles at time 0 h, but all other times presented differences between them. For 1 h, $p < 0.001$; for 2 h $p < 0.01$; for 4 h, 8 h and 24 h the difference is $p < 0.0001$. While for the uptake there is no difference between the nanoparticles at time 0 h and 24 h, for the others time points the difference has a $p < 0.0001$ for 1 h and 2 h, $p < 0.001$, for 4 h and $p < 0.01$ for 8 h (Fig. 3).

3.4. Internalization of nanoparticles

The images show both nanoparticle formulations inside the tumor cells (in yellow) at all time points. However, Fig. 3 shows that more PLGA-PEG-FA nanoparticles than the PLGA-PEG were able to enter the tumor cells (Fig. 3).

3.5. Viability test

PLGA-PEG did not show cytotoxicity at any time point (Fig. 2S). After 24 h, the free OXA showed cytotoxicity at 5, 10, 20 and 50 µg/mL (p

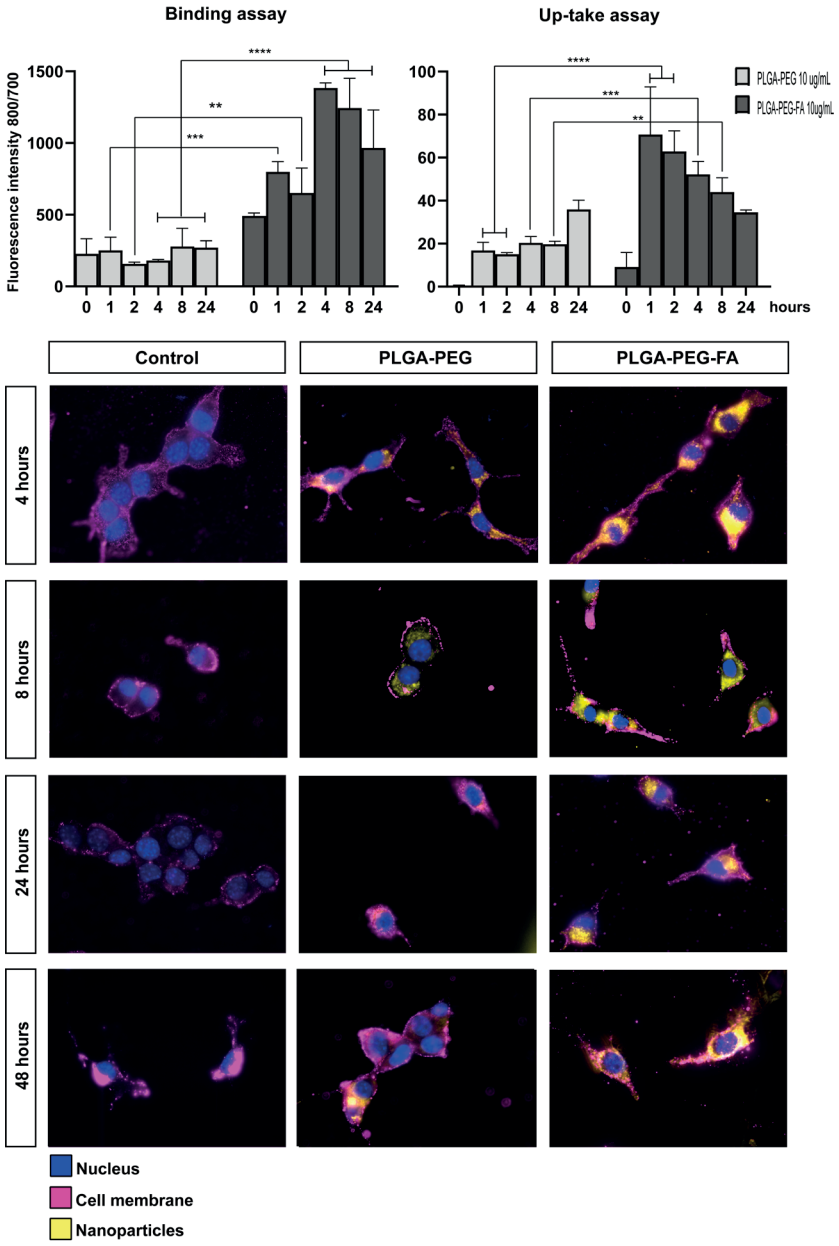

Figure 3 Binding, uptake, and Internalization assays of nanoparticles by CT-26 cells. The graphs show the fluorescence intensity (y axis) for the dye contained in the nanoparticles when the cells are treated with 10 μg/mL PLGA-PEG and PLGA-PEG-FA for several hours (X axis). The images show the PLGA-PEG and PLGA-PEG-FA nanoparticles (in yellow) at a concentration 10 μg/mL inside the cancer cells after 4, 8, 24, and 48 h of incubation. Pink: membrane. Blue: nucleus. Magnification: 63×. (For interpretation of the references to colour in this figure legend, the reader is referred to the web version of this article).

< 0.0001), PLGA-PEG (OXA) showed similar cytotoicity than OXA (p <0.001 at 5, 10 and 50 μg/mL and p < 0.001 for 20 μg/mL). The activity of PLGA-PEG-FA (OXA) was detected at all concentration (p < 0.0001), also at the lower dose, 1 μg/mL (Fig. 2SA). After 48 h, treatment with free OXA, PLGA-PEG (OXA) and PLGA-PEG-FA (OXA) at all concentrations further decreased the number of viable cells [p < 0.0001, except for 1 μg/mL OXA (p < 0.01)] (Fig. 2SB). After 72 h of treatment, the result was comparable, but 1 μg/mL OXA did not show significant cytotoXicity (Fig. 2SC).

3.6. Flow cytometry

The data showed that only PLGA-PEG-FA (OXA) induced cell death at a concentration of 20 μg/mL (p < 0.001) after 24 h compared to the control (Fig. 4A). After 48 h, the percentage of cell death for the three compounds was higher than that of the control. The activity of 10 μg/mL OXA and 10 μg/mL PLGA-PEG (OXA) was higher (p < 0.0001) then 20 μg/mL OXA, 20 μg/mL PLGA-PEG (OXA) and 10 μg/mL and 20 μg/mL PLGA-PEG (OXA) (p < 0.01) (Fig. 4B). Treatment groups [OXA, PLGA-PEG-FA (OXA) and PLGA-PEG (OXA)-FA] were compared at the same concentration (10 μg/mL) and same treatment time (48 h), the result were that PLGA-PEG-FA (OXA) induced more cell death than others samples in the same condition, p < 0.5 for comparison with OXA and p< 0.001 for comparison with PLGA-PEG-FA (OXA) (Fig. 4B).

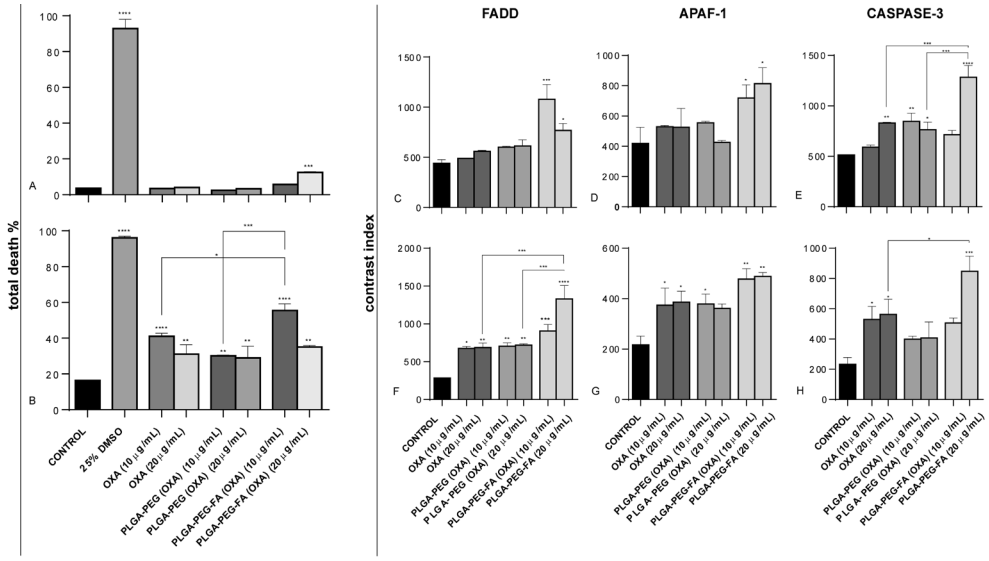

Figure 4 Total death, and Contrast index for immunofluorescence. The graph A and B displays the total cell death after 24 h (A) and 48 h (B) of treatment. The contrast index for FADD, APAF-1, and caspase-3 of CT-26 after treatment with the nanoparticles and free OXA for 24 h (C, D and E, respectively) and for 48 h (F, G and H, resectively) are displayed. * $p < 0.05$, ** $p < 0.01$, *** $p < 0.001$, and **** $p < 0.0001$.

3. RESULTS

3.7. Immunofluorescence

To analyze the apoptosis pathway induced by nanoparticles, cells were labelled with fluorescent antibodies and subsequently imaged. After 24 h of treatment, only 10 µg/mL and 20 µg/mL PLGA-PEG-FA (OXA) induced apoptosis through the extrinsic route (FADD) and intrinsic route (APAF-1) compared to the negative control. Regarding the common route (caspase-3), only OXA and PLGA-PEG (OXA) at a concentration of 10 µg/mL did not show a significant difference when compared with the control. However, 20 µg/mL PLGA-PEG-FA (OXA) showed a significant difference between treatments when compared to OXA and PLGA-PEG (OXA) at the same dose ($p < 0.001$) (Figs. 4C–E and 5).

After 48 h, all three formulations of both doses induced statistically significant apoptosis via the extrinsic route (FADD) and intrinsic route (APAF-1) when compared to the control group, with the exception of PLGA-PEG (OXA) at 20 µg/mL. The intensity of the fluorescence intensity of FADD labelling of cells treated with 20 µg/mL PLGA-PEG-FA (OXA) was increased when compared to the other two treatments, OXA and PLGA-PEG (OXA), at the same concentration ($p < 0.0001$).

Caspase-3 detection results showed that only OXA in both concentrations ($p < 0.5$) and PLGA-PEG-FA (OXA) at 20 µg/mL ($p < 0.001$) induced apoptosis. It is worth noting that when comparing 20 µg/mL of free OXA with PLGA-PEG-FA (OXA) there is a difference between these treatments, showing greater apoptosis induction by the nanoparticle DDS ($p < 0.5$; Fig. 4F–H and 5).

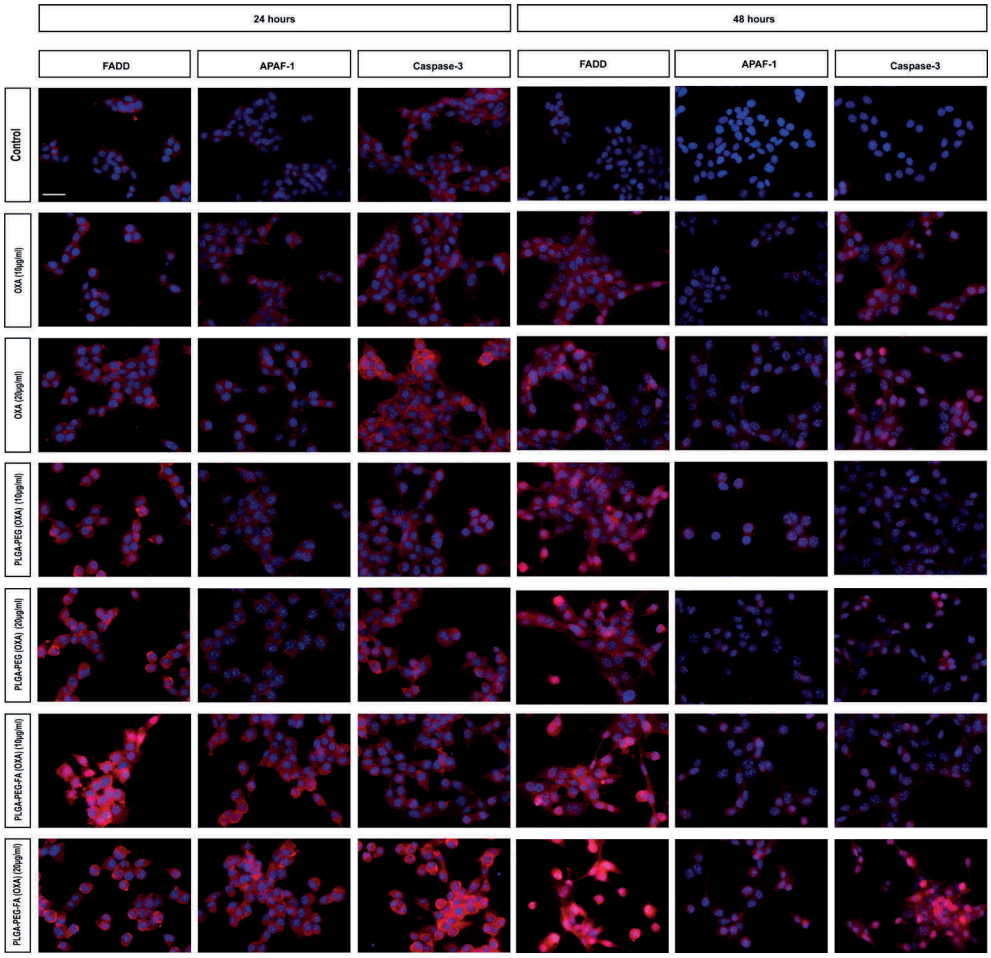

Figure 5 Detection of FADD, APAF-1, and caspase-3 after 24 and 48 h of treatment. CT-26 cells stained with DAPI (blue) as well as anti-FADD, anti- APAF-1, or anticaspase-3 antibodies (red). Scale bar: 50 μm. (For interpretation of the references to colour in this figure legend, the reader is referred to the web version of this article.)

3. RESULTS

3.8. *In vivo* study

The *in vivo* model was applied to analyze the activity of the nanoparticulate systems and compare them with the free drug in relation to apoptosis, drug resistance, and metastasis factors. The macroscopic results showed a tumor growth curve with a difference in all treated groups in relation to the saline group (negative control), with $p < 0.0001$ (Fig. 6A–E). Tumor weight decreased considerably among the treated groups, which was contrary to the saline group ($p < 0.0001$). There was also a significant difference between the treatment with free OXA and PLGA-PEG-FA (OXA) ($p < 0.01$; Fig. 6F).

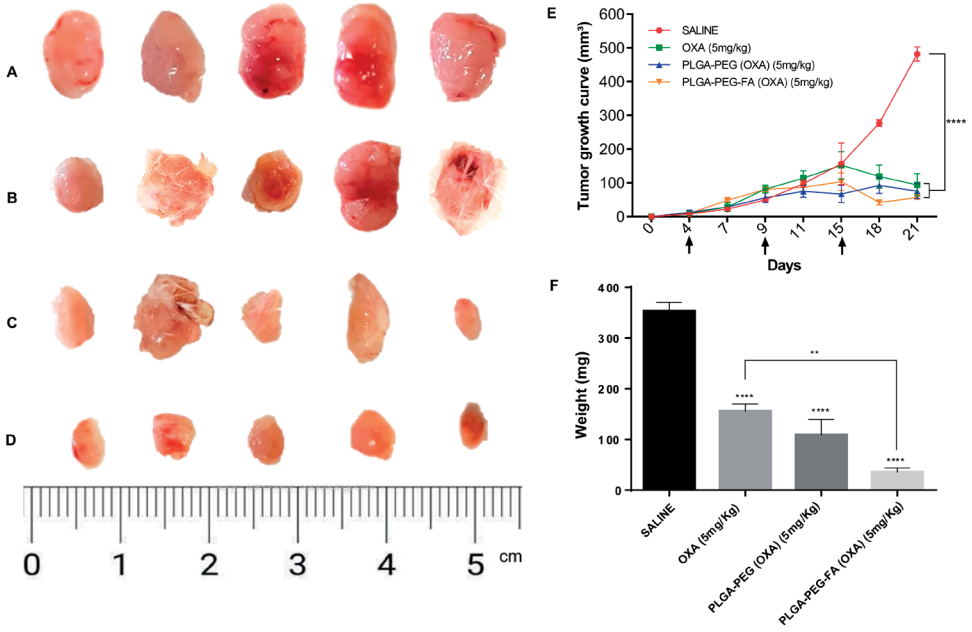

Figure 6 Macroscopic results of the CRC *in vivo* xenograft model. Morphology of the tumors collected from Saline (A), OXA (5 mg/Kg) (B), PLGA-PEG (OXA) (5 mg/Kg) (C), and PLGA-PEG-FA (OXA) (5 mg/Kg) (D) groups. Tumor growth curve (E) and weight graph (F) of the xenograft tumors with different treatments. All treatment groups were compared with saline group. ** $p < 0.01$ and **** $p < 0.0001$.

For analysis of the tumors, immunohistochemistry and RT-PCR were applied. Immunohistochemical analyses showed that all treated groups had low expression of survivin compared to the saline group: $p< 0.001$ for

free OXA and p < 0.0001 for both nanoparticle formulations (Fig. 7I). There was also a statistically significant difference when the treated groups were compared between each other: p < 0.01 for OXA X PLGA-PEG (OXA), p < 0.0001 for OXA X PLGA-PEG (OXA), and PLGA-PEG (OXA) X PLGA-PEG-FA (OXA). Regarding the analysis of the common pathway of apoptosis (caspase-3), the expression was increased in all groups when compared to the control: p < 0.01 for free OXA and p < 0.0001 for both nanoparticle formulations. The comparison between the treated groups showed a difference between the nanoparticle groups and free OXA group: p < 0.0001 for the two analyses (Fig. 7J).

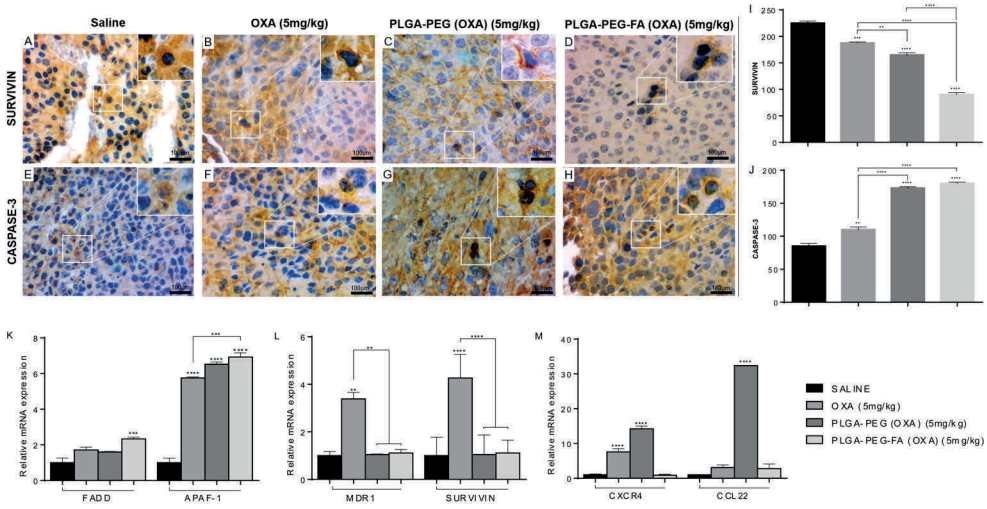

Figure 7 Analysis of apoptosis, drug resistance, and metastasis factors. Representative images of immunohistochemistry of tumor fragments of mice treated with saline, OXA, and nanoparticles (A–H). Immunohistochemistry score by anti-survivin (I) and anti-caspase-3 (J). Relative mRNA expression by of FADD and APAF-1 (K), MDR1 and survivin (L), and CXCR4 and CCL22 (M) as determined by RT-PCR. All treatment groups were compared with the negative control group and between the treated groups. ** p < 0.01, *** p < 0.001, and **** p < 0.0001. Magnification (A-H): 40×.

The apoptosis-related gene expression analysis showed that only PLGA-PEG-FA (OXA) had expression of FADD when compared to the negative control (p < 0.001) (Fig. 7K). Also, for APAF-1, all treated groups had increased expression when compared to the negative control (p < 0.0001). In addition, the groups free OXA and PLGA-PEG-FA (OXA) also showed a significant difference between each other (p < 0.001) in terms of the expression of APAF-1 (Fig. 7K). The increase in mRNA expression for MDR1 and survivin was only observed for the OXA group

in relation to control ($p < 0.01$ and $p < 0.001$, respectively). The same results were obtained when OXA was compared with PLGA-PEG (OXA) and PLGA-PEG-FA (OXA) (Fig. 7).

CXCR4 expression was increased for free OXA and PLGA-PEG (OXA) in comparison to the control and for CCL22 expression only in the PLGA-PEG (OXA) group, $p < 0.0001$. Interestingly, PLGA-PEG-FA (OXA) did not increase the expression of these mRNAs.

4. DISCUSSION

Using the double-emulsion solvent evaporation method of water-oil-water (W/O/W) allowed us to obtain nanoparticles with a range of sizes in which nanoparticles can be actively taken up by cells via endocytosis [34,35]. The nanoparticles showed a good stability since the zeta potential was between 20 mV and 24 mV, which are values that are typically indicative of high nanoparticles stability (Table 1) [36,37]. The differences in encapsulation efficiency were probably because of the chemistry of the formulated co-polymers. PLGA-PEG-FA nanoparticles loaded with the NIR dye and co-loaded with OXA did encapsulate almost 10% less of NIR dye than the PLGA-PEG nanoparticles. This is probably duo to the encumberment of the FA bound to the PLGA-PEG. The sizes obtained by TEM were slightly smaller (Fig. 2A–D) than those determined by DLS (Table 1). The difference is likely due to different sample preparation methods since hydrated particles were used for DLS, whereas rehydrated nanoparticles were used for TEM [38]. The pattern of release of OXA by the particulate systems, [PLGA-PEG (OXA) and PLGA-PEG-FA (OXA)], was continuous and slow, this shows that the drug was kept trapped inside the DDS for a long period of time [5,39]. PLGA-PEG-FA (OXA) released even slower than PLGA-PEG (OXA), this release pattern can ensure that the drug will not be released before its internalization in tumor cells, allowing to increase its accumulation in tumor tissues with the consequent decrease in possible side effects caused by OXA [5,40].

The binding and uptake tests complement each other and prove the acid folic target's effectiveness in maximizing OXA activity. In this study, we

were able to confirm that the system with FA works. During the same time period, PLGA-PEG-FA greatly improved the binding and internalization of the nanoparticles by tumor cells when compared to PLGA-PEG, which did not possess FA [41]. As CRC cells overexpress FA receptors, this system is of great use in the treatment of this kind of tumors [41]. The microscopic images corroborate these results and allow the visualization of the nanoparticles, due to the presence of the dye inside the cells [42,43].

Since nanoparticles, which contained FA for targeting purposes, were internalized at a higher rate, cytotoxicity and the percentage of cell death increased due to the improved effectiveness of the OXA treatment. The FA-containing DDS already induces cell death after 24h. This activity is sustained, showing higher rates after 48 h, the second time of analysis [44]. This initial activity of the tumor cells is not observed for free OXA, since the internalization of free OXA is not facilitated by the target, i.e. FA, and the tumor cells developed a resistance to treatment with OXA [42,45]. This evidence reveals the importance of using a DDS to circumvent treatment barriers, such as drug resistance.

Evasion of apoptosis, drug resistance, and metastasis are interconnected factors, which are present in tumor malignancy. These factors can be the reason for the failure of a cancer treatment, that, as a result, allow tumor progression or recurrence [7,46,47]. Therefore, DDSs with therapeutic action via induction of apoptosis are promising [48]. Our immunofluorescence data showed an increase in apoptosis in tumor cells when treated with PLGA-PEG-FA (OXA), when compared to free OXA.

Our *in vitro* results of apoptosis induction were confirmed *in vivo* by means of a regression of the tumor size. In relation to free OXA, tumor size was decreased by 3 times after treatment with PLGA-PEG-FA (OXA). Drug resistance is a known characteristic of treatment with OXA [49]. Our data shows decreased OXA resistance when cells are treated with PLGA-PEG-FA (OXA), which indicates that cells are more susceptible to the action of OXA when it is incorporated into the PLGA system targeted with FA. These results corroborate other studies and, thereby, confirm the efficiency of this target system and uptake by the cells via endocytosis [50,51].

The tumor microenvironment, invasion, and metastasis are also targets of antitumor therapies. Hence, we went beyond the study of apoptosis

and drug resistance [52]. We also analyzed the expression of CXCR4, a chemokine receptor, overexpressed in metastases, tumor growth, proliferation, and invasion, and CCL22, a macrophage-derived chemokine that attracts regulatory T cells to the tumor microenvironment, thereby, decreasing anti-cancer immunity [53–56]. The groups treated with free OXA and PLGA-PEG (OXA) showed an increase for CXCR4 compared to the saline group, while treatment with PLGA-PEG-FA (OXA) did not show a difference. Regarding CCL22, only PLGA-PEG (OXA) increased levels in relation to the control. These results reveal that the PLGA-PEG-FA (OXA) DDS does not interfere in the expression of CXCR4 and CCL22 that are related to tumor microenvironment and tumor progression.

Our results showed that PLGA-PEG-FA increased the antitumor effectiveness of OXA by functioning as a facilitator of drug delivery in CRC. These results contribute to our understanding of the drug delivery mechanisms that underlie the antitumor effects of chemotherapy in nanoscale.

APPENDIX TO CHAPTER 4

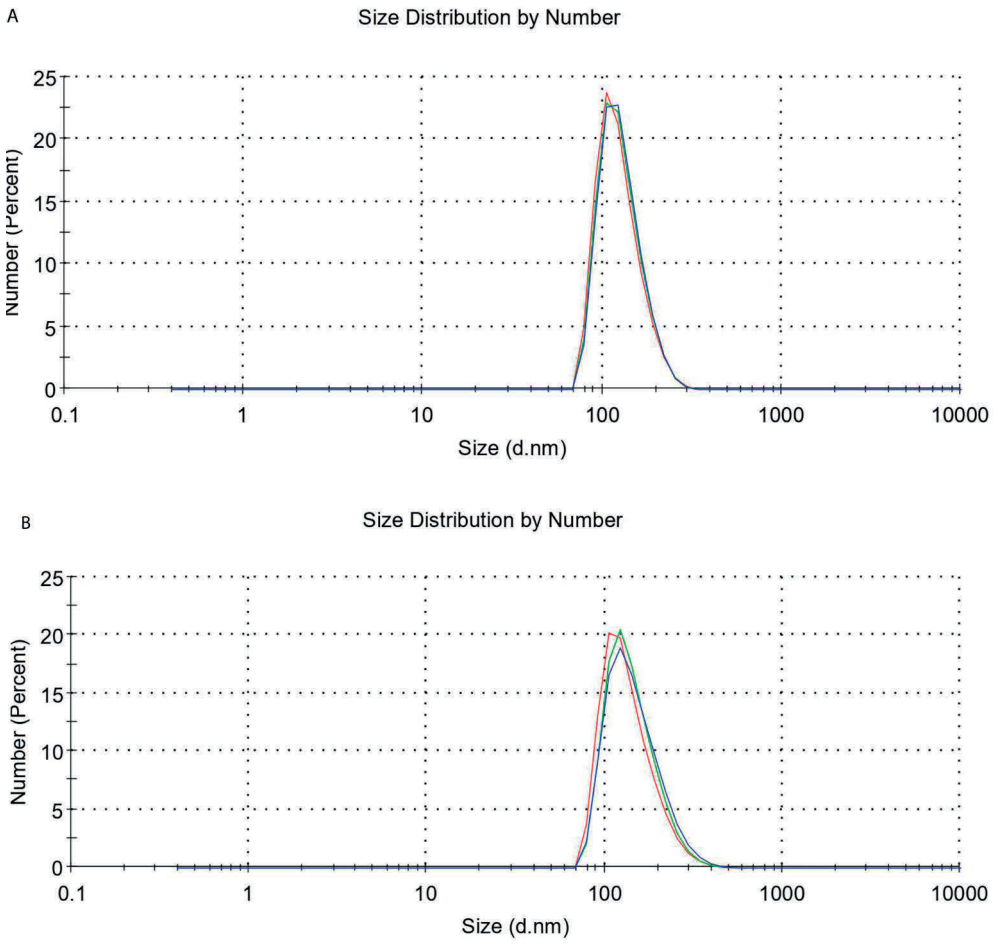

Figure S1 DLS curves. DLS curves are representative for the PLGA-PEG (OXA) (A) and for PLGA-PEG-FA (OXA) (B).

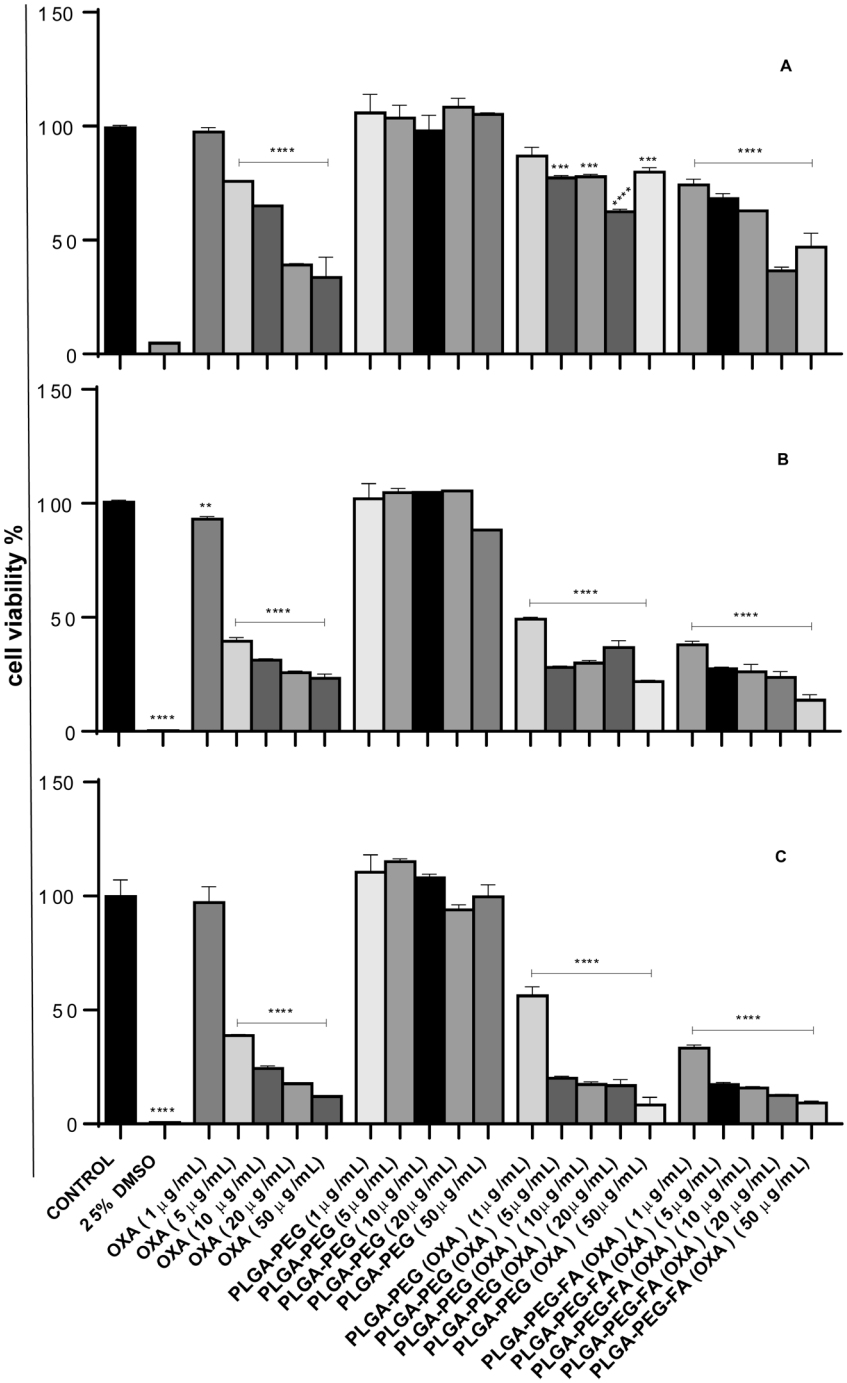

Figure S2 Cell viability. Mean cell viability of CT-26, the cells were treated with OXA and PLGA nanoparticles for 24 hours (A), for 48 hours (B), and for 72 hours (C). ** p<0.01, *** p<0.001, and **** p<0.0001.

APPENDIX TO CHAPTER 4

mRNA	Oligonucleotides Primers		Temp-erature
β-actina	5' AAC TTT GGC ATCGTG GAA GG 3'	5'GTGGATGCAGGGAT-GATGTTC 3'	60°C
FAAD	5' AGAAGAAGAACG-CCTCGGTG 3'	5' GCTCACAGATTCCTG-GGCTT 3'	56.5°C
APAF-1	5'TTCCAGTGGCAAGGA-CACAG 3'	5` CCACTCTCCACAGGG-ACAAC 3'	56.8°C
MDR1	5' TCAGCAACAG-CAGTCTGGAG 3'	5' ACTATGAGCACAC-CAGCACC 3'	55.2°C
Survivin	5'AGAACAAAATTG-CAAAGGAGACA 3'	5'GGCATGTCACTCAG-GTCCAA 3'	55.2°C
CXCR4	5'ACCTCGGT-GTCCTCTTGCTGTCCA3'	5'GCTTGACGTTGGCTCTG-GCGATGT` 3	56.5°C
CCL22	5'GAGACAACAGTGGTC-CCAGG 3'	5` CTGGCACTGTCAATC-CCTGT 3'	56.8°C

REFERENCES

1. E.J. Kuipers, W.M. Grady, D. Lieberman, T. Seufferlein, J.J. Sung, P.G. Boelens, C.J. H. van de Velde, T. Watanabe, Nature Reviews Disease Primers 1 (2015) 15065.
2. F. Bray, J. Ferlay, I. Soerjomataram, R.L. Siegel, L.A. Torre, A. Jemal, CA Cancer J. Clin. 68 (2018) 394–424.
3. A. Guerra, L.A.L. Soares, M.R.A. Ferreira, A.A. Araújo, H.A.O. Rocha, J.S. Medeiros, R.D.S. Cavalcante, R.F.A. Júnior, Biomedicine & pharmacotherapy Biomedecine & pharmacotherapie 92 (2017) 696–706.
4. A.L.C. de S.L. Oliveira, R.F.d. Araújo Júnior, T. Gomes de Carvalho, A.B. Chan, T. Schomann, F. Tamburini, L.-F. de Geus-Oei, L.J. Cruz, Pharmaceutics 12 (2020) 193.
5. A.L.C.S.L. de Oliveira, A.M. dos Santos-Silva, A.A. da Silva-Júnior, V.B. Garcia, A. A. de Araújo, L.-F. de Geus-Oei, A.B. Chan, L.J. Cruz, R.F. de Araújo Júnior, Journal of Nanoparticle Research 22 (2020) 115.
6. R.S. Wong, Journal of experimental & clinical cancer research: CR 30 (2011) 87.
7. D. Hanahan, R.A. Weinberg, Cell 144 (2011) 646–674. [8] M.S. D'Arcy, Cell Biol. Int. 43 (2019) 582–592.
8. B.A. Carneiro, W.S. El-Deiry, Nature reviews, Clin. Oncol. 17 (2020) 395–417.
9. Y. Shi, B. Tang, P.-W. Yu, B. Tang, Y.-X. Hao, X. Lei, H.-X. Luo, D.-Z. Zeng, PLoS One 7 (2012), e51076.
10. T.V. Rakitina, I.A. Vasilevskaya, P.J. O'Dwyer, Biochem. Pharmacol. 73 (2007) 1715–1726.
11. B. Stordal, N. Pavlakis, R. Davey, Cancer Treat. Rev. 33 (2007) 347–357.
12. Z.P. Hong, L.G. Wang, H.J. Wang, W.F. Ye, X.Z. Wang, Phytomedicine 39 (2018) 168–175.
13. W. Cheng, J. Nie, N. Gao, G. Liu, W. Tao, X. Xiao, L. Jiang, Z. Liu, X. Zeng, L. Mei 27 (2017) 1704135.
14. N. Ashwanikumar, N.A. Kumar, S.A. Nair, G.S.V. Kumar, Colloids Surf B Biointerfaces 122 (2014) 520–528.
15. W. Ni, Z. Li, Z. Liu, Y. Ji, L. Wu, S. Sun, X. Jian, X. Gao, J. Pharm. Sci. 108 (2019) 1284–1295.
16. C. Liang, H. Wang, M. Zhang, W. Cheng, Z. Li, J. Nie, G. Liu, D. Lian, Z. Xie,
17. L. Huang, X. Zeng, J. Colloid Interface Sci. 525 (2018) 1–10.
18. Z. Eskandari, F. Kazdal, F. Bahadori, N. Ebrahimi, Journal of Drug Delivery Science and Technology 48 (2018) 393–402.
19. X. Luo, Y. Yang, F. Kong, L. Zhang, K. Wei, Int. J. Pharm. 564 (2019) 340–349.
20. X. Song, J. Wang, Y. Xu, H. Shao, J. Gu, Colloids Surf. B: Biointerfaces 180 (2019) 110–117.
21. A. Banerjee, S. Pathak, V.D. Subramanium, D.G Murugesan .R., R.S. Verma, Drug Discov Today 22 (2017) 1224–1232.
22. W. Cheng, X. Zeng, H. Chen, Z. Li, W. Zeng, L. Mei, Y. Zhao, ACS Nano 13 (2019) 8537–8565.
23. Y. Wang, P. Li, L. Chen, W. Gao, F. Zeng, L.X. Kong, Drug Delivery 22 (2015) 191–198. M.M El-Hammadi, A.V Delgado, C. Melguizo, J.C. Prados, J.L. Arias, Int. J. Pharm. 516 (2017) 61-67.
24. L.J. Cruz, P.J. Tacken, F. Rueda, J.C. Domingo, F. Albericio, C.G. Figdor, Methods Enzymol. 509 (2012) 143–163.
25. M.V.d.M. Ribeiro, I.d.S. Melo, F.d.C.d.C. Lopes, G.C. Moita, Brazilian Journal of Pharmaceutical Sciences 52 (2016) 741–750.
26. S.H. Boddu, R. Vaishya, J. Jwala, A. Vadlapudi, D. Pal, A.K. Mitra, 2 (2012) 068–075.
27. P. García-Manrique, N.D. Machado, M.A. Ferna´ndez, M.C. Blanco-Lo´pez, M. Matos, G. Guti´errez, Colloids Surf. B: Biointerfaces 186 (2020) 110711.
28. W. Zhang, F. Wang, X. Hu, J. Liang, B. Liu, Q. Guan, S. Liu, Oncol. Lett. 17 (2019) 815–822.
29. L. Liu, P.A. Mayes, S. Eastman, H. Shi, S. Yadavilli, T. Zhang, J. Yang, L. Seestaller- Wehr, S.Y. Zhang, C. Hopson, L. Tsvetkov, J. Jing, S. Zhang, J. Smothers, A. Hoos, Clin. Cancer Res. 21 (2015) 1639–1651.

30. Y. Liu, N. Zhang, Q. Cao, X. Cui, Q. Zhou, C. Yang, Biomedicine & pharmacotherapy Biomedecine & pharmacotherapie 90 (2017) 47–52.
31. Y. Liu, N. Zhang, Q. Cao, X. Cui, Q. Zhou, C. Yang, Biomedicine & pharmacotherapy Biomedecine & pharmacotherapie 90 (2017) 47–52.
32. H. Liu, H.W. Xu, Y.Z. Zhang, Y. Huang, G.Q. Han, T.J. Liang, L.L. Wei, C.Y. Qin, C. K. Qin, World J. Gastroenterol. 21 (2015) 10367–10374.
33. E. Charafe-Jauffret, C. Tarpin, V.-J. Bardou, F. Bertucci, C. Ginestier, A.-C. Braud, B. Puig, J. GeneiX, J. Hassoun, D. Birnbaum, J. Jacquemier, P. Viens, J. Pathol. 202 (2004) 265–273.
34. L. Shang, K. Nienhaus, G.U. Nienhaus, J Nanobiotechnology 12 (2014) 5.
35. J.P. Marshalek, P.S. Sheeran, P. Ingram, P.A. Dayton, R.S. Witte, T.O. Matsunaga, J. Control. Release 243 (2016) 69–77.
36. V. Ayala, A.P Herrera, M. Latorre-Esteves, M. Torres-Lugo, C. Rinaldi, J. Nanopart, Res. 15 (2013) 1874. S. Bathattacharjee, J. Control. Realese 235 (2016) 337-351.
38. R.F. Domingos, M.A. Baalousha, Y. Ju-Nam, M.M. Reid, N. Tufenkji, J.R. Lead, G.G. Leppard, K.J. Wilkinson, Environmental Science & Technology 43 (2009) 7277–7284.
39. S.A. Sufi, M. Hoda, S. Pajaniradje, V. Mukherjee, S.M. Coumar, R. Rajagopalan, Int. J. Pharm. 588 (2020) 119738.
40. B. Gibbens-Bandala, E. Morales-Avila, G. Ferro-Flores, C. Santos-Cuevas, L. Mele´ndez-Alafort, M. Trujillo-Nolasco, B. Ocampo-García, Mater. Sci. Eng. C 105 (2019) 110043.
41. A. Narmani, M. Kamali, B. Amini, A. Salimi, Y. Panahi, Process Biochem. 69 (2018) 178–187.
42. A. Akbarian, M. Ebtekar, N. Pakravan, Z.M. Hassan, Int. J. Biol. Macromol. 152 (2020) 90–101.
43. J. Hu, J.D. Obayemi, K. Malatesta, A. Ko˘smrlj, W.O. Soboyejo, Mater. Sci. Eng. C 88 (2018) 32–45.
44. Z. Wang, X. Duan, Y. Lv, Y. Zhao, Life Sci. 239 (2019) 117013.
45. W. Gao, X. Jia, J. Wu, Y. Song, J. Yin, M. Zhang, N. Qiu, X. Li, P. Wu, X. Qi, Z. Liu, Journal of Drug Delivery Science and Technology 54 (2019) 101349.
46. B.D. Kurmi, P. Patel, R. Paliwal, S.R. Paliwal, Journal of Drug Delivery Science and Technology 57 (2020) 101682.
47. C. BoX, S.J. Rogers, M. Mendiola, S.A. Eccles, Semin. Cancer Biol. 20 (2010) 128–138.
48. M.C. Pfeffer, T.K.A. Singh, International Journal of Molecular Sciences, 19, 2018.
49. D.B. Longley, P.G. Johnston, J. Pathol. 205 (2005) 275–292.
50. H. Tonbul, A. Sahin, E. Tavukcuoglu, G. Esendagli, Y. Capan, Journal of Drug Delivery Science and Technology 54 (2019) 101380.
51. J.L. Markman, A. Rekechenetskiy, E. Holler, J.Y. Ljubimova, Adv. Drug Deliv. Rev. 65 (2013) 1866–1879.
52. F. Guo, Y. Wang, J. Liu, S.C. Mok, F. Xue, W. Zhang, Oncogene 35 (2016) 816–826.
53. E. Martinenaite, S. Munir Ahmad, M. Hansen, O¨ . Met, M.W. Westergaard, S. K. Larsen, T.W. Klausen, M. Donia, I.M. Svane, M.H. Andersen, Oncoimmunology 5 (2016) e1238541.
54. A. Maolake, K. Izumi, K. Shigehara, A. Natsagdorj, H. Iwamoto, S. Kadomoto, Y. Takezawa, K. Machioka, K. Narimoto, M. Namiki, W.-J. Lin, G. Wufuer, A. Mizokami, Oncotarget 8 (2017) 9739–9751.
55. C. Xu, L. Zheng, D. Li, G. Chen, J. Gu, J. Chen, Q. Yao, Life Sci. 208 (2018) 333–340.
56. M.V. C´espedes, U. Unzueta, P. A´lamo, A. Gallardo, R. Sala, I. Casanova, M.A. Pavo´n, M.A. Mangues, M. Trías, A. Lo´pez-Pousa, A. Villaverde, E. Va´zquez, R. Mangues, Nanomedicine: Nanotechnology, Biology and Medicine 12 (2016) 1987–1996.

CHAPTER
FIVE

SUMMARY, GENERAL DISCUSSION AND FUTURE PERSPECTIVES

SUMMARY

The field of nanomedicine is constantly improving due to its use of modern techniques. With these techniques, nanostructures with pharmacokinetics and pharmacodynamics suitable for treating various diseases, including cancer are formulated. It is important to consider the heterogeneity of primary tumors for cancer treatment to be effective. Tumor heterogeneity favors tumor tissue to survive and resist drugs, leading to the failure of chemotherapeutic agents to induce a therapeutic response. In addition, the absorption mechanisms, metabolism and excretion of chemotherapeutic drugs, which are commonly used for cancer patients and the lack of specific targeting of these drugs can cause adverse effects on treated patients. Thus, the general objective of this thesis is to investigate the biological activity of targeted poly (lactic-co-glycolic acid) (PLGA) nanoparticles (NPs) as a drug delivery system (DDS) for carvedilol (CVDL) or oxaliplatin (OXA), *in vitro* and *in vivo*, to treat colorectal cancer (CRC). DDSs were formulated to achieve this goal. Subsequently, the formulations were characterized in order to obtain information about their size, shape, encapsulation rate and zeta potential. As a common result of this thesis, all formulations showed a spherical shape and smooth surface. Inflammation studies were performed, since the progression of CRC is related to the induction of a chronic and recurrent inflammatory process (Chapter 2). In Chapter 2, nanoparticles functionalized with cholesterol (CHO) decreased leukocyte migration when compared to free CVDL when used at the same concentration. Furthermore, the nanoformulations showed similar activities when used at lower doses than CVDL, at higher concentration, in relation to malondialdehyde (MDA) and glutathione (GSH) levels. *In vitro* studies, such as analysis of cell viability and cell death were carried out in order to analyze the antitumor activity of the systems (Chapters 2, 3 and 4). The *in vitro* results showed that the PLGA polymer is non-toxic, and that the use of NPs increased the drug's effectiveness against tumor cells. Tests to evaluate the efficiency of targeting the NPs by means of CHO or folic acid (FA) were executed to prove that there is an increase in the targeting efficiency of the systems for CT-26 murine CRC cells (Chapters 3 and 4). These tests showed that targeted NPs bind to the cell surface and internalize in the cell in greater quantity than NPs without the target. Finally, animal models were developed to study apoptosis and resistance to drugs as well as metastases (Chapters 3 and 4). The results of an animal study confirmed our *in vitro* results, showing that the use of

NPs reduced tumor volume and acted on tumor modulation. In chapters 2, 3 and 4, our studies were discussed in detail on the formulations and characterizations of NPs as DDSs with ideal characteristics to increase the therapeutic range of drugs at the tumor site. As well as the biological evaluation of these DDS when its anti-inflammatory activity (Chapter 2) and its antitumor activity *in vitro* (Chapters 2, 3 and 4) and *in vivo* (Chapters 3 and 4). Taken together, all the DDSs studied in this thesis were able to improve the chemotherapeutic efficiency of the drugs studied in Chapters 2, 3 and 4.

MAIN OUTCOMES AND RESPECTIVE IMPLICATIONS

Objective 1: Formulating nanoparticles with satisfactory physico-chemical characteristics used as a drug delivery system

The development of nanoparticles (NPs) consisting of biodegradable materials with surface functionalization enables advancement towards achieving new treatment strategies in medicine. When used as a DDS, NPs and other colloidal systems have the ability to modify the kinetics, body distribution and release of drugs incorporated into these systems [1]. Thus, nanoparticles were formulated to achieve this goal, and were subsequently characterized in terms of size, shape, potential (surface) charge and encapsulation rate.

For this thesis, NPs consisting of polyethylene glycol (PEG) and poly (lactic-co-glycolic acid) (PLGA) were formulated. These PEG-PLGA-NPs were loaded with OXA and retinoic acid (RA) or CVDL and functionalized with CHO or FA in order to increase the therapeutic efficacy of the drugs encapsulated in the DDS [2-4]. The resulting DDS formulations had spherical shape, smooth surfaces and uniform size distribution. The morphology of the NPs influenced both pharmacokinetics and cell absorption [5]. Therefore, the spherical form of our NPs played an important role in reducing cytotoxicity compared to other forms [6]. Studies using NPs for the treatment of breast cancer, CRC and glioblastomas show that the most effective formulations have a spherical shape [7-9].

Due to the satisfactory volume, surface and size of the NPs, delivery of the encapsulated drugs is optimized and there is an increase in their pharma-

cological activity [10-12]. The therapeutic content has to be released in a controlled manner within the tumor microenvironment (TME) in order to achieve the objective of using nanoformulations in cancer treatment [13]. Several studies have shown the importance of encapsulation efficiency in formulating NPs related to the optimization of cell uptake, suggesting improved therapeutic efficacy and reduced cell toxicity [14, 15]. The encapsulation rates for this thesis (Chapter 2, 3 and 4) were high, which led to an increase in antitumor activity of the encapsulated/loaded drugs in comparison to the free drugs. [16, 17]. Also, a reduction in the inflammatory activity (Chapter 2) of the encapsulated drug in relation to the free drug was also observed for NPs containing CVDL. This shows the importance of using DDSs to fight cancer [18, 19].

Higher encapsulation rates of the drugs are desirable, especially for application of *in vivo* studies, since a solution with a higher concentration is needed in a small volume to be injected during animal experiments. However, when the encapsulation efficiency is low, it is necessary to have a greater number of NPs within a small volume to obtain a therapeutic concentration. This can create a viscous solution, which makes it difficult to solubilize the NPs and consequently makes administration *in vivo* difficult.

Regarding the zeta potential values, previous studies have determined that relative values with variation in the range between 0 mV and ± 5 mV indicate increased instability of NPs, and consequently rapid aggregation. However, values of ± 30 mV imply greater stability for the colloidal system [20]. The results of the present thesis (Chapters 3 and 4) show that the zeta potentials of the nanoparticulate formulations ranged from -20 mV to -29.6 mV. Thus, our values indicate that the molecules of the PLGA-NP groups were stable and they had reduced cytotoxic effects[21]. This supports other studies which had similar zeta potentials for their NPs used as DDS against cancer [7, 22].

In contrast, the results obtained in Chapter 2 for NPs with CVDL and CVDL-CHOL were not within this range. The zeta potential of these NPs was -2.04 mV and -2.08 mV, respectively. However, no problems were observed regarding the stability of these formulations in stability studies; the samples remained stable for up to seven weeks. There was stability because these nanoparticles did not undergo the lyophilization process.

They were maintained in colloidal solution right from when they were formulated, characterized until the experiments were conducted.

Another physicochemical characteristic that requires attention is the size of our NPs, as it is strongly associated with cell uptake, biodistribution and the half-life of the NPs in circulation [23]. Thus, the smaller the NPs, the faster would the body absorb, metabolize and excrete them [24]. However, very small sizes are not desirable, since NPs between 14 and 74 nm show a half-life between 2 and 24 hours [25]; while sizes larger than 200 nm are quickly eliminated by the spleen [26].

The average sizes of the NPs in this study were around 234 nm in diameter (formulation of Chapter 2), 400 nm (formulation of Chapter 3) and 197 nm (formulation of Chapter 4). The noticeable difference between the nanoparticle sizes used in Chapter 3 and those in Chapters 2 and 4 is due to the number of components incorporated in them. Besides OXA, RA was also added to these formulations, which resulted in a larger diameter of the nanoparticles. Such results directly influence the circulation time of the nanoformulations, the size-dependent biodistribution, the penetration into target cells and the elimination from tumor tissue, which lead to improved anticancer efficacy. The uptake and elimination of the NPs can be compromised when nanoparticles are very small due to accelerated elimination, hindering the EPR effect [27]. Therefore, the average dimensions achieved by the nanoformulations in this study led to improved EPR effect, inducing efficient cancer treatment, *in vitro* and *in vivo* [28].

Additionally, our results can contribute to developing nanoscale therapeutic systems and provide information on nanotoxicity in the treatment of CRC. This may result in better prognosis, due to a more specific treatment and fewer side effects of the anticancer drug.

Objective 2: Increasing the efficiency of drugs when encapsulated in a drug delivery system

Conventional chemotherapy is often associated with low solubility and limited tumor targeting. These unbeneficial treatment characteristics prevent the drug from efficiently reaching the tumor and furthermore, it leads to side effects [29]. Incorporating drugs within functionalized NPs can be helpful to solve these disadvantages of chemotherapy. It reduces

non-specific dissemination of the drug and thereby reduces side effects [30]. It increases the efficiency of the drug and circumvents cancer cells from resisting drugs [31, 32].

The NPs formulated in Chapters 2, 3 and 4 were studied to prove that there was an increase in the efficiency of drugs when they were encapsulated in a system in order to achieve a more specific treatment. We decided to use the polymer PLGA for the formulation of polymeric NPs because it stands out among the DDS formulations for cancer. This is due to its biodegradability and biocompatibility, which makes it a safe candidate as DDS [33, 34]. The results obtained in our study did not show antiproliferative activity when the cells were treated with empty PLGA NPs. This can be seen in the results of the viability assays (MTS) where the empty nanoparticles did not show cytotoxic activity. Our data confirmed the results of other studies and proved that PLGA is an efficient DDS for different active components. In addition, the hydrolysis of PLGA leads to lactic acid and glycolic acid monomers that are endogenous and easily metabolized by the body via the Krebs cycle, with minimal associated systemic toxicity [34, 35].

In this study, the release time of free drugs (CVDL and OXA) was compared with the same drugs encapsulated in NPs. A slow, gradual and progressive release was observed in the nanosystems over time when compared to the free drugs. This increased the efficiency of the drugs in the nanoparticulate systems [8, 36].

The therapeutic efficacy of the drugs CVDL and OXA was also assessed using cell viability and flow cytometry techniques; also, immunofluorescence was used for OXA. These techniques aim to quantify the proliferation and death rates of cells, which will occur if the drug is delivered successfully and in appropriate concentrations to act on these cellular processes. Our results show that the encapsulated drugs are capable of maximizing the therapeutic activity induced by the free drug when it is in a DDS [37, 38]. This maximization of the drug's effect when encapsulated in a DDS was confirmed by our results when the cells were treated with our NPs and compared to free drugs (OXA and CVDL) [39, 40].

Cancer cells that do not undergo apoptosis end up proliferating more than normal, resulting in a malignant tumor process [41]. Therefore,

studying the mechanisms, which initiate apoptosis is extremely important to stop carcinogenesis. Studies showed that there is a correlation between improved chemotherapy results and reduced BCL-2 expression [42]. Furthermore, our results showed that small concentrations of OXA encapsulated in a nanoparticulate DDS induced apoptosis at the same way as when the free OXA is used in higher concentrations. The use of drugs in the system lead to lower side effects and reduction in drug resistance rates, since the drug will be released into the system only at the tumor site [22, 43].

Apoptosis induction was investigated in our study to prove that our DDS increased the efficiency of free drug in the treatment of CRC. The data show low expression of the anti-apoptotic molecule BCL-2, and greater expression of caspase 3, FADD and APAF-1. This proves there is greater induction of the extrinsic and intrinsic pathways of apoptosis in tumor cells when treated with DDS containing OXA compared to the free drug. However, further investigations need to be done in the future in order to understand which apoptosis pathway is triggered the most.

In addition to all of the antitumor activity described, synergy activity was observed when RA and OXA were internalized together in nanoparticles. There was an improvement in the antitumor activity of OXA, showing the occurrence of synergy between them. Previous studies have shown that RA induces apoptosis, thus corroborating the data presented in this study [44, 45].

All the findings of this study together with data from the literature endorse the importance of studying the area of DDSs in order to improve the existing treatment for CRC.

Objective 3: Proving the efficiency of the target by increasing the binding and internalization of the nanoparticles in the cancer cell

Since the targets of many therapeutic agents are usually located in intracellular compartments, superficial modulation of NPs is necessary to facilitate their binding and internalization by target cells. A detailed study of the interactions between NPs and target cells is relevant to enable efficient cell adsorption or endocytosis across the plasma membrane [46]. Targeted therapies are ideal to be used as DDS, since its therapeutic

content will only be released at the tumor site [47]. Therefore, the functionalization of NPs in such a way that they directly interact with cancer cells is crucial to assess the effects of NPs and their toxicity.

Cancer cells demand an intense biosynthesis of CHO and an abundant supply of reduced folate (the main functional form of FA), for there to be intense neoplastic proliferation [48, 49]. The metabolic dependence of CHO and FA cancer cells is related to the construction of new plasma membranes and use for nucleotide biosynthesis, respectively, which are indispensable for maintaining cell growth. Such nutritional requirements of the tumor are reflected by the increased attraction and endocytosis of molecules, such as CHO and FA [48-51].

The drugs in the present study were delivered through active targeting, in which CHO (Chapter 2 and 3) or FA (Chapter 4) was added to the surface of the NPs. All functionalized NPs showed a higher internalization or binding rate. They also had greater antitumor activity when compared to nanoparticles without active targeting. CHO is a widely explored targeting moiety for DDSs for cancer, and our data confirm the results of other studies which indicate the contributory role of CHOL in the internalization of DDDs through endocytosis [52, 53]. Better internalization directly reflects greater availability of the drug in the cell interior, leading to maximization of the antitumor effect of the drug [54, 55].

The successful delivery of functionalized systems was also achieved when FA was used as a targeting moiety. Thus, two techniques were studied in our DDS: binding and uptake through the fluorescence analysis of the dye added inside the nanoparticles. We chose to use FA because CRC cells show an overexpression of FA receptors, which makes FA a promising targeting moiety for this type of cancer [56]. In these studies, we observed an improved internalization of the DDSs. Both the binding of the DDSs at the surface receptors and their internalization inside the cell were confirmed by an increase of the fluorescence signal of the incorporated dye as well as the fluorescence signal obtained from immunocytochemistry [56]. The fluorescence signal for nanoparticles without the targeting moiety was weaker than the fluorescence signal of the targeted nanoparticles. These data, together with the increase in cell death, confirm that functionalized NPs are more efficient than the free drug. [57].

The increased delivery efficiency of OXA and CVDL to the tumor site by DDSs functionalized with CHO and FA resulted in reduced proliferation and increased tumor cell mortality rates, demonstrating the therapeutic importance of these systems.

Objective 4: Modulating tumour progression when using treatment with nanoparticulate systems

Tumor progression includes mechanisms which involve genetic, biochemical and phenotypic changes used by neoplastic cells to grow, proliferate, survive, invade and metastasize [58, 59]. By acquiring the ability to survive, cancer cells in the TME gain new characteristics of escape from the immune system as well as apoptosis, which results in failed response to drugs [58, 59].

For the *in vivo* studies of this thesis related to tumor progression, we subcutaneously inoculated CT-26 cells into the right flank of Balb/c mice [60]. This cell line originates from fibroblasts and is an undifferentiated strain of colon carcinoma induced by N-nitrous-N-methylurethane (NNMU). To obtain these cells, the CT-26 WT strain was transduced with the retroviral vector LXSN, which contained the lacZ gene and encoded the tumor-associated model antigen (TAA) as well as beta-galactosidase (beta-gal) to generate the lethal CT-26 subclone gene [61]. A lethal tumor rapidly develops when the CT-26 cell line is inoculated subcutaneously in Balb/c mice. This results in a rapidly growing grade IV carcinoma, which is easily implanted and promptly metastasizes. Therefore, these characteristics were the reason for choosing this strain for our study, this strain is one of the most used in drug development, as it shares molecular characteristics with aggressive, undifferentiated and refractory cells of human colorectal carcinomas [62]. After the inoculation of CT-26 cells, we expected the tumor volume to reach 3-4 mm. The animals were randomly divided into four groups based on the treatment received: saline, free OXA, NP-OXA and NP-OXA functionalized. [60]. Subsequently, NPs were peritumorally injected to treat the mice. This treatment route was chosen because the regions adjacent to the tumor ensured complete absorption of the formulation by the tumor, avoiding losses by metabolism in the liver and losses due to kidney clearance. In addition, the route was chosen because the molecules and cells of the immune system were similar to the tumor mass. Previous studies have shown responses to treatments

using this route [63-65]. Other studies quantitatively analyzed the tumor and its surroundings in order to obtain relevant data regarding the biological characteristics of the cancer and the probability of response to targeted therapy [66]. Information on the peritumoral immune response could be used to predict the impact on the intratumoral environment. Treatment via the peritumoral environment can predict the safety of DDDs, like the ones used in this thesis [63]. However, this administration route of the NPs could become a limitation for a clinical application, since in general systemic administration routes are used to administer drugs, since metastases are not often located superficially and are in most cases disseminated all over the body. Therefore, it is necessary to develop studies where the administration route of NPs is systematic so that our formulations can be translated to clinical settings. Future studies are required, which analyze the interaction of NPs with barriers in the human body that will be faced after systemic administration.

Our *in vivo* study covered the following topics: a) inflammation, b) survival and proliferation, c) apoptosis, d) drug resistance and e) metastasis. Next, we will point out the main conclusion of each subitem.

a. Inflammation

Tumors are known as “wounds that do not heal” (Hal Dvorak, 1986), due to the immunosuppressive characteristics of the TME [67]. The onset of CRC progression is triggered by persistent chronic inflammation, passing through stages, which include the formation of aberrant polyps, adenomas and carcinomas. Subsequent mutations activate signaling pathways and pro-inflammatory transcription factors, promoting the release of inflammatory cytokines [68-70]. The immune system plays a crucial role in gastrointestinal tract health, intervening during infections. However, the recurrence of the presence of pro-inflammatory molecules at the site causes damage to the intestinal mucosa, which leads to tumor progression [68-70].

Based on the results found in Chapter 2, it was possible to observe a reduction in the global leukocyte count in the peritonitis model induced from treatment with nanocomposites containing CVDL and CHO. Thus, the treatment proved to be efficient in reducing the inflammatory response present in peritonitis. In addition, reduced levels of

malondialdehyde (MDA), glutathione peroxidase (GSH) and leukocyte migration were observed. It does not only reduce inflammation, but also reduces oxidative stress.

MDA is an indicator of the presence of oxidative stress, since MDA is the final product of lipid peroxidation. MDA levels in cancer patients are higher compared to individuals without cancer [71]. While, the GSH marker is an antioxidant enzyme, which eliminates reactive species under physiological conditions. The glutathione metabolism is disrupted in cancer, promoting tumor progression and therapeutic resistance, because the genes involved in using GSH are controlled by classic tumorigenic pathways, such as the hypoxia-inducible factor 1 (HIF1) pathway that activates GSH synthesis in a hypoxic situation and shows a greater amount of stem cells in the tumor tissue after chemotherapy in breast cancer [72, 73].

Oxidative stress occurs when ROS levels replace antioxidant defense mechanisms. Many studies have demonstrated a correlation between tumor progression and oxidative stress, since excess ROS can cause damage to genomic and mitochondrial DNA. This results in damage to DNA, mutation of several molecules and also changes in signaling pathways, promoting tumor initiation and progression [74, 75]. Therefore, the use of an anti-inflammatory drug encapsulated in NPs can decrease the oxidative stress of the tumor, thus preventing tumor progression [76-78].

b. Survival and proliferation

The recurrence and persistence of inflammation at the same location in the intestine leads to cellular neoformations, and therefore changes in the immune system cell phenotype pattern in the TME. Such a change leads to loss of immune surveillance over the excessive proliferation of neoplastic cells, which induces tumor growth [79]. Survival and proliferation markers, such as SURVIVIN and Ki-67, respectively, were measured in the tumor mass (Chapters 3 and 4), and their reduced expression was observed during treatment of human CRC cell lines with our DDSs. SURVIVIN and Ki-67 are described in literature as overexpressed in cancer, promoting activation of the cell cycle and inhibiting apoptosis in cancer cells [80, 81]. We hypothesized that the groups of animals

used for our *in vivo* studies treated with our DDSs show a reduction in tumor weight and a decline in tumor growth, when compared to treatment groups treated with free OXA. The hypothesis was confirmed, since a reduction in proliferation markers and an induction of apoptosis was observed.

c. Apoptosis

Cancer cells acquire the ability to overcome programmed cell death, activating anti-apoptotic machinery molecules and inhibiting pro-apoptotic molecules [82]. The escape mechanisms used by the cells can contemplate deregulation in both the intrinsic and extrinsic pathways [83]. As the avoidance of apoptosis by cancer cells is a major problem, apoptosis activation plays an important role in the treatment of cancer [84]. In analyzing our results, it was possible to verify the reduction of BCL-2 as an anti-apoptotic marker, and the increase in caspase-3 and caspase-8 as pro-apoptotic markers, including an increase of intrinsic (APAF-1) and extrinsic (Fas, FADD) pathway markers. RA can molecularly interact with nuclear receptors (heterodimers of the retinoic acid receptor and the retinoid X receptor), which can inhibit cell cycle-promoting proteins, such as p27, and can activate regulatory proteins in the cell cycle, such as Cdk5 [85]. Thus, RA as part of the nanosystem can lead to growth inhibition and apoptosis in tumor cells [86, 87]. The results of Chapter 3 indicate the effectiveness of the treatment with our DDS, in which cell death was induced either by direct action of RA, which promotes the regulations of proteins in the apoptotic pathway, or by indirect action stimulated by targeted nanoparticles containing FA and CHO, which favors binding, internalization and containment of the drug [45, 56]. The activation of apoptosis by the nanoparticulate complex was the objective outlined and achieved by the studies performed in Chapter 3.

d. Drug resistance

The tolerance to drugs developed in cancer can originate from mutations in DNA and metabolic alterations that promote inhibition,

degradation or efflux of the drug. In drug resistant cells, the mechanisms used by chemotherapeutics are modified in such a way that changes in the drug's target are generated, which activates pro-survival pathways and render cell death induction approaches unusable [88, 89].

The multiple resistance gene (MDR-1) is amplified in the drug resistance process developed by tumor cells [90-92]. In the results obtained by the Chapter 3 and 4 it was possible to visualize reduced expression of the MDR-1 gene when treatment using nanoparticulate systems was compared with treatment with free OXA. When such results are associated with reduced SURVIVIN labeling after treatment, attenuation of drug resistance is observed along with the consequent inhibition of neoplastic cell survival. This indicates greater susceptibility of the cells to the treatment with OXA encapsulated with PLGA, FA or CHOL, and RA. This increases the therapeutic potential through modulating MDR, which confirms the efficiency of the target system by promoting the endocytosis of the DDS [93-96].

In addition, some recent studies demonstrate there is a direct correlation between the epithelial-mesenchymal transition (EMT) process and drug resistance. EMT is a process present in tumor progression, whereby epithelial cells can convert into a mesenchymal phenotype. This transition can culminate in metastasis, generating tumor cells with stem cell properties that play an important role in resistance to cancer treatment [97]. Thus, by reversing the tumor's drug resistance, it would be possible to hamper the EMT process, delay metastases, and therefore improve patients' prognosis [98, 99].

e. Metastasis

Invasiveness, migration and metastasis are inherent characteristics to tumor progression, directly related to tumor aggressiveness [100]. The metastatic cascade involves tumor cells detaching from the primary tumor, entering into the circulatory and lymphatic systems, preventing the immune attack, and finally reaching distant capillary vessels, invading and proliferating in distant organs [101, 102].

According to the results obtained of our study described in Chapter

3 and 4, there was a reduction in the expression of C-X-C chemokine receptor type 4 (CXCR4) and monocyte-derived chemokine (CCL22) in the tumor after treatments with NP-OXA functionalized with CHOL and RA. Furthermore, in our CRC xenograft *in vivo* model, the treatments with NP-OXA and FA only demonstrated the relevant expression reduction profile for CCL22 when compared to the control groups in *in vivo* experiment. The results showed that the targeted nanoconjugates were able to control inflammatory cytokines in the TME and were able to suppress tumor progression [103, 104].

Tumor progression is composed of a series of interrelated steps, sequential or not, which lead to tumor extension and tumor spread. Many authors study tumor metastatic potential and report the association with prognosis; they highlight the importance of developing new treatment strategies, which can prevent or control this process [105, 106].

Following this line of research, it was extremely important to analyze the action of nanoconjugates functioning as possible proliferation and survival blockers, activators of apoptosis, inhibitors of drug resistance, and finally inhibitors of the metastatic cascade [107, 108]. All of these behavioral responses observed in neoplastic cells occurred due to the successful encapsulation of drugs in nanoparticulate systems, resulting in improved internalization. This approach has increased the effectiveness of treatment for CRC when drugs are encapsulated in PLGA systems. [109-111].

FUTURE PERSPECTIVES

In the past decades, important advances have been made in the use of nanomedicine to improve cancer treatment. A variety of methods have been applied to design efficient DDSs, to improve the efficacy of the drug, decrease its associated side effects, and counteract drug resistance.

To take the next steps forward, future experiments should be conducted in order to formulate nanoparticulate systems with smaller sizes with regard to the NPs studied in Chapter 3 and with greater encapsulation efficiency with regard to the NPs studied in Chapters 3 and 4. Better pharmacokinetics can be achieved by obtaining NPs with more suitable sizes, and consequently fewer toxic effects.

The results obtained with the target moiety FA showed great potential, but additional studies should be carried out using free FA to evaluate the competition between free FA and bound FA, which is located on the NP surface. It is important to study this competition in order to strengthen our hypothesis.

The use of another animal model may also add more value to this research and answer questions, which have not been answered herein, such as microscopic analysis of animal organs in order to search for possible metastases in the treated and control groups. The use of specific markers will be useful to identify the intracellular pathway(s) activated during the treatment with DDSs.

In addition, the use of 3D solid tumor models can be a promising approach in the search for more information, regarding tumor growth, differentiation, cell structure and the TME. Studies focused on organoids seek to create a 3D culture which can approach *in vivo* conditions in order to obtain relevant results similar to the human physiology. Furthermore, orthotopic animal models could be used, which are based on tumor cell line implants or tumor cell xenografts derived from patients, in order to create a situation which is very close to human physiology.

REFERENCES

[1] S. Parveen, R. Misra, S.K. Sahoo, Nanomedicine : nanotechnology, biology, and medicine, 8 (2012) 147-166.
[2] S.P. Chandran, S.B. Natarajan, S. Chandraseharan, M.S.B. Mohd Shahimi, Journal of Cancer Research and Practice, 4 (2017) 45-48.
[3] A. Gulbake, A. Jain, A. Jain, A. Jain, S.K. Jain, World J Gastroenterol, 22 (2016) 582-599.
[4] C.-S. Lee, H. Kim, J. Yu, S.H. Yu, S. Ban, S. Oh, D. Jeong, J. Im, M.J. Baek, T.H. Kim, European Journal of Medicinal Chemistry, 142 (2017) 416-423.
[5] N.P. Truong, M.R. Whittaker, C.W. Mak, T.P. Davis, Expert Opin Drug Deliv, 12 (2015) 129-142.
[6] B. Zhang, P. Sai Lung, S. Zhao, Z. Chu, W. Chrzanowski, Q. Li, Scientific reports, 7 (2017) 7315.
[7] F. Madani, S.S. Esnaashari, M.C. Bergonzi, T.J. Webster, H.M. Younes, M. Khosravani, M. Adabi, Life Sciences, 256 (2020) 117943.
[8] S.A. Sufi, M. Hoda, S. Pajaniradje, V. Mukherjee, S.M. Coumar, R. Rajagopalan, International journal of pharmaceutics, 588 (2020) 119738.
[9] E. Akbari, H. Mousazadeh, Z. Sabet, T. Fattahi, A. Dehnad, A. Akbarzadeh, E. Alizadeh, Journal of Drug Delivery Science and Technology, 61 (2021) 102294.
[10] M. Caldorera-Moore, N. Guimard, L. Shi, K. Roy, Expert Opin Drug Deliv, 7 (2010) 479-495.
[11] S. Venkataraman, J.L. Hedrick, Z.Y. Ong, C. Yang, P.L.R. Ee, P.T. Hammond, Y.Y. Yang, Advanced Drug Delivery Reviews, 63 (2011) 1228-1246.
[12] L. Guerrini, R.A. Alvarez-Puebla, N. Pazos-Perez, 11 (2018) 1154.
[13] A. Rajendra, R. Ariane, H. Philip Michael, R. Michael John, D. Kamal, B. Mary, Current Drug Targets, 19 (2018) 1696-1709.
[14] T. Sadhukha, S. Prabha, AAPS PharmSciTech, 15 (2014) 1029-1038.
[15] X. Gu, Y. Wei, Q. Fan, H. Sun, R. Cheng, Z. Zhong, C. Deng, Journal of Controlled Release, 301 (2019) 110-118.
[16] X. Montané, A. Bajek, K. Roszkowski, J.M. Montornés, M. Giamberini, S. Roszkowski, O. Kowalczyk, R. Garcia-Valls, B. Tylkowski, Molecules, 25 (2020) 1605.
[17] C. Deng, Q. Zhang, J. Guo, X. Zhao, Z. Zhong, Advanced Drug Delivery Reviews, 160 (2020) 199-211.
[18] S. Alqahtani, L. Simon, C.E. Astete, A. Alayoubi, P.W. Sylvester, S. Nazzal, Y. Shen, Z. Xu, A. Kaddoumi, C.M. Sabliov, Journal of Colloid and Interface Science, 445 (2015) 243-251.
[19] M.C. Pereira, D.A. Oliveira, L.E. Hill, R.C. Zambiazi, C.D. Borges, M. Vizzotto, S. Mertens-Talcott, S. Talcott, C.L. Gomes, Food Chemistry, 240 (2018) 396-404.
[20] Q. Abbas, B. Yousaf, Amina, M.U. Ali, M.A.M. Munir, A. El-Naggar, J. Rinklebe, M. Naushad, Environment International, 138 (2020) 105646.
[21] Y. Zhang, M. Yang, N.G. Portney, D. Cui, G. Budak, E. Ozbay, M. Ozkan, C.S. Ozkan, Biomedical Microdevices, 10 (2008) 321-328.
[22] S. Ghosh, S. Dutta, A. Sarkar, M. Kundu, P.C. Sil, Colloids and Surfaces B: Biointerfaces, 197 (2021) 111404.
[23] N. Hoshyar, S. Gray, H. Han, G. Bao, Nanomedicine (Lond), 11 (2016) 673-692.
[24] M.J. Ernsting, M. Murakami, A. Roy, S.D. Li, Journal of controlled release : official journal of the Controlled Release Society, 172 (2013) 782-794.
[25] B.D. Chithrani, A.A. Ghazani, W.C.W. Chan, Nano Letters, 6 (2006) 662-668.
[26] T. Sun, Y.S. Zhang, B. Pang, D.C. Hyun, M. Yang, Y. Xia, Angewandte Chemie (International ed. in English), 53 (2014) 12320-12364.
[27] L. Tang, X. Yang, Q. Yin, K. Cai, H. Wang, I. Chaudhury, C. Yao, Q. Zhou, M. Kwon, J.A. Hartman, I.T. Dobrucki, L.W. Dobrucki, L.B. Borst, S. Lezmi, W.G. Helferich, A.L. Ferguson, T.M. Fan, J. Cheng, 111 (2014) 15344-15349.

[28] H. Maeda, Bioconjug Chem, 21 (2010) 797-802.
[29] A. Ediriwickrema, W.M. Saltzman, ACS Biomaterials Science & Engineering, 1 (2015) 64-78.
[30] J. Cassidy, J.-L. Misset, Seminars in Oncology, 29 (2002) 11-20.
[31] Y. Zhong, T. Su, Q. Shi, Y. Feng, Z. Tao, Q. Huang, L. Li, L. Hu, S. Li, H. Tan, S. Liu, H. Yang, International journal of nanomedicine, 14 (2019) 8543-8560.
[32] A. Tiwari, S. Saraf, A. Jain, P.K. Panda, A. Verma, S.K. Jain, Drug Delivery and Translational Research, 10 (2020) 319-338.
[33] D.N. Kapoor, A. Bhatia, R. Kaur, R. Sharma, G. Kaur, S. Dhawan, Therapeutic Delivery, 6 (2015) 41-58.
[34] F. Sadat Tabatabaei Mirakabad, K. Nejati-Koshki, A. Akbarzadeh, M.R. Yamchi, M. Milani, N. Zarghami, V. Zeighamian, A. Rahimzadeh, S. Alimohammadi, Y. Hanifehpour, S.W. Joo, Asian Pacific journal of cancer prevention : APJCP, 15 (2014) 517-535.
[35] A. Kumari, S.K. Yadav, S.C. Yadav, Colloids and Surfaces B: Biointerfaces, 75 (2010) 1-18.
[36] B. Layek, J. Singh, International journal of molecular sciences, 20 (2019).
[37] L. Frungillo, D. Martins, S. Teixeira, M.C. Anazetti, P.d.S. Melo, N. Durán, Journal of Pharmaceutical Sciences, 98 (2009) 4796-4807.
[38] N. Vilaça, A.R. Bertão, E.A. Prasetyanto, S. Granja, M. Costa, R. Fernandes, F. Figueiredo, A.M. Fonseca, L. De Cola, F. Baltazar, I.C. Neves, Materials Science and Engineering: C, (2020) 111721.
[39] Y. Xu, Y. Zi, J. Lei, X. Mo, Z. Shao, Y. Wu, Y. Tian, D. Li, C. Mu, Carbohydrate polymers, 233 (2020) 115858.
[40] M. Kundu, S. Chatterjee, N. Ghosh, P. Manna, J. Das, P.C. Sil, Materials Science and Engineering: C, 116 (2020) 111239.
[41] X. Zhou, Y. Chen, F. Wang, H. Wu, Y. Zhang, J. Liu, Y. Cai, S. Huang, N. He, Z. Hu, X. Jin, Chemico-Biological Interactions, 331 (2020) 109273.
[42] W. Ke, X. Zhao, Z. Lu, Biomedicine & Pharmacotherapy, 135 (2021) 111213.
[43] H.S. Zavareh, M. Pourmadadi, A. Moradi, F. Yazdian, M. Omidi, Int J Biol Macromol, 165 (2020) 1422-1430.
[44] H. Futami, R. Sakai, Cancer Letters, 297 (2010) 220-225.
[45] H. Watabe, Y. Soma, M. Ito, Y. Kawa, M. Mizoguchi, The Journal of investigative dermatology, 118 (2002) 35-42.
[46] N. Kamaly, Z. Xiao, P.M. Valencia, A.F. Radovic-Moreno, O.C. Farokhzad, Chemical Society Reviews, 41 (2012) 2971-3010.
[47] D.-J. Jang, C. Moon, E. Oh, Biomedicine & Pharmacotherapy, 80 (2016) 162-172.
[48] X. Ding, W. Zhang, S. Li, H. Yang, Am J Cancer Res, 9 (2019) 219-227.
[49] J.E. Baggott, R.A. Oster, T. Tamura, Cancer Epidemiology, 36 (2012) 78-81.
[50] O.F. Kuzu, M.A. Noory, G.P. Robertson, Cancer Research, 76 (2016) 2063.
[51] T.N. Wien, E. Pike, T. Wisløff, A. Staff, S. Smeland, M. Klemp, BMJ Open, 2 (2012) e000653.
[52] J.-J. Lee, S.Y. Lee, J.-H. Park, D.-D. Kim, H.-J. Cho, International journal of pharmaceutics, 509 (2016) 483-491.
[53] A.A. Radwan, F.K. Alanazi, Saudi Pharmaceutical Journal, 22 (2014) 3-16.
[54] I.A. Khalil, K. Kogure, H. Akita, H. Harashima, Pharmacological reviews, 58 (2006) 32-45.
[55] T.-G. Iversen, T. Skotland, K. Sandvig, Nano Today, 6 (2011) 176-185.
[56] A. Narmani, M. Kamali, B. Amini, A. Salimi, Y. Panahi, Process Biochemistry, 69 (2018) 178-187.
[57] A. Akbarian, M. Ebtekar, N. Pakravan, Z.M. Hassan, Int J Biol Macromol, 152 (2020) 90-101.
[58] R.D. Schreiber, L.J. Old, M.J. Smyth, Science, 331 (2011) 1565.
[59] D.F. Quail, J.A. Joyce, Nature medicine, 19 (2013) 1423-1437.
[60] W. Zhang, F. Wang, X. Hu, J. Liang, B. Liu, Q. Guan, S. Liu, Oncol Lett, 17 (2019) 815-822.
[61] S.Y. Owyang, M. Zhang, G.A. Walkup, G.E. Chen, H. Grasberger, M. El-Zaatari, J.Y. Kao, Immunol Lett, 191 (2017) 47-54.

[62] J.C. Castle, M. Loewer, S. Boegel, J. de Graaf, C. Bender, A.D. Tadmor, V. Boisguerin, T. Bukur, P. Sorn, C. Paret, M. Diken, S. Kreiter, Ö. Türeci, U. Sahin, BMC Genomics, 15 (2014) 190-190.
[63] R. Li, JAMA Network Open, 3 (2020) e2016125-e2016125.
[64] C. Sun, X. Tian, Z. Liu, W. Li, P. Li, J. Chen, W. Zhang, Z. Fang, P. Du, H. Duan, P. Liu, L. Wang, C. Chen, J. Tian, EBioMedicine, 46 (2019) 160-169.
[65] Y. Hu, C. Xie, H. Yang, J.W.K. Ho, J. Wen, L. Han, K.W.H. Chiu, J. Fu, V. Vardhanabhuti, JAMA Network Open, 3 (2020) e2015927-e2015927.
[66] N. Braman, P. Prasanna, J. Whitney, S. Singh, N. Beig, M. Etesami, D.D.B. Bates, K. Gallagher, B.N. Bloch, M. Vulchi, P. Turk, K. Bera, J. Abraham, W.M. Sikov, G. Somlo, L.N. Harris, H. Gilmore, D. Plecha, V. Varadan, A. Madabhushi, JAMA Network Open, 2 (2019) e192561-e192561.
[67] J.S. Byun, K. Gardner, Am J Pathol, 182 (2013) 1055-1064.
[68] H. Raskov, J. Burcharth, H.-C. Pommergaard, J Cancer, 8 (2017) 3378-3395.
[69] Y. Xiong, Y. Wang, K. Tiruthani, Nanomedicine : nanotechnology, biology, and medicine, 21 (2019) 102034.
[70] C.R.L.V. Figueiredo, 55 (2019) 321-332.
[71] J. Didžiapetrienė, B. Kazbarienė, R. Tikuišis, A. Dulskas, D. Dabkevičienė, V. Lukosevičienė, E. Kontrimavičiūtė, K. Sužiedėlis, V. Ostapenko, Medicina, 56 (2020).
[72] A. Bansal, M.C. Simon, J Cell Biol, 217 (2018) 2291-2298.
[73] E. Desideri, F. Ciccarone, M.R. Ciriolo, Nutrients, 11 (2019) 1926.
[74] J.E. Klaunig, Current pharmaceutical design, 24 (2018) 4771-4778.
[75] J.D. Hayes, A.T. Dinkova-Kostova, K.D. Tew, Cancer Cell, 38 (2020) 167-197.
[76] J. Sun, I. Kato, Genes & Diseases, 3 (2016) 130-143.
[77] T. Atsumi, R. Singh, L. Sabharwal, H. Bando, J. Meng, Y. Arima, M. Yamada, M. Harada, J.-J. Jiang, D. Kamimura, H. Ogura, T. Hirano, M. Murakami, Cancer Research, 74 (2014) 8.
[78] L.M. Coussens, Z. Werb, Nature, 420 (2002) 860-867.
[79] R.F. de Araujo Junior, C. Eich, C. Jorquera, T. Schomann, F. Baldazzi, A.B. Chan, L.J. Cruz, Molecular and cellular biochemistry, 468 (2020) 153-168.
[80] L.T. Li, G. Jiang, Q. Chen, J.N. Zheng, Molecular medicine reports, 11 (2015) 1566-1572.
[81] S. Khan, J.M.S. Jutzy, J.R. Aspe, D.W. McGregor, J.W. Neidigh, N.R. Wall, Apoptosis, 16 (2011) 1-12.
[82] K. Fernald, M. Kurokawa, Trends in cell biology, 23 (2013) 620-633.
[83] J.L. Koff, S. Ramachandiran, L. Bernal-Mizrachi, International journal of molecular sciences, 16 (2015).
[84] R.S.Y. Wong, Journal of Experimental & Clinical Cancer Research, 30 (2011) 87.
[85] M.C. Chen, S.L. Hsu, H. Lin, T.Y. Yang, BioMedicine, 4 (2014) 22.
[86] P. Nagar, P. Goyal, A. Gupta, A.K. Sharma, P. Kumar, Nano-Structures & Nano-Objects, 14 (2018) 110-117.
[87] M.H. Akanda, R. Rai, I.J. Slipper, B.Z. Chowdhry, D. Lamprou, G. Getti, D. Douroumis, International journal of pharmaceutics, 493 (2015) 161-171.
[88] C. Holohan, S. Van Schaeybroeck, D.B. Longley, P.G. Johnston, Nature Reviews Cancer, 13 (2013) 714-726.
[89] G. Housman, S. Byler, S. Heerboth, K. Lapinska, M. Longacre, N. Snyder, S. Sarkar, Cancers, 6 (2014).
[90] R.L. Linardi, C.C. Natalini, 36 (2006) 336-341.
[91] E. Balcerczak, M. Panczyk, S. Piaskowski, G. Pasz-Walczak, A. Sałagacka, M. Mirowski, International Journal of Colorectal Disease, 25 (2010) 1167-1176.
[92] P.C. Huber, C.H. Maruiama, W.P. Almeida, 33 (2010) 2148-2154.
[93] S. Kapse-Mistry, T. Govender, R. Srivastava, M. Yergeri, Front Pharmacol, 5 (2014) 159-159.
[94] T. Lv, Z. Li, L. Xu, Y. Zhang, H. Chen, Y. Gao, Acta biomaterialia, 76 (2018) 257-274.
[95] J.L. Markman, A. Rekechenetskiy, E. Holler, J.Y. Ljubimova, Advanced Drug Delivery Reviews, 65 (2013) 1866-1879.

[96] H. Tonbul, A. Sahin, E. Tavukcuoglu, G. Esendagli, Y. Capan, Journal of Drug Delivery Science and Technology, 54 (2019) 101380.
[97] J. Roche, Cancers (Basel), 10 (2018) 52.
[98] A. Singh, J. Settleman, Oncogene, 29 (2010) 4741-4751.
[99] Y. Shang, X. Cai, D. Fan, Current cancer drug targets, 13 (2013) 915-929.
[100] C.L. Chaffer, R.A. Weinberg, Science, 331 (2011) 1559.
[101] D. Tarin, Seminars in cancer biology, 21 (2011) 72-82.
[102] A.F. Chambers, A.C. Groom, I.C. MacDonald, Nature reviews. Cancer, 2 (2002) 563-572.
[103] P.J. Sarvaiya, D. Guo, I. Ulasov, P. Gabikian, M.S. Lesniak, Oncotarget, 4 (2013) 2171-2185.
[104] A. Maolake, K. Izumi, K. Shigehara, A. Natsagdorj, H. Iwamoto, S. Kadomoto, Y. Takezawa, K. Machioka, K. Narimoto, M. Namiki, W.-J. Lin, G. Wufuer, A. Mizokami, Oncotarget, 8 (2017) 9739-9751.
[105] J. Massagué, A.C. Obenauf, Nature, 529 (2016) 298-306.
[106] N.J. Birkbak, N. McGranahan, Cancer Cell, 37 (2020) 8-19.
[107] I. Pastushenko, C. Blanpain, Trends in cell biology, 29 (2019) 212-226.
[108] M. Saitoh, Journal of biochemistry, 164 (2018) 257-264.
[109] C. Fernandes, D. Suares, M.C. Yergeri, 9 (2018).
[110] L. Wang, M. Huo, Y. Chen, J. Shi, Advanced Healthcare Materials, 7 (2018) 1701156.
[111] T. Wu, Y. Dai, Cancer Letters, 387 (2017) 61-68.

APPENDICES

NEDERLANDSE SAMMENVATTING

Het gebruik van moderne technologie komt het nanogeneeskundig onderzoek steeds meer ten goede. Deze technieken maken het mogelijk om nanostructuren dusdanig te aan te passen, dat ze de gewenste farmacokinetische en farmacodynamische eigenschappen bezitten die gunstig zijn voor de behandeling van verschillende ziekten, zoals kanker. Voor de effectieve behandeling van kanker is het belangrijk om de heterogeniteit van primaire tumoren in acht te nemen. Tumorheterogeniteit bevordert de overleving van tumorweefsel en zorgt ervoor dat dit minder gevoelig is voor de werking van medicijnen, waardoor bijvoorbeeld behandelingen met chemotherapie minder goed aanslaan. De bijwerkingen van de huidige chemotherapieën zijn met name te wijten aan de manier waarop de chemotherapeutica worden opgenomen, afgebroken en uitgescheiden, alsook de niet doelgerichte afgifte van de medicijndeeltjes.
Het algemene doel van dit proefschrift was het inkapselen van carvedilol of oxaliplatin in doelgerichte PLGA nanodeeltjes. Hierbij zijn *in vitro* en *in vivo* experimenten uitgevoerd zijn om de biologische activiteit te testen om een indruk te krijgen of de nanodeeltjes effectief zijn tegen colorectale kanker. Hiertoe zijn verschillende afgiftesystemen gemaakt en gekarakteriseerd om een beeld te krijgen van de grootte, de vorm, de hoeveelheid ingekapselde medicijndeeltjes en de zeta spanning. Omdat er een samenhang is tussen chronische en terugkerende ontsteking en het verloop van colorectale kanker, hebben wij de ontsteking onderzocht (Hoofdstuk 2). Met *in vitro* experimenten, waarbij we bijvoorbeeld keken naar celoverleving en celdood, hebben wij onderzocht in welke mate de afgiftesystemen toxisch zijn voor tumorcellen. In hoofdstuk 3 en 4 hebben wij onderzocht of nanodeeltjes die met CHO en FA zijn gekoppeld, ook doelgericht CT-26 colorectaal kankercellen kunnen targeten.
Ten slotte stonden in hoofdstuk 3 en 4 dierstudies met apoptose, behandelresistentie en metastases centraal. De belangrijkste resultaten van dit onderzoek zijn samengevat in het eerste deel van dit proefschrift, welk als een algemeen overzicht fungeert. Daarnaast worden factoren besproken die mogelijk van invloed geweest waren op de onderzoeksresultaten.
In het tweede gedeelte gaan wij alleen in op de plannen voor verder onderzoek.

PORTUGUESE SUMMARY

O campo da nanomedicina está em constante aperfeiçoamento devido ao uso de técnicas modernas. Com essas técnicas, são formuladas nanoestruturas com farmacocinética e farmacodinâmica adequadas para o tratamento de várias doenças, incluindo o câncer. É importante considerar a heterogeneidade dos tumores primários para que o tratamento do câncer seja eficaz. A heterogeneidade do tumor favorece a sobrevivência do tecido tumoral e a resistência aos medicamentos, levando à falha dos agentes quimioterápicos em induzir uma resposta terapêutica. Além disso, os mecanismos de absorção, metabolismo e excreção dos quimioterápicos, comumente utilizados em pacientes com câncer, e a falta de direcionamento específico desses medicamentos podem causar

efeitos adversos nos pacientes tratados. Assim, o objetivo geral desta tese é investigar a atividade biológica de nanopartículas (NPs) poli (ácido lático-co-glicólico) (PLGA) como um sistema de distribuição de drogas (DDS) para carvedilol (CVDL) ou oxaliplatina (OXA), *in vitro* e *in vivo*, para tratar o câncer colorretal (CRC). Os DDSs foram formulados para atingir esse objetivo. Posteriormente, as formulações foram caracterizadas a fim de se obter informações sobre seu tamanho, forma, taxa de encapsulação e potencial zeta. Como resultado comum desta tese, todas as formulações apresentaram forma esférica e superfície lisa. Estudos de inflamação foram realizados, uma vez que a progressão do CCR está relacionada à indução de um processo inflamatório crônico e recorrente (Capítulo 2). No Capítulo 2, nanopartículas funcionalizadas com colesterol (CHO) diminuíram a migração de leucócitos quando comparadas com CVDL livre quando usadas na mesma concentração. Além disso, as nanoformulações apresentaram atividades semelhantes quando utilizadas em doses menores que o CVDL, em maior concentração, em relação aos níveis de malondialdeído (MDA) e glutationa (GSH). Estudos *in vitro*, como análise de viabilidade celular e morte celular, foram realizados para analisar a atividade antitumoral dos sistemas (Capítulos 2, 3 e 4). Os resultados *in vitro* mostraram que o polímero PLGA é atóxico e que o uso de NPs aumentou a eficácia do medicamento contra células tumorais. Testes para avaliar a eficiência do direcionamento dos NPs por meio de CHO ou ácido fólico (FA) foram realizados para comprovar que há um aumento na eficiência do direcionamento dos sistemas para células CRC murinas CT-26 (Capítulos 3 e 4). Esses testes mostraram que NPs direcionados se ligam à superfície da célula e internalizam na célula em maior quantidade do que NPs sem o alvo. Finalmente, modelos animais foram desenvolvidos para estudar apoptose e resistência a drogas, bem como metástases (Capítulos 3 e 4). Os resultados de um estudo em animais confirmaram nossos resultados *in vitro*, mostrando que o uso de NPs reduziu o volume do tumor e atuou na modulação do tumor. Nos capítulos 2, 3 e 4, nossos estudos foram discutidos em detalhes sobre as formulações e caracterizações de NPs como DDSs com características ideais para aumentar a gama terapêutica de drogas no local do tumor. Bem como a avaliação biológica desses DDS quando sua atividade antiinflamatória (Capítulo 2) e sua atividade antitumoral *in vitro* (Capítulos 2, 3 e 4) e *in vivo* (Capítulos 3 e 4). Tomados em conjunto, todos os DDSs estudados nesta tese foram capazes de melhorar a eficiência quimioterapêutica das drogas estudadas nos Capítulos 2, 3 e 4.

LIST OF ABBREVIATIONS

ACE	Acetone
ACE	Apoptosis-inducing factor
AFM	Atomic force microscopy
AP	Aqueous Phase
APAF-1	Anti-apoptotic protease activating factor 1
ASGP	Asialoglycoprotein
ATR-FTIR	Transform infrared spectroscopy
AuNPs	Gold NPs
BBB	Blood-brain barrier
BTB	Blood-tumor barrier
BSA	Bovine serum albumin
CAP	Capecitabine
CCL22	Chemokine ligand 22 of the C-C motif
CHOL/CHO	Cholesterol
CRC	Colorectal cancer
CT	Threshold cycle
CVDL	Carvedilol
CXCR4	C-X-C chemokine receptor type 4
DAPI	Diamidino-2-phenylindole; 4,6-diamidino-2-phenylindole
DCM	Dichloromethane
DDS	Drug delivery systems
DISC	Death-inducing signaling complex
DMEM	Dulbecco's modified eagle medium
DMSO	Dimethyl sulfoxide
DNA	Deoxyribonucleic acid
DOX	Doxorubicin
DSL	Dynamic light scattered
EDTA	Ethylenediamine tetraacetic acid
EE	Encapsulation efficiency
EGFR	Epidermal growth factor receptor
EMA	European Medicines Agency
EMT	Epithelial-mesenchymal transition
EPR	Enhanced Permeation and Retention
FA	Folic Acid
FAAD	Fas-associated death domain protein
FBS	Fetal bovine serum
FDA	Food and Drug Administration
FITC	Fluorescein isothiocyanate
GSH	Glutathione

HA	Hyaluronic acid
HRP	Haptoglobin Related Protein
IAP	Apoptosis inhibitor proteins
IHC	Immunohistochemistry
IRI	Irinotecan
LAS X	Leica Application Suite X
MDA	Malondialdehyde
MDR-1	Multidrug resistance protein 1
MOMP	Mitochondrial outer membrane permeabilization
MPS	Mononuclear phagocyte system
mRNA	Messenger ribonucleic acids
MSNs	Mesoporous silica NPs
MTS	[3-(4,5-dimethylthiazol-2-yl)-5-(3-carboxymethoxyphenyl)-2-(4-sulfophenyl)-2H-tetrazolium, inner salt]
mV	Millivolt
NADPH	Nicotinamide adenine dinucleotide phosphate?
NF-kb	Factor nuclear kappa B
NHS	N-hydroxysuccinimide
NIR	Near infrared 780 dye
Nm	Nanometer
NPs	Nanoparticles
OXA	Oxaliplatin
PAA	Polyacrylic acid
PBS	Phosphate-buffered saline
PCL	Poly-ε-caprolactone
PDI	Polydispersity Index
PEG	Polymeric polyethylene glycol
PLA	Polymers polylactic acid
PLGA	Poly (D, L-lactide-co-glycolide)
PTX	Paclitaxel
PVA	Polyvinyl alcohol
PVP	Polyvinyl pyrrolidone
qPCR	Real-time quantitative polymerase chain reaction
RA	Retinoic acid
RAR	Retinoic acid receptor
RES	Reticuloendothelial system
RNA	Ribonucleic acid
RNI	Reactive nitrogen intermediates
ROS	Reactive oxygen species

RP-HPLC	Reversed-phase high-performance liquid chromatography
RT-PCR	Reverse transcription polymerase chain reaction
RXR	Retinoid X receptor
SMAC	Second mitochondria-derived activator of caspases
SD	Standard deviation
STAT-3	Signal transducers and activatores of transcription
TCA	Trichloroacetic acid
TEA	Triethylamine
TEM	Transmission electron microscopy
TGF-β	Transforming growth factor beta
TMA	Tissue microarray
TME	Tumor microenvironment
TNF	Tumor necrosis factor
VEGF	Vascular endothelial growth factor

LIST OF PUBLICATIONS

1. Nanocarriers as a Tool for the Treatment of Colorectal Cancer. Ana Luiza C. de S. L. Oliveira, Timo Schomann, Lioe-Fee de Geus-Oei, Ellen Kapiteijn, Luis J. Cruz*, Raimundo F. de Araújo Júnior*. August 2021. Pharmaceutics. DOI: 10.3390/pharmaceutics13081321. * Authors to whom correspondence should be addressed.

2. Maximizing the potency of oxaliplatin coated nanoparticles with folic acid for modulating tumor progression in colorectal cancer. Ana Luiza C. de S. L. Oliveira, Luana Zerillo, Luis J. Cruz*, Timo Schomann, Alan B. Chan, Thaís Gomes de Carvalho, Shirley Vitória de P. Souza, Aurigena A. Araújo, Lioe-Fee de Geus-Oei, Raimundo F. de Araújo Júnior*. January 2021. Materials Science and Engineering C. DOI: 10.1016/j.msec.2020.111678. * Authors to whom correspondence should be addressed.

3. Cholesterol-functionalized carvedilol-loaded PLGA nanoparticles: anti-inflammatory, antioxidant, and antitumor effects. Ana Luiza C. de S. L. Oliveira, Alaine M. dos Santos-Silva, Arnóbio A. da Silva-Júnior, Vinícius B. Garcia, Aurigena A. de Araújo, Lioe-Fee de Geus-Oei, Alan B. Chan, Luis J. Cruz and Raimundo F. de Araújo Júnior. May 2020. Journal of Nanoparticle Research. DOI: 10.1007/s11051-020-04832-8

4. Effect of Oxaliplatin-Loaded Poly (d,l-Lactide-co-Glycolic Acid) (PLGA) Nanoparticles Combined with Retinoic Acid and Cholesterol on Apoptosis, Drug Resistance, and Metastasis Factors of Colorectal Cancer. Ana Luiza C. de S. L. Oliveira, Raimundo Fernandes de Araújo Júnior*, Thaís Gomes de Carvalho, Alan B. Chan, Timo Schomann, Filippo Tamburini, Lioe-Fee de Geus-Oei and Luis J. Cruz*. February 2020. Pharmaceutics. DOI: 10.3390/pharmaceutics12020193. * Authors to whom correspondence should be addressed.

5. Self-Assembled Benznidazole-Loaded Cationic Nanoparticles Containing Cholesterol/Sialic Acid: Physicochemical Properties, *In Vitro* Drug Release and *In Vitro* Anticancer Efficacy. Alaine Maria dos Santos-Silva, Lilia Basílio de Caland, Ednaldo Gomes do Nascimento, Ana Luiza C. de S.L. Oliveira, Raimundo F. de Araújo-Júnior, Alianda Maira Cornélio, Matheus F. Fernandes-Pedrosa and Arnóbio Antônio da Silva-Júnior.

May 2019. International Journal of Molecular Sciences 20(9). DOI: 10.3390/ijms20092350

6. Hydrophilic and hydrophobic polymeric benznidazole-loaded nanoparticles: Physicochemical properties and *in vitro* antitumor efficacy. Alaine Maria dos Santos Silva, Lilia Basílio de Caland, Polyanne Nunes de Melo Doro, Ana Luiza C. de S. L. Oliveira, Raimundo F. de Araújo-Júnior, Matheus F. Fernandes-Pedrosa,Eryvaldo Sócrates Tabosa do Egito, Arnóbio Antônio da Silva-Junior. April 2019. Journal of Drug Delivery Science and Technology. DOI: 10.1016/j.jddst.2019.04.005.

7. Designing structural features of novel benznidazole-loaded cationic nanoparticles for inducing slow drug release and improvement of biological efficacy. Alaine M. dos Santos-Silva, Lilia B. de Caland, Ana Luiza C. de S. L. Oliveira, Raimundo F. de Araújo-Júnior, Matheus F. Fernandes-Pedrosa, Alianda Maira Cornélio, Arnóbio A. da Silva-Júnior. April 2017. Materials Science and Engineering C. DOI: 10.1016/j.msec.2017.04.053

8. Anti-inflammatory, analgesic and anti-tumor properties of gold nanoparticles. Raimundo Fernandes de Araújo Júnior, Aurigena Antunes de Araújo, Jonas Bispo Pessoa, Franscisco Paulo Freire Neto, Gisele Ribeiro da Silva, Ana Luiza C.S. Leitão Oliveira, Thaís Gomes de Carvalho, Heloiza F.O. Silva, Mateus Eugênio, Celso Sant'Anna, Luiz H.S. Gasparotto. September 2016. Pharmacological reports. DOI: 10.1016/j.pharep.2016.09.017

9. Environmentally compatible bioconjugated gold nanoparticles as efficient contrast agents for colorectal cancer cell imaging. Kássio M.G. Lima, Raimundo F. Araújo Júnior, Aurigena A. Araújo, Ana Luiza C.S. Leitão Oliveira and Luiz H.S.Gasparotto. February 2014. Sensors and Actuators B Chemical. DOI: 10.1016/j.snb.2014.02.008.

10. The use of EEM fluorescence data and OPLS/UPLS-DA algorithm to discriminate between normal and cancer cell lines: A feasibility study. Ana Carolina de Oliveira Neves, Raimundo Fernandes de Araújo Júnior, Ana Luiza Cabral de Sá Leitão Oliveira, Aurigena Antunes de Araújo and Kássio Michell Gomes de Lima. April 2014. The Analyst. DOI: 10.1039/c4an00296b

11. Telmisartan induces apoptosis and regulates Bcl-2 in human renal

cancer cells. Raimundo Fernandes de Araújo Júnior*, Ana Luiza C.S. Leitão Oliveira*, RaniereFagundes de Melo Silveira, Hugo Alexandre de Oliveira Rocha, Pedro de França Cavalcanti, and Aurigena Antunes de Araújo. *These authors contributed equally. August 2014. Experimental Biology and Medicine. DOI: 10.1177/1535370214546267. * Equal contribution.

12. Maytenus ilicifolia dry extract protects normal cells, induces apoptosis and regulates Bcl-2 in human cancer cells. Raimundo Fernandes de Araújo Júnior*, Ana Luiza Cabral de Sá Leitão Oliveira*, Jonas Bispo Pessoa, Vinícios Barreto Garcia, Gerlane Coelho Bernardo Guerra,Luiz Alberto Lira Soares5, Tatiane Pereira de Souza, Pedro Ros Petrovick andAurigena Antunes de Araújo. *These authors contributed equally. July 2013. Experimental Biology and Medicine. DOI: 10.1177/1535370213494563. * Equal contribution.

13. A dry extract of Phyllanthus niruri protects normal cells and induces apoptosis in human liver carcinoma cells. Raimundo Fernandes de Araújo Júnior, Tatiane Pereira de Souza, Júlia Glória Lucatelli Pires, Luiz Alberto Lira Soares, Aurigena Antunes de Araújo, Pedro Ros Petrovick, Helainy Daline Oliveira Mâcedo, Ana Luiza Cabral de Sá Leitão Oliveira, Gerlane Coelho Bernardo Guerra. November 2012. Experimental Biology and Medicine. DOI: 10.1258/ebm.2012.012130

Patent

Araujo Junior, R. F.; Garcia, V. B.; Oliveira, A. L. C. S. L.; Gasparotto, L.H.S.; Silva, H. F. O.; Araujo, A. A. Nanoparticulated gold system and its way of obtaining applied to the immunofluorescence technique in paraffinized tissue. 2016, Brasil. Type of Patent: Innovation Privilege. Register number: BR10201602447. Registration institution: INPI - National Institute of Industrial Property. Issued date: 08/09/2021

CURRICULUM VITAE

Ana Luiza Cabral de Sá Leitão Oliveira was born in the city of Natal, Rio Grande do Norte, Brazil. She graduated with a degree in Biomedical Sciences at the Universidade Federal do Rio Grande do Norte (UFRN) in 2012, where she also completed her Master's degree in Pharmaceutical Sciences in 2014. She has worked in the Laboratory of Inflammation and Cancer Investigation with Professor Dr. Raimundo Fernandes de Araújo Júnior since the end of her graduation, who was her advisor throughout her academic period. She was a student tutor in the discipline of Pathology during her graduation studies, which touched her interest in teaching and led her to seek becoming a teacher. She was a lecturer in professional technical courses at UFRN-Escola Agrícola de Jundiaí, UFRN/EAJPRONATEC, Brazil, in 2014 and at the Universidade Potiguar, UnP, Brazil, from 2015 to 2019. Her PhD in 2015 at UFRN followed the same research line as her Master's degree, but this time working with a drug delivery system for colorectal cancer. She started an internship at the Leiden University Medical Center, the Netherlands, with Professor Dr. Luis Cruz in August 2017, working with evaluating drug delivery systems with *in vitro* and *in vivo* models. The internship partnership was renewed and transformed into an agreement between the two universities (UFRN and Leiden University) which culminated in the defense of a Doctorate degree in the Netherlands in 2022. From April 2020 to the present, Ana Luiza has been working at the Percuros B. V. company in the Netherlands as a Research Scientist.

ACKNOWLEDGEMENTS

The PhD was not an easy journey, and I had many wonderful people with me during it who directly and indirectly contributed to me being able to finish this very important cycle, and it is time to thank them.

I would like to thank Graduate Program of Brazil, the Health Sciences Graduation Program and CAPES for all the opportunities and funding that have been granted to me. I would also like to thank the University of Leiden and LUMC for receiving me and for making this collaboration happen.

I would like to thank my supervisor Dr. Raimundo Fernandes for all the learning, opportunities, patience and support. We had a long and fruitful partnership and I am very grateful. Thank you to Dr. Luis Cruz for opening the doors of his laboratory, which allowed me to experience another reality and opened my eyes to so many possibilities. Thank you to Prof. Dr. Lioe-Fee, for not giving up on our partnership, for all your patience and help. You are an inspiration to me as a woman and an excellent professional.

To Alan Chan, thank you for all the opportunities you have given me. To all the other professors and collaborators, such as Aurigena, Arnóbio, Alaine, who participated in this journey, it was a pleasure to work with all of you.

To my colleagues at the laboratory in Brazil, UFRN, thank you very much for all your support. You are part of this achievement and without you it would not have happened. I am very grateful to all of you. To my colleagues in the TNI group: thank you very much for warmly welcoming

me. Especially Chih Kit, who has always been very kind and willing to help me. To Silvia Sobol, my thanks for all the support and help at the end of this journey.

To my paranymphs: Timo Schomann and Carla Jorquera, I have no words to express all my gratitude. You are more than colleagues, you are friends. Timo was my encourager, my guide during the writing process and my benchmate. Carla was my friendly shoulder, always willing to listen to me. Thanks for everything.

My friends: Andreza Verás, thank you very much for all your help, encouragement and complicity. Kellen Passos, thank you for all the support in such a stressful ending. Natália Feitosa and Shirley Paiva, I have no words for you, thank you for holding my hand when I thought about giving up. Anouk, thank you for making my life in Leiden lighter.

To my Dutch family, Jannie, Martin and Stefano van Bovene: thank you very much for the warm welcome and all the encouragement. Especially to my husband Stefano for understanding all my stress in the final stage of preparing the thesis, thank you for being much better than I expected, for not letting me give up. And of course, thank you for giving me my greatest gift, our daughter, Kiara, who was my company during the writing process of the thesis. Kiara, my sweetheart, you were the strength I needed to finish this doctorate.

To my beloved grandmother Ana Maria (*in memorium*) and grandfather Joaquim, my greatest supporters, I am forever grateful for the sweetest words heard during this process.

My sister, Raquel, thank you so much for always believing that I am capable, for listening, helping and encouraging me. And my mother, Andréa, the main person responsible for getting me here, thank you very much. Andréa is synonymous with courage and love and it was these elements that brought me here. Thank you so much for teaching me to be the protagonist of my life, to be honest, strong and brave, and to always treat everyone with love and respect.